DEVELOPMENT OF A TISSUE ENGINEERING STRATEGY TO CREATE HIGHLY COMPLIANT BLOOD VESSELS

A Dissertation
Presented to
The Academic Faculty

by

Peter Maughan Crapo

In Partial Fulfillment
of the Requirements for the Degree
Doctor of Philosophy in Bioengineering

Georgia Institute of Technology

May 2009

DEVELOPMENT OF A TISSUE ENGINEERING STRATEGY

TO CREATE HIGHLY COMPLIANT BLOOD VESSELS

Approved by:

Dr. Yadong Wang, Advisor
School of Biomedical Engineering
Georgia Institute of Technology

Dr. Todd C. McDevitt
School of Biomedical Engineering
Georgia Institute of Technology

Dr. Samuel C. Dudley
College of Medicine, Section of Cardiology
University of Illinois at Chicago

Dr. David W. Rosen
School of Mechanical Engineering
Georgia Institute of Technology

Dr. Andres J. Garcia
School of Mechanical Engineering
Georgia Institute of Technology

Date Approved: November 25, 2008

To my eternally loving wife, Kristie

and to the advancement of medicine

for the extension of life

and the fulfillment of dreams

ACKNOWLEDGEMENTS

I am sincerely grateful to Dr. Yadong Wang for his mentoring, kindness, and encouragement in the completion of this work. He graciously allowed me to take stewardship of this research when other opportunities became impractical. Yadong provided many hours of stimulating conversation and trusted my judgment in directing key aspects of the research.

I would like to thank Dr. Jin Gao for teaching me principles of cell and tissue culture and helping me to learn the application of these principles. His contribution was invaluable in the development of the protocols used for this research. I would also like to thank Christiane Gumera and Blaine Zern for providing information regarding laboratory procedures and equipment and for their input regarding current literature as it related to aspects of this research. Jin, Christiane, and Blaine all provided encouragement and comradery during long hours of laboratory research.

I would like to thank Dr. Robert Nerem, for the use of the uniaxial tensile testing system in his laboratory, and technical assistance generously provided by Dr. Ann Ensley and Stacey Schutte.

I would like to especially thank Dr. Stephen Hanson, Dr. Monica Hinds, and Ulla Marzec at Oregon Health & Science University for generous providing baboon arteries, including excision and shipment. I would also like to thank Dr. Edward Balog for providing access to porcine tissue.

I would like to thank Dr. Rudolph Gleason for generously allowing me to use the pressure-diameter testing system he and his students developed. William Wan, Daniel

Howell, Julia Raykin, and Michael Zaucha provided excellent technical assistance as well as highly valuable troubleshooting assistance.

Finally and most importantly, I am sincerely grateful to my wife, Kristie, for her enduring support and patience during the completion of this work.

TABLE OF CONTENTS

LIST OF TABLES

LIST OF FIGURES

LIST OF ABBREVIATIONS

A_C	footprint area after transverse compression testing
A_{lumen}	lumen cross-sectional area before ultimate tensile stress
$A_{\sigma o}$	lumen cross-sectional area at zero stress
$A_{\sigma max}$	lumen cross-sectional area at ultimate tensile stress
bFGF	basic fibroblast growth factor (human recombinant)
BrdU	5-bromo-2-deoxyuridine
CNBr	cyanogen bromide
D_1	artery or construct diameter at initial (low) pressure
D_2	artery or construct diameter at target (high) pressure
DAPI	4',6-diamidino-2-phenylindole
dH_2O	deionized water
D_{hook}	hook diameter
DMEM	Dulbecco's modified Eagle's medium
DMSO	dimethyl sulfoxide
E_c	elastic modulus in transverse compression
EC	endothelial cell
ECM	extracellular matrix
EGF	epidermal growth factor (human recombinant)
E_{linear}	elastic modulus in uniaxial tension
EPC	endothelial progenitor cell
ePTFE	expanded poly(tetrafluoroethylene)
FBS	fetal bovine serum

FITC	fluorescein isothiocyanate
F_{max}	maximum force
H&E	hematoxylin and eosin
HBSS	Hank's balanced salt solution
HS	heat-shrinkable
HCl	hydrochloric acid
ID	inner diameter
IGF-1	insulin-like growth factor 1 (human recombinant)
L_{hook}	hook separation distance
l_{seg}	scaffold segment length
min	minutes
MTT	3-(4,5-dimethylthiazol-2-yl)-2,5-diphenyltetrazolium bromide
n	number of samples
NGS	normal goat serum
OD	outer diameter
P_1	initial (low) pressure
P_2	target (high) pressure
PBS	phosphate buffered saline without calcium and magnesium
$PBS_{Ca/Mg}$	phosphate buffered saline with calcium and magnesium
PC	poly(carbonate)
PET	poly(ethylene terephthalate)
PGA	poly(glycolic acid)
PGS	poly(glycerol sebacate)
PLA	poly(lactic acid)
PLGA	poly(lactide-co-glycolide)

PTFE	poly(tetrafluoroethylene)
SEM	scanning electron microscopy
SMC	smooth muscle cell
TCPS	tissue culture-treated polystyrene
THF	tetrahydrofuran
TGF-β1	transforming growth factor β1
t_{min}	minimum wall thickness
TUNEL	terminal deoxynucleotidyl transferase dUTP nick end labeling
VEGF	vascular endothelial growth factor (human recombinant)
vWF	von Willebrand factor

LIST OF SYMBOLS

$\varepsilon_{\sigma(0.40)max}$	strain at 40% of the ultimate tensile stress
$\varepsilon_{\sigma(0.80)max}$	strain at 80% of the ultimate tensile stress
ε_{Tmax}	strain at ultimate tensile stress, or strain at failure
$\varepsilon_{C(0.50)max}$	strain at half of maximum compressive force
ε_{Cmax}	strain at maximum compressive force
μ	dynamic viscosity
σ_o	unstressed or zero-stress state
σ_{max}	ultimate tensile stress
τ	shear stress

SUMMARY

Compliance mismatch is a significant hurdle to long-term patency in small-diameter arterial bypass grafts. Vascular tissue engineering has the potential to produce compliant, non-thrombogenic small-diameter grafts. However, current engineered grafts are relatively non-compliant, leading to undesirable tissue remodeling such as intimal hyperplasia and resultant graft occlusion when subjected to arterial pressures. This study investigates the mechanical and biological properties of engineered vascular constructs based on a biodegradable synthetic elastomer, poly(glycerol sebacate) (PGS). Several methods for fabricating porous PGS scaffolds in a tubular geometry were developed and compared. Adult baboon vascular cells were cultured in the scaffolds *in vitro*, and the resultant engineered vessels were tested to determine their mechanical and biological properties.

An initial method was developed to create porous tubular scaffolds composed of PGS, a biodegradable elastomer with advantages over current benchmark biomaterials such as PLGA. Iterative improvements of the initial scaffold fabrication method significantly increased yield and decreased wall thickness while eliminating seams and maintaining high porosity. Culture of SMCs or coculture of SMCs and EPCs on type II and III scaffolds showed increases in cell quantity and ECM synthesis and deposition over time and led to constructs with high compliance compared to reports of other engineered blood vessels in the literature, demonstrating their potential for engineering blood vessels and other soft tissues with tubular structures. Further iterative improvements to scaffold fabrication retained high porosity and yield while significantly decreasing wall thickness, eliminating external seams, and improving handling and tolerances of mechanical properties. Culture on type V scaffolds decreased SMC culture time required to reach luminal confluence from 10 to less than seven days.

Doubling the initial quantity of SMCs seeded into type IV scaffolds shifted SMCs, and therefore collagen and elastin, to the abluminal rather than luminal surface of constructs. Constructs seeded with twice as many SMCs contained significantly more collagen and significantly less elastin. Type V constructs contained significantly more insoluble elastin and were significantly more compliant than type IV constructs, with type V construct compliance similar to baboon carotid arteries at low pressures. Decreasing SMC culture time in type V scaffolds from 21 to 10 days significantly decreased collagen and insoluble elastin content as well as soluble elastin synthesis, significantly increased compliance, and did not significantly affect burst pressure.

Altering type V scaffold material from PGS to PLGA did not affect yield, porosity, or SMC luminal confluence after 10 days of culture but did accelerate scaffold compaction. Degradation rates of PGS and PLGA scaffolds in culture medium without SMCs were not significantly different over 10 days. Both materials became significantly stiffer in transverse compression up to 50% strain as a result of 10-day SMC culture, but deformation mechanics were plastic in PLGA-based constructs and PLGA scaffolds in contrast to elastic and reversible deformation in porcine carotid arteries, PGS-based constructs, and PGS scaffolds. The compressive modulus of porcine carotid arteries and PGS-based constructs were significantly different but within the same order of magnitude, whereas the compressive modulus of PLGA-based constructs was an order of magnitude higher. Compliance and elastic recovery in porcine carotid arteries and PGS-based constructs were similar at low pressures. Altering type V scaffold material from PGS to PLGA significantly increased collagen content and significantly decreased insoluble elastin content without affecting soluble elastin synthesis. Insoluble elastin content in PLGA scaffolds did not differ significantly from uncultured PGS or PLGA scaffolds, indicating that PLGA may inhibit elastin crosslinking by SMCs.

Increasing hydrostatic pressure during SMC culture on type V scaffolds significantly increased collagen and insoluble content of constructs, soluble elastin

synthesis, and burst pressure but did not affect elastic recovery. Constructs cultured under increased hydrostatic pressure had significantly lower compliance than baboon carotid arteries, but their baseline hydrostatic pressure counterparts did not.

The iterative improvement of tubular porous PGS scaffolds and the development of methods for culturing adult vascular cells in these scaffolds provide tools for engineering tubular soft tissues. The systematic investigation of culture conditions, including initial cell seeding density, the type of scaffold used for culture, culture time, scaffold material, and hydrostatic pressure, provide insights into the control of engineered blood vessel properties. Overall, this work provides a foundation for PGS-based vascular tissue engineering.

CHAPTER 1

INTRODUCTION

Autologous vessels remain the only suitable source of grafts for small-diameter (<5 mm) arterial bypass procedures. More than one tenth of coronary artery bypass grafts (~50,000 grafts annually) occlude significantly within the first year.[1] Autologous vessels also negatively impact patient health by requiring multiple surgical procedures and the sacrifice of healthy tissue separate from the pathological site. Engineered grafts suitable for coronary bypass would provide a clinical alternative capable of reducing patient mortality, tissue morbidity, and demand for donor hearts. However, current engineered grafts are challenged by (1) thrombosis and (2) compliance mismatch, resulting in undesirable tissue remodeling and graft occlusion.

Tissue engineering combines cells and scaffolds and has the potential to produce compliant, non-thrombogenic small-diameter grafts. Early efforts indicate that cells and scaffolds can indeed be combined to engineer vascular tissues in a clinically relevant period of time for urgent clinical care.[2-4] There are numerous efforts to engineer blood vessels by incorporating vascular cells[5-8] or peripheral blood- or bone marrow-derived progenitor cells[3,9,10] with biodegradable non-compliant polymers,[6,9,11] biodegradable elastomers,[12-15] naturally-derived materials,[7,16-18] or sheets of *in vitro* cell-derived matrix.[5,19] The choice of scaffold material and the selection of one or more cell types with accompanying sources (or the decision to omit either scaffold or cells) are major considerations in vascular tissue engineering. Autologous cell sources are indicated as the best choice by early clinical successes, including progenitor cells[2] and adult cells.[20]

Tissue engineering has produced grafts with super-physiologic burst pressures and *in vivo* patency rates of ~80% at time points beyond three months (see Background: Tissue-engineered Vascular Grafts and Table 3.1). These results indicate that aneurysm

and thrombosis, challenges which cause graft failure in the short-term, are being overcome. However, tissue engineering has yet to produce a graft with physiologic compliance. Compliance mismatch causes intimal hyperplasia and is associated with graft failure in the long-term.[21-25] Elastomeric materials may provide a foundation for increased compliance and improvements in long-term patency in engineered vasculature.

The research presented in this dissertation investigates the mechanical and biological properties of engineered vascular constructs based on a biodegradable synthetic elastomer, poly(glycerol sebacate) (PGS). The unique, tunable properties of PGS and the potential role of elastomers in vascular tissue engineering motivated the development of a method to fabricate porous PGS scaffolds in a tubular geometry, with subsequent iterative revisions. Vascular cells were cultured in the scaffolds in a bioreactor providing pulsatile perfusion, and the resultant constructs were probed to determine their protein synthesis and content as well as various mechanical properties, including compliance. Scaffold material and stiffness are expected to be key determinants of construct mechanical properties and ECM synthesis and deposition by vascular cells. The influence of scaffold material was investigated by culturing vascular cells on scaffolds composed of PGS or PLGA having similar degradation rates. Finally, in an effort to increase construct burst pressure toward physiologic values, construct mechanical properties and protein synthesis and contents were compared under different culture conditions, including variations in cell seeding density, scaffold type on which the constructs were based, culture time, and hydrostatic pressure. These studies pursue two avenues of contribution to the field of biomedical engineering generally and tissue engineering specifically: (1) the generation of new methods for engineering tubular tissues; and (2) the formation of insights into PGS-based engineered vasculature.

CHAPTER 2

CENTRAL HYPOTHESIS AND SPECIFIC AIMS

The creation of a clinically successful engineered vascular graft requires compliance matching and incorporation of a robust and functional endothelium. The relationship between graft compliance and long-term patency in combination with the prevalence of coronary heart disease and the associated frequency of bypass procedures as a treatment mode motivated this work.

Central Hypothesis

The central hypothesis of this work is that grafts engineered from compliant poly(glycerol sebacate) scaffolds and adult vascular cells under biomimetic in vitro *culture conditions can possess compliance comparable to autologous vessels.*

Three specific aims were defined to address the central hypothesis.

Specific Aim 1

To develop a reproducible and scalable method for fabricating porous tubular PGS scaffolds with properties conducive to engineering tubular tissues.

A series of scaffold fabrication methods were developed and evaluated by qualitatively assessing scaffold handling characteristics and quantitatively comparing process yield and scaffold geometry, porosity, and mechanical properties. Cell-scaffold interactions were assessed for scaffolds fabricated using select methods. Coculture of SMCs and EPCs or culture of SMCs alone were each investigated. Results of the first three methods are presented in Chapter 5. Shortcomings of these methods necessitated

further iterative improvement, particularly reproducibility, scalability, handling, and geometry. In Chapter 6, two additional methods are presented for comparison to the previous methods, with a method sandwiching the scaffold between a glass tube coated with hyaluronic acid and an inner tube composed of heat-shrinkable material identified as superior on the basis of metrics. Culture of SMCs alone was investigated in the newer scaffolds.

Specific Aim 2

To compare tissue-engineered vascular constructs based on porous tubular scaffolds composed of PGS or PLGA cultured with adult baboon SMCs under identical conditions.

Scaffolds composed of compliant PGS or rigid PLGA were fabricated using the method identified as superior in Specific Aim 1 (see Chapters 5 and 6). Degradation characteristics of the PLGA were selected to match those of PGS. The scaffolds were evaluated separately under three different conditions: (1) culture with adult baboon arterial SMCs for 10 days; (2) degradation in culture medium for 10 days; or (3) uncultured and without degradation. Qualitative comparison of uncultured scaffolds, engineered constructs, and porcine carotid arteries (positive control) included gross construct morphology, SEM, and staining with H&E. Quantitative comparison included scaffold fabrication yield, scaffold porosity, mechanical properties, collagen content and insoluble elastin content of arteries and constructs, and soluble elastin concentration in culture medium. Results are presented in Chapter 10.

Specific Aim 3

To increase the load-bearing capacity of engineered vessels based on porous tubular PGS scaffolds by systematically investigating various tissue culture conditions.

Vascular constructs were created from PGS scaffolds cultured with adult baboon arterial SMCs. The effects of four independent variables were investigated separately in culture: (1) initial SMC seeding density; (2) scaffold type (comparison of scaffolds made using different fabrication methods); (3) culture length; or (4) hydrostatic pressure. Qualitative comparisons of uncultured scaffolds, engineered constructs, and baboon carotid arteries (positive control) included gross construct morphology, SEM, staining with H&E, and visualization of immunofluorescently-labeled collagens I and III. Quantitative comparison included mechanical properties of arteries and constructs, collagen content and insoluble elastin content, and soluble elastin concentration in culture medium. Results are presented in Chapters 7, 8, 9, and 11.

CHAPTER 3

BACKGROUND

Coronary Heart Disease and Vascular Grafts

Coronary heart disease is the leading cause of death in the U.S., with an estimated annual cost of more than $150 billion.[26] Approximately half-a-million (500,000) coronary artery bypass graft procedures and an even greater number of percutaneous arterial procedures (coronary angioplasty, stent revascularization, endarterectomy, etc.) are performed annually. Coronary artery bypass is associated with better outcomes compared to percutaneous procedures.[27] Only autologous vessels remain patent as bypass grafts, with 10 – 20% becoming significantly occlusive within the first year.[1] Autologous vessels that are routinely used as bypass grafts include the internal thoracic (also called the internal mammary), radial, and gastroepiploic arteries and the saphenous vein. The internal thoracic artery is the benchmark for coronary bypass, but its use is limited by issues of accessibility and length.[28] Saphenous vein grafts are easiest to access and have the least impact on tissue morbidity and patient health. However, saphenous vein grafts used for coronary bypass occlude at much higher rates (50% within 10 years) compared to arterial grafts,[29] underscoring the need to match the biological and mechanical properties of the specific artery being replaced. Complex biological responses caused by stress and hemodynamic changes regulate graft remodeling and stenosis and determine the degree of graft occlusion and intimal hyperplasia.

Artery Structure and Function

Arteries are composed of three layers with distinct cellular composition and physiological properties (Figure 3.1). The innermost *tunica intima* is composed of a

single layer of ECs which provide hemocompatibility. An underlying basement membrane provides functional support and a proteinaceous anchor for the endothelium, which is composed primarily of collagen IV, glycosaminoglycans, elastin, and laminin.[30,31] The *tunica media* contains concentric layers of SMCs that provide vasoresponsive function (vasodilation and vasoconstriction) and remodeling of the ECM according to physiological cues. The medial layer's ECM is composed of elastic protein fibers formed from collagens I and III, elastin, and proteoglycans and aligned circumferentially to aid the vessel in withstanding arterial pressure.[30,31] The primary load-bearing element of an artery is the *tunica media*. The outermost *tunica externa*, or *tunica adventitia*, is less dense and more closely resembles connective tissue in its cell and protein composition, with fibroblasts and collagens as its chief components. Elastin organized into functional elastic fibers and collagen III within the *tunica media* are the most significant contributors to vascular compliance.[32-34] Cell-cell communication between ECs, SMCs, and fibroblasts is vital to normal cell function and ECM synthesis in the arterial *tunicae* and therefore to normal artery structure and function.

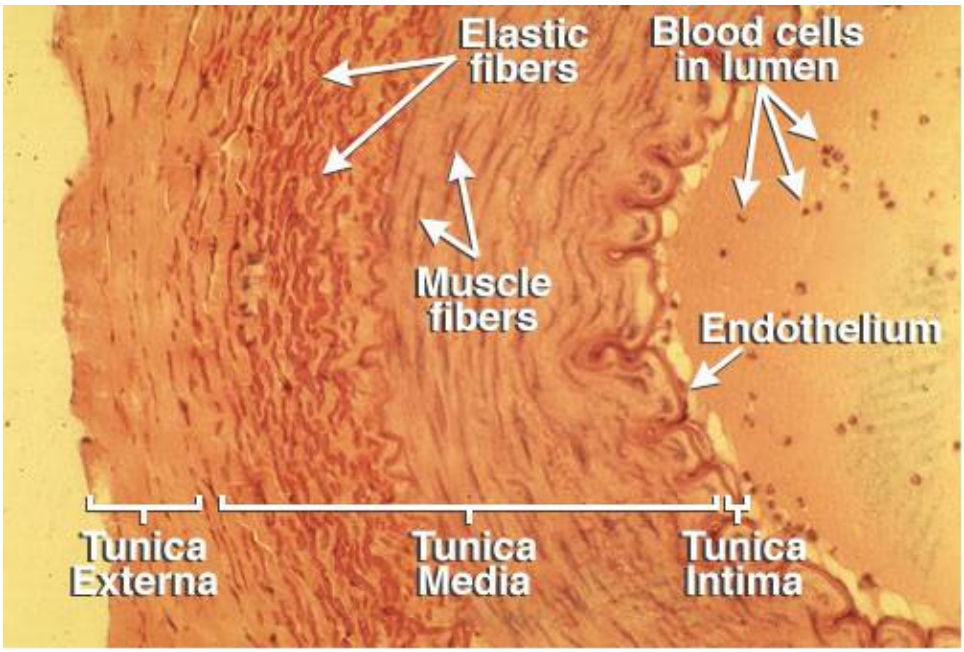

Figure 3.1: Small-diameter Artery Histology. Three distinct layers with distinct functions exist: the *tunicae intima*, *media*, and *externa*.[35]

Vascular Grafts

An extracorporeal source of small-diameter vascular grafts possessing physiologic compliance and antithrombogenicity would prevent the consumption of multiple native vessels when unfavorable remodeling occurs and would provide an alternative when autologous grafts are unavailable due to a patient's condition or other complications. Undesirable responses can be caused by compliance mismatch between the graft and adjoining artery, influencing a variety of flow and wall shear stress parameters.[36]

The Role of Compliance in Vascular Graft Outcomes

Compliance mismatch results in intimal hyperplasia at the downstream anastamosis.[22] It has been suggested that abnormal shear stress as a result of compliance

mismatch is the true cause of intimal hyperplasia.[25] The importance of compliance matching was first established by Abbott et al. using a canine model to investigate compliance.[21] Canine carotid artery autografts were treated with glutaraldehyde in a variable manner to differentially alter compliance and then implanted end-to-end with the femoral artery. Compliance of grafts and arteries were either matched (1:1) or mismatched (2:5), resulting in patencies of 85% or 37% at 90 days post-implantation, respectively. Occlusive arteries that were compliance-matched failed only after their counterpart and within 24 hours. Interestingly, Sonoda et al. achieved a patency rate similar to that of Abbot et al. (86%, also in canine common carotid) at 365 days post-implantation using biodegradable synthetic grafts with initial physiologic compliance.[37] Grafts were composed of an outer segmented poly(urethane) sleeve and an inner crosslinked gelatin tube and retained their original compliance at 30 days. Remodeling caused compliance mismatch at 90 and 180 days, but at 365 days compliance matching was restored following complete degradation of the poly(urethane) layer. Patency at other mid-points was not reported. These results indicate a role for compliance matching in vascular graft patency.

The effect of compliance mismatch on end-to-side grafting *in vivo* has been investigated using a femoropopliteal ovine model with constraint of the venous graft and/or artery by a PET mesh sleeve.[24] The thickness of intimal hyperplasia at regular intervals along the graft-artery conduit was not significantly affected by equivalent constraint of both the graft and artery by PET sleeves or by lack of constraint of both the graft and artery. However, constraint of the graft by PET while the artery remained unconstrained caused a significantly increase in the thickness of intimal hyperplasia along the lengths of the graft and artery.

In contrast to these studies, abluminal constraint of canine common iliac artery sections *in vivo* (simulating end-to-end anastamosis) suggests that compliance mismatch alone does not cause intimal hyperplasia.[38] However, there is evidence to suggest that

compliance mismatch may cause intimal hyperplasia indirectly. Shear stress increases significantly with compliance mismatch and may thereby directly affect intimal hyperplasia.[39] Flow irregularities at the downstream anastamosis influence protein transport and are likely to contribute to intimal hyperplasia by increasing residence time of particles such as chemotactic factors.[23,40] Compliance mismatch also increases suture line stresses at the junction of bypass grafts and native vessels, though this phenomenon can be alleviated by elliptical graft geometries.[41] It is unknown whether the elliptical geometry can be preserved over time as graft remodeling occurs.

The selection of venous or arterial grafts also influences patency by altering remodeling. Following implantation of bovine vessels into inbred rats for 28 days, excision, and *in vitro* testing, vein grafts released significantly higher concentrations of growth factors associated with intimal hyperplasia and atherosclerosis as well as mitogenic factors associated with higher cell proliferation compared to arterial grafts.[42] Intimal hyperplasia was observed in vein grafts but not in arterial grafts.

Non-autologous Vascular Grafts

Allografts and xenografts require ongoing medication or decellularization to prevent immune rejection. Their lack of cells contributes to undesirable graft remodeling and thrombogenicity, which ultimately lead to graft dilation and failure.[43] Synthetic vascular grafts are commonly based on PET or ePTFE. Large-diameter (>6 mm) synthetic grafts remain patent for extended periods but may still have associated inflammation and thromboembolism. Small-diameter (<5 mm) synthetic grafts exhibit severe thrombogenicity leading to occlusion.[44] Endothelialization of synthetic grafts can prevent thrombogenicity if the endothelium remains intact, but intimal hyperplasia caused by compliance mismatch still causes graft failure at more immediate time points than those of venous grafts[21,24,45]. Other long-term complications include foreign body reaction and infection caused by non-resorbable graft materials.[46]

Tissue-engineered Vascular Grafts

Traditional tissue engineering of vascular grafts combines vascular cells and a biologic or synthetic scaffold, typically incorporating only some of the elements found in native arteries. Examples of arterial element combinations include ECs and SMCs in a collagen-PET scaffold,[47] ECs and SMCs in a synthetic mesh made from PGA,[6,48,49] SMCs dispersed in tubular fibrin gel,[7,50-52] EPCs seeded on the lumen of decellularized xenogeneic arteries,[3] everted granulation tissue formed in the graft recipient's own peritoneal cavity,[4] and decellularized xenogeneic non-vascular tissue.[19] Elastogenesis has been relatively rare in tissue-engineered blood vessels, especially in adult SMCs.[33,53] Successes in vascular graft engineering are outlined in Table 3.1 and include physiologic burst pressure,[3-6,19] vasodilation and vasoconstrictive in response to various biological agents, [3,4,6,54,55] stable endothelium under physiologic shear stress,[3,7,56] endothelium production of vWF and prostacyclin,[47] co-expression of elastin and collagen by SMCs cultured in fibrin with insulin and TGF-β1 medium supplementation,[52] and *in vivo* patency of multiple weeks in various animal models,[3-6] with the notable exception being physiologic compliance (Table 3.1). Coordinate realization of many of these mechanical and biological features is the current challenge for engineered vascular grafts.

Table 3.1: Successes in Blood Vessel Tissue Engineering. See citations in text for references and additional details. Grafts from various investigative groups possess a biomimetic property only as indicated ("X"), and uninvestigated graft properties are differentially indicated ("?").

Investigator	**Kaushal et al.**	**Campbell et al.**	**L'Heureux et al.**	**Niklason et al.**	**Tranquillo et al.**
Graft Material	Decellularized Porcine Iliac Vessels	Peritoneal ECM (Derived *In Vivo*)	ECM & Cell Sheets (Derived *In Vitro*)	PGA	Fibrin Gel
Cell Source	Ovine	Rat or Rabbit	Human	Bovine or Porcine	Rat
Cell Type	EPC	Fibroblast, SMC, Mesothelial	Fibroblast, EC	SMC, EC	Neonatal SMC
↓ Biomimetic Property ↓					
Physiologic Burst Pressure	X	X	X	X	?
Response to Vasodilators	X	X	X	?	?
Response to Vasoconstrictors	X	X	X	X	?
Stable Endothelium Under Physiologic Shear Stress (~15 dynes/cm^2)	X		X	?	X
Elastin & Collagen Co-expressed	?	X			X
Physiologic Compliance	?	?			?
Animal Model	Ovine	Rat or Rabbit	Rat	Porcine	N/A
Position of *In Vivo* Testing	Carotid Artery	Descending Aorta or Carotid Artery	Aorta	Saphenous Artery	N/A
Duration of *In Vitro* Preparation (Days)	2	14	~200	56	42
Duration of *In Vivo* Patency (Days)	130+	120+	225	28+	?

Although tissue engineering has yet to produce a vascular graft with compliance similar to human arteries,[45] the results of vascular graft engineering do indicate that autologous graft properties are likely to be best mimicked by incorporating all major types of native cells and proteins. Physiologic burst pressure, suturability, and *in vivo* patency of 85% for up to 225 days in an immune-compromised animal model were demonstrated for grafts created by L'Heureux et al. from layered sheets of human fibroblasts, smooth muscle cells, and fibroblast-derived ECM with ECs seeded during the final week of culture,[5,56] and these vessels were then transitioned to clinical trials.[5,20] However, increasing the number of elements extended culture time to an impractical length exceeding four months. Engineered graft compliance in the 80-120 mmHg range ($1.5 \pm 0.3\%$, $n = 3$) was comparable to that of saphenous vein grafts (0.7 – 1.5%) but not internal thoracic and radial arteries (4.5 – 6.2%).[5] While elastin was detected in these constructs it was synthesized by fibroblasts in the adventitia-like layer rather than SMCs in the media-like layer and did not result in compliance comparable to autologous coronary artery grafts. The protein homology of the fibroblast-synthesized and SMC-synthesized elastin was not assessed.

Vascular Cell Behavior and Interactions

Smooth Muscle Cells

SMCs are known to respond to mechanical stimuli such as shear stress, cyclic stretch, and hydrostatic pressure. Arterial shear stress is inversely related to SMC proliferation,[57-59] and subjection to shear increases ECM synthesis by SMCs[58] although there is no relationship between shear stress magnitude and ECM synthesis rates by SMCs.[59] Cyclic stretch influences SMC and collagen fibril orientation, both being oriented parallel to the direction of stretch.[60] Cyclic stretch also increases synthesis of collagens I and III and some glycosaminoglycans such as hyaluronic acid and chondroitin

6-sulfate.[61] Cyclic stretch does not affect the proliferation of arterial SMCs but does increase the proliferative rate of venous SMCs.[62] The effect of cyclic stretch on SMC proliferation is also ligand-dependent; when cell adhesion is mediated by serum proteins such as fibronectin or vitronectin and cycled at 1.0 Hz[63] SMC proliferation increases, but when cell adhesion is mediated by elastin at 0.87 Hz[61] (interestingly, the culture used 10% serum) or by collagen or laminin at 1.0 Hz[63] SMC proliferation is unaffected. Coincidentally, substrate also influences ECM synthesis by SMCs without mechanical stimulation; culture on PGA favors elastin synthesis while culture on collagen I favors collagen synthesis.[64] This phenomenon may be related directly to ligand-mediated adhesion since vitronectin is the primary ligand adsorbed onto PGA while fibronectin and vitronectin both adsorb onto collagen I sponges.

Recently, hydrostatic pressure has been shown to influence three-dimensional (Boyden chamber) SMC migration, with pulsatile rather than steady hydrostatic pressure and higher pulse frequencies causing an increase in SMC migration.[65] Migration also increased when pulsatile hydrostatic pressure had a higher mean pressure or covered a wider pressure range at constant frequency. Pulsatile hydrostatic pressure is directly proportional to two-dimensional SMC proliferation,[66,67] though the phenomenon is frequency-dependent. Pulsing hydrostatic pressure at frequencies of 1.0 Hz[66] and 0.1 Hz[67] significantly increases SMC proliferation while a frequency of 0.02 Hz[67] does not. In contrasting studies, steady hydrostatic pressure has been shown to increase SMC rates of proliferation[66] and apoptosis[68] in monoculture, with the proliferative effect having greater weight and causing an overall increase in SMC quantities *in vitro*. A study using sections of rabbit pulmonary arteries and hydrostatic pressures of 12, 25, or 45 mmHg suggested that hydrostatic pressure does not affect SMC protein synthesis.[69] However, separate studies of porcine aortic valves suggest that SMC collagen synthesis is proportional to the magnitude of mean pulsatile hydrostatic pressure cycled at 1.17 Hz[70] and that SMC collagen synthesis increases under steady hydrostatic pressures of 140 or 170 mmHg but

not 100 mmHg[71]. Therefore, correlations between hydrostatic pressure and SMC protein synthesis may be dependent on species, location in the circulatory system, and magnitude of hydrostatic pressure.

Endothelial Cells

Like SMCs, ECs also respond to mechanical stimuli such as shear stress, cyclic stretch, and hydrostatic pressure. However, because SMCs synthesize the load-bearing constituents of the artery wall but proliferate at significantly lower rates in a heparan sulfate-mediated manner when cocultured with ECs,[72-74] vascular tissue engineering must rely on one of three strategies: (1) a period of SMC-only culture followed by coculture with ECs; (2) coculture of SMCs with ECs in the presence of matrix metalloproteinases[75] or antagonists against heparan sulfate;[72] or (3) coculture of SMCs with cells that differentiate into ECs after sufficient time for ECM synthesis and organization. Therefore, EC behavior and the effect of ECs on SMCs in coculture are both presented for consideration.

EC proliferation is shear stress-dependent, with peak proliferative rates around 5.0 dynes/cm^2 and complete cessation of proliferation at super-physiologic shear stress.[76] EC proliferation in monoculture is increased by cyclic stretch[77] and altered by pulsatile hydrostatic pressure at 1.0 Hz in a serum- and mean pressure-dependent manner, with lower mean pressure (~80 mmHg and lower) increasing proliferation and higher mean pressure (~135 mmHg) decreasing proliferation under 10% serum conditions.[78,79] ECs subjected to shear stress stimulate SMC migration by releasing chemotactic factors.[80] Coculture of ECs and SMCs under steady hydrostatic pressure in the physiologic range decreases SMC proliferation,[68] while coculture with or without hydrostatic pressure decreases EC proliferation.[81] Coculture with ECs also increases SMC rates of apoptosis, and this effect appears to be amplified by steady hydrostatic pressure.[68] Interestingly, these trends are likely to be dependent on tissue source, either arterial or veinous.[82]

Endothelial Progenitor Cells

EPCs are known to coordinate vasculogenesis and angiogenesis and can differentiate into both ECs and SMCs.[83-85] While ECs are known to inhibit SMC proliferation and ECM synthesis when confluent (forming a shear-protective layer), ECs are also known to attract SMCs and pericytes prior to confluence by secreting chemoattractant growth factors.[86-88] SMC behaviors such as increased proliferation and ECM synthesis are associated with pathologies such as restenosis and atherosclerosis *in vivo*.[89] EPCs therefore present the potential to form a confluent non-thrombogenic surface while encouraging non-pathologic SMC function in culture. These facts taken together suggest that EPCs and SMCs could be cocultured to create physiologic vascular tissue in an *in vitro* environment that mimics vasculogenesis.

Poly(glycerol sebacate) and Cardiovascular Tissue Engineering

PGS is synthesized from biocompatible monomers, glycerol and sebacic acid, and its elastic modulus and degradation rate can be controlled by altering monomer ratio, crosslink density, and polymer porosity.[90] The elastic modulus of PGS can be matched to that of myocardial tissue,[91] and its strain at failure resembles that of native arteries.[92] In contrast to PLGA, PGS swells only a few percent in water and is biodegraded completely without fibrous capsule formation or foreign body giant cell formation within 60 days of subcutaneous implantation.[93] Similar results showing acute (PGS) rather than chronic (PLGA) inflammation were obtained for intramuscular implantation.[94] PGS degrades *in vivo* primarily through surface erosion[93] via hydrolytic and enzymatic resorption modes, allowing it to retain shape and mechanical strength during degradation.

ECs, SMCs, and fibroblasts have been demonstrated to adhere to and proliferate on PGS surfaces *in vitro*,[95-98] and the phenotypic protein expression of primate SMCs is preserved during culture on PGS films.[99] Recent work has also demonstrated the ability of PGS to support co-expression of elastin and collagen by baboon SMCs in three-

dimensional *in vitro* culture with or without EPCs present, resulting in highly distensible pieces of engineered tissue.[95] *It is important to note that the presence of EPCs during SMC culture did not produce significant changes in the mechanical properties of the tissue.* In summary, the mechanical and biochemical properties of PGS are well-suited to cardiovascular tissue engineering applications.

CHAPTER 4

MATERIALS AND METHODS

Synthesis of Poly(glycerol sebacate)

Anhydrous glycerol was obtained from Lancaster Synthesis (Pelham, NH). Sebacic acid (EMD Chemicals, Gibbstown, NJ) was purified by dissolving 100 g in 2.0 liters of 95% ethanol at 55°C and immediately passing the solution through a 0.2 μm filter followed by incubation at 4°C for 72 hours to crystallize the sebacate and a second 0.2-μm filtration. The purification process was completed at least three times and the final crystallization was dried in a vacuum oven (Lindberg/Blue M, Asheville, NC) at 100 mTorr and 60°C overnight prior to sabacic acid use.

Short-chain pre-polymer was synthesized by polycondensation of equimolar amounts of glycerol and purified sebacic acid at 120°C under pure nitrogen (Airgas, Radnor, PA) until water production was no longer visible (20 to 26 hours, medium stir rate). Stirring was continued under vacuum (40 mTorr) until the stirring was significantly but not completely inhibited (72 to 96 hours, depending on pressure), with polymer chain length measured indirectly using a viscometer (Chemglass, Vineland, NJ) to aid in reproducibility.

Scaffold Fabrication

General Tubular Scaffold Fabrication Procedures

PGS pre-polymer or PLGA (5050 DLG 5E; Lakeshore Biomaterials, Birmingham, AL) was dissolved in THF (Fisher Scientific, Pittsburgh, PA) at a mass ratio of 1:5. Sodium chloride (EMD) was ground and sieved using a set of USA standard testing sieves purchased from VWR International (West Chester, PA) to select salt

particles with a size range of 75-90 or 75-150 μm. After addition to individual molds, the salt was fused into a template at 37°C and dried overnight in a vacuum oven at 100 mTorr.[100] PGS-THF or PLGA-THF solution was added in a fume hood at 4.0 mg polymer per mm salt template length, and THF was allowed to evaporate for at least one hour. The PGS was cured at 150°C and 100 mTorr for 24 hours, or the PLGA was placed overnight in a vacuum oven to remove all THF. A series of 2-3 water baths (~24 hours in first bath, >48 hours in subsequent baths) was used to dissolve the salt template. Individual scaffolds were obtained by cutting the tubes into 30-mm sections, with PLGA scaffolds being placed on a horizontal metal rod to allow one wall to be cut in compression without irreversibly compressing the entire scaffold. Scaffolds were lyophilized (Labconco, Kansas City, MO) and stored dry.

Scaffold Nomenclature

Scaffolds were designated sequentially according to their chronological order of development. Table 4.1 outlines scaffold nomenclature used throughout this work. In addition to sequential designations, mold dimensions and mold assembly clearances (space between the outer mold and the mandrel) are presented in Table 4.1 for comparison.

Table 4.1: Scaffold Nomenclature, Mold Dimensions, and Mold Assembly Clearances.

Scaffold Type	Outer Mold	Outer Mold ID (mm)	Mold Release Coating Material	Mandrel	Mandrel OD (mm)	Clearance (mm)
I	Bifurcated PTFE Mold	7.14	(None)	Paraffin	4.76	1.19
II	Bifurcated PTFE Mold	7.14	Lecithin Spray	PTFE Tubing	4.76	1.19
III	Bifurcated PTFE Mold	7.94	Lecithin Spray	Heat-shrinkable Poly(olefin)	5.28	1.33
IV	PTFE Tubing	7.94	Lecithin Spray	Heat-shrinkable Poly(olefin)	5.28	1.33
V	Glass Tubing	7.00	Hyaluronic Acid	Heat-shrinkable Poly(olefin)	5.28	0.86

Tubular Scaffold Fabrication Using Bifurcated Molds

Fabrication Using Bifurcated Molds and Paraffin Mandrels

(These scaffolds were designated as type I scaffolds.)

In-house molds with two mating halves were machined from PTFE rectangular stock (McMaster-Carr, Aurora, OH) to have two coaxial cylindrical recesses flanked by holes for inserting thumb screws and wing nuts to provide alignment (Figure 4.1). The smaller recess constrained a solid cylindrical mandrel made of paraffin wax (OD 4.76 mm; Acros Organics, Geel, Belgium) and the larger recess (ID 7.14 mm, length 60 mm) held salt particles. Paraffin mandrels were created by placing wax pellets into a funnel and melting them into silicone tubing (ID 4.76 mm; VWR) with one end plugged. The paraffin was allowed to solidify, the silicone was cut away (taking care not to remove paraffin), and the paraffin mandrel was rolled across a warm PTFE plate at ~65°C and cooled on a flat surface to ensure straightness. Each mold was assembled with a paraffin

mandrel and filled with salt (75-150 μm), after which the upper half of the mold was removed and the salt was reshaped with a spatula to correct disturbances caused by mold disassembly. The salt was fused for two hours at 95% humidity and dried at 20°C,[100] PGS-THF solution was added, and the THF was allowed to evaporate. Each mold was turned on end and the paraffin mandrel was melted out of the salt template's lumen at 75°C. The PGS was cured and the molds and scaffolds were immersed in two hexane baths in hexane (24 hours each) prior to salt leaching, sectioning, and lyophilization.

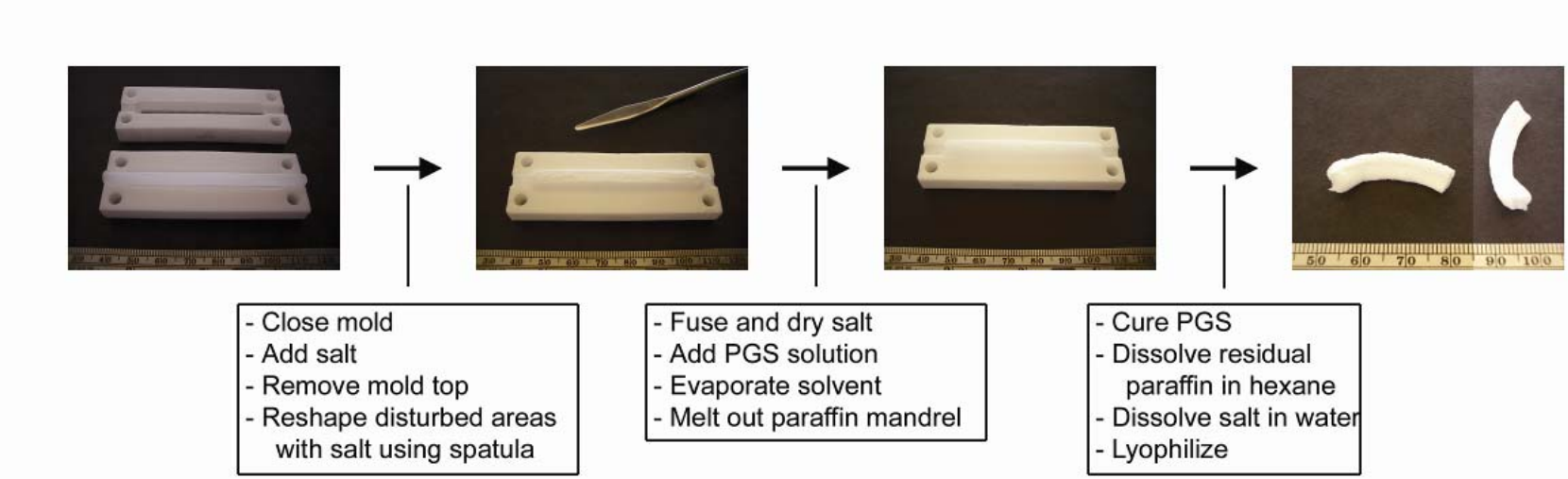

Figure 4.1: Scaffold Fabrication Using a Paraffin Mandrel. The outer PTFE mold was closed around a paraffin mandrel and filled with salt. The mold top was removed and areas of the salt disturbed by mold top removal were reshaped with a metal spatula. The salt was fused and dried into an interconnected salt template to which a PGS solution was added. After the solvent was evaporated, the paraffin mandrel was melted out of the template and the PGS was cured. The resultant PGS tube was placed in a hexane bath to dissolve residual paraffin, a water bath to dissolve salt, sectioned into 30-mm scaffolds, and lyophilized. Ruler divisions are 1.0 mm.

Fabrication Using Bifurcated Molds and Rigid Mandrels

(These scaffolds were designated as type II scaffolds.)

A second scaffold fabrication process was developed to eliminate the possibility of contamination from traces of wax or solvents with the intent of simultaneously increasing yield and reducing scaffold defects. The same set of PTFE molds was used in the second process, but with two coats of lecithin mold release (Diversified Brands, Cleveland, OH) on all salt-contacting mold surfaces to reduce salt adhesion. A stainless steel rod encased by PTFE tubing (OD 4.76 mm; McMaster-Carr) was used as the mandrel (Figure 4.2), around which salt particles (75-150 μm) were loaded. The upper half of each PTFE mold was retained during salt fusion for 6.5 hours at 88% humidity and drying at 60°C to reduce variations in salt template thickness. Unlike paraffin, the PTFE mandrels had sufficient strength and stiffness to remove the salt template from the PTFE mold halves after salt fusion and drying. Intact release of the salt template at this stage was improbable without lecithin mold release. Each PTFE mandrel and attached salt template were re-enclosed in the loosely-assembled, aligned mold halves so that the mandrel could be slid out of the salt template in the axial direction without disrupting the template or re-adhering it to the mold halves. Polymer addition and curing, salt leaching, sectioning, and lyophilization were completed with the same procedures used for type I scaffolds.

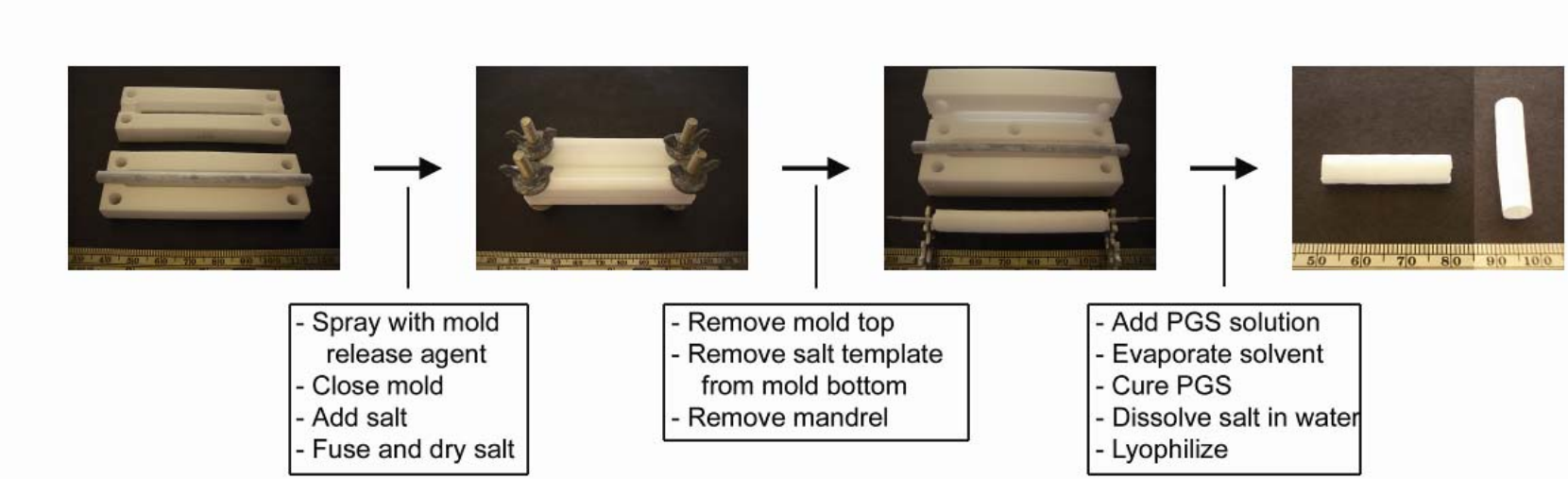

Figure 4.2: Scaffold Fabrication Using a Rigid Poly(tetrafluoroethylene) Mandrel. The PTFE mold was coated with lecithin mold release and closed around a mandrel made of PTFE tubing straightened by an internal steel rod. Salt was loaded into the mold, fused, and dried into an interconnected salt template. The mold top was removed and the PTFE mandrel was used to pull the salt template from the mold bottom. The template was returned to the mold and the PTFE mandrel was slid out. A PGS solution was added to the template, the solvent was evaporated, and the PGS was cured. The resultant PGS tube was placed in a water bath to dissolve salt, sectioned into 30-mm scaffolds, and lyophilized. Ruler divisions are 1.0 mm.

Fabrication Using Bifurcated Molds and Heat-shrinkable Mandrels

(These scaffolds were designated as type III scaffolds.)

A HS sleeve made of translucent food-grade acrylated poly(olefin) (OD 5.28 mm, ID 4.76 mm; McMaster-Carr) was placed around the mandrel used to create type II scaffolds with the intent of further reducing scaffold defects by reducing salt template disruption and adhesion to mandrels (Figure 4.3). New molds (upper and lower halves, ID 7.94 mm, length 60 mm) were designed to preserve salt recess width (1.33 mm for type III molds vs. 1.19 mm for type I/II molds), and therefore scaffold wall thickness, as closely as possible while accommodating the 0.5-mm increase in mandrel diameter. The new molds were machined from the same PTFE stock and with the same milling machine (Grizzly Industrial, Bellingham, WA) as the previous molds. The remainder of the type III scaffold fabrication process was similar to the type II fabrication process, including two coats of lecithin mold release. Two additional steps after drying the salt template were required to remove the HS sleeve from the salt template by shrinking it onto a metal rod at 120°C (≤ 5 min) and cool the salt template to 20°C before obtaining the final scaffold.

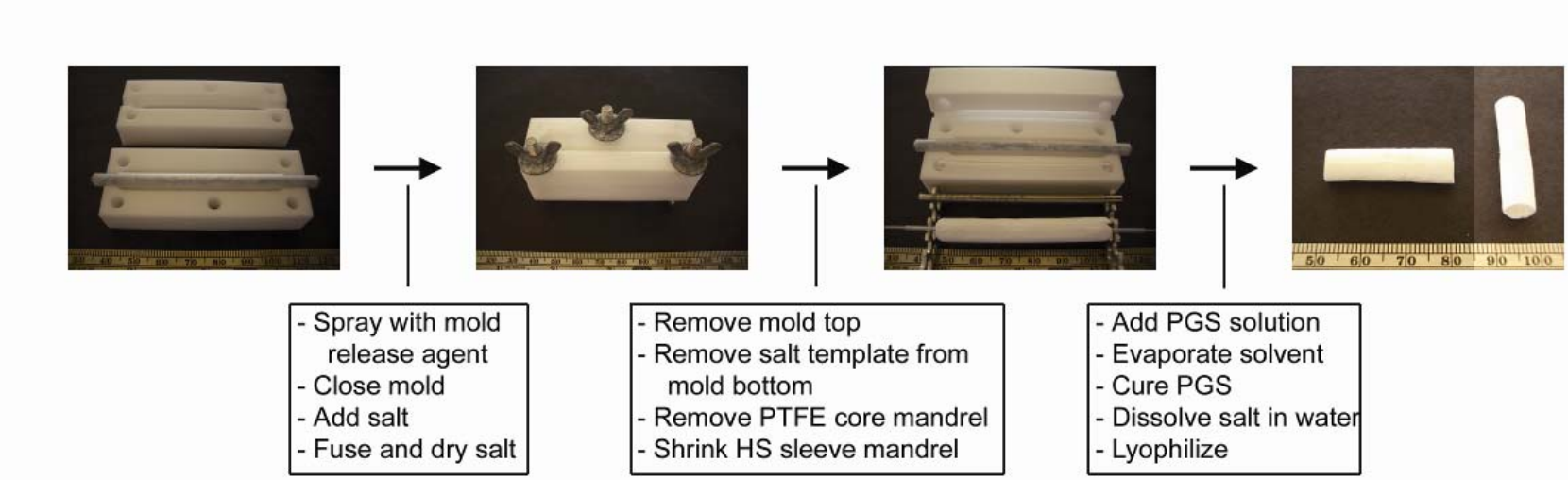

Figure 4.3: Scaffold Fabrication Using a Heat-shrinkable Mandrel. The PTFE mold was coated with lecithin mold release and closed around a heat-shrinkable mandrel over PTFE tubing straightened by an internal steel rod. Salt was loaded into the mold, fused, and dried into an interconnected salt template. The mold top was removed and the PTFE tubing and steel rod were used to pull the salt template from the mold bottom. The template was returned to the mold and the PTFE tubing and steel rod were slid out. The heat-shrinkable mandrel was removed from the inside of the salt template by heating at 120°C, and the salt template was cooled prior to PGS addition, solvent evaporation, and curing. The resultant PGS tube was placed in a water bath to dissolve salt, sectioned into 30-mm scaffolds, and lyophilized. Ruler divisions are 1.0 mm.

Tubular Scaffold Fabrication Using Tubular Molds

Fabrication Using Polymer Tubes and Heat-shrinkable Mandrels

(These scaffolds were designated as type IV scaffolds.)

Extruded PTFE tubing (OD 12.7 mm, ID 7.94 mm; McMaster-Carr) was cut into 90-mm lengths, effectively replacing the bifurcated molds while preserving outer mold diameter (Figure 4.4). The same PTFE mandrels and HS sleeves from type II and III molds were used for fabrication, with the addition of a single ring-shaped piece of extruded PTFE tubing (OD 7.94 mm, ID 4.76 mm, 1.0 mm length; McMaster-Carr) for spacing and concentricity between the outer tubular mold and the PTFE mandrel. Sections of the ring-shaped piece's outer diameter were cut away to provide ventilation without compromising alignment or spacing. Two coats of lecithin mold release were applied by spraying into the outer PTFE mold parallel to its axis. The mold assembly was held vertically with the spacer ring at its bottom, and the upper end of the mandrel was manually centered during salt loading. The salt was fused for 6.5 hours at 88% humidity and dried. The spacer ring was used to retain the HS sleeve and prevent its movement while pushing the PTFE mandrel out through the bottom of the assembly, thereby minimizing lateral forces exerted on the salt template. The HS sleeve was then shrunk at 120°C (~30 min) and the salt template cooled to 20°C before adding PGS-THF solution to the salt template's inner surface and curing. After 24 hours in the first water bath the scaffold freely slid inside the outer tubular mold. Sectioning and lyophilization were completed to obtain the final scaffold.

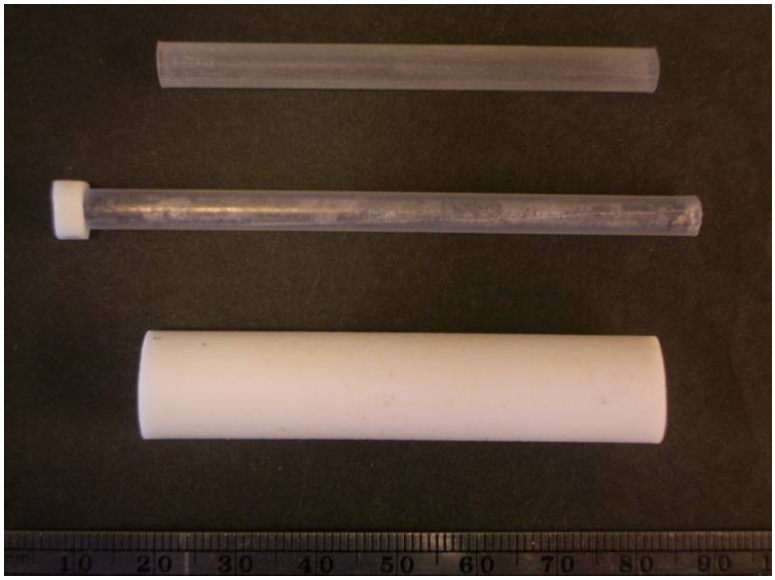

Figure 4.4: Materials for Scaffold Fabrication Using a Polymer Tube and a Heat-shrinkable Mandrel. The same mandrel from type III scaffold fabrication was used to fabricate type IV scaffolds, but with an outer tubular mold made of PTFE. The outer tubular PTFE mold was coated with lecithin mold release. A heat-shrinkable mandrel was placed over PTFE tubing straightened by an internal steel rod and inserted into the outer tubular PTFE mold. A PTFE ring served as a spacer and provided ventilation and alignment at one end of the mandrel. The mold was held vertical with the spacer at the bottom while salt was loaded, fused, and dried into an interconnected salt template. The PTFE tubing and steel rod were slid out through the spacer, leaving the heat-shrinkable mandrel in place. The heat-shrinkable mandrel was removed from the inside of the salt template by heating at 120°C, and the salt template was cooled prior to PGS addition, solvent evaporation, and curing. The outer tubular PTFE mold and resultant PGS tube were placed in a water bath to dissolve salt. After 24 hours in the water bath the PGS tube moved freely in the outer tubular PTFE mold and was removed to a second water bath. The PGS tube was sectioned into 30-mm scaffolds and lyophilized. Ruler divisions are 1.0 mm.

Fabrication Using Glass Tubes and Heat-shrinkable Mandrels

(These scaffolds were designated as type V scaffolds.)

Glass tubing (OD 9.0 mm, wall thickness 1.0 mm; Small Parts, Miramar, FL) was cut into 70-mm lengths and used in place of tubular PTFE outer molds (Figure 4.5). The

same PTFE mandrels and HS sleeves from previous molds were used, as well as modified PTFE spacers similar to the spacers used for ventilation, alignment, and spacing in type IV molds. In lieu of lecithin mold release, the glass tubes were coated with 1.0% hyaluronic acid, which was dried overnight at 37°C and 100 mTorr. The mold assembly was held vertically with the spacer ring at its bottom, and the upper end of the mandrel was manually centered during salt loading. The salt was fused for 20 min at 88% humidity and dried. (The significant reduction in salt fusion time required to produce cohesive but unsaturated salt templates was likely a result of increased moisture sequestering by the thin coating of hyaluronic acid during fusion.) The remainder of the type V scaffold fabrication process using glass molds was similar to the type IV scaffold fabrication process.

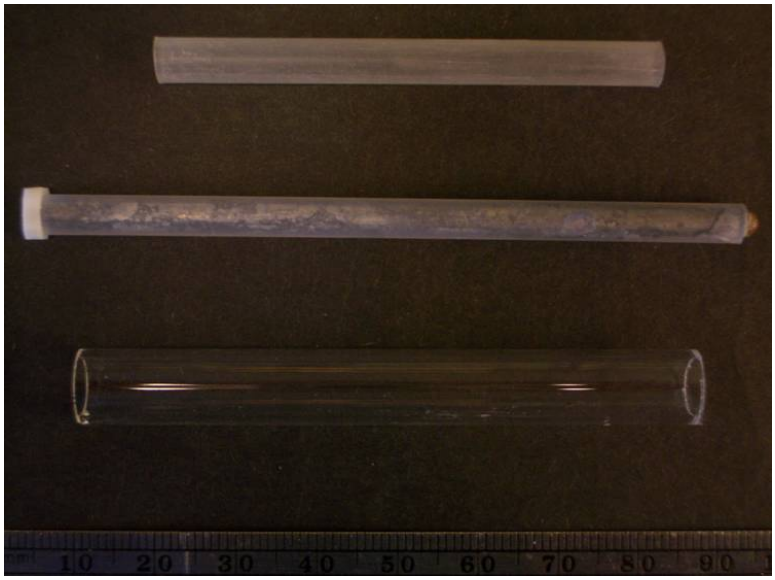

Figure 4.5: Materials for Scaffold Fabrication Using a Glass Tube and a Heat-shrinkable Mandrel. The same mandrel from type III and IV scaffold fabrication was used to fabricate type V scaffolds, but with an outer tubular mold made of glass. The outer tubular glass mold was coated with 1.0% hyaluronic acid and dried overnight. A heat-shrinkable mandrel was placed over PTFE tubing straightened by an internal steel rod and inserted into the outer tubular glass mold. A PTFE ring similar to those used for type IV scaffold fabrication served as a spacer and provided ventilation and alignment at one end of the mandrel. The mold was held vertical with the spacer at the bottom while salt was loaded, fused, and dried into an interconnected salt template. The PTFE tubing and steel rod were slid out through the spacer, leaving the heat-shrinkable mandrel in place. The heat-shrinkable mandrel was removed from the inside of the salt template by heating at 120°C, and the salt template was cooled prior to PGS addition, solvent evaporation, and curing. The outer tubular glass mold and resultant PGS tube were placed in a water bath to dissolve salt. After 24 hours in the water bath the PGS tube moved freely in the outer tubular glass mold and was removed to a second water bath. The PGS tube was sectioned into 30-mm scaffolds and lyophilized. Ruler divisions are 1.0 mm.

Evaluation of Scaffolds

Overall Process Yields and Scaffold Physical Properties

Overall Yields

Overall yields of the various scaffold fabrication methods were determined by recording quantities of usable and unusable scaffolds created from each process. A usable scaffold was free of through-cracks and holes along its entire length (30 mm). Scaffold wall thickness homogeneity was compared macroscopically by sectioning whole scaffolds at 5-mm intervals along their entire length and measuring segment wall thicknesses in digital images captured with a CCD Monochrome Video Camera (model CS8420i; Tokyo Electronic Industry Company, Tokyo, Japan) using Matrox Inspector 8.0 imaging software (Matrox Electronic Systems, Dorval, Quebec). The mean and standard deviation of each segment's wall thickness were calculated from measurements at eight evenly-spaced intervals around the segment's circumference. The minimum wall thickness was recorded at the thinnest of all locations, not including defect sites that did not span the entire segment length (0.5 mm).

Scaffold Geometry, Microstructure, and Porosity

Detailed inspections of wall cross-sections and luminal microstructure were completed on randomly-selected scaffold segments using SEM. Scaffold samples were attached to aluminum mounts with carbon tape, sputter-coated with gold (~35 nm thickness) using a Polaron SC7640 High Resolution Sputter Coater (Quorum Technologies, Newhaven, United Kingdom), and observed with a Leo 1550 SEM (5-20 kV). Porosity was calculated using an ethanol displacement method previously described.[101] Although techniques such as mercury porosimetry and flow porosimetry are expected to be more accurate,[102] these techniques were not used for scaffold evaluation due to the fragile nature of the scaffolds. Ethanol rather than water submersion was used

to reduce air bubble retention by scaffold pores.[102,103] A graduated cylinder (maximum volume 10.0 ml) was filled with an initial volume of ethanol (V_1), the scaffold was submerged in the ethanol and briefly compressed to eliminate any residual air bubbles (V_2), the scaffold was removed, and the remaining volume of ethanol was measured (V_3). Porosity (P) was defined as the ratio of the volume of the scaffold's pores to its total volume using the following equation: $P = (V_1-V_3)/(V_2- V_3)$. Porosity in two 5.0-mm scaffold segments was measured by micro-computed tomography and showed reasonable agreement with ethanol submersion results, but micro-computed tomography was not used to evaluate porosity due to resolution (voxel size of 6.0 μm was only one order of magnitude smaller than porogen size of 75-90 μm prior to shrinkage during salt fusion) and prohibitive time and cost requirements.

Scaffold Degradation

Scaffolds were cut into segments (length ~5 mm) and placed in pre-weighed microcentrifuge tubes (2.0 ml; Eppendorf, Westbury, NY). Scaffold segments were sterilized by steam autoclaving for PGS (15 min) or ethylene oxide gas for PLGA (>48 hours of subsequent outgassing) and weighed. Culture medium was added to each tube (2.00 ml) and the tubes were rotated horizontally in a hybridization chamber (Model 1000; Robbins Scientific Corp., Sunnyvale, CA) at 2.0 rpm for 10 days. The ratio of surface area to volume for degraded scaffolds segments was identical to the ratio of surface area to volume for scaffolds in culture, both being 79 mm^2/ml (scaffold segments: mean length of 5.0 mm, mean surface area of 160 mm^2, and medium volume of 2.00 ml, compared to scaffolds in culture: mean length of 30 mm, mean surface area of 940 mm^2, and culture chamber volume of 12 ml). After transverse compression testing scaffolds were returned to their tubes, frozen, lyophilized, and re-weighed. Pre-weighed microcentrifuge tubes containing culture medium only were likewise frozen, lyophilized, and re-weighed to determine the change in mass contributed by lyophilized medium.

Mechanical Properties of Scaffolds

Uniaxial Tensile Testing of Scaffolds

Three scaffolds from each fabrication method were sectioned into 5-mm-long segments, and three, four, or five segments from each scaffold were tested to failure under uniaxial tension (0.20 mm/s) after soaking for 24 hours in PBS. All segments were tested on an Instron 5842 Materials Testing System (Instron Corporation, Canton, MA) using a 5 N load cell (type 2530-439), Merlin 5.30 software, and identical hooks with known D_{hook} separated by a variable L_{hook}. Force-extension and video data (collected with Matrox Inspector 8.0) were correlated to determine mechanical properties for individual scaffold segments. Measurements of l_{seg} prior to testing and t_{min} in the first video frame (at σ_o) were used to determine wall cross-sectional area. Cracks and voids were ignored in measuring t_{min} if they did not span l_{seg} entirely. σ_{max} was calculated as F_{max} held by the scaffold segment's walls per unit of wall cross-sectional area using the following equation: $\sigma_{max} = F_{max}/(2t_{min}l_{seg})$. When a segment was not fully stretched, A_{lumen} and $A_{\sigma 0}$ were calculated as the area of an ellipse using measurements of the semi-major and semi-minor axes (designated a and b, respectively) from the following equation: A_{lumen} or $A_{\sigma 0} = \pi(a+b)(1+3h/\{10+\sqrt{(4-3h)}\}$, where $h = \{(a-b)/(a+b)\}^2$ and $b > \sim 0.002a$.[104] $A_{\sigma max}$ for a fully-stretched segment was calculated as the sum of the rectangular and two half-circular areas encompassed by the lumen using D_{hook} and L_{hook} according to the following equation: $A_{\sigma max} = (D_{hook})(L_{hook})(\pi/4)(D_{hook})^2$. ε_{Tmax} was calculated from the σ_{max} and σ_o states according to the following equation: $\varepsilon_{Tmax} = (A_{\sigma max} - A_{\sigma 0})/ A_{\sigma 0}$. Intermediate strain values were also calculated by normalizing to the unstressed state. E_{linear} was calculated for the linear stress-strain region of 40-80% σ_{max} (Figure 4.6) and was defined as the ratio of the change in stress to the change in strain according to the following equation: $E_{linear} = (0.80\sigma_{max}-0.40\sigma_{max})/(\varepsilon_{\sigma(0.80)max}-\varepsilon_{\sigma(0.40)max})$.

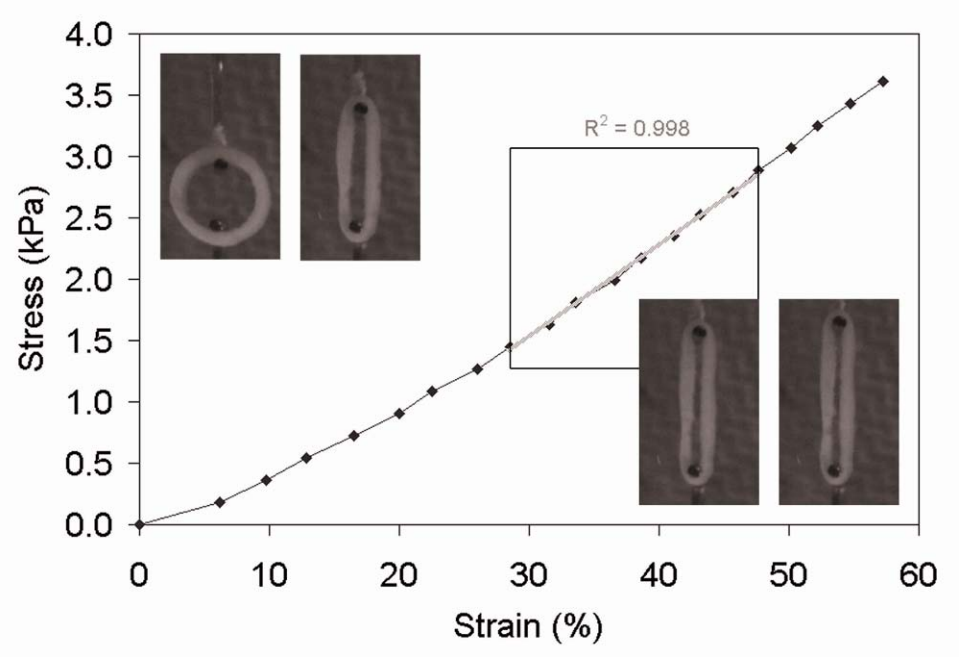

Figure 4.6: Scaffold Stress-strain Behavior. Stress-strain behavior is shown during a representative uniaxial tensile test, with video frame insets showing the tested scaffold segment's geometry at 0%, 40%, 80%, and 100% of σ_{max}. Each plot's linear region spanning 40-80% σ_{max} (boxed area) was used to calculate E_{linear}. All stress-strain data plots were linear ($R^2 \geq 0.95$) in the 40-80% σ_{max} region.

Transverse Compression Testing of Scaffolds

Three type V scaffolds composed of either PGS or PLGA were sectioned into 5-mm-long segments, and at least three segments from each scaffold were tested to failure in transverse compression (compression in a single axis perpendicular to the construct/segment axis at 0.0167 mm/s) after soaking for 24 hours in PBS. Degraded scaffold segments were already wetted and were therefore not soaked prior to testing. Each segment was tested with its axis horizontal on a Synergie 100 Testing System (MTS Systems Corporation, Eden Prairie, MN) using a 50 N load cell and compression platen (1.00 mm separation distance for all segments). Scaffold segments were pre-cycled to 5% strain until load stabilized, which was 0.02-0.07 N for all segments. Five compression

cycles to 50% strain were completed in rapid succession and the segments were photographed to determine A_C. Photographs were analyzed with Photoshop Elements 6.0 (Adobe Systems Incorporated, San Jose, CA) and A_C was determined by using the quick selection tool (brush size 50 pixels) to select once at the center of each segment's image and record the uncached pixel count. F_{max} for the second, third, and fourth compression cycles were taken directly from the raw data, as were ε_{Cmax} and $\varepsilon_{C(0.50)max}$ at F_{max} and 50% of F_{max}, respectively. E_c for the segment was taken as the mean of E_c for cycles 2-4, which was calculated according to the following equation: $E_c = (F_{max}-0.50F_{max})/\{A_C(\varepsilon_{Cmax}-\varepsilon_{C(0.50)max})\}$.

Cell and Tissue Culture

Bioreactor Design

First-generation Bioreactor Design

A simple pulsatile perfusion bioreactor was designed for culturing vascular cells on tubular porous PGS scaffolds *in vitro*. The bioreactor included a Masterflex L/S pump (model 77301-22; Cole-Parmer Instrument Company, Vernon Hills, IL) beside a base plate with four medium reservoirs mounted on top, with eight flow circuits comprised of longer lengths of silicone tubing continuous with coiled silicone tubing (gas-permeable) for gas exchange, scaffold-containing chambers with shorter tubing assemblies that could be detached from the bulk of each circuit, and a shorter length of silicone tubing (Figure 4.7). The base plate was made from PC (thickness 6.35-mm; McMaster-Carr) sized to fit beside the pump in a standard CO_2 incubator. Bioreactor components were held in position using stainless steel slotted spring pins (OD 6.35 mm, length 25.4 mm, alloy 316; McMaster-Carr) inserted into holes (ID 6.35 mm) drilled in the base plate. Reservoirs were 1000 ml Erlenmeyer flasks (VWR) with 24/40 stoppers (VWR), each drilled with four ~3.18-mm-ID holes. Each reservoir was connected to the inlet and outlet

of two circuits, with the circuit inlets extending to the reservoir bottom and the circuit outlets protruding ~50 mm past the stopper within the reservoir.

Figure 4.7: First-generation Bioreactor with Pulsatile Perfusion. Reservoirs, gas exchange coils, and the pump head can be seen on the incubator's upper shelf. Scaffolds and chambers were placed below to maximize low-level hydrostatic pressure.

Starting at the reservoir, the flow of medium entered each flow circuit through PTFE tubing (OD 4.0 mm, ID 2.0 mm, length ~250 mm; McMaster-Carr) and passed into platinum-cured silicone tubing (ID 3.18 mm, OD 6.35 mm; VWR). The medium then passed through a peristaltic pump interface consisting of 3.18-to-1.59-mm barbed PC reducing coupling (McMaster-Carr), wear-resistant platinum-cured silicone tubing for use with peristaltic pumps (ID 1.0 mm; Dow Corning, Midland, MI), a second reducing coupling connected to silicone tubing, a third reducing coupling, wear-resistant platinum-cured silicone tubing for use with peristaltic pumps (ID 1.6 mm; Dow Corning, Midland, MI), and a fourth reducing coupling connected to silicone tubing. When low flow rates were required the first section of wear-resistant tubing (ID 1.0 mm) was placed in the pump cartridges, and when higher flow rates were required the second section of wear-resistant tubing (ID 3.1 mm) interfaced with the pump. Desired flow rates were calculated based on desired shear stress in the scaffold lumen and calculated according to Poiseuille's Law: $\tau = (4\mu Q)/(\pi r^3)$, where μ was taken at 37°C, Q was the experimentally determined volumetric flow rate, and r was taken as the initial scaffold ID, nominally 0.5 mm. Based on Poiseuille's Law, the shear stress could be varied from 1.1 dynes/cm^2 at the minimum possible flow rate (~1.0 ml/min) to 15 dynes/cm^2 at a flow rate of ~14 ml/min. The pump interface was followed by silicone tubing (length ~1.0 m) coiled around PTFE or PC tubes (OD ~ 30 mm, ID ~25 mm, length ~ 200 mm; McMaster-Carr) which served as a gas exchanger, and a 3.18-to-3.18-mm barbed PC tubing coupling (McMaster-Carr) connected to the remainder of the flow circuit.

The next portion of the flow circuit was the detachable scaffold-chamber circuit, which could be closed to form a fully-isolated and independent loop to allow removal from sterile environments (Figure 4.8). The detachable circuit began with a short segment of silicone tubing (length ~40 mm) and a PC wye tubing connector (all connections 3.18 mm; McMaster-Carr) which separated flow into two lengths of silicone tubing for luminal and abluminal flow (lengths ~100 and ~150 mm, respectively). Luminal flow

proceeded into PTFE tubing (ID 2.0 mm, OD 4.0 mm, length ~180 mm; McMaster-Carr) which penetrated a stopper (size 0; VWR) through a drilled hole (ID ~3.18-mm) to enter the scaffold chamber and attached to the proximal end of the scaffold. A second segment of PTFE tubing (length ~50 mm) attached the scaffold's distal end exited the chamber by passing through an opposing drilled stopper and connecting to silicone tubing (length ~80 mm) to rejoin common flow at a second wye connector.

Figure 4.8: Detachable Scaffold-chamber Circuit. The culture chamber and scaffold could be isolated by clamping proximal and distal tubing and closing the ends in an independent circuit while the bioreactor was in a sterile environment, allowing transport through non-sterile environments.

Abluminal flow passed into and out of the scaffold chamber through a 20G1-1/2" blunt-end needle (VWR) attached to a 3.18-mm-to-Luer-Lock barbed PC tubing connector, with a distal segment of silicone tubing (length ~50 mm) connected to the second wye connector. A pre-formed hole for the 20G needle was made in each stopper by passing a sharp 20G needle through the stopper parallel to stopper's PTFE tubing while the stopper and tubing were inserted into the chamber end. This design allowed each chamber to have independent luminal and abluminal flow, enabling flow to be routed through the scaffold lumen or through the scaffold wall through the application of clamps the exterior of the tubing (Figure 4.9, bottom and top, respectively). Chambers were constructed from PC tubes (OD 15.9 mm, ID 9.53 mm, length ~90 mm; McMaster-Carr) threaded at each end with a 5/8"NF-18 die and fitted with center-drilled (ID 9.53 mm) stainless steel pipe end caps (3/8" NPT, alloy 316; McMaster-Carr) to prevent leakage and stopper ejection at high pressures. silicone tubing (length ~500 mm) and a tubing coupling returned flow to the bulk of the bioreactor circuit. The bioreactor circuit concluded with silicone tubing attached to the reservoir by the PTFE tubing circuit outlet.

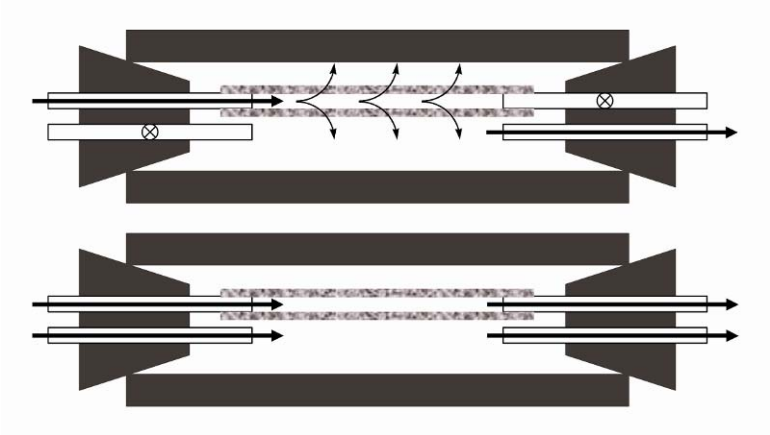

Figure 4.9: Diagram of Flow Schemes Used During Scaffold Preparation, Cell Seeding, and Cell Culture in the Bioreactor. (Top) Through-wall flow: luminal inlet and abluminal outlet are open; luminal outlet and abluminal inlet are closed. Flow is forced through the wall of the porous tubular PGS scaffold. (Bottom) Luminal and abluminal flow: luminal inlet and outlet and abluminal inlet and outlet are open. Figure not to scale.

The entire bioreactor could be repeatedly sterilized by opening the flow circuits and steam autoclaving at 120°C for 30 min. Sterility between uses was aided by immediately flushing with bleach twice, soaking all internal and external surfaces in bleach for no more than 24 hours, flushing with water twice, soaking all internal and external surfaces in water for at least 24 hours, and flushing as much water as possible from the system followed by partial disassembly and air drying. All parts were inspected between uses and replaced as necessary. Needles were tested for blockage before each use and replaced regularly since they were more susceptible to corrosion by bleach.

Second-generation Bioreactor Design

A new bioreactor was built by modifying the initial design to incorporate hydrostatic pressure and reduce part count and assembly time by using a common flow circuit with manifolds to accommodate multiple scaffold chambers (Figure 4.10). A

needle valve (part 4A-V4LN-SS; Parker) was placed downstream from the scaffold chambers, and downstream and upstream pressure transducers (part PM/4; Living Systems, Burlington, VT) monitored real-time pressure. The transducers were calibrated using a mercury manometer (part P/MM; Living Systems) prior to each use. The second-generation bioreactor used the same Masterflex L/S pump with a like-sized aluminum base plate (thickness 6.35-mm; McMaster-Carr) to avoid cracks and wear after extensive use. Bioreactor components were constrained by slotted spring pins inserted into holes in the base plate as before. Up to four detachable scaffold-chamber circuits identical to those of the first-generation bioreactor could be cultured simultaneously (see Figure 4.8).

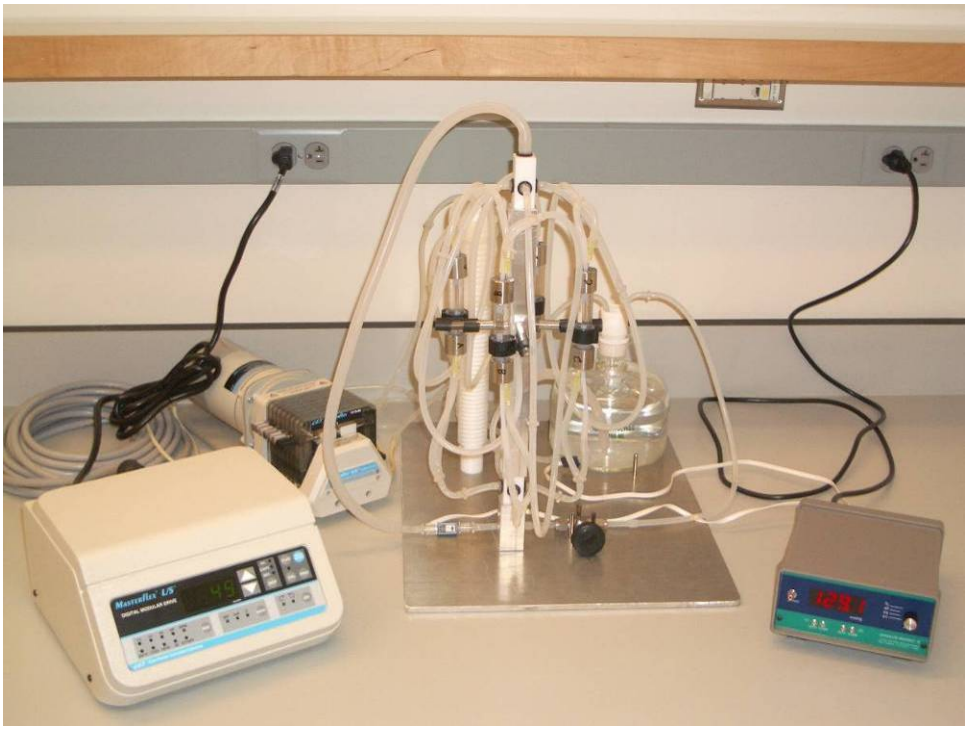

Figure 4.10: Second-generation Bioreactor Incorporating Hydrostatic Pressure. A modification of the earlier bioreactor used a needle valve downstream from the scaffold chambers to increase hydrostatic pressure, which was simultaneously monitored at locations upstream and downstream from the chambers. The flow scheme was revised to

allow culture of up to four scaffolds at the same time on a shared circuit with a single reservoir.

The reservoir was a custom-made 1000 ml flask (OD 140 mm, height 150 mm; Chemglass) which allowed entry and exit from a standard biosafety cabinet without requiring the sash to be drawn above the limit for maintenance of sterility. The reservoir was fitted with a 29/42 stopper (VWR) breached by two ~3.18-mm-ID holes for the circuit inlet and outlet. The flow circuit included similar lengths of platinum-cured silicone tubing split into two pump interface segments followed by two coiled sections of silicone tubing (length ~2.0 m) for gas exchange. The pump interface used 1.6-mm and 3.1-mm wear-resistant platinum-cured silicone tubing for use with peristaltic pumps (Dow Corning) with couplings and reducing couplings as appropriate to provide a range of flow rates and accommodate higher flow rates required by a single flow circuit. Based on Poiseuille's Law (see First-generation Bioreactor Design), the shear stress could be varied from 1.1 dynes/cm^2 at the minimum possible flow rate (~4.0 ml/min) to 15 dynes/cm^2 at a flow rate of ~55 ml/min. Each gas exchange coil included 1.0 m of silicone tubing identical to the first-generation bioreactor gas exchanger followed by 1.0 m of thin-walled platinum-cured silicone tubing (ID 3.18 mm, OD 4.76 mm; Small Parts).

Flow from the gas exchange coils was reunited and passed through the upstream pressure transducer flanked by 3.18-mm-to-Luer-Lock barbed PC tubing connectors. Flow continued through a 3.18-to-6.35-mm reducing coupling (McMaster-Carr) and platinum-cured silicone tubing (ID 6.35 mm, OD 9.53 mm; VWR) into the lower manifold through the detachable scaffold-chamber circuits, and into the upper manifold. The manifolds were machined in-house from 19.05 mm PTFE square bar stock with similar but not identical dimensions. Positioned as used, the non-identical dimensions of each manifold were its height (79.4 mm for lower manifold, 66.8 mm for upper manifold) and the depth of its initial vertical cavity (ID 7.94 mm, centered) extending down from the upper surface (depth 25.4 mm for lower manifold, 12.7 mm for upper manifold).

These dimensions were varied to especially encourage uniform flow in the lower manifold prior to division of the flow into the four detachable circuits.

The upper portion of the initial vertical cavity was threaded with a tap (3/8”-27 NPT) and fitted with a 6.35-mm-to-1/8” NPT barbed tubing connector (McMaster-Carr). A horizontal plane orthogonal to and intersecting the bottom of the initial vertical cavity was used as a datum reference for the remainder of the machining. A narrower continuation of the cavity (ID 6.35 mm, depth 28.6 mm) was machined with a ball end mill to the mill’s maximum depth (~13 mm) and completed with a drill bit. This was the only portion of the machining not completed using a ball end mill. One hole (ID 6.35 mm) was centered on each side of the manifold perpendicular to its vertical recess with its center 15.9 mm below the datum plane. Each side hole was threaded with a tap (5/16”-27 NPT) and fitted with a 3.18-mm-to-1/16” NPT barbed tubing connector (McMaster-Carr).

Pieces of aluminum square tube (width 25.4 mm, wall thickness 6.35 mm; McMaster-Carr) were used as spacers between the base plate and the lower manifold (height ~50 mm) and between the lower and upper manifolds (height ~300 mm). The aluminum spacer between the manifolds also supported bracket clamps (McMaster-Carr) holding the scaffold chambers vertically with flow directed upward. The detachable circuits were unaltered from their initial design. The upper manifold was connected to 6.35-mm-ID silicone tubing which extended to the base plate, where it joined with a reducing coupling and 3.18-mm-ID silicone tubing. Flow then passed through the downstream pressure transducer, again flanked by Luer Lock tubing connectors, through the needle valve, flanked by stainless steel tubing (ID 3.86 mm, OD 6.35 mm, length ~38 mm; McMaster-Carr) and returned to the reservoir.

The entire bioreactor could be repeatedly sterilized by steam autoclaving at 120°C for 30 min with the exception of the pressure transducers and removable needle valve knob, which required ethylene oxide gas sterilization and reassembly in a biosafety hood.

Other cleaning, sterilization, and maintenance procedures followed those of the first-generation bioreactor.

Scaffold Attachment to the Bioreactor

Attachment of Compliant Poly(glycerol sebacate) Scaffolds

Each scaffold made of PGS was attached to the luminal tubing in its chamber using poly(olefin) HS bands (red, 2:1 shrink ratio, prior to shrinking: ID 6.35 mm and cut to length ~1.0 mm; McMaster-Carr). The proximal (longer) section of 4.0-mm-OD PTFE tubing was pushed through its stopper until it protruded at least 4 mm from the opposite end of the PC chamber. The proximal stopper was then pushed firmly into the chamber. The proximal end of the scaffold was fitted with one HS band and slipped over the PTFE tubing. The assembly was heated at 120°C until the band no longer changed dimensions (~30 min) and then cooled. The proximal PTFE tubing was slid back through the stopper, taking care not to abrade the attached scaffold against the chamber wall, until the scaffold protruded ~4 mm from the chamber.

The distal end of the scaffold was fitted with one HS band and slipped over the distal (shorter) section of 4.0-mm-OD PTFE tubing. The assembly was again heated at 120°C to shrink the second band (~30 min), taking care to minimize forces applied to the scaffold by the assembly during transport and heating. The cooled assembly was placed on the bench, and the proximal stopper was held between the thumb and forefinger of the non-dominant hand while the remaining fingers of this hand secured the chamber against the bench. The dominant hand gripped the proximal PTFE tubing securely and held it stationary while the non-dominant hand exerted force on the proximal stopper and slid it, in brief, short movements, along the proximal PTFE tubing until the distal stopper contacted the chamber. (This required a smooth bench top surface.) The assembly could then be lifted and the distal stopper pushed firmly into the chamber, taking care to

minimize compression of the scaffold by adjusting the sections of PTFE tubing relative to their stoppers. The scaffold was likewise centered within the chamber and each stainless steel end cap was placed over its stopper in turn. As the end cap initially contacted its stopper a 20G blunt-end needle was passed through its pre-formed hole. Tightening of the end cap caused the stopper to compress and twist, requiring adjustment of the proximal and distal PTFE tubing in turn and careful monitoring of the scaffold. Once fully tightened the end caps were reversed until the 20G needles were parallel to the PTFE tubing (~1/4 turn). The remainder of the detachable scaffold-chamber circuit assembly was attached to facilitate ease of handling and preservation of sterility subsequent to autoclaving.

Attachment of Rigid Poly(lactide-co-glycolide) Scaffolds

Each scaffold made of PLGA was attached to the luminal tubing in its chamber using short bands of 3.18-mm-ID silicone tubing fitted over the proximal (longer) and distal (shorter) sections of 4.0-mm-OD PTFE tubing and positioned 1.0 mm from the sections' interior ends. (PLGA could not be attached using HS bands because its melting point is typically less than 100°C, whereas the HS bands require 100°C for shrinking.) The proximal PTFE tubing, band, and stopper were inserted into the chamber at their desired final position, the proximal stopper was pushed firmly into place, and the chamber was held vertically. The scaffold was lowered into the chamber delicately with forceps until it fit over the proximal PTFE tubing and contacted the silicone band.

The position of the distal stopper on its PTFE tubing was arranged so that the silicone band would just contact the scaffold when the stopper was fully inserted. The distal tubing, band, and stopper were inserted into the chamber, taking care to minimize forces exerted on the scaffold to avoid irreversible compression of the PLGA scaffold. The proximal and distal PTFE tubing and silicone sleeves were adjusted to center and securely hold the scaffold without causing it to buckle. Each stainless steel end cap was

placed over its stopper in turn. As the end cap initially contacted its stopper a 20G blunt-end needle was passed through its pre-formed hole. Tightening of the end cap caused the stopper to compress and twist, requiring adjustment of the proximal and distal PTFE tubing in turn and careful monitoring of the scaffold. Once fully tightened the end caps were reversed until the 20G needles were parallel to the PTFE tubing (~1/4 turn). The remainder of the detachable scaffold-chamber circuit assembly was attached to facilitate ease of handling and preservation of sterility subsequent to autoclaving.

Cell Source and Culture

Adult arterial SMCs and EPCs were isolated from the carotid arteries of juvenile male baboons (*Papio anubis*) and characterized prior to passaging and seeding.[105] SMC medium contained MCDB 131 medium (Mediatech, Inc., Herndon, VA) with 10% irradiated FBS (lot 01113030; Lonza, Walkersville, MD), 1.0% L-glutamine (Mediatech), and 50 μg/ml ascorbic acid (Sigma-Aldrich, St. Louis, MO). SMC medium employed 20 μg/ml gentamicin sulfate (Mediatech) or 100 IU/ml penicillin, 100 μg/ml streptomycin, and 0.25 μg/ml amphotericin B (Mediatech) as antibiotics and antimycotics. EPC medium was gentamicin-containing SMC medium supplemented with 0.002 μg/ml bFGF (Invitrogen Co., Carlsbad, CA), 0.01 μg/ml EGF (Invitrogen), 0.002 μg/ml IGF-1 (Invitrogen), 0.001 μg/ml VEGF (Invitrogen), and 1.0 μg/ml hydrocortisone (Sigma-Aldrich). Coculture medium was gentamicin-containing SMC medium supplemented with 0.002 μg/ml bFGF and 0.005 μg/ml EGF.

SMCs and EPCs were passaged separately in TCPS Petri dishes with 10 ml medium at 37°C and 5% CO_2. Cells were trypsinized, collected, centrifuged, resuspended, and replated according to standard cell culture procedures. A single passage was typically three days (range of two to four days) for SMCs and four days (range of three to six days) for EPCs. Cells were cryopreserved in 10% DMSO and culture medium

and immersed in liquid nitrogen for long-term storage. SMCs at passage 9 and EPCs at passage 18 tested negative for mycoplasma (MycoAlert; Lonza).

Cell Seeding

In preparation for cell seeding, scaffolds were sterilized by steam autoclaving (for PGS, 15 min) or ethylene oxide gas (for PLGA, >48 hours of subsequent outgassing following a 24-hour gas purge cycle) and pretreated. Briefly, scaffolds enclosed in bioreactor chambers were sterilized and then perfused at the minimum flow rate with 70% ethanol for 1 hour, 50% ethanol for 1 hour, 25% ethanol for 1 hour, and PBS (Mediatech) for 2 hours to remove any unreacted monomers and oligomers and residual salt prior to cell seeding. Scaffolds were then conditioned with culture medium for 2 hours. During no less than five minutes of perfusion with each pretreatment fluid, flow was forced through the scaffold wall by clamping the luminal tubing outlet (see Figure 4.8, top).

Each scaffold and chamber was detached from their flow circuit, and SMCs (passage 4-9) were seeded in the scaffold lumen by injecting a cell suspension containing 2.0×10^6 SMCs per cm^2 of luminal surface area (nominal ID 5.0 mm). The optimum cell seeding density was determined in previous experiments[95] using a hemacytometer to quantify cells washed out of the scaffold during seeding. The cell suspension volume was matched to 80% of the scaffold's luminal volume (nominal ID 5.0 mm) to ensure that the cells were completely contained within the lumen. During injection the 1-ml syringe holding the cell suspension was held vertical with its port down and the chamber was held vertical with its proximal end down, with the silicone tubing between them curved at 180°, taking care to avoid kinking. If the cell suspension overflowed the scaffold lumen the distal luminal tubing was clamped and the excess cell suspension was slowly filtered through the scaffold walls. The seeded scaffolds were oriented horizontally and rotated in a hybridization chamber at 2.0 rpm for 4 hours (Figure 4.11). Reservoirs with medium

used for scaffold conditioning were exchanged for reservoirs with fresh medium (125 ml per scaffold on the reservoir's flow circuit). The scaffolds and chambers were reattached to their flow circuits and perfusion was resumed at the minimum flow rate by either allowing medium to flow freely through the lumen (luminal flow) or by clamping the distal luminal tubing and forcing flow through the scaffold walls (through-wall flow, with the scaffold essentially serving as a filter for the cells) for 15 min (with one experimental group receiving through-wall perfusion for 240 min) followed by luminal flow.

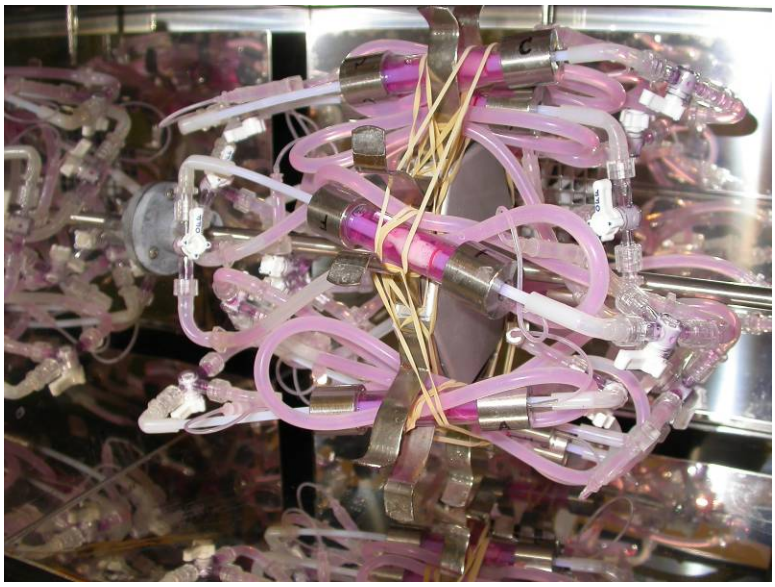

Figure 4.11: Rotation of Scaffold Chambers. Scaffold chambers were rotated in a heated hybridization chambers for four hours immediately following scaffold seeding by luminal injection of an SMC suspension.

Scaffolds and chambers receiving EPCs were seeded subsequently by detachment from their flow circuit, and EPCs (passage 11-18) were seeded in the scaffold lumen by

injecting a cell suspension containing 2.0×10^6 EPCs per cm^2 of luminal surface area (nominal ID 5.0 mm) in the same manner as the SMC suspension. The seeded scaffolds were oriented horizontally and rotated in a hybridization chamber at 2.0 rpm for 4 hours, reattached to their flow circuits, and reperfused without through-wall flow.

Culture of Engineered Constructs

Sterile surgical gloves were used to exchange medium every seventh day of culture. One alternate reservoir for each reservoir in use was capped with two layers of aluminum foil, autoclaved, and moved into a biosafety hood to fully cool beforehand. Medium was prepared no more than 48 hours in advance and 125 ml medium was added to each cooled reservoir per scaffold on the reservoir's flow circuit. Care was taken to maintain the sterility of the foil caps and reservoirs were recapped after medium addition. Flow circuit pump interfaces were detached from pump cartridges and the entire bioreactor was removed from the incubator, sprayed thoroughly with 70% ethanol, and moved into the biosafety hood containing the alternate reservoirs. Stopper edges were folded up and loosened from reservoir necks, and each stopper with its inlet and outlet tubing was carefully removed from the current reservoir and inserted into the reservoir containing new medium. Extreme care was taken to avoid contact between inlet and outlet tubing and any other surface. Additional ascorbic acid (6.25 mg in PBS) was injected into each medium reservoir three days and five days after each medium exchange.

The flow rate was steadily increased during the course of culture by no more than 1.0 ml/min per day to gradually increase shear stress inside each scaffold. In the first-generation bioreactor, baseline hydrostatic pressure was 10 mmHg (± 5 mmHg due to pulsatile perfusion) throughout the culture period. In the second-generation bioreactor, hydrostatic pressure was steadily increased from an initial mean value of 60 mmHg (± 10 mmHg due to pulsatile perfusion) to 120 mmHg by day seven (± 20 mmHg due to

pulsatile perfusion and increased flow rates). At the conclusion of the tissue culture period the detachable scaffold-chamber circuits were removed from the bioreactor and the constructs (cultured scaffolds) isolated by reversing the scaffold attachment process, taking care not to damage the construct during removal. Compaction during culture often caused the construct to pull away from the chamber inlet or outlet, making construct removal easier. If construct detachment occurred at either end the direction of flow through the chamber circuit could be reversed easily, ensuring that the proximal end of the construct was always attached to the upstream luminal tubing to guarantee the desired level of shear stress. Irregular flow patterns and shear were also maintained in the case of construct detachment by progressively pushing luminal tubing ends further into the chamber to eliminate the gap between the tubing and the end of the construct, taking care not to push the portion of the luminal tubing outside the chamber far enough to expose it to media. Longitudinal construct compaction was typically ~10% of the scaffold length.

Potential Sources of Contamination

Contamination by bacteria and/or fungus was a major concern during tissue culture and was attributed to a variety of causes. Initial sterility could be lost by seeding with a contaminated cell suspension if any of the Petri dishes from which cells were collected were contaminated. Inadequate bleaching of the bioreactor after use or inadequate aluminum foil coverage during autoclaving could also compromise initial sterility. Contact between ***any*** internal bioreactor surface exposed to medium during culture and ***any*** external "sterile" surface such as gloves, biosafety hood surfaces, autoclaved flask exteriors, and similar surfaces could result in contamination. This was especially pertinent during cell seeding or medium exchange. Disintegration of connector and coupling walls caused by residual bleach or repeated autoclaving without careful monitoring also contributed to contamination (Figure 4.12). Repeated contamination of entire sets of constructs was caused by sterile-packaged three-way valves as supplied for

clinical use, with more than two dozen (three sets of eight) constructs contaminated at intermediate time points due to these valves (see Figures 4.7 and 4.11, with white valve handles and stems visible at ends of chambers). Extreme care was necessary to ensure repeatability by avoiding potential sources of contamination.

Figure 4.12: Disintegration of Connector and Coupling Walls. Walls of connectors and couplings disintegrated over time, possibly due to residual bleach or repeated autoclaving. Regular inspection and periodic replacement were necessary to avoid contamination due to connector and coupling disintegration. Ruler divisions are 1.6 mm.

Evaluation of Engineered Vascular Constructs

Positive Controls

Porcine Carotid Arteries

The left and right common carotid arteries of Large White/Yorkshire pigs (~30 kg, *Sus scrofa domestica*) were excised immediately following anesthesia (ketamine and xylazine) and euthanasia (pentobarbital). Artery lengths prior to and following excision were noted. Each artery was rinsed in HBSS (Mediatech) and the *tunica adventitia* was removed using scissors and a scalpel, leaving the *tunica media* and *tunica intima* intact. Artery segments at different distances from the aorta were used so that a range of compliance representative of the baboon common carotid artery could be used for comparison.

Baboon Carotid Arteries

The left and right common carotid arteries of baboons (~15 kg, ~5 years old, *Papio anubis*) were excised immediately following anesthesia and euthanasia. Each artery and any attached tissue were rinsed in HBSS and shipped overnight at 4°C in 200 IU/ml penicillin, 200 µg/ml streptomycin, and 0.50 µg/ml amphotericin B. Upon receipt the artery and attached tissue were rinsed a second time and excess tissue and the *tunica adventitia* were removed using scissors and a scalpel, leaving the *tunica media* and *tunica intima* intact. Artery segments at different distances from the aorta were used so that a range of compliance representative of the baboon common carotid artery could be used for comparison.

Cell-scaffold Interactions

Cell Seeding Efficiency

Cell seeding efficiency was compared for two perfusion methods. In the first method, flow was routed solely through the scaffold wall for 240 min at 2.0 ml/min (see Figure 4.8, top). Flow was then routed through the scaffold lumen for an additional 12 hours at 2.0 ml/min (see Figure 4.8, bottom) before removing the scaffolds from the bioreactor to assess seeding efficiency. In the second method, flow was routed through the scaffold lumen for 20 hours at 2.0 ml/min (see Figure 4.8, bottom) before assessing seeding efficiency.

A crystal violet solution for staining cell nuclei was prepared with 0.1 M citric acid (Mallinckrodt Baker, Inc., Phillipsburg, NJ) and 0.1 % crystal violet (Fisher) in deionized water.[106] Each scaffold was removed from the bioreactor, cut into 1-2 mm segments, and chopped into finer pieces with scissors. Scaffold pieces were transferred to a 15-ml centrifuge tube, and the dish was rinsed twice with filtered crystal violet solution (~10 ml followed by ~5 ml), which were transferred to the tube. Each tube was vortexed for five min to free as many cell nuclei as possible from the scaffold and then incubated at 37°C. Tubes were vortexed for an additional five min before determining the concentration of stained SMC nuclei using a hemacytometer. Incubation at 37°C continued until cell nuclei concentration stabilized for the solution ($\geq$ 48 h) and repeated compression of the largest scaffold fragments with forceps appeared to release no cell nuclei while observed under a microscope. Cell nuclei appeared oval and translucent, while microscopic fragments of stained scaffold had irregular morphologies and were opaque. The concentrations of SMC nuclei were multiplied by the respective total volume of each tube to quantify cells retained by each scaffold.

Chronological Quantification of Live Cells

Type III scaffolds were seeded with SMCs and removed from the bioreactor (initial design) after six, eight, or 10 days of culture and longitudinally divided. One half of the scaffold was processed for assessment of cellular confluence (see next section: Cellular Confluence) and the other half was processed the same as scaffolds used in assessing cell seeding efficiency (see Cell Seeding Efficiency), with vortex times up to 15 min because of increased cell adhesion and quantities. Crystal violet-stained SMC nuclei were quantified using a hemacytometer. The rate of change in cell quantity over time (r) was calculated by assuming the mean seeding efficiency (e) for the through-wall perfusion seeding method and using the following equation to comparing the ratio of seeded cells (Q_S) to live cells at each discrete time point (Q_T) in each scaffold: $r = \{Q_T/(eQ_S)\}^{1/t}$, where r is the rate of change in cell quantity over time, Q_T is the quantity of live cells at a discrete point in time, e is the mean seeding efficiency, Q_S is the quantity of seeded cells, and t is time. For comparison, SMCs (passage 5-9) were statically cultured on TCPS for six to eight days (two passages). Rates of change in cell quantity over time for static SMCs were calculated in the same manner with an assumed cryopreservation viability of 95% substituted for the mean seeding efficiency.

Cellular Confluence

To investigate the length of culture time required and to demonstrate cellular confluence, constructs (cultured scaffolds) were removed from the bioreactor after various lengths of culture and sectioned to expose their luminal surface and wall cross-section. Samples were rinsed in PBS (×3) and fixed overnight with 2.5 % glutaraldehyde in PBS (4°C, ≥ 14 hours). After rinsing in $PBS_{Ca/Mg}$ (×3) and distilled water (×1), constructs were dehydrated in a series of histology-grade acetone baths (20 min each at 25%, 30%, 50%, 70%, 80%, 90%, and 100% ×3). Substitution of acetone with liquid CO_2 was completed using a critical point dryer (Quorum Technologies). Dried samples were

attached to aluminum mounts with carbon tape, sputter-coated with gold (~35 nm thickness), and observed with a Leo 1550 SEM (5-20 kV). Cellular confluence on scaffold luminal surfaces and cell incorporation into the scaffolds were assessed qualitatively.

Gross Construct Morphology

Visual Observations

The macroscopic appearance of engineered vessels and porcine and baboon carotid arteries were compared qualitatively, including color, shape, and handling characteristics.

Histology

Construct segments (length 2-5 mm) were rinsed gently with PBS and embedded in Tissue-Tek Optimal Cutting Temperature (OCT) Compound (Sakura Finetek USA, Torrance, CA) for cryosectioning. Segments were cut in cross-section at a thickness of 8 μm. Cryosections were stained with hematoxylin and eosin using a Leica Autostainer XL (Leica Microsystems, Bannockburn, IL), cover-slipped, and imaged at 4X using a Nikon TE-2000U inverted microscope equipped with a 4-megapixel Diagnostics Spot Flex digital camera (Nikon Corporation, Tokyo, Japan).

Mechanical Properties of Engineered Constructs

Transverse Compression Testing of Construct Segments

Type V scaffolds composed of either PGS or PLGA were cultured with baboon vascular SMCs for 21 days. Upon termination of culture the constructs (cultured scaffolds) were sectioned into segments (length 3-5 mm depending on scaffold compaction), and at least three segments from each construct were tested to failure in transverse compression (compression in a single axis perpendicular to the construct /

segment axis at 0.0167 mm/s). Porcine carotid arteries and uncultured type V scaffolds composed of PGS or PLGA were similarly segmented (lengths ~5 mm) and tested. Each segment was tested with its axis horizontal on a Synergie 100 Testing System using a 50 N load cell and compression platen. Tissue segments were pre-loaded to 0.02 N, causing platen separation distances to vary (0.85-1.02 for porcine carotid arteries, 0.93-2.30 mm for PGS-based constructs, and 2.63-3.91 mm for PLGA-based constructs). Five compression cycles to 50% strain were completed in rapid succession and the segments were photographed to determine A_C. Photographs were analyzed with Photoshop Elements 6.0 and A_C was determined by using the quick selection tool (brush size 50 pixels) to select once at the center of each segment's image and record the uncached pixel count, which was then converted to mm^2. Porcine carotid artery segments recovered to a cylindrical geometry after testing, and A_C for artery segments was therefore multiplied by a correctional factor of $\pi/2$. Elastic recovery by vessel segments was determined by comparing force-extension curves and F_{max} for each five-cycle compression series. Values of F_{max} for comparison of cycles and calculations of E_c were taken directly from the raw data, as were ε_{Cmax} and $\varepsilon_{C(0.50)max}$ at F_{max} and 50% of F_{max}, respectively. E_c for the segment was taken as the mean of E_c for cycles 2-4, which were calculated according to the following equation: $E_c = (F_{max}\text{-}0.50F_{max})/\{A_C(\varepsilon_{Cmax}\text{-}\varepsilon_{C(0.50)max})\}$.

Pressure-diameter Testing of Whole Constructs

The entire length of engineered constructs and porcine and baboon carotid arteries of similar length (~3 cm) were measured prior to testing. Artery or construct ends were attached to glass cannulae connected to a flow circuit, and the artery or construct was submerged in and perfused with DMEM (Mediatech) until all air bubbles were purged from the circuit and then stretched to 120% of its length prior to attachment. The internal pressure of the circuit was cycled between zero and a target pressure, which was incrementally increased by 5 or 10 mmHg after three complete cycles. The circuit's

pressure was increased at a rate of ~60 mmHg/min and decreased at a rate of ~40 mmHg/min. Two pressure transducers measured and recorded pressure at a frequency of 0.25-1.0 Hertz. The diameter of the artery or construct was observed via light microscopy and a video camera, with images of the external diameter recorded and the diameter measured at the same time points and frequency as the pressure. Dynamic pressure control and data collection were performed using LabVIEW (National Instruments, Austin, TX).

Pressure-diameter data were used to determine burst pressure, elastic recovery, and compliance of engineered vessels and elastic recovery and compliance of carotid arteries up to the maximum pressure of the system (200 mmHg). Irregular cross-sectional geometries required that diameter be calculated along a portion of the vessel length rather than at a single point. Agreement between length-averaged and single-point mean diameter was excellent for control arteries and generally good for engineered vessels, with a few poor matches for engineered vessels. Compliance was proportional to the change in diameter over a given pressure range and was defined as the inverse of Peterson's elastic modulus[107] according to the following equation: $C = \{(D_2-D_1)/D_1\}/(P_2-P_1)$, where C is compliance. Failure modes of engineered vessels were noted by inspection after burst.

Extracellular Matrix Synthesis in Engineered Constructs

Collagen Content

Immunofluorescence

Primary and secondary antibodies were selected to allow coordinate imaging of collagens I and III in each individual tissue section. Primary antibodies were mouse monoclonal anti-collagen III (catalog # MAB3392; Millipore Corporation, Billerica, MA) and rabbit polyclonal anti-collagen I (catalog # AB745; Millipore) and were diluted 1:50

in 1% NGS (Sigma-Aldrich). Secondary antibodies were Rhodamine-conjugated goat polyclonal anti-mouse IgG (catalog # 12-509; Millipore) and FITC-conjugated goat polyclonal anti-rabbit IgG catalog # 12-507; Millipore) and were diluted 1:200 in 1% NGS. Nuclei were stained using VectaShield mounting medium containing DAPI (catalog # H-1200; Vector Laboratories, Burlingame, CA). Cryosections of tissues and scaffolds were rinsed twice with PBS, incubated with 5% NGS for 60 min at 37°C, incubated with primary antibodies in 1% NGS for 45 min at 37°C, and rinsed twice with PBS. Without exposure to light, cryosections were incubated with secondary antibodies in 1% NGS for 45 min at 37°C, rinsed twice with PBS, rinsed once with dH_2O, and received 3-4 drops of VectaShield mounting medium before cover-slipping. Cryosections were imaged immediately at 10X using a Nikon TE-2000U inverted microscope equipped with a 4-megapixel Diagnostics Spot Flex digital camera, and images were compared qualitatively.

Colorimetric Analysis of Collagen Content

Tissue samples were evaluated for hydroxyproline content similar to previously reported methods.[108,109] Assay buffer with a pH of 7.0 was prepared by combining citric acid (2.5g; Acros), glacial acetic acid (0.6 ml; EMD), sodium acetate (6.0 g; Acros), sodium hydroxide (1.7 g; EMD), and dH_2O to bring the total volume to 50.0 ml. The majority of the assay buffer (40.0 ml) was used to make a chloramine T solution containing chloramine T (705 mg; TCI America, Portland, OR), isopropanol (5.0 ml; VWR), and dH_2O (5.0 ml). An aldehyde-perchloric solution was prepared by combining p-dimethylaminobenzaldehyde (7.5 g; TCI) isopropanol (31.0 ml), and 60% perchloric acid (13.0 ml). A hydroxyproline standard was made by dissolving L-hydroxyproline (100 µg; TCI) in 1.0 ml of HCl (1.0 N, diluted from 12 N; EMD).

Construct and scaffold segments (length 3-5 mm) were cut into pieces no larger than 1.0 mm, placed in pre-weighed 2.0-ml microcentrifuge tubes and wet weight was

recorded. In a fume hood, 800 µl of CNBr (100mg/ml; Acros Organics, Geel, Belgium) fully dissolved in 70% formic acid (EMD) was added to each sample, taking care to avoid exposure to the highly volatile CNBr. The samples were left in the hood overnight and then centrifuged at 12,100×g in a MiniSpin microcentrifuge (model 5452; Eppendorf) for 30 min to pellet insolubles such as elastin. A small volume (50 µl) from the middle portion of the supernatant was transferred to a new microcentrifuge tube, frozen, and lyophilized. The residue was resuspended in 1.0 ml of HCl (6.0 N, diluted from 12 N), heated overnight at 110°C in an oil bath, frozen, lyophilized, and resuspended in 1.5 ml of dH_2O.

A small volume of the final resuspension (80 µl for engineered vessel samples cultured 10 days, 30 µl for all other engineered vessel samples, or 10 µl for carotid artery samples) was transferred to a 15-ml centrifuge tube (VWR) and increased to a total volume of 100 µl by adding assay buffer. The hydroxyproline standard was prepared in duplicate from volumes of 0, 10, 30, 50, and 70 µl brought to a total volume of 100 µl by adding assay buffer. Each sample received 1.0 ml of the chloramine T solution, after which the samples were vortexed and incubated for 20 min at 20°C. Each sample subsequently received 1.0 ml of the aldehyde-perchloric solution, after which the samples were vortexed and incubated for 15 min in a water bath at 65°C. Samples were cooled to 20°C and 200 µl of each samples was transferred to a clear-bottom 96-well plate. Absorbance at 550 nm was measured in the wells in triplicate using a SpectraMax M2^e plate reader (Molecular Devices, Sunnyvale, CA), and total collagen per wet weight of the sample was calculated from the hydroxyproline standard curve. Standard duplicates had means within 5% of one another, and triplicate absorbance measurements also varied less than 5%.

Elastin Content

Elastin Autofluorescence

Elastin and collagen both autofluoresce, but at different excitation and emission wavelengths (respectively ~488 and ~522 nm for elastin[110] and ~370 and ~440 nm for collagen[111]) and with different intensities, that of elastin being much greater.[112] Collagen autofluorescence was therefore not practical because PGS is also weakly autofluorescent in the 370-440 nm range. Elastin autofluorescence was imaged in cryosections using a Zeiss Axiovert 100M microscope coupled to an argon-ion laser and fitted with a Zeiss LSM 510 scanning module (Carl Zeiss, Inc, Oberkochen, Germany). Since PGS is weakly autofluorescent at 488 nm, scaffold cryosections were used for image thresholding prior to imaging tissue cryosections (pinhole 275, detector gain 480, amplifier offset -2, and amplifier gain 1). Images were compared qualitatively.

Colorimetric Analysis of Soluble and Insoluble Elastin Content

Medium was collected from each chamber at the termination of culture and evaluated for soluble elastin content using a Fastin™ Elastin Assay kit (kit F2000; Biocolor Ltd., Carrickfergus, United Kingdom). Chamber medium samples (~2.0 ml) were placed in 2.0-ml microcentrifuge tubes and centrifuged at 12,100×g for 30 min in a MiniSpin microcentrifuge to pellet tissue fragments, cells, and other debris and insolubles. Samples were run in duplicate, as were a sample of unused culture medium incubated with an uncultured scaffolds and a set of elastin standards prepared from the α-elastin solution provided with the kit. Elastin precipitation and resuspension, dye binding, recovery of the elastin-dye complex, and dye release were completed as outlined in the assay kit. The complete final sample (250 µl) containing the recovered dye was transferred from each tube to a clear-bottom 96-well plate and absorbance at 513 nm was measured in the wells in triplicate using a SpectraMax M2^e plate reader. Elastin concentration in culture medium from the scaffold chambers was calculated from the elastin standard curve. Standard duplicates had means within 5% of one another, and sample duplicates also varied less than 10% as allowed by kit instructions.

Tissue samples were evaluated for insoluble elastin content using a Fastin™ Elastin Assay kit (kit F2000) after acid hydrolysis of the tissue to destroy all other proteins, including soluble elastin. Construct and scaffold segments (length 3-5 mm) were cut into pieces no larger than 1.0 mm, placed in pre-weighed 15-ml centrifuge tubes and wet weight was recorded. Tissue was digested with ~4 ml of oxalic acid in a 100°C water bath for 60 min with the tube's cap loosened. The tube was cooled, centrifuged at 3000 rpm for 10 min, and the supernatant collected. Oxalic acid digestion and collection of supernatant was repeated four times for carotid artery digestion and three times for engineered tissue and scaffold digestion. The volume of the pooled supernatant was measured and elastin precipitation and resuspension, dye binding, recovery of the elastin-dye complex, and dye release were completed as outlined in the assay kit. Samples were run in duplicate, as were a set of elastin standards prepared from the α-elastin solution provided with the kit each time the assay was run. Supernatant from the final digestion of each positive control was initially assayed separately to confirm that it contained no elastin, ensuring that elastin extraction was complete. The complete final sample (250 µl) containing the recovered dye was transferred from each tube to a clear-bottom 96-well plate and absorbance at 513 nm was measured in the wells in triplicate using a SpectraMax M2^{e} plate reader. Total elastin per wet weight of the sample was calculated from the elastin standard curve. Standard duplicates had means within 5% of one another, and sample duplicates also varied less than 10% as allowed by kit instructions.

Statistical Analysis

Three or more experimental groups were compared using one-way analysis of variance and a Tukey-Kramer *post-hoc* test in all cases, with $p < 0.05$ in all cases of statistical significance unless otherwise stated. If only two experimental groups were being compared a Student two-tailed *t*-test was used, with $p < 0.05$ in all cases of statistical significance unless otherwise stated. Variance was proportional to the ratio of a

group's standard deviation to its mean and was noted but not compared statistically. Graphical representations of all data show mean ± standard deviation.

CHAPTER 5

INITIAL TUBULAR SCAFFOLD FABRICATION AND EVALUATION[113]

Introduction

Existing approaches for tubular scaffold fabrication include manufacturing a polymer mesh which can be sutured into a tubular geometry,[6,114] electrospinning fibers onto a rotating cylindrical mandrel,[8] or forming a hydrogel around a solid mandrel *in situ*.[51,115] Scaffolds, whether biologic or synthetic, are critical in laying the foundation for engineered tissue; defective scaffolds are likely to spatiotemporally restrict graft remodeling either by producing defective tissue or by excessively lengthening *in vitro* culture time required to create a uniform construct. Defects that are orders of magnitude larger than individual cells may be difficult to correct by extracellular matrix synthesis and cell proliferation without an extended *in vitro* culture period prior to implantation.

A method was initially developed to create compliant, tubular scaffolds of various diameters from any soluble polymer for engineering tubular soft tissues (Figures 5.1 and 5.2).[97] The initial method modified a salt casting technique previously developed[100] to accommodate a tubular geometry using an inner paraffin mandrel and a bifurcated outer PTFE mold. These scaffolds were highly porous and fabricated without seams in the luminal surface. However, the overall process yield was low, geometric tolerances were poor, and complete removal of paraffin was difficult to achieve. We subsequently developed two new scaffold fabrication methods and compared them to the original method by examining overall yields and scaffold characteristics such as defect frequency and severity, wall thickness homogeneity, microstructure, porosity, and mechanical properties.[113] The methods differ in their mandrel materials, mold coating conditions, and

mold configurations during various stages of fabrication. We also investigated cell seeding methods, cell retention, and cellular confluence in the scaffolds as well as the mechanical properties and SMC and protein distribution in constructs (cultured scaffolds). Materials and methods used in this chapter are described in Chapter 4.

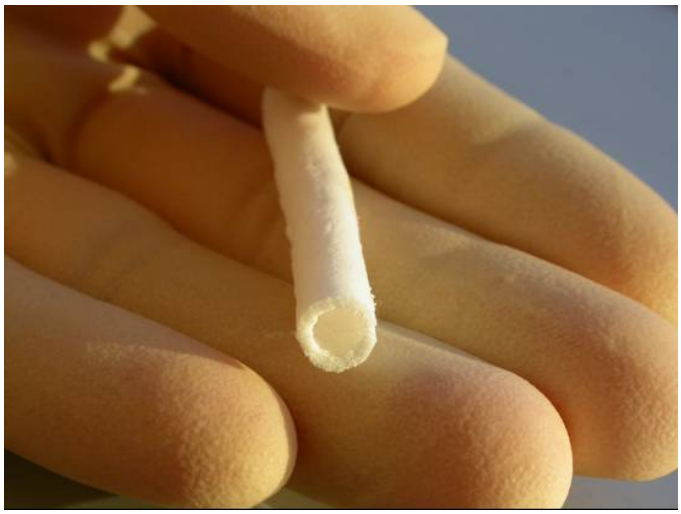

Figure 5.1: Small-diameter Porous Tubular Scaffold Composed of Poly(glycerol sebacate). Scaffolds with an inner diameter of 5 mm and wall thickness of 1 mm have been fabricated at lengths up to 60 mm.

Figure 5.2: Large-diameter Porous Tubular Scaffold Composed of Poly(glycerol sebacate). Scaffolds with an inner diameter of 20 mm and wall thickness of 1 mm have been fabricated at lengths up to 75 cm.

Experimental Design

Salt templates and type I scaffolds adhere to PTFE molds while submerged in water after curing. Porous PGS scaffolds are easily damaged when hydrated, and releasing the scaffolds from the molds decreases yield due to tearing and cracking. Salt templates appear to withstand greater tensile forces than PGS scaffolds. Molds were coated with a food-grade lecithin mold release spray to permit salt template release after drying and before PGS addition. The amount of mold release agent used to coat PTFE molds was optimized by qualitatively assessing salt template yield while controlling the number of mold release applications (with drying between) and their duration. The effect of improved salt template release on yield was investigated.

Type I scaffolds underwent non-symmetric thermal expansion of their molds during fabrication. The coefficient of thermal expansion for the unconstrained upper half of the scaffold and the enclosed bottom half caused cracks at the interface of the scaffold

halves during curing. The effect of salt template release from molds prior to polymer addition and curing on yield was investigated.

Early mandrel materials such as paraffin and starch left residues in scaffolds that could potentially contaminate cell culture or alter cell function. Paraffin also increased scaffold handling and lengthened the fabrication process. Starch residues did not dissolve in water after curing. Hollow PTFE mandrels appeared to decrease process yield by increasing forces on the ends of salt templates during mandrel removal in the axial direction. PTFE mandrels were reinforced by encasing a steel rod within their lumen (type II scaffolds). PGS adhesion to PTFE mandrels sprayed with lecithin mold release was compared to salt template adhesion to heat-shrinkable poly(olefin) sleeves fitted around PTFE mandrels by comparing yields of type II and III scaffolds. PTFE mandrels were pushed out of the polyolefin sleeve after salt template removal from the mold halves. The salt template and attached poly(olefin) were suspended on a metal rod and heated (120°C) until the polyolefin shrank, freeing the salt template.

In an initial experiment, baboon SMCs (passage 5-9) were seeded in type II scaffolds with through-wall flow for 240 min followed by luminal flow on the first-generation bioreactor. The flow rate was increased gradually from 2.0 ml/min (2.2 dynes/cm^2) on day 16 to 14 ml/min (15 dynes/cm^2) on day 38. Culture was continued until day 49, when EPCs (passage 11 or 18) were seeded. Perfusion resumed at 2.0 ml/min (2.2 dynes/cm^2) and was increased steadily to 6.0 ml/min (6.5 dynes/cm^2) on day 53. This flow rate was maintained until the end of the culture period (day 56). Medium was changed weekly without any additional medium components being injected into the medium reservoirs. Cultured type II scaffolds are denoted as type II constructs.

In a subsequent experiment, baboon SMCs (passage 4-5) were seeded in type III scaffolds with through-wall flow for 15 min followed by luminal flow on the first-generation bioreactor. The flow rate was increased steadily from 1.0 ml/min (1.1 dynes/cm^2) on day one to 14 ml/min (15 dynes/cm^2) on day 14. Flow was maintained at

14 ml/min until the end of the culture period (day 21). Medium was changed weekly with additional ascorbic acid being injected into the medium reservoirs three and five days after medium exchange. Cultured type III scaffolds are denoted as type III constructs.

Results and Discussion

Overall Process Yields and Scaffold Physical Properties

Overall Yields

Overall yields of type I and II scaffolds were 46% and 37%, respectively, while 95% of type III scaffolds were free from through-cracks and holes and were therefore usable (n = 26, 30, and 14, respectively; Figure 5.3). The significant differences in yield were likely due to differences in stress concentrations during scaffold fabrication. Type I scaffolds (made with paraffin mandrels) adhered to PTFE molds at the edges of each salt recess, which caused stress concentrations during separation. Type II salt templates (made with PTFE mandrels) were easily disrupted by frictional forces during mold and mandrel removal because of low tensile strength between fused salt crystals. These forces resulted in defective salt templates, with defects transferred to type II scaffolds. Crack formations in type II salt templates were observed during PTFE mandrel removal. Type III salt templates (made with HS mandrels) underwent uniform stresses due to uniform reduction of the mandrel diameter upon heating, and type III salt templates experienced decreased forces because they were not in direct contact with PTFE tubing during its removal. Reduced stress concentrations and frictional forces in type III salt templates produced fewer defects in type III scaffolds.

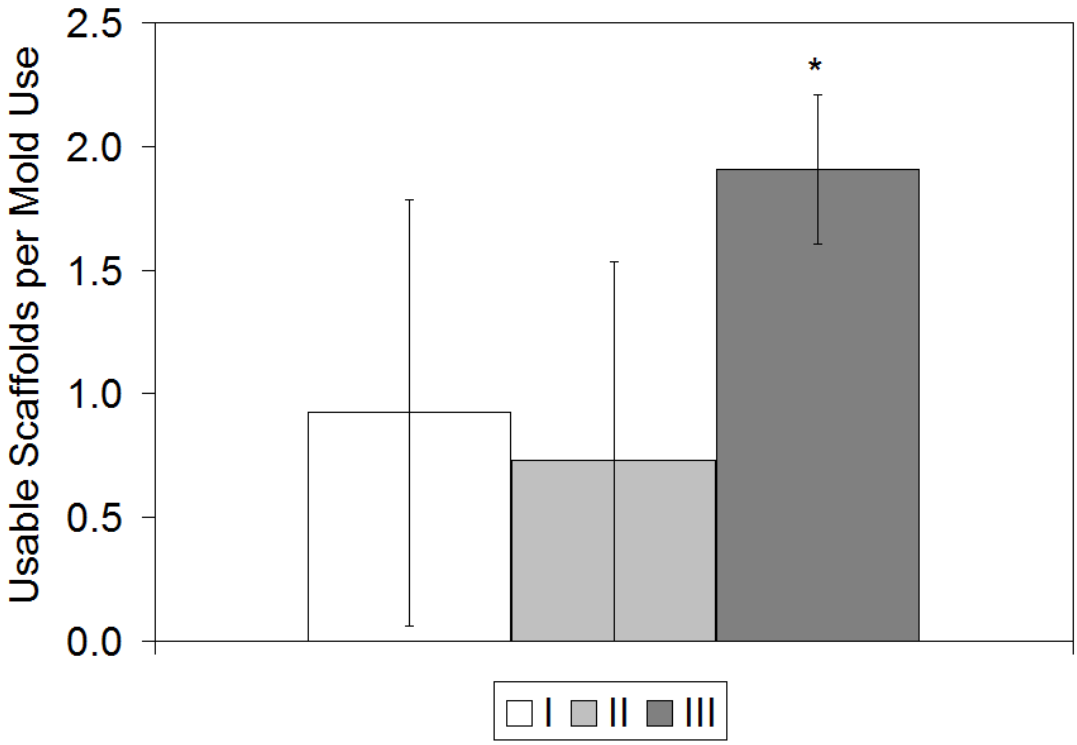

Figure 5.3: Overall Yields of Type I, II, and III Scaffolds. Type I, II, and III scaffolds were fabricated with paraffin, PTFE, or HS mandrels, respectively. *Yield was significantly higher for type III scaffolds compared to other scaffold types ($p < 0.01$, n = 26, 30, and 14, respectively).

Scaffold Geometry, Microstructure, and Porosity

The average, minimum, and standard deviation of wall thickness were compared for segments from type I, II, and III scaffolds (n = 9, 11, and 11, respectively). In comparison to other scaffold types, type I scaffolds had equivalent average wall thickness, significantly lower minimum wall thickness ($p < 0.01$), and significantly higher standard deviation of wall thickness ($p < 0.01$) (Figure 5.4A). Usable type I scaffolds had a high probability of incorporating defects in the form of non-homogeneous wall thickness or partial-thickness voids (Figure 5.4B). Partial-thickness defects in type I

scaffolds appeared to result from scaffold adhesion to PTFE molds at various stages and flaws in the easily-deformed paraffin mandrels. Paraffin also introduced the possibility of contamination from wax or solvents. The use of lecithin mold release and PTFE mandrels and the retention of upper mold halves during salt fusion and drying appeared to reduce the incidence and magnitude of partial-thickness defects in type II scaffolds: cracks and voids occurred less frequently and with lesser magnitude but were not eliminated (Figure 5.4C). Defects in usable type II scaffolds appeared to result from salt template adhesion to PTFE molds and mandrels. Type III scaffolds demonstrated fewer partial-thickness defects than other scaffold types (Figure 5.4D). As with yield, reducing the stress concentrations and frictional forces applied to salt templates likely reduced defect frequency in type III scaffolds.

A: 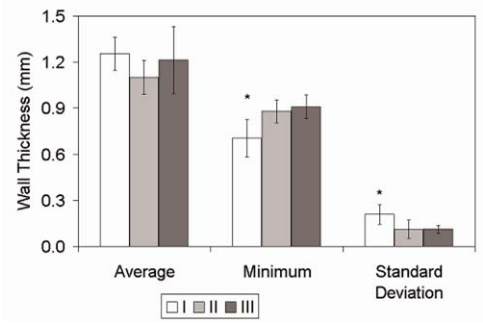

B: 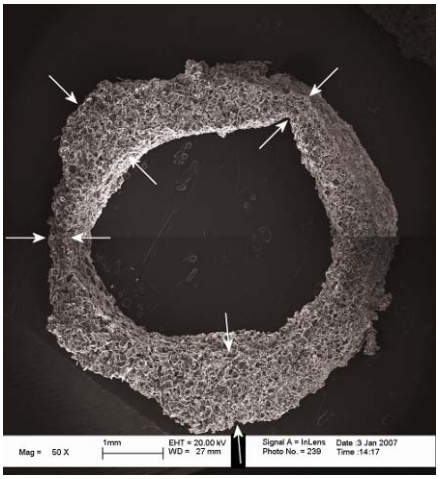

C: 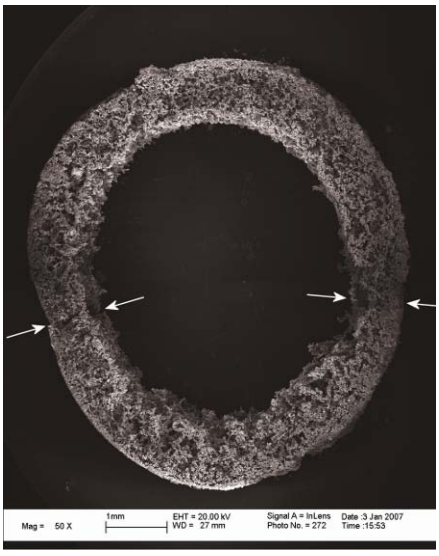

D: 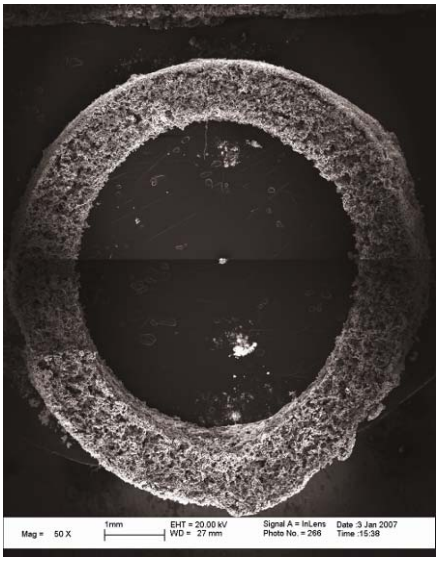

Figure 5.4: Wall Thickness of Type I, II, and III Scaffolds. Type I, II, and III scaffolds were fabricated with paraffin, PTFE, or HS mandrels, respectively. (A) Average, minimum, and standard deviation of wall thickness were determined by measuring at least three 5-mm segments from each of three different type I, II, or III scaffolds. Wall thickness was measured at eight evenly-spaced intervals around each scaffold segment's circumference. There was no correlation between average wall thickness and clearances between outer molds and mandrels, which were 1.19, 1.19, and 1.33 mm for type I, II, and III scaffolds, respectively. *Minimum wall thickness was significantly lower and standard deviation of wall thickness was significantly higher in type I scaffolds compared to other scaffold types ($p < 0.01$, $n = 9$, 11, and 11, respectively). (B) Wall thickness in type I scaffolds ranged from >1000 μm to <250 μm. (C) Type II scaffolds also possessed critical defects such as cracks (arrows at left) or voids (arrows at right) rendering them unusable. (D) Wall thickness in type III scaffolds appeared homogeneous and fewer partial-thickness defects were apparent. Severe defects are indicated by arrows. Segments were randomly selected for SEM inspection. Micrographs (scale bars = 1.0 mm) were

merged to show the complete cross-section, with multiple cutting planes on some specimens.

Individual scaffold porosities ranged from 86% to 95% for type I, II, and III scaffolds (n = 4 for each type). The mean porosity of type III scaffolds was significantly higher than the mean porosity of type II scaffolds (Figure 5.5A). Differences in luminal microstructure were apparent from SEM inspection. Type I scaffolds contained fewer micropores (< 20 μm), with some sections of the scaffold surface void of micropores (Figure 5.5B). The lack of micropores, which are caused by glycerol evaporation during PGS curing, suggested an inhibitory or interactive role for paraffin during PGS curing. Micropores are likely to aid in cell infiltration and attachment within the scaffold during seeding and culture. Microstructure was comparable in type II and III scaffolds, though the overall quality of the microstructure in type III scaffolds appeared higher because they contained fewer voids > 200 μm (exceeding an individual cell's diameter by approximately one order of magnitude; Figures 5.4C-D, 5.5C-D) and significantly higher mean porosity (Figure 5.5A). Differences in porosity and microstructure probably resulted from voids in salt templates caused by salt adhesion to PTFE mandrels and collapses in salt templates caused by stress concentrations during PTFE mandrel removal.

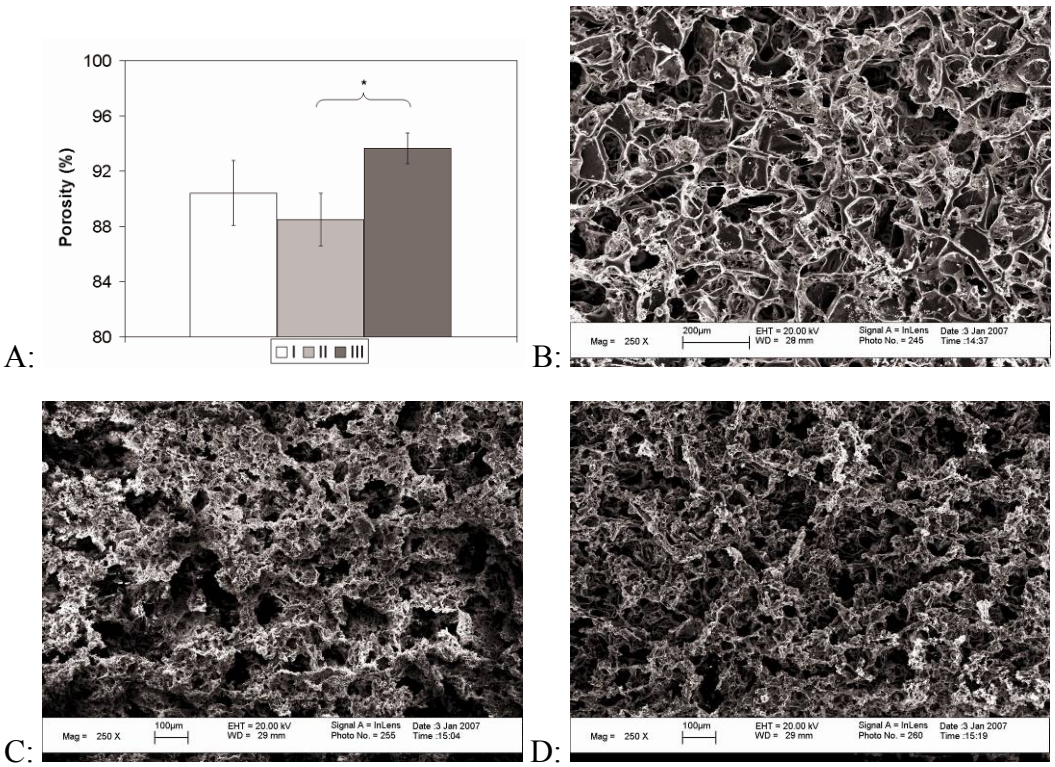

Figure 5.5: Porosity and Luminal Microstructures of Type I, II, and III Scaffolds. Type I, II, and III scaffolds were fabricated with paraffin, PTFE, or HS mandrels, respectively. (A) Individual scaffold porosity ranged from 86% to 95% for all scaffold types. *Porosity was significantly higher in type III scaffolds compared to type II scaffolds (n = 4 for all scaffold types). (B) Fewer, less-evenly distributed micropores were observed on the luminal surfaces of type I scaffolds (scale bar = 200 µm). (C) Type II scaffolds had voids > 200 µm throughout their luminal surfaces (scale bar = 100 µm). (D) Type III scaffolds contained fewer voids of lesser magnitude than those found in type II scaffolds (scale bar = 100 µm). Microstructure in type III scaffolds appeared to be of higher quality. Segments were randomly selected for SEM inspection. Micrographs are from randomly selected areas.

Mechanical Properties of Scaffolds

Uniaxial Tensile Testing of Scaffolds

Partial-thickness defects were observed to harbor stress concentrations during mechanical testing of scaffold segments. The significantly lower t_{min} of type I scaffolds resulted in apparent mechanical properties that were not comparable to other scaffold types (σ_{max} = 4.32 ± 1.22 kPa, ε_{Tmax} = 28.0 ± 13.0 %, and E_{linear} = 22.2 ± 8.4 kPa; see Figures 5.4A-D). Comparisons of σ_{max}, ε_{Tmax}, and E_{linear} for type II and III scaffolds revealed no significant differences, though data for type II scaffolds did have greater standard deviations in comparison to their means (n = 11 for each type; Figure 5.6). The greater variability in mechanical properties of type II scaffolds was probably caused by partial-thickness defects spanning nearly the entire wall thickness in some but not all of the tested segments. This variance was large enough that a significant difference was unlikely to be established even if the number of samples used for comparison was to be increased an order of magnitude.

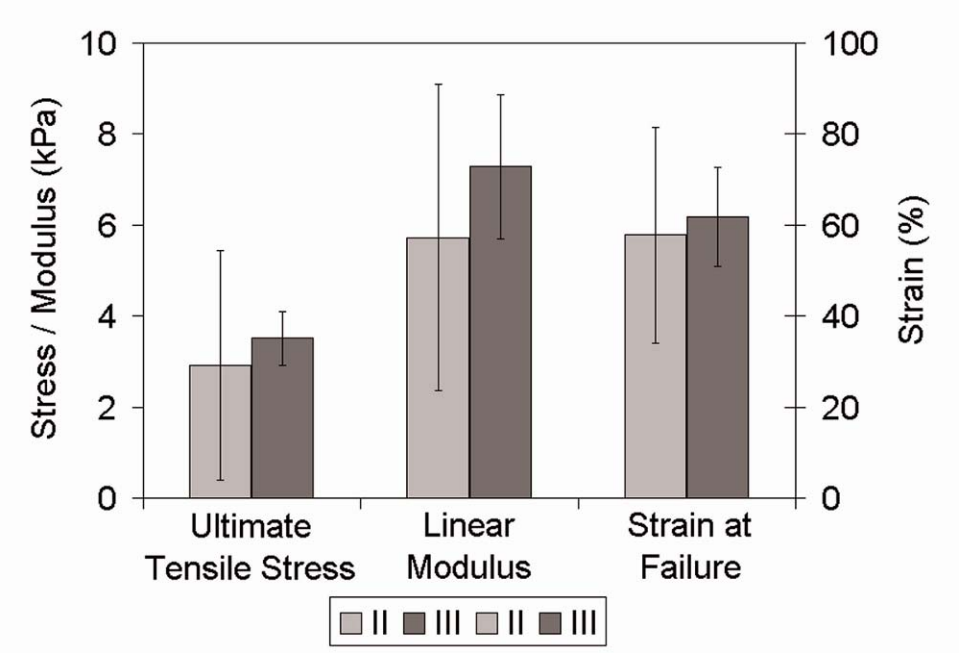

Figure 5.6: Ultimate Tensile Stress, Linear Modulus of Elasticity, and Strain at Failure of Type II and III Scaffolds. Type II and III scaffolds were fabricated with PTFE and HS mandrels, respectively. No significant differences were found, though data from type II scaffolds had greater variance (n = 11 for each scaffold type). Type I scaffolds had significantly lower minimum wall thickness, making their mechanical properties artificially higher and therefore not comparable to other scaffold types (see Figure 5.4A).

Cell-Scaffold Interactions

Cell Seeding Efficiency

Type III scaffolds seeded with SMCs using through-wall perfusion retained 74 ± 4% of seeded cells (individual scaffolds: 77%, 74%, and 69%) as quantified by hemacytometer observations of crystal violet-stained nuclei following mechanical disruption. Type III scaffolds seeded with an SMC suspension followed by immediate luminal flow resulted in 44 ± 8% seeding efficiency (individual scaffolds: 54%, 41%, and

39%). Perfusing the same density of SMCs through scaffold walls for an initial brief period significantly increased cell seeding efficiency, likely by forcing a greater number of SMCs further into the scaffold, thereby decreasing cell washout during subsequent luminal perfusion.

Chronological Quantification of Live Cells

Type III scaffolds cultured with SMCs for six, eight, or 10 days in the first-generation bioreactor (n = 3; 1 per time point) had a rate of change in cell quantity over time of 19 ± 3% per day (day six: 20.5%, day eight: 15.4%, day 10: 19.7%). The live SMC population doubled slower under pulsatile flow conditions (every 4.1 ± 0.6 days) compared to static conditions (every 2.6 ± 0.2 days) due to perfusion-induced shear.[57]

Cellular Confluence

Type II scaffolds cultured with SMCs for 49 days followed by coculture with EPCs for another seven days (n = 4) were confluent over the entire luminal surface (Figure 5.7A). Type III scaffolds cultured with SMCs for 21 days (n = 3) contained cells throughout their entire wall thickness (Figure 5.7B) and a confluent layer of cells on their luminal surface (Figure 5.7C). SMCs seeded in type III scaffolds reached luminal confluence by day 10, while bare scaffold was visible in the lumen on days six and eight (data not shown).

A:

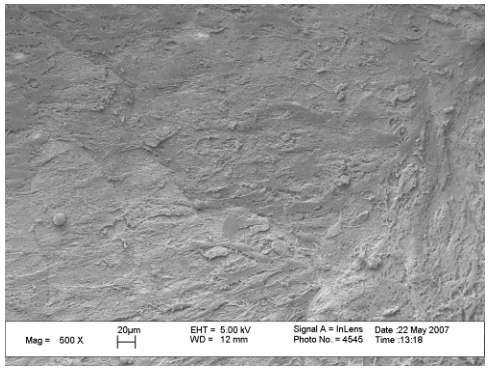

A:

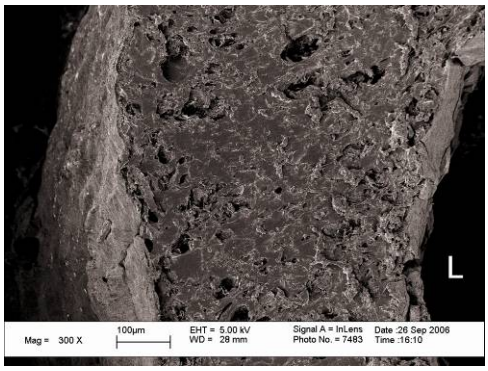

B:

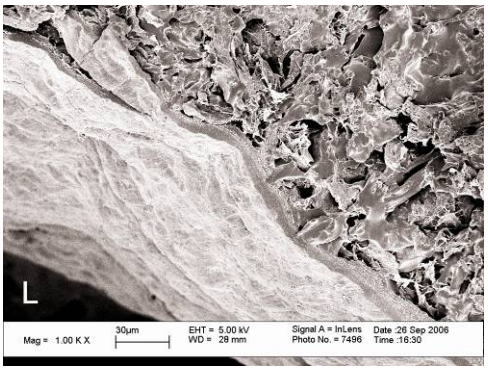

Figure 5.7: Distribution and Luminal Confluence of Adult Baboon Vascular Cells Cultured in Type II Scaffolds for Fifty-six Days or Type III Scaffolds for Twenty-one Days. Type II scaffolds were cultured with SMCs for 49 days and cocultured with SMCs and EPCs for an additional seven days. Type III scaffolds were cultured with SMCs only for 21 days. (A) Luminal surfaces of type II constructs were confluent at the termination of culture (scale bar = 20 µm). (B) Biological material such as SMCs and protein was observed within the pores of type III scaffold segments sectioned perpendicular to the construct axis (scale bar = 100 µm). (C) Type III scaffold luminal surfaces showed that the SMCs were confluent (scale bar = 30 µm). L indicates luminal space.

Gross Construct Morphology

Visual Observations

Engineered type II and III constructs visibly distended in a cyclic manner while subjected to pulsatile perfusion during *in vitro* culture. Upon removal from the first-generation bioreactor on day 56, cultured type II constructs appeared pink and retained

their cylindrical shape in contrast to uncultured scaffolds, which collapsed flat when wet. Type III constructs were similar in appearance to type II constructs. Cultured scaffolds could withstand forces exerted on them during removal from their chamber and handling required for analysis. The tissue did not disintegrate with careful handling but could not withstand normal forces exerted on native tissues such as those required by clinical tissue handling.

Histology

Type II SMC-EPC constructs stained with H&E, which stained cell nuclei purple and cytosol and ECM pink, showed concentrations of cell nuclei and protein at the luminal and abluminal surfaces and throughout the construct wall (Figure 5.8A). Type III SMC-only constructs showed similar concentrations of cell nuclei and protein at the luminal and abluminal surfaces and throughout the construct wall (Figure 5.8B). Multiple areas that stained pink were distant from cell nuclei and were likely to be ECM rather than cytosol.

A:

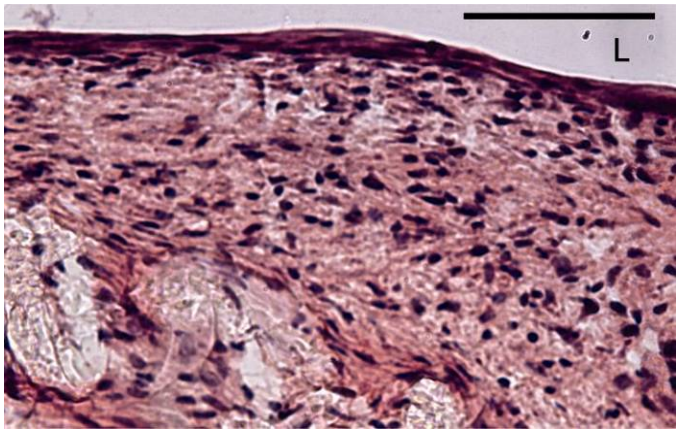

B:

Figure 5.8: Histological Appearance of Type II Poly(glycerol sebacate)-based Tissue-engineered Constructs Cultured for Fifty-six Days or Type III Constructs Cultured for Twenty-one Days. Type II scaffolds were cultured with adult baboon SMCs for 49 days and cocultured with SMCs and EPCs for an additional seven days. Type III scaffolds were cultured with SMCs only for 21 days. (A) Type II SMC-EPC constructs had concentrations of cell nuclei and proteins at the luminal and abluminal surfaces and cell nuclei distributed throughout the scaffold walls (scale bar = 1.0 mm). The scaffold appeared wrinkled, probably as a result of compaction by SMCs. (B) Distributions of cell nuclei and protein in type III SMC-only constructs appeared similar to type II SMC-EPC constructs (scale bar = 50 μm). Multiple areas that stained pink were distant from nuclei and were likely to be ECM rather than cytosol. This finding encouraged further investigation of protein synthesis and incorporation into ECM by adult baboon SMCs cultured in PGS scaffolds. L indicates luminal space.

Mechanical Properties of Engineered Constructs

Pressure-diameter Testing of Whole Constructs

Type II scaffolds cultured with SMCs for 49 days and subsequently cocultured with SMCs and EPCs for an additional seven days were subjected to pressure-diameter testing to determine whether PGS scaffolds showed potential in creating compliant engineered vascular constructs. Almost the entire length of each construct was used for pressure-diameter testing to burst. (A small section near either end of each construct was cut off and set aside for cryosectioning and histological analysis prior to pressure-diameter testing.) In some cases the constructs were damaged during attachment to cannulae or stretch prior to testing, in which case the longest intact section of the construct was tested. The engineered constructs showed hysteresis during the first cycle to each target pressure, but subsequent cycles demonstrating complete elastic recovery (Figure 5.9).

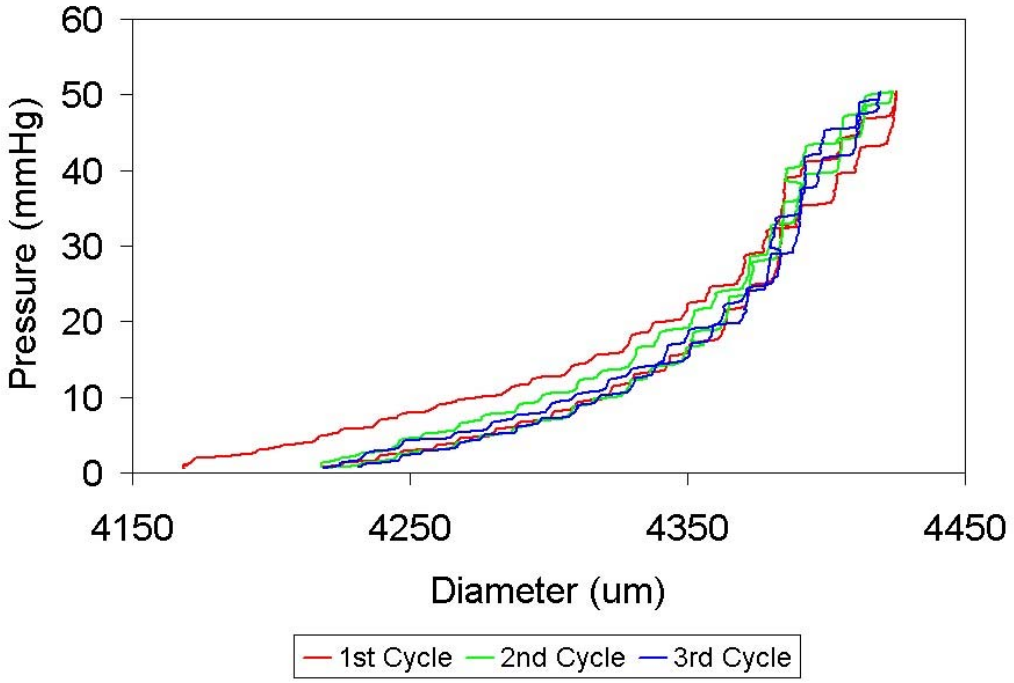

Figure 5.9: Elastic Recovery of Whole Poly(glycerol sebacate)-based Type II Constructs Cultured for Fifty-six Days. Pressure-diameter testing of whole constructs was performed after type II scaffolds were cultured with adult baboon SMCs for 49 days and cocultured with adult baboon EPCs for an additional seven days. Complete elastic recovery was observed after the initial cycle to each target pressure in type II constructs up to pressures near their burst pressure (cycles to a target pressure of 50 mmHg are shown for a construct with a burst pressure of 81 mmHg).

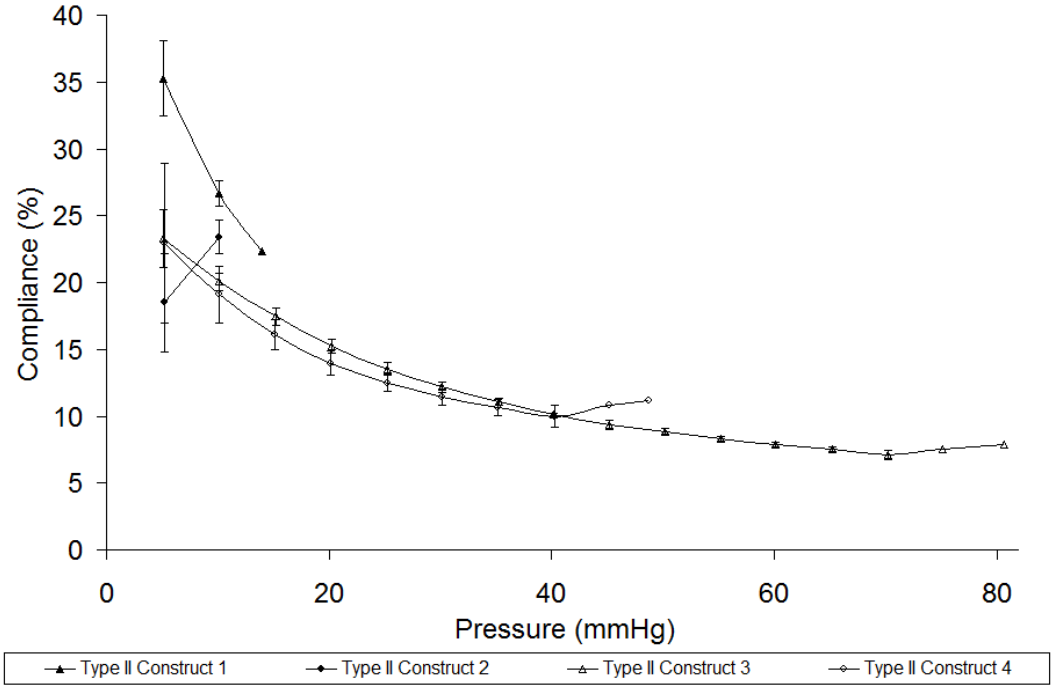

Figure 5.10: Compliance of Whole Type II Constructs. Pressure-diameter testing of whole constructs was performed after PGS type II scaffolds were cultured with adult baboon SMCs for 49 days and cocultured with EPCs for an additional seven days. Compliance was calculated for changes in diameter at each given zero-to-target pressure value. Sharp increases in compliance immediately prior to vessel failure were most likely caused by tearing in luminal SMC sheets that circumferentially wrinkled the scaffolds (see Figure 5.8). At pressure up to 80 mmHg, type II constructs (n = 4) had relatively high compliance compared to other tissue-engineered constructs reported in the literature. Inverse relationships appeared to exist between target pressure and compliance for individual constructs and between burst pressure and compliance at burst for the entire group.

Extracellular Matrix Synthesis in Engineered Constructs

Collagen Content

Immunofluorescence

Collagen distribution was imaged in initial experiments using Masson's trichrome stain, which showed concentrations of collagen at the luminal surface of constructs. Subsequent imaging of collagens I and III and cell nuclei in type II constructs showed concentrations of collagen I and cell nuclei at the luminal and abluminal surfaces with collagens I and III and cell nuclei distributed throughout the construct wall (Figure 5.11).

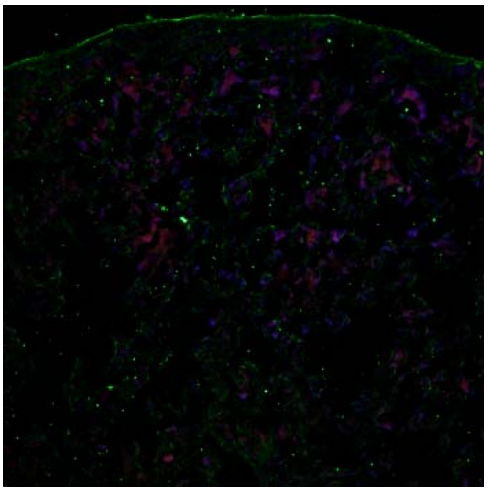

Figure 5.11: Distributions of Collagens I and III in Type II Constructs. Segments of PGS type II scaffolds cultured with adult baboon SMCs for 49 days and cocultured with EPCs for an additional seven days were snap-frozen and cryosectioned. Cryosections were immunofluorescently stained against collagen I (FITC) and collagen III (Rhodamine) to assess collagen distribution (magnification 100X). Staining with DAPI was used to assess distribution of SMCs. Collagens I and III and cell nuclei were stained and imaged in single locations, with images subsequently merged. Type II constructs showed collagen I and cell nuclei concentrated at the luminal and abluminal surfaces with collagens I and III and cell nuclei throughout the construct wall. Image is oriented with the luminal surface facing down.

Elastin Content

Elastin Autofluorescence

Elastin distribution was imaged in initial experiments using autofluorescence, which showed concentrations of elastin at the luminal surface of constructs. Subsequent autofluorescence imaging of elastin in type II constructs also showed concentrations of elastin at the luminal surface (Figure 5.12).

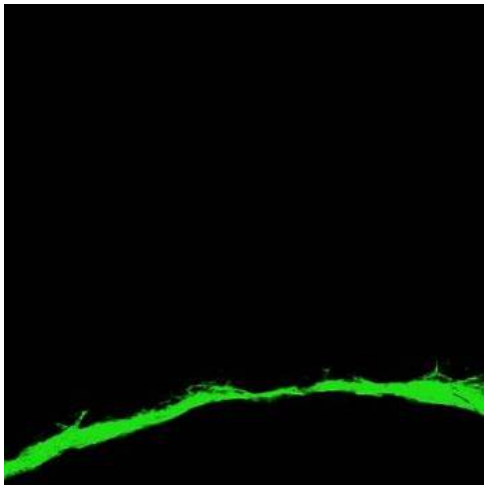

Figure 5.12: Elastin Distribution in Type II Constructs. Segments of PGS type II scaffolds cultured with adult baboon SMCs for 49 days and cocultured with EPCs for an additional seven days were snap-frozen and cryosectioned. Cryosections were excited at 488 nm and imaged to assess elastin distribution via autofluorescence (magnification 100X). Type II constructs showed a concentration of elastin at the luminal surface. The weak autofluorescence of uncultured PGS scaffolds was used for image intensity thresholding (data not shown). Image is oriented with the luminal surface facing down.

Limitations of the Experimental Approach and Recommendations

Fabrication of scaffolds using bifurcated molds was time-intensive due to part counts of the mold assemblies. Type II and III scaffolds were even more time-intensive if sufficient care was taken in the extensive handling required for the delicate salt templates. The process was complicated and yield was significantly lower for an inexperienced fabricator.

Communication between multiple cell types, especially when separated by the entire thickness of the scaffold wall, could inhibit development of engineered vascular tissue. The relationship between scaffold impedance to diffusive biomolecule transport and PGS density in the scaffolds could be investigated. The density currently used (4.0 mg/mm relative to scaffold length) was determined qualitatively by SEM and by handling scaffolds at various densities (0.5-10 mg/mm).

While SMCs adhered to the surface and became confluent, the calculated rate of change in cell quantity over time did not eliminate the possibility of cytotoxicity. A live/dead assay (or assessment using trypan blue at the very least) would conclusively investigate cytotoxicity. Seeding efficiency might be lower than desirable values for a tissue engineering process that would be clinically implemented and could be increased to reduce cost by reducing time required for cell expansion and the quantity of cells not contributing to tissue development in culture. Alternatively, recapturing washed out SMCs from medium reservoirs and reseeding prior to luminal SMC confluence could increase seeding efficiency to levels near 100%. A thin PGS membrane (on the order of tens of μm) could have been cured around the outside of each scaffold following fabrication to provide a barrier against cell washout, with micropores still providing through-wall flow during seeding. The membrane could also provide improved scaffold handling and mechanical properties. The abluminal flow circuit would prevent the PGS membrane from acting as a nutrient barrier during culture.

Mold release agents other than lecithin may improve yield for salt template release, such as food-grade silicone or PTFE dry films. Other HS polymers may be substituted in place of poly(olefin), such as PVC. It is anticipated that systematic refinement of scaffold processing and handling techniques and establishment of standard protocols for fabrication will decrease handling forces and flaws and increase yield.

Conclusions

A high-yield method was developed for creating internally seamless tubular scaffolds of uniform wall thickness made from a biodegradable elastomer. Type III scaffolds (created with HS mandrels) exhibited four advantages: (1) higher yield due to decreased frequency and severity of critical defects; (2) tighter wall thickness tolerance; (3) greater porosity; and (4) a greater number of more evenly-distributed micropores. Culture results indicate that type II and III scaffolds are cytocompatible, conducive to cell adhesion and increases in cell quantity over time, and promote co-expression of collagen and elastin, demonstrating their potential for engineering soft tissues with tubular structures. Culture of type II scaffolds led to highly compliant constructs with elastic recovery during pressurization, demonstrating the potential of PGS scaffolds for creating tissue-engineered blood vessels. A combined discussion of results from this and all other chapters and their implications is presented in Chapter 12.

CHAPTER 6

MODIFIED TUBULAR SCAFFOLD FABRICATION AND EVALUATION

Introduction

The desire to simplify the process for fabricating porous tubular PGS scaffolds and enable large-scale production through the elimination of machining requirements and assembly part count motivated a revision of prior scaffold fabrication processes. Shortcomings of initial scaffold fabrication methods, particularly geometry and handling, also motivated further improvement. It was expected that tubular PGS scaffolds for blood vessel tissue engineering with thinner walls and lower wall thickness variance would lead to constructs that better matched the properties of the *tunica media* of native healthy arteries. The elimination of seams from the abluminal surface was also desirable so that the scaffolds would be truly seamless on all surfaces and therefore provide better handling by minimizing stress concentrations in the walls. Two additional methods are presented and compared to the previous methods, with one method identified as superior on the basis of metrics. Materials and methods used in this chapter are described in Chapter 4.

Experimental Design

The approach for improving fabrication was based around developing a process that would be easy to learn, highly reproducible, and capable of automation. The reduction of stress concentrations was viewed as a key to scaffold improvement. The development of new scaffold fabrication methods centered on the reduction of stress concentrations during separation of the mandrel and outer mold from the salt template or

scaffold. Scaffolds from the resulting modified fabrication methods (types IV and V) were compared to scaffolds from two of the initial methods (types II and III). Scaffolds were compared for wall thickness homogeneity, microstructure, porosity, and mechanical properties with the same experimental design used in Chapter 5.

Results and Discussion

Overall Process Yields and Scaffold Physical Properties

Overall Yields

Process yields were quantitatively assessed after method development and during instruction to undergraduates learning the modified fabrication methods. Yields for type IV and V scaffolds were comparable to yields for type III scaffolds and significantly higher than yields for type II scaffolds (Figure 6.1). However, yield of type IV scaffolds steadily decreased over time as PTFE tubes became worn by salt loading and packing. (The hardness of salt exceeds that of PTFE.) PTFE tube wear necessitated production of new type IV molds, and geometrical tolerances and surface roughness of supply materials were inconsistent and therefore problematic. Yields for type V scaffolds were consistently high when coating with hyaluronic acid was completed correctly. Coating with less than 1.0% hyaluronic acid or incomplete coating of surfaces caused PGS to adhere to type V molds. Slow end-over-end rotation (~0.1 rpm) of glass tubes during hyaluronic acid coating provided reproducible scaffold release from type V molds. Observation of inexperienced fabricators indicated that the type V fabrication process significantly reduced the user-dependent nature of yield.

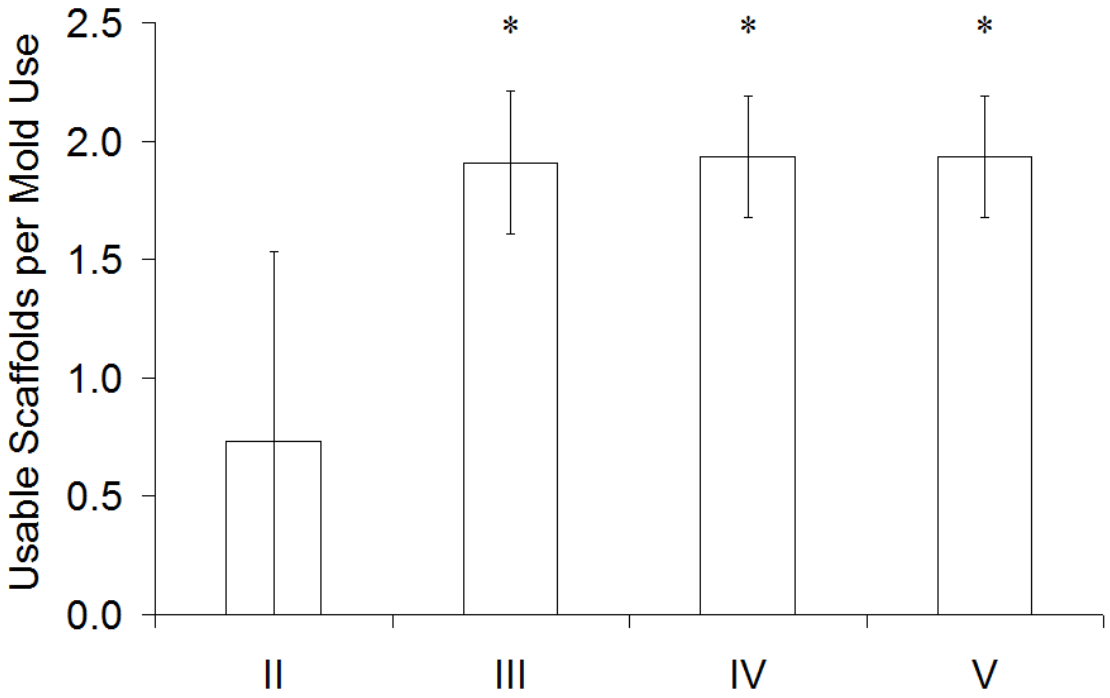

Figure 6.1: Overall Yields of Type II, III, IV, and V Scaffolds. Type II scaffolds were fabricated with PTFE mandrels, while type III, IV, and V scaffolds were fabricated with HS mandrels. Type II and III scaffolds were fabricated with bifurcated PTFE outer molds, while type IV scaffolds were fabricated with tubular PTFE outer molds and type V scaffolds were fabricated with tubular glass outer molds. *Yield was significantly higher for types III, IV, and V scaffolds compared to type II scaffolds (n = 30, 22, 30, and 30from left to right).

Scaffold Geometry, Microstructure, and Porosity

Mean wall thickness of type IV scaffolds was significantly lower compared to type II and III scaffolds, but variance was higher (Figure 6.2A). Wall thickness of type V scaffolds was significantly lower than all other scaffold types, with variance comparable to that of type III scaffolds. Evidence from SEM at higher magnification confirmed this improvement (Figures 6.2B-C). Porosity in type IV scaffolds was comparable to type II

scaffolds and significantly lower than type III scaffolds (Figure 6.3A). Porosity in type V scaffolds was significantly lower than other scaffold types but was still 84.6 ± 0.6%. Porosities of all individual scaffolds tested fell within a narrow range (84-95%), and all scaffold types were therefore expected to similarly accommodate cell penetration during seeding and increases in cell quantity during culture. Comparison of luminal scaffold surfaces using SEM showed equivalent microstructures and fewer out-of-plane microstructures and voids on the luminal surface of type V scaffolds (Figures 6.3B-E).

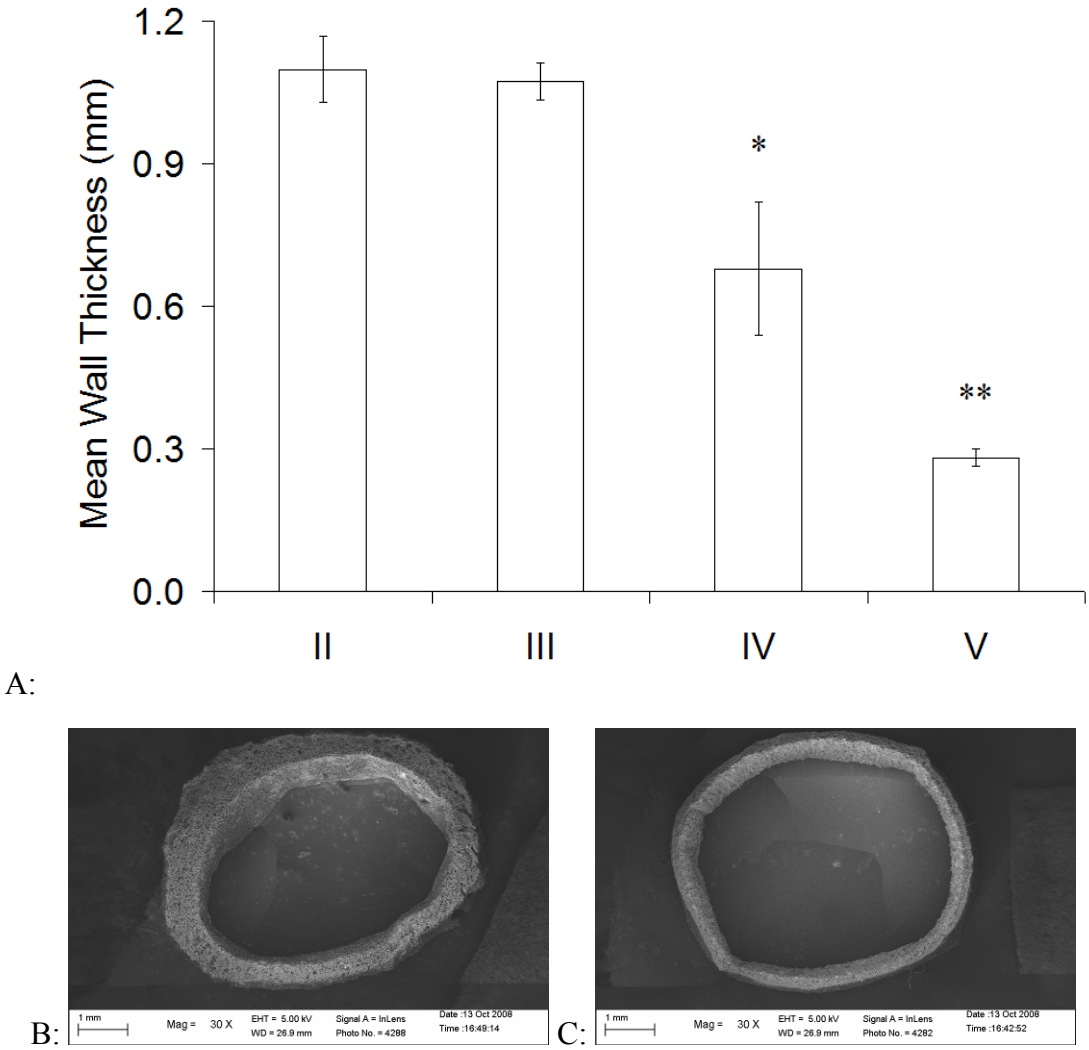

Figure 6.2: Wall Thickness of Type II, III, IV, and V Scaffolds. Type II scaffolds were fabricated with PTFE mandrels, while type III, IV, and V scaffolds were fabricated with HS mandrels. Type II and III scaffolds were fabricated with bifurcated PTFE outer molds, while type IV scaffolds were fabricated with tubular PTFE outer molds and type V scaffolds were fabricated with tubular glass outer molds. Clearances between outer molds and mandrels were 1.19, 1.33, 1.33, and 0.86 mm for type II, III, IV, and V scaffolds, respectively. (A) Mean wall thickness was determined from measurements of unstressed scaffolds immediately prior to mechanical testing (n = 11, 11, 20, and 14 from left to right). *Type IV scaffolds had significantly thinner walls compared to type II and III scaffolds. **Type V scaffolds had significantly thinner walls than all other scaffold types and decreased wall thickness variance compared to type IV scaffolds. (B) Wall thickness in type IV scaffolds ranged from 300 to 800 μm. (C) Wall thickness in type V scaffolds ranged from 200 to 350 μm and appeared more homogeneous. Segments were randomly selected for SEM inspection. Micrographs (scale bars = 1.0 mm) were merged to show the complete cross-section.

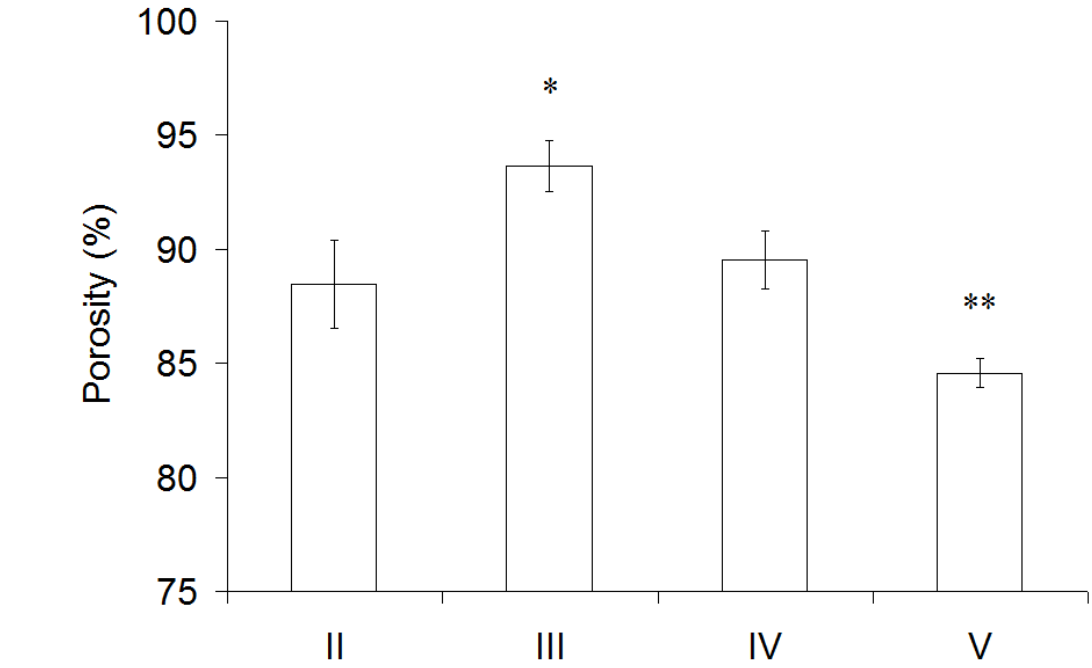

A:

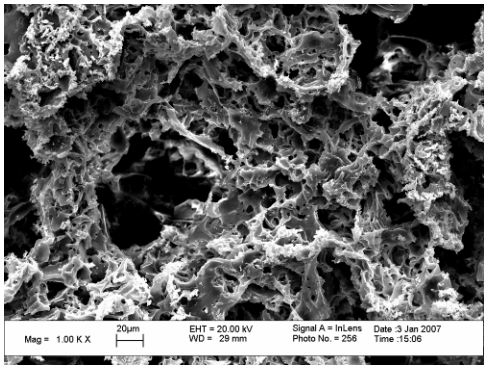

B:

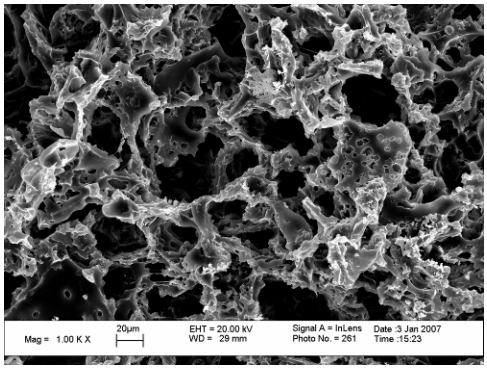

C:

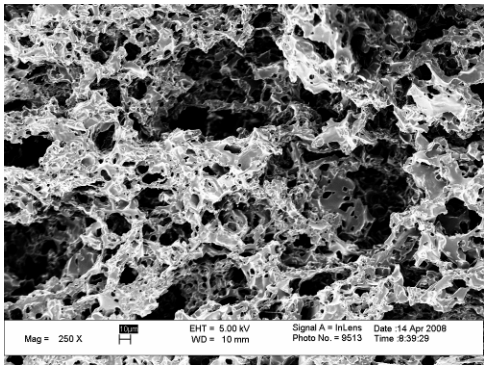

D:

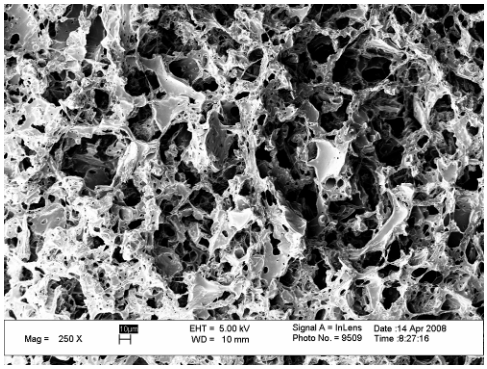

E:

Figure 6.3: Porosity and Luminal Microstructures of Type II, III, IV, and V Scaffolds. Type II scaffolds were fabricated with PTFE mandrels, while type III, IV, and V scaffolds were fabricated with HS mandrels. Type II and III scaffolds were fabricated

with bifurcated PTFE outer molds, while type IV scaffolds were fabricated with tubular PTFE outer molds and type V scaffolds were fabricated with tubular glass outer molds. Salt porogen sizes were 75-90 μm for all scaffold types. (A) Measurements of scaffold porosity were determined from volumetric ethanol submersion (n = 4 for all scaffold types). *Type III scaffolds had significantly higher porosity compared to other scaffolds. **Type V scaffolds had significantly lower porosity compared to other scaffolds. Microstructure was similar in (B) type II and (C) type III scaffold luminal surfaces (scale bars = 20 μm), as well as in (D) type IV and (E) type V scaffold luminal surfaces (scale bars = 10 μm). Type V scaffolds appeared more planar at the microscopic level, with fewer pits and raised areas.

Mechanical Properties of Scaffolds

Uniaxial Tensile Testing of Scaffolds

Type V scaffolds had significantly higher σ_{max} and E_{linear} than all other scaffold types (Figure 6.4), and σ_{max} and E_{linear} were also significantly higher for type IV scaffolds compared to type II and III scaffolds. However, higher σ_{max} and E_{linear} for type IV scaffolds were coupled with greater variance. The significant increases in E_{linear} for type IV and V scaffolds were not expected since E_{linear} is a material property. The increase in E_{linear} was likely due to the elimination of abluminal scaffold seams and an associated significant reduction in stress concentrations around the outer circumference of scaffold segments during uniaxial tensile testing. If stress concentrations were truly reduced, E_{linear} for type IV and V scaffolds more accurately reflected the material properties of porous PGS. Other possible contributors to the significant increase in E_{linear} included PGS pre-polymer batch variation or variations in scaffold microstructure not observable by SEM inspection of scaffold wall cross-sections and the luminal and abluminal surfaces. Variance in E_{linear} was comparable for type III and V scaffolds and was much higher for other scaffold types. Type IV scaffolds had significantly lower values of ε_{Tmax} compared to type II and III scaffolds (Figure 6.4). This was most likely a result of the combination

of decreased wall thickness coupled with greater variance in wall thickness (see Figure 6.2A). Variance of ε_{Tmax} was similar in all groups employing HS mandrels (all except type II scaffolds). Type V scaffolds generally displayed significantly tighter control of geometry and mechanical properties in comparison to all other scaffold types (see Figures 6.2 and 6.4).

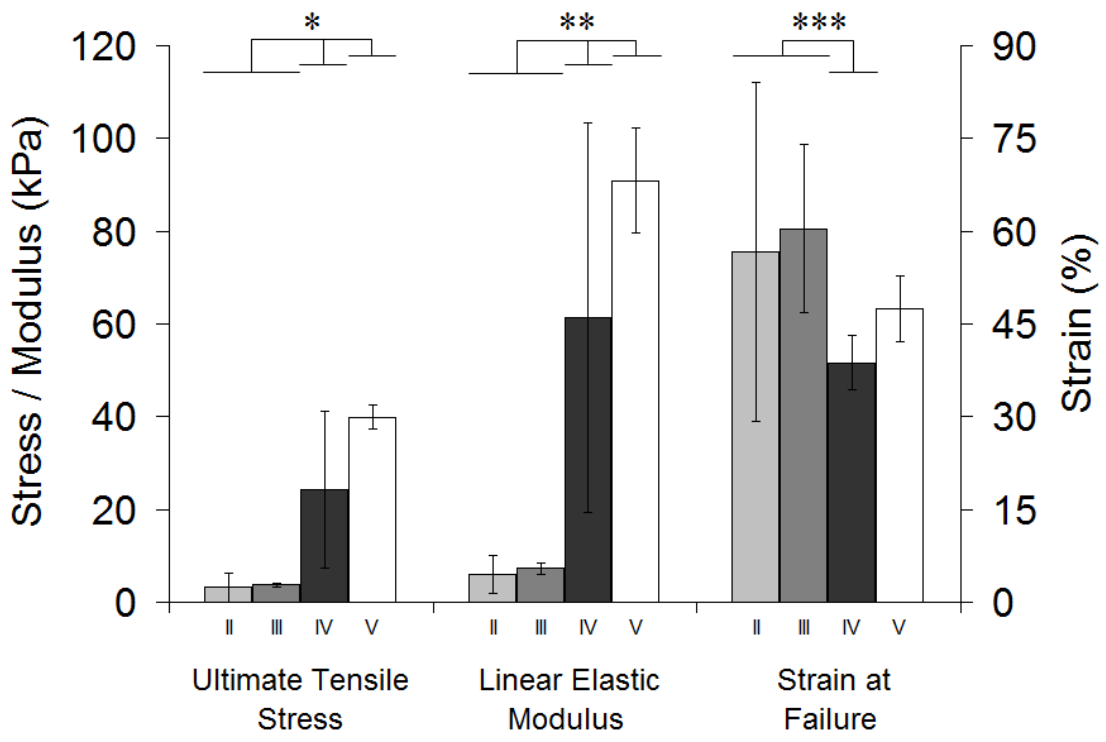

Figure 6.4: Ultimate Tensile Stress, Linear Modulus of Elasticity, and Strain at Failure of Type II, III, IV, and V Scaffolds. Scaffold segments were tested uniaxially with video capture to determine σ_{max}, E_{linear}, and ε_{Tmax} (n = 11, 11, 20, and 14 from left to right). *Type V scaffolds segments had significantly higher σ_{max} compared to all other scaffold types. Type IV scaffolds segments had significantly higher σ_{max} compared to type II and III scaffold segments. Type V scaffold segments had lower variance in σ_{max} compared to type IV scaffold segments. ** Type V scaffolds segments had significantly higher E_{linear} compared to all other scaffold types. Type IV scaffolds segments had significantly higher E_{linear} compared to type II and III scaffold segments. Type V scaffold segments had lower variance in E_{linear} compared to type IV scaffold segments. ***Type IV scaffold segments had significantly higher ε_{Tmax} compared to type II and III scaffold segments. Type IV and V scaffolds segments had lower variance in ε_{Tmax} compared to type II and III scaffolds segments.

Scaffold Attachment to the Bioreactor

Increased mechanical properties coupled with lower tolerances allowed more aggressive handling of type V scaffolds during attachment to the bioreactor despite their

significantly reduced wall thickness. The improved mechanical properties led to fewer scaffold losses during attachment preparatory to culture.

Cell-Scaffold Interactions

Cell Seeding Efficiency

Seeding efficiency was compared for type II scaffolds (previous data, see Chapter 5) and type V scaffolds. Type V scaffolds seeded with SMCs using through-wall perfusion retained 80 ± 6% of seeded cells (individual scaffolds: 85%, 82%, and 74%) compared to 74 ± 4% (77%, 74%, and 69%) retained in through-wall-perfused type II scaffolds. No significant difference in cell seeding efficiency existed between the two scaffold types.

Cellular Confluence

After seven days in culture SMCs had reached confluence on type V scaffold lumens (Figure 6.5A). Microscopic fenestrations were observed in SMC monolayers on the luminal surface at sizes of five μm or less (Figure 6.5B). Scaffold cross-sections showed that SMCs had formed multiple layers on the luminal surface, and a semi-confluent monolayer of SMCs appeared to have formed on each scaffold's abluminal surface from cells washed out of the scaffold during seeding (Figure 6.5C). The presence of multi-layered luminal SMCs indicated that confluence was probably reached earlier than day seven. The barrier formed by multiple layers of SMCs with maximum fenestrations of approximately five μm were expected to prevent luminally seeded ECs or EPCs from crossing into the abluminal space or abluminally seeded fibroblasts from crossing into the lumen.

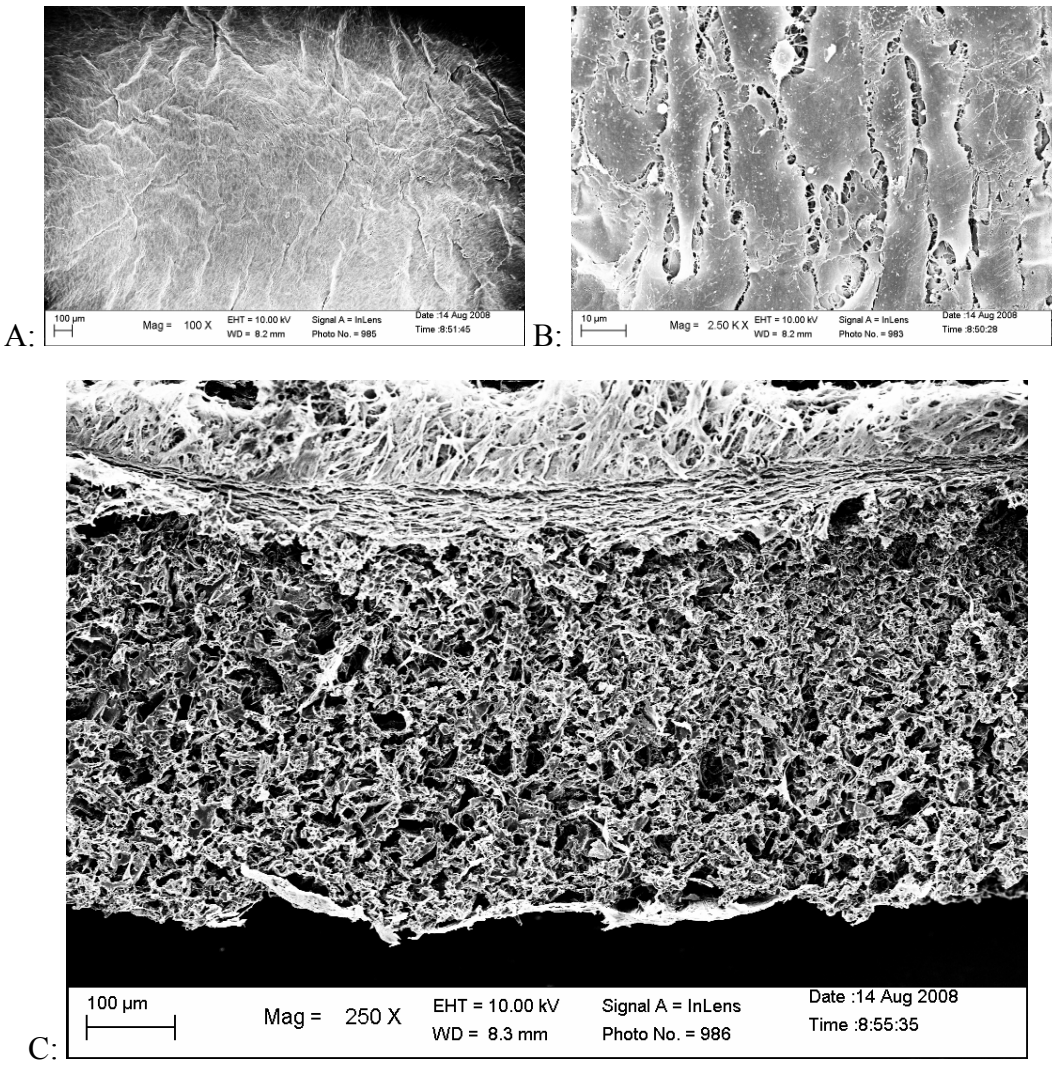

Figure 6.5: Distribution and Luminal Confluence of Adult Baboon Smooth Muscle Cells Cultured in Type V Scaffolds for Seven Days. Type V scaffolds seeded with SMCs were confluent within seven days. Luminal and abluminal surfaces are at top and bottom of image, respectively. (A) SMCs appeared confluent over the entire luminal surface of the scaffold on day seven (scale bar = 100 µm). (B) Fenestrations in confluent SMC monolayers were 5 µm or less in all areas inspected by SEM (scale bar = 10 µm). (C) Multiple SMC monolayers were observed in cross-section, indicating that penetration of the luminal surface by cells was not possible (scale bar = 100 µm). Biological materials such as SMCs and protein were observed throughout the wall of transversely sectioned type V scaffold segments and a partially-confluent layer of SMCs was visible on the abluminal surface.

Limitations of the Experimental Approach and Recommendations

Despite the implementation of detailed protocols, type V process yield and scaffold quality remained somewhat user-dependent, though to a lesser extent than other scaffold fabrication methods. Reproducible, small-scale partial automation in a laboratory could be achieved by using manually-operated equipment to load and pack salt (for example, by using a fixed salt mass, an appropriately-sized loading funnel, and a shaker), remove mandrels uniformly (using a hydraulic press with custom fixtures to hold glass tubing), and add PGS solution uniformly (using a syringe pump) similar to the slow end-over-end rotation already implemented for coating of glass tubes with hyaluronic acid.

This study neglected the effect of pore size and pore interconnectivity on scaffold properties and more especially on cell seeding efficiency and cellular confluence. Decreasing the pore size from 75-90 μm to values closer to the diameter of an individual unadhered SMC (which would be less than the diameter of ~10-20 μm observed on luminal surfaces after confluence) would be likely to improve cell adhesion to the scaffold and therefore seeding efficiency and cellular confluence. This study also presumptively focused on SMC-scaffold interactions and ignored interactions of other cell types with the scaffold, which may play a role in engineered vessel development, especially in the case of fibroblasts seeded abluminally.

Conclusions

A previously developed high-yield scaffold fabrication method was modified in two different ways to enable creation of truly seamless porous tubular scaffolds made from a biodegradable elastomer. Type V scaffolds (created with glass tubular molds and HS mandrels) exhibited five advantages over scaffolds made using other methods: (1) a decrease in wall thickness of 3.8-fold compared to type II and III scaffolds and 2.4-fold compared to type IV scaffolds; (2) tighter wall thickness tolerance; (3) improved mechanical properties and handling; (4) tighter tolerances for mechanical properties; and

(5) less time required to reach luminal cellular confluence. Type V scaffolds also exhibited other desirable qualities comparable to scaffolds made using other methods, including high yield and porosity, with similar microstructure, cell retention, and increases in cell quantity over time. A combined discussion of results from this and all other chapters and their implications is presented in Chapter 12.

CHAPTER 7

ENGINEERED VASCULAR CONSTRUCTS – INVESTIGATION OF THE EFFECT OF SMOOTH MUSCLE CELL SEEDING DENSITY

Introduction

SMC densities in initial engineered constructs based on PGS scaffolds compared poorly to native arteries in earlier experiments (see Figure 5.8). A simple way to substantially increase SMC densities and accelerate tissue development would be to increase the initial seeding density by saturating the scaffolds with an excess of SMCs. Since seeding efficiencies in earlier experiments were ~80% and SMC population doubling time was ~4.1 days during the first 10 days of culture, the scaffolds would likely accept a greater number of cells initially without adverse necrotic effects such as metabolite accumulation or CO_2 shortages. The purpose of this study was to compare engineered vascular constructs based on porous tubular PGS scaffolds and cultured with adult vascular SMCs seeded at two different densities and cultured under identical conditions, thereby providing insights into the effect of SMC seeding density on the properties of engineered vascular constructs. Materials and methods used in this chapter are described in Chapter 4.

Experimental Design

Baboon SMCs (passage 4-5) were seeded in two sets of PGS type IV scaffolds with through-wall flow for 15 min followed by luminal flow. One set of four type IV scaffolds received the normal initial density of SMCs and the other set received twice the normal initial density of SMCs. All scaffolds were cultured on the first-generation bioreactor. The flow rate was increased steadily from 1.0 ml/min (1.1 dynes/cm^2) on day

one to 14 ml/min (15 dynes/cm^2) on day 14. Flow was maintained at 14 ml/min until the end of the culture period (day 21). Medium was changed weekly with additional ascorbic acid being injected into the medium reservoirs three and five days after medium exchange. Cultured type IV scaffolds are denoted as type IV constructs.

Qualitative comparisons of uncultured scaffolds, engineered constructs, and baboon carotid arteries (positive control) included gross construct morphology, SEM, staining with H&E, and visualization of immunofluorescently-labeled collagens I and III. Quantitative comparisons included mechanical properties, total collagen and insoluble elastin content of wet tissue, and soluble elastin concentration in culture medium at the termination of culture.

Results and Discussion

Cell-Scaffold Interactions

Cell Seeding Efficiency

Cell seeding efficiency was evaluated qualitatively by macroscopically inspecting reservoir bottoms for cell aggregates and thick, confluent cell layers. Large cell aggregates and thick layers of cells had been visible within 24 hours of low-efficiency luminal (not through-wall) flow seeding (44 ± 8% versus 74 ± 4% seeding efficiency, respectively; see Chapter 5). A single large, tubular cell aggregate or sheet (longest dimension ~30 mm) was discovered on day seven in a reservoir used with type IV scaffolds receiving twice the normal initial density of SMCs (Figure 7.1). One of the constructs on this reservoir's circuit was flaccid rather than firm during removal from the bioreactor on day 21. This construct was excluded from analysis since it was assumed that the SMCs lining the lumen had been stripped out of the construct at some point during the first week of culture. Its paired construct was also excluded from analysis since the aggregate could have formed from cells shed to the reservoir by either construct

and collected at the circuit inlet by fluid currents. An exception to the paired construct's exclusion was later made during analysis of pressure-diameter data since its compliance closely matched that of other constructs in the group, but the construct had already been discarded and inclusion in other analyses was therefore impossible. No large aggregates or thick cell sheets were visible in any of the other reservoirs at any time point.

Figure 7.1: Adult Baboon Smooth Muscle Cell Loss from a Poly(glycerol sebacate) Type IV Scaffold Seeded at Twice-normal Smooth Muscle Cell Density. Photograph of a tubular cell aggregate or sheet (longest dimension ~30 mm) discovered at the end of the first week of culture in a reservoir feeding the flow loops of scaffolds receiving twice the normal initial density of SMCs.

Cellular Confluence

The luminal surface of baboon carotid arteries showed cellular confluence without cells adhering to the lumen (Figures 7.2A). Luminal surfaces of type IV constructs had confluent cellular layers with SMCs aligned perpendicular to the direction of flow and individual SMCs visible on construct lumens (Figures 7.2B-C). Larger quantities of individual cells could be seen on the luminal surfaces of type IV constructs seeded at twice-normal SMC density (Figure 7.2C). The luminal surface of type IV constructs appeared similar to over-confluent SMCs viewed with phase contrast microscopy in two-dimensional Petri dish culture, and this observation could indicate that higher SMC densities in three-dimensional culture may push SMCs toward a synthetic, proliferative phenotype.

A:

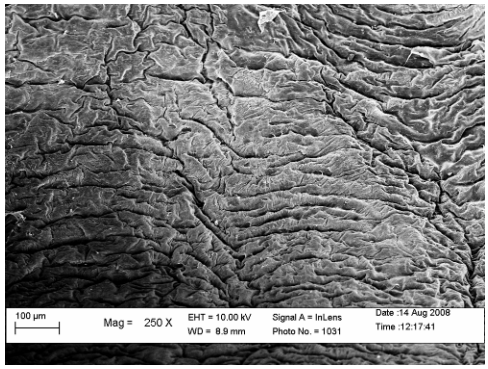

B:

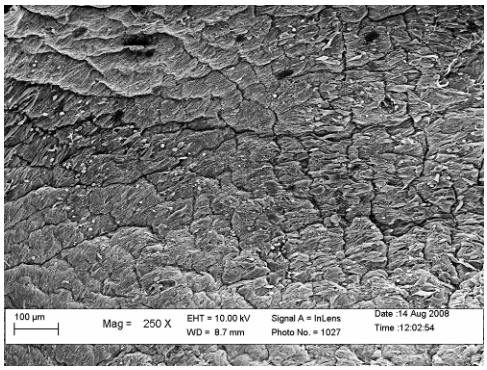

C:

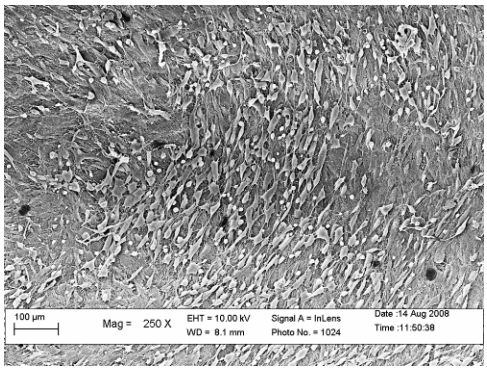

Figure 7.2: Effect of Smooth Muscle Cell Seeding Density on Luminal Confluence of Adult Baboon Smooth Muscle Cells Cultured in Poly(glycerol sebacate) Type IV Scaffolds for Twenty-one Days. Luminal surfaces of (A) baboon carotid arteries were confluent and devoid of cells, while luminal surfaces of type IV scaffolds seeded with adult baboon SMCs at (B) normal and (C) twice-normal cell density and cultured for 21 days were confluent but had individual SMCs visible on their luminal surfaces (scale bars = 100 µm). Larger quantities of SMCs were visible on lumens of type IV scaffolds seeded at twice-normal SMC density.

Gross Construct Morphology

Visual Observations

Engineered constructs visibly distended in a cyclic manner while subjected to pulsatile perfusion during *in vitro* culture. Type IV constructs retained a cylindrical shape upon removal from the bioreactor and had a wrinkled appearance that varied from the

smoother surface of baboon carotid arteries. No differences in handling were noted between type IV constructs seeded at normal or twice-normal SMC density, though both were less robust than baboon carotid arteries.

Histology

Baboon carotid arteries were compact and cells and protein were organized into circumferential bands within the artery wall, with some remaining *tunica adventitia* visible (Figure 7.3A). Type IV scaffolds showed minor absorption of H&E (Figure 7.3B). Type IV constructs seeded at normal SMC density had concentrations of cell nuclei and proteins at the luminal and abluminal surfaces, cell nuclei scattered throughout the scaffold walls, and circumferential wrinkles caused by compaction and filled by SMCs (Figure 7.3C). Doubling the initial SMC density appeared to shift the highest concentration of cells to the abluminal surface and also showed a lack of filling of compaction wrinkles by SMCs (Figure 7.3D).

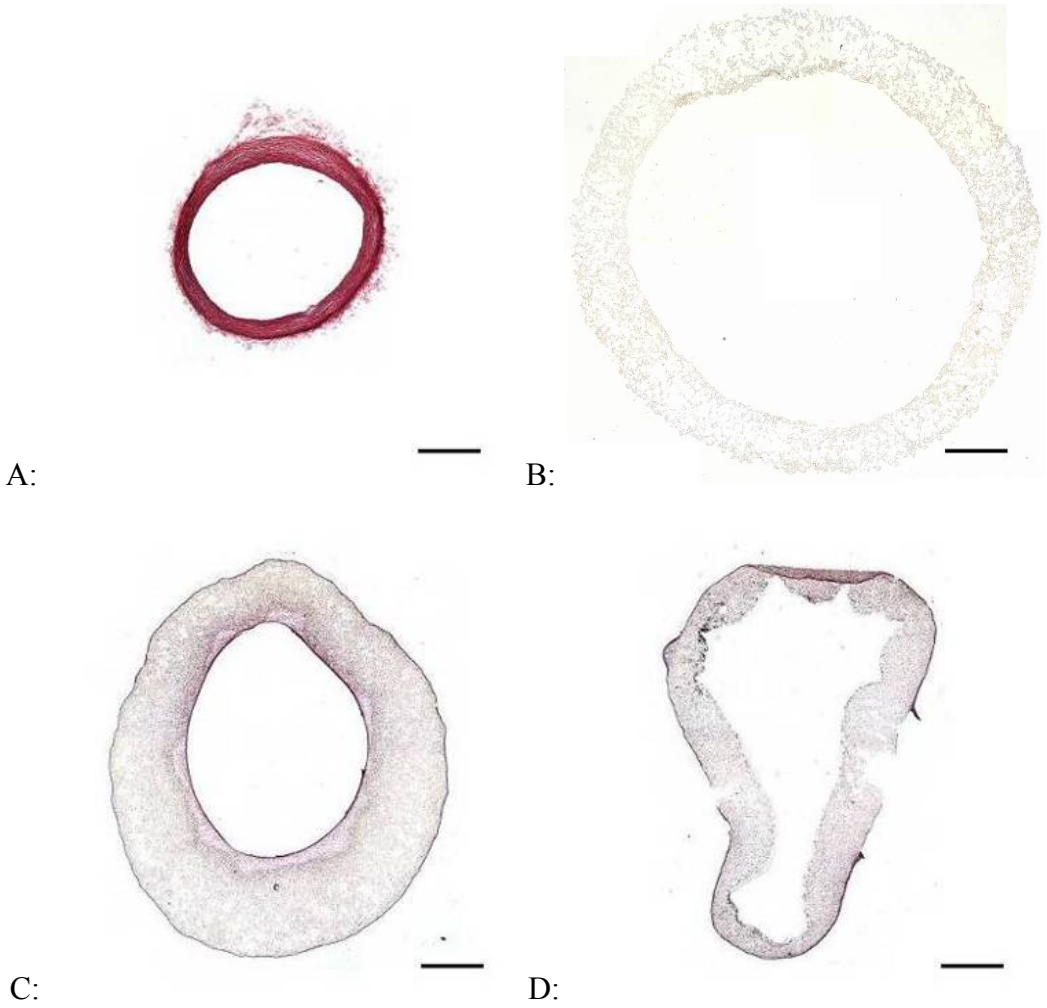

Figure 7.3: Effect of Smooth Muscle Cell Seeding Density on Histological Appearance of Type IV Constructs. Segments of baboon carotid arteries, type IV scaffolds cultured with adult baboon SMCs for 21 days, and uncultured type IV scaffolds were snap-frozen and cryosectioned. Cryosections were stained with H&E to qualitatively assess cell and protein distribution (scale bars = 1 mm). The *tunica adventitia* of baboon carotid arteries was removed prior to snap-freezing, and the artery cross-section shown has only the *tunicae media* and *intima* intact. (A) Baboon carotid arteries were dense and highly organized. (B) Uncultured type IV scaffolds showed minor absorption of H&E. (C) Type IV constructs seeded at normal SMC density had concentrations of cell nuclei and proteins at the luminal and abluminal surfaces and cell nuclei distributed throughout the scaffold walls. The scaffold appeared wrinkled, probably as a result of compaction by SMCs. (D) Type IV constructs seeded at twice-normal SMC density appeared to have a higher concentration of cell nuclei on the abluminal surface with a lack of luminal wrinkle-filling by SMCs.

Mechanical Properties of Engineered Constructs

Pressure-diameter Testing of Whole Constructs

Almost the entire length of each type IV construct was used for pressure-diameter testing to burst. (A small section near either end of each construct was cut off and set aside for cryosectioning and histological analysis prior to pressure-diameter testing.) In some cases the constructs were damaged during attachment to cannulae or stretch prior to testing, in which case the longest intact section of the construct was tested. The mode of failure in constructs was generally short longitudinal slits (~5 mm) that were approximately linear (see Figure 11.4). Other failure modes included circumferential slits and pinholes. Hysteresis in baboon carotid arteries and engineered constructs was observed only during the first cycle to each target pressure, with subsequent cycles demonstrating complete elastic recovery (data not shown).

Type IV constructs seeded at normal SMC density were significantly less compliant than baboon carotid arteries for target pressures of 55 mmHg and less, and type IV constructs seeded at twice-normal SMC density were also significantly less compliant than baboon carotid arteries for target pressures of 50 mmHg and less (Figure 7.4). Carotid arteries excised at different distances from the aorta showed the range of compliance in the baboon common carotid, with artery segments isolated at locations closer to the aorta showing higher compliance at a given pressure. Sharp increases in compliance immediately prior to vessel failure were most likely a result of tearing in luminal SMC sheets that had circumferentially wrinkled the scaffolds (see Visual Observations and Figure 7.3C).

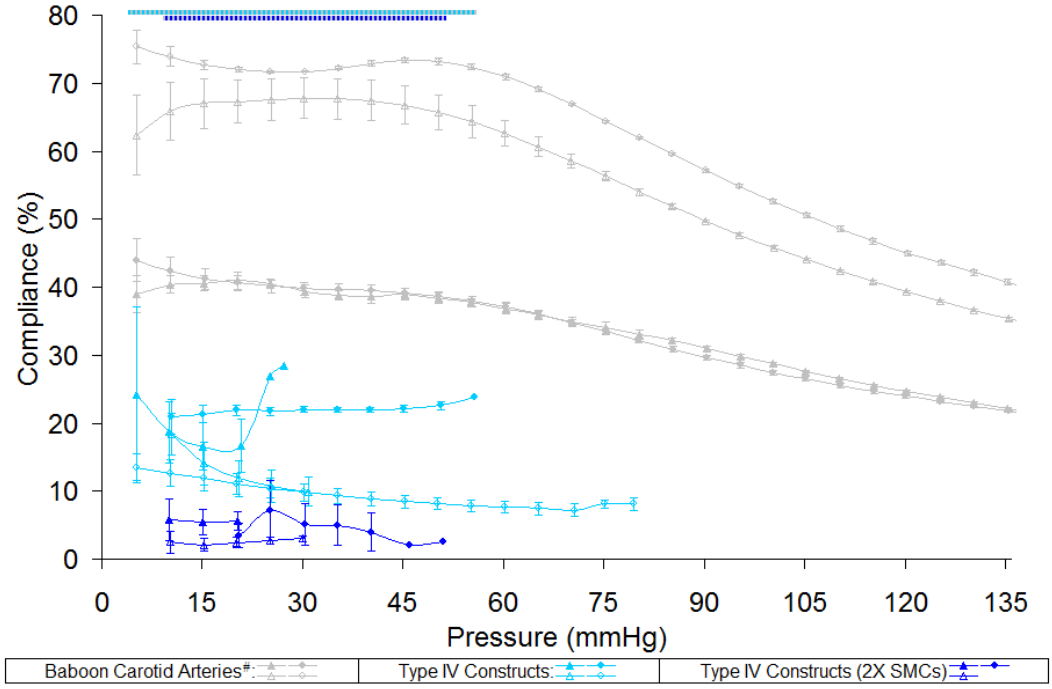

Figure 7.4: Effect of Smooth Muscle Cell Seeding Density on Compliance of Whole Type IV Constructs. Pressure-diameter testing of whole constructs was performed after type IV scaffolds were cultured for 21 days with adult baboon SMCs. Compliance was calculated for changes in diameter for each given zero-to-target pressure interval. Sharp increases in compliance immediately prior to vessel failure were most likely caused by tearing in luminal SMC sheets that circumferentially wrinkled the scaffolds (see Figure 7.3C). Similar lengths of baboon carotid arteries were tested for comparison. #The *tunica adventitia* of baboon carotid arteries was removed prior to testing, and results therefore represent properties of the *tunicae media* and *intima* only. The gray-and-light blue striped line indicates that type IV constructs seeded at normal SMC density (light blue, n = 4) were significantly less compliant than baboon carotid arteries (gray, n = 4) for target pressures of 55 mmHg and less. The gray-and-dark blue striped line indicates that type IV constructs seeded at twice-normal SMC density (dark blue, n = 3) were significantly less compliant than baboon carotid arteries (gray, n = 4) for target pressures of 50 mmHg and less.

The mean burst pressures of type IV constructs seeded at normal or twice-normal SMC density were not significantly different (Figure 7.5).

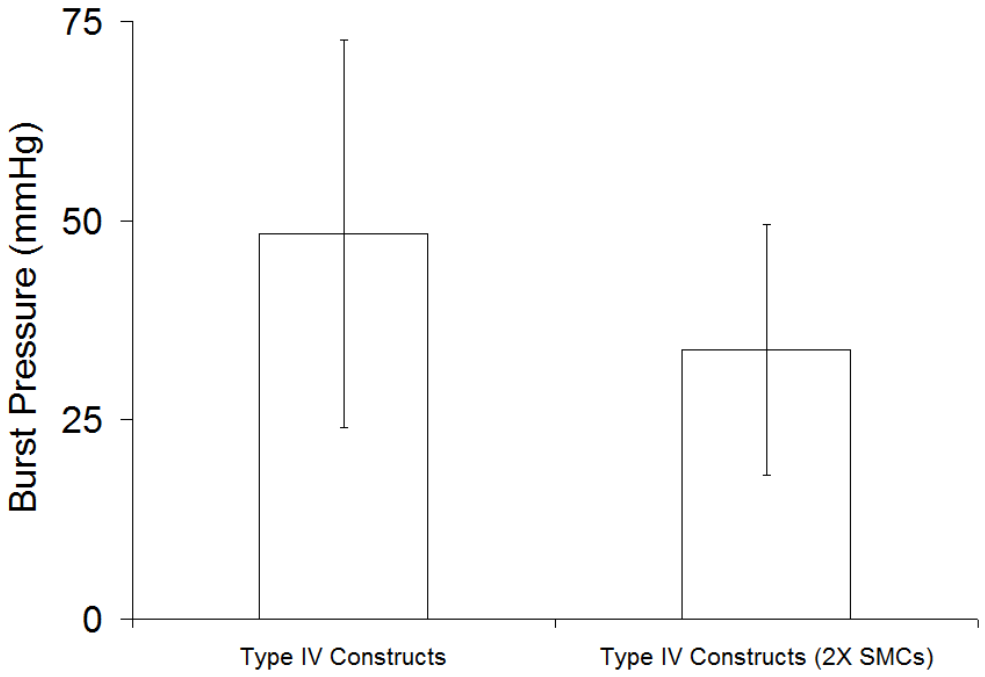

Figure 7.5: Effect of Smooth Muscle Cell Seeding Density on Burst Pressure of Whole Type IV Constructs. Pressure-diameter testing of whole constructs was performed after type IV scaffolds were cultured for 21 days with adult baboon SMCs. Burst pressure was taken as the highest pressure withstood by a construct at a rate of pressure increase of ~60 mmHg/min. Mean burst pressures of type IV constructs seeded at normal or twice-normal SMC density were not significantly different (n = 4 and 3 from left to right).

Extracellular Matrix Synthesis in Engineered Constructs

Collagen Content

Immunofluorescence

Baboon carotid arteries showed circumferentially-organized collagen I (FITC), collagen III (Rhodamine), and cell nuclei throughout the artery wall (Figure 7.6A). Uncultured type IV scaffolds absorbed DAPI and faintly autofluoresced but did not show antibody attachment (Figure 7.6B). Type IV constructs seeded at normal density showed collagen I and cell nuclei concentrated at the luminal and abluminal surfaces with collagens I and III and cell nuclei distributed throughout the construct wall (Figure 7.6C), while type IV constructs seeded at twice-normal density showed collagen I and cell nuclei concentrated at the abluminal surface and discontinuous concentrations of collagen I at the luminal surface with similar distributions of collagens I and III and cell nuclei throughout the construct wall (Figure 7.6D).

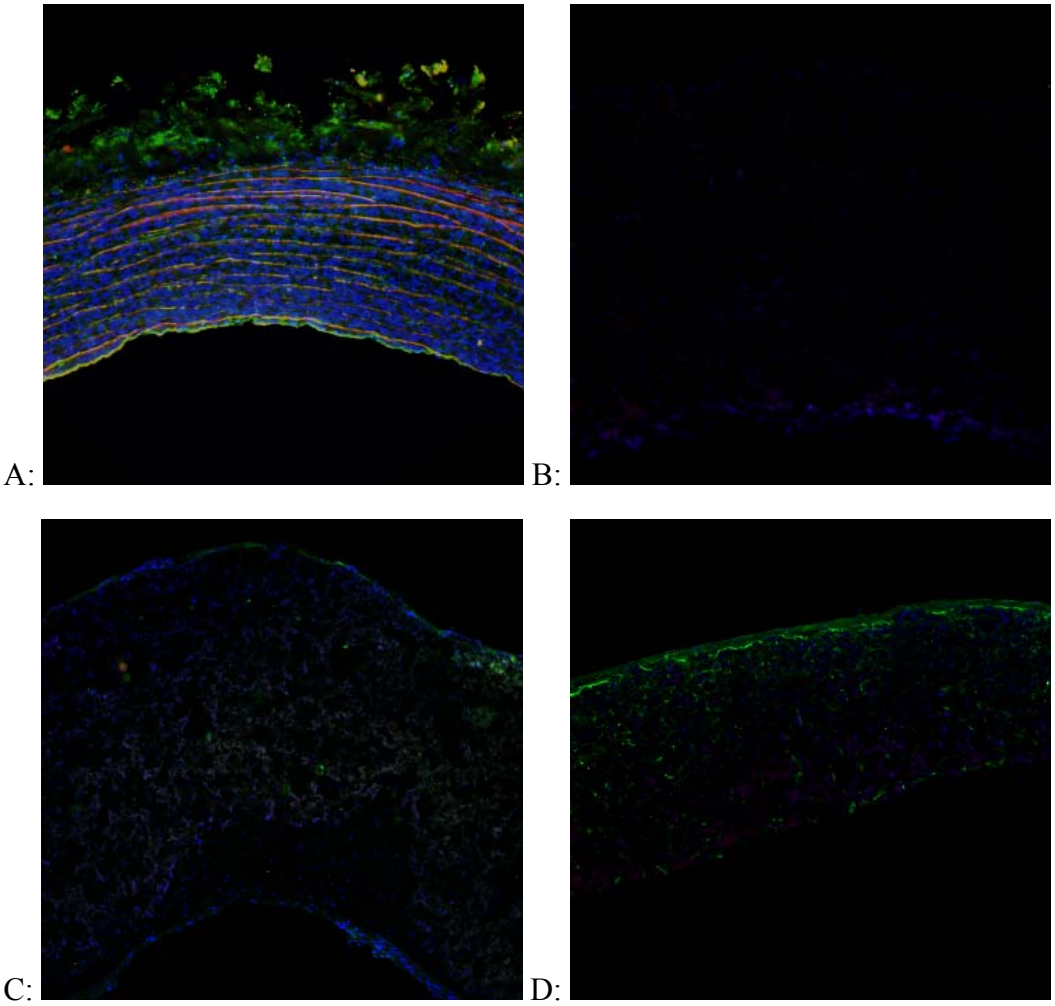

Figure 7.6: Effect of Smooth Muscle Cell Seeding Density on Distributions of Collagens I and III in Type IV Constructs. Segments of baboon carotid arteries, type IV scaffolds cultured with adult baboon SMCs for 21 days, and uncultured type IV scaffolds were snap-frozen and cryosectioned. Cryosections were immunofluorescently stained against collagen I (FITC) and collagen III (Rhodamine) to assess collagen distribution (magnification 10X). Staining with DAPI was used to assess distribution of SMCs. Collagens I and III and cell nuclei were stained and imaged in single locations, with images subsequently merged. All images are oriented with the luminal surface facing down. The *tunica adventitia* of baboon carotid arteries was removed prior to snap-freezing, and the artery cross-section shown has only the *tunicae media* and *intima* intact. (A) Baboon carotid arteries showed circumferentially-organized collagens I and III with cell nuclei throughout the artery wall. (B) Uncultured type IV scaffolds absorbed DAPI and faintly autofluoresced but did not show antibody attachment. (C) Type IV constructs seeded at normal SMC density showed collagen I and cell nuclei concentrated at the luminal and abluminal surfaces with collagens I and III and cell nuclei distributed throughout the construct wall. (D) Type IV constructs seeded at twice-normal SMC density showed collagen I and cell nuclei concentrated at the abluminal surface and

discontinuous concentrations of collagen I at the luminal surface with collagens I and III and cell nuclei distributed throughout the construct wall.

Colorimetric Analysis of Collagen Content

Baboon carotid arteries contained more collagen than Type IV constructs by more than an order of magnitude (Figure 7.7A). A statistical analysis performed by excluding the positive control (to create a valid basis of statistical comparison between experimental groups and controls by equalizing magnitudes in the standard deviations of the data) showed that all constructs had significantly higher collagen content than uncultured type V scaffolds and that type IV constructs seeded at twice-normal SMC density contained significantly more collagen than type IV constructs seeded at normal SMC density (Figure 7.7B).

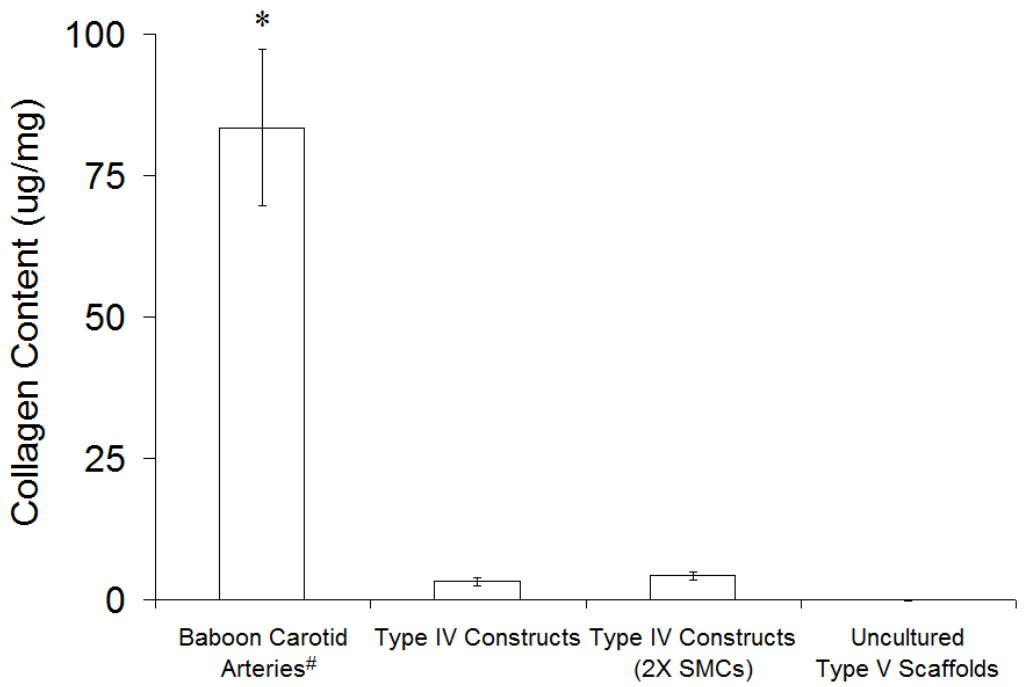

A:

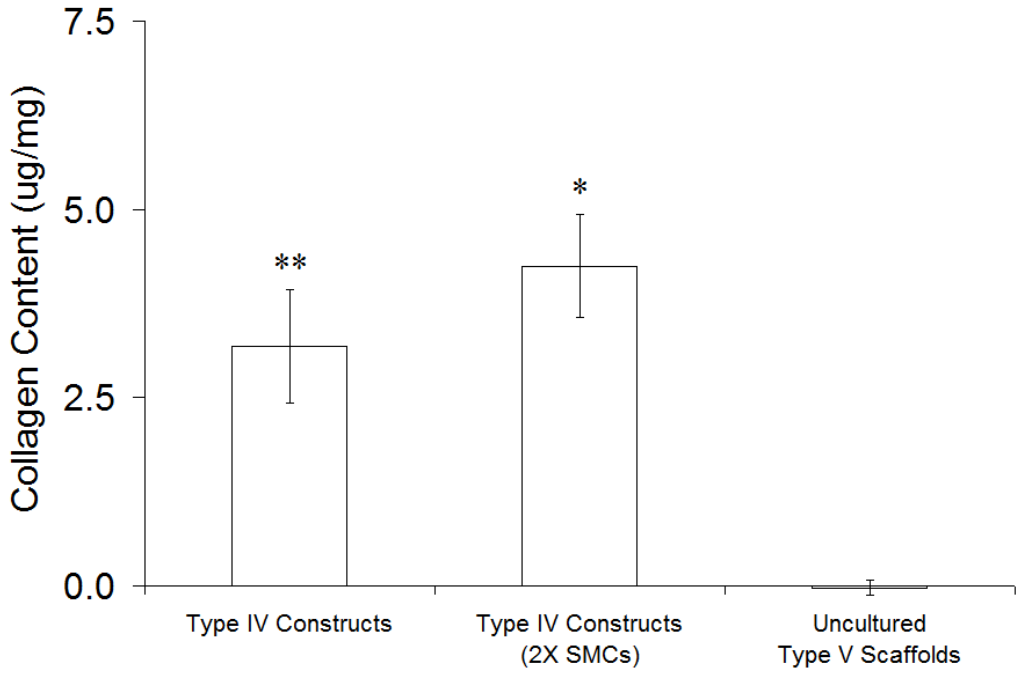

B:

Figure 7.7: Effect of Smooth Muscle Cell Seeding Density on Total Collagen Content in Type IV Constructs. Total collagen contents of baboon carotid arteries, type IV scaffolds cultured with adult baboon SMCs for 21 days, and uncultured type V scaffolds were measured indirectly by colorimetric quantification of hydroxyproline content. #The *tunica adventitia* of baboon carotid arteries was removed prior to testing, and results

therefore represent properties of the *tunicae media* and *intima* only. (A) All experimental groups and controls were initially included in the analysis (n = 4, 4, 2, and 8 from left to right). *Baboon carotid arteries had significantly higher collagen content than all other groups. (B) Dissimilar magnitudes of standard deviation between the positive control and all other groups prompted subsequent comparison of the experimental groups and the negative control only. *Type IV constructs seeded at twice-normal SMC density contained significantly more collagen than all other groups. **Type IV constructs seeded at normal SMC density contained significantly more collagen than uncultured type V scaffolds.

Elastin Content

Elastin Autofluorescence

Baboon carotid arteries showed circumferentially-organized elastin throughout the artery wall (Figure 7.8A). Uncultured type IV scaffolds were used for image thresholding and showed spots of faint autofluorescence under imaging conditions (Figure 7.8B). Type IV constructs seeded at normal density showed a concentration of elastin at the luminal surface (Figure 7.8C), while type IV constructs seeded at twice-normal density showed a concentration of elastin at the abluminal surface (Figure 7.8D).

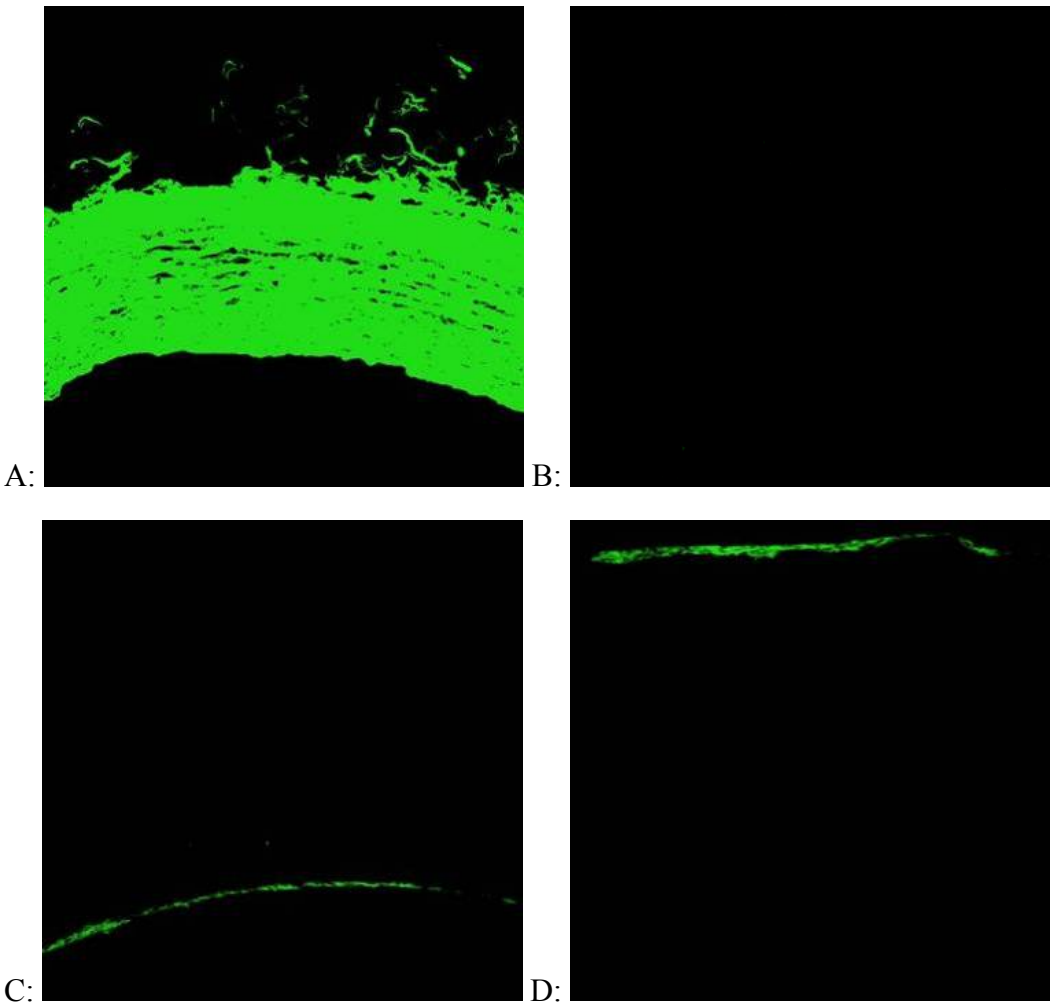

Figure 7.8: Effect of Smooth Muscle Cell Seeding Density on Elastin Distribution in Type IV Constructs. Segments of baboon carotid arteries, type IV scaffolds cultured with adult baboon SMCs for 21 days, and uncultured type IV scaffolds were snap-frozen and cryosectioned. Cryosections were excited at 488 nm and imaged to qualitatively assess elastin via autofluorescence (magnification 10X). All images are oriented with the luminal surface facing down. The *tunica adventitia* of baboon carotid arteries was removed prior to snap-freezing, and the artery cross-section shown has only the *tunicae media* and *intima* intact. (A) Baboon carotid arteries showed circumferentially-organized elastin throughout the artery wall. (B) The weak autofluorescence of uncultured type IV scaffolds was used for image intensity thresholding. (C) Type IV constructs seeded at normal SMC density showed a concentration of elastin at the luminal surface. (D) Type IV constructs seeded at twice-normal SMC density showed a concentration of elastin at the abluminal surface.

Colorimetric Analysis of Soluble and Insoluble Elastin Content

The soluble elastin concentration in culture medium collected from all construct chambers was higher than unused culture medium incubated with uncultured type V scaffolds (Figure 7.9). There was no significant difference in soluble elastin concentrations of medium collected from type IV constructs seeded at normal or twice-normal SMC density. Seeding type IV constructs at twice-normal SMC density was expected to increase the concentration of soluble elastin in medium by increasing quantities of SMCs during culture, suggesting that either (1) SMC quantities increased at lower rates when seeded at higher densities or (2) SMCs sensed the concentration of soluble elastin in their microenvironment and inversely altered elastin synthesis.

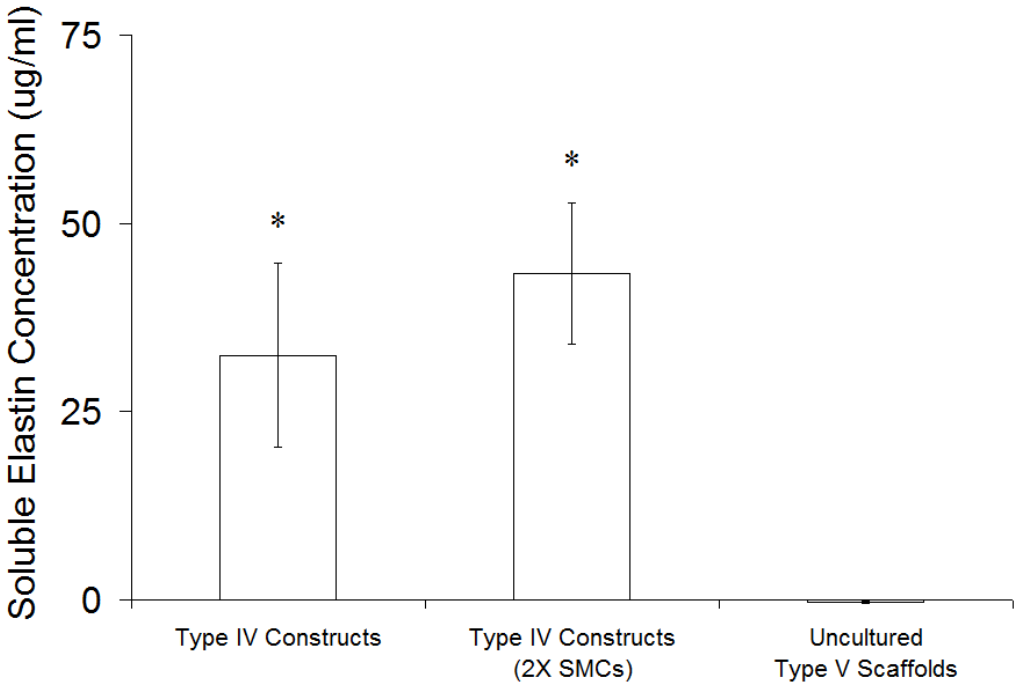

Figure 7.9: Effect of Smooth Muscle Cell Seeding Density on Soluble Elastin Concentration in Culture Medium of Type IV Constructs. Soluble elastin concentrations in culture medium collected at the termination of culture of type IV scaffolds for 21 days with adult baboon SMCs and in unused medium incubated with uncultured type V scaffolds were measured indirectly by a dye-binding assay and colorimetric quantification after centrifugation of medium to remove any insoluble elastin (n = 4, 2, and 10 from left to right). *Constructs seeded at normal or twice-normal SMC density released similar concentrations of soluble elastin into the culture medium which were significantly higher than concentrations measured in unused medium incubated with uncultured type V scaffolds.

Baboon carotid arteries contained significantly more insoluble elastin than all other groups (Figure 7.10). All type IV constructs had significantly more insoluble elastin content than uncultured type V scaffolds. Type IV constructs seeded at normal SMC density contained significantly more insoluble elastin than type IV constructs seeded at twice-normal SMC density, suggesting an inverse relationship between SMC density and

elastin crosslinking and incorporation into the ECM or between compliance and elastin crosslinking and deposition by SMCs.

Equal soluble elastin concentrations and significantly different insoluble elastin contents were possibly a result of high SMC density causing SMCs to shift from a synthetic, proliferative phenotype to a contractile, quiescent phenotype.[116] The lack of differences in elastin synthesis and crosslinking between type IV constructs seeded at different SMC densities indicated that SMCs might be shifting from a synthetic to a contractile phenotype in less than 21 days in three-dimensional *in vitro* culture under pulsatile flow. Another possible cause may be an inverse relationship between cell density and elastin crosslinking and incorporation into the ECM.

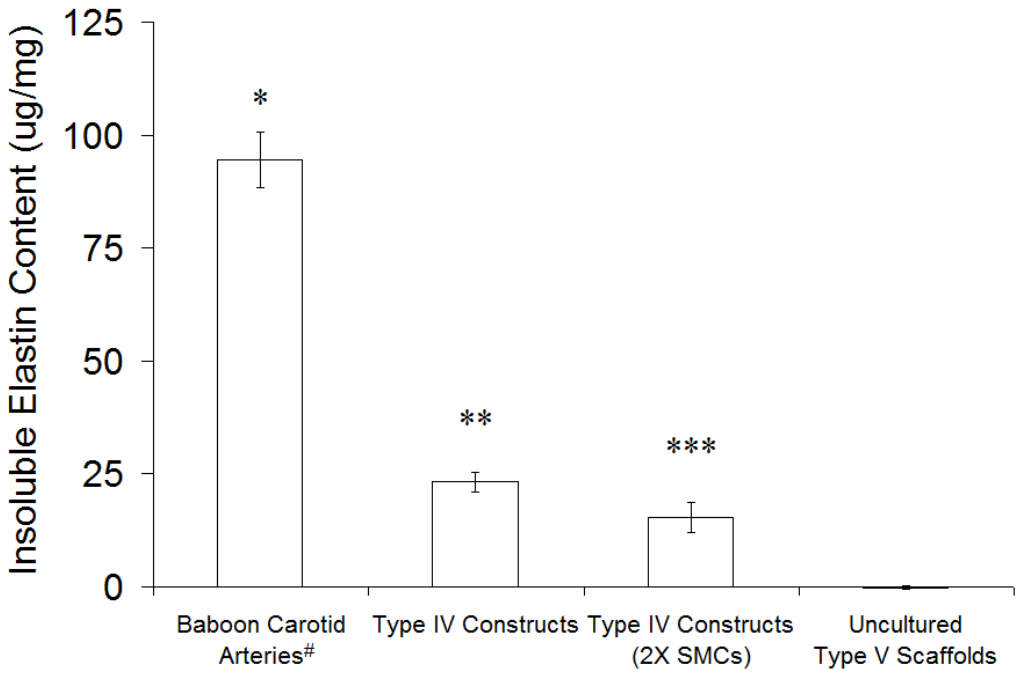

Figure 7.10: Effect of Smooth Muscle Cell Seeding Density on Insoluble Elastin Content in Type IV Constructs. Insoluble elastin contents of baboon carotid arteries, type IV scaffolds cultured with adult baboon SMCs for 21 days, and uncultured type V scaffolds were measured indirectly by a dye-binding assay and colorimetric quantification after acid hydrolysis, which destroyed all proteins except elastin, and centrifugation, which eliminated soluble elastin (n = 4, 4, 2, and 9 from left to right). #The *tunica adventitia* of baboon carotid arteries was removed prior to testing, and results therefore represent properties of the *tunicae media* and *intima* only. *Baboon carotid arteries contained significantly more insoluble elastin than all other groups. **Type IV constructs seeded at normal SMC density contained significantly more insoluble elastin compared to type IV constructs seeded at twice-normal SMC density and uncultured type IV scaffolds. ** Type IV constructs seeded at twice-normal SMC density contained significantly more insoluble elastin compared to uncultured type V scaffolds.

Limitations of the Experimental Approach and Recommendations

Medium components known to affect ECM synthesis and organization such as TGF-β1,[52] insulin,[52] and cupric sulfate activation of lysyl oxidase[117] would have the potential to increase collagen III and elastin synthesis and crosslinking, thereby

increasing compliance and the rate of development of engineered constructs *in vitro*. Lysyl oxidase is known to increase crosslinking of both elastin and collagen and would be most likely to alter construct compliance.[117,118] Results of this study also suggest that seeding at less-than-normal SMC density would increase the compliance of type IV constructs and shift it toward the compliance of native arteries.

Conclusions

Seeding type IV constructs with higher densities of SMCs appeared to shift SMCs, collagen I, and elastin toward the abluminal surface of constructs, significantly increased collagen content, and significantly decreased insoluble elastin content. A combined discussion of results from this and all other chapters and their implications is presented in Chapter 12.

CHAPTER 8

ENGINEERED VASCULAR CONSTRUCTS – INVESTIGATION OF THE EFFECT OF SCAFFOLD TYPE

Introduction

Defects that are orders of magnitude larger than individual cells may be difficult to correct by ECM synthesis and cell proliferation and migration without an extended *in vitro* culture period prior to implantation. Scaffold geometry and mechanical properties may therefore predict the mechanical properties of engineered constructs and be limiting factors in the potential development of homogeneous, dense, and highly-ordered engineered vascular constructs. Tolerances of scaffold properties may also be linked directly to tolerances in compliance and burst pressure of engineered constructs. The purpose of this study was to compare engineered vascular constructs based on porous tubular PGS type IV and V scaffolds cultured with adult vascular SMCs under identical conditions, thereby providing insights into the effect of scaffold type on the properties of engineered vascular constructs. Materials and methods used in this chapter are described in Chapter 4.

Experimental Design

Baboon SMCs (passage 4-5) were seeded at normal density in sets of four PGS type IV and V scaffolds with through-wall flow for 15 min followed by luminal flow. All scaffolds were cultured on the first-generation bioreactor. The flow rate was increased steadily from 1.0 ml/min (1.1 dynes/cm^2) on day one to 14 ml/min (15 dynes/cm^2) on day 14. Flow was maintained at 14 ml/min until the end of the culture period (day 21). Medium was changed weekly with additional ascorbic acid being injected into the

medium reservoirs three and five days after medium exchange. Cultured type IV and V scaffolds are respectively denoted as type IV and V constructs.

Qualitative comparisons of uncultured scaffolds, engineered constructs, and baboon carotid arteries (positive control) included gross construct morphology, SEM, staining with H&E, and visualization of immunofluorescently-labeled collagens I and III. Quantitative comparisons included mechanical properties, total collagen and insoluble elastin content of wet tissue, and soluble elastin concentration in culture medium at the termination of culture.

Results and Discussion

Cell-Scaffold Interactions

Cell Seeding Efficiency

Cell seeding efficiency was evaluated qualitatively by macroscopically inspecting reservoir bottoms for cell aggregates and thick, confluent cell layers. Large cell aggregates and thick layers of cells had been visible within 24 hours of low-efficiency luminal (not through-wall) flow seeding (44 ± 8% versus 74 ± 4% seeding efficiency, respectively; see Chapter 5). No large aggregates or thick cell sheets were visible in any of the reservoirs at any time point.

Cellular Confluence

The luminal surface of baboon carotid arteries showed cellular confluence without cells adhering to the lumen (Figures 8.1A). Luminal surfaces of type IV and V constructs had confluent cellular layers with SMCs aligned perpendicular to the direction of flow and individual SMCs visible on construct lumens (Figures 8.1B-C).

A:

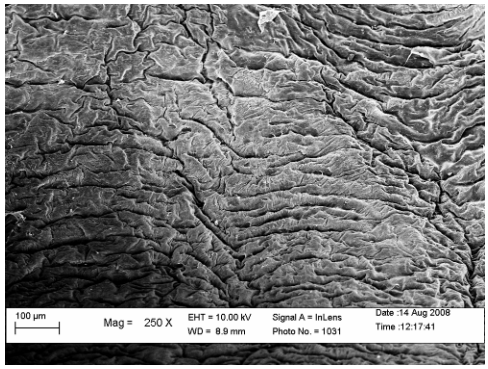

B:

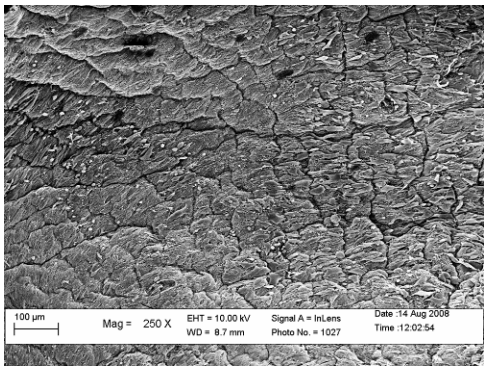

C:

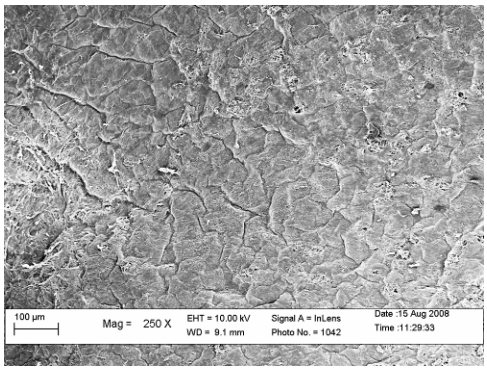

Figure 8.1: Effect of Scaffold Type on Luminal Confluence of Adult Baboon Smooth Muscle Cells Cultured in Poly(glycerol sebacate) Scaffolds for Twenty-one Days. Luminal surfaces of (A) baboon carotid arteries were confluent and devoid of cells, while luminal surfaces of (B) type IV and (C) type V scaffolds cultured with adult baboon SMCs for 10 days were confluent but had individual SMCs visible on their surfaces (scale bars = 100 µm).

Gross Construct Morphology

Visual Observations

Engineered constructs visibly distended in a cyclic manner while subjected to pulsatile perfusion during *in vitro* culture. Constructs retained a cylindrical shape upon removal from the bioreactor and had a wrinkled appearance that varied from the

smoother surface of baboon carotid arteries. No differences in handling were noted for type IV and V constructs, though both were less robust than baboon carotid arteries.

Histology

Baboon carotid arteries were compact and cells and protein were organized into circumferential bands within the artery wall, with some remaining *tunica adventitia* visible (Figure 8.2A). Type IV scaffolds showed minor absorption of H&E (Figure 8.2B), as did type V scaffolds (Figure 8.2C). Type IV constructs had concentrations of cell nuclei and proteins at the luminal and abluminal surfaces, cell nuclei scattered throughout the scaffold walls, and circumferential wrinkles caused by compaction and filled by SMCs (Figure 8.2D). Type V constructs appeared similar to type IV constructs (Figure 8.2E). Many of the engineered constructs showed the ability of the cells to fill macroscopic voids such as wrinkles after only days of *in vitro* culture, which was evidence against the hypothesis that macroscopic scaffold defects cannot be corrected by protein synthesis, ECM deposition and remodeling, and cell proliferation and migration without an extended *in vitro* culture period.

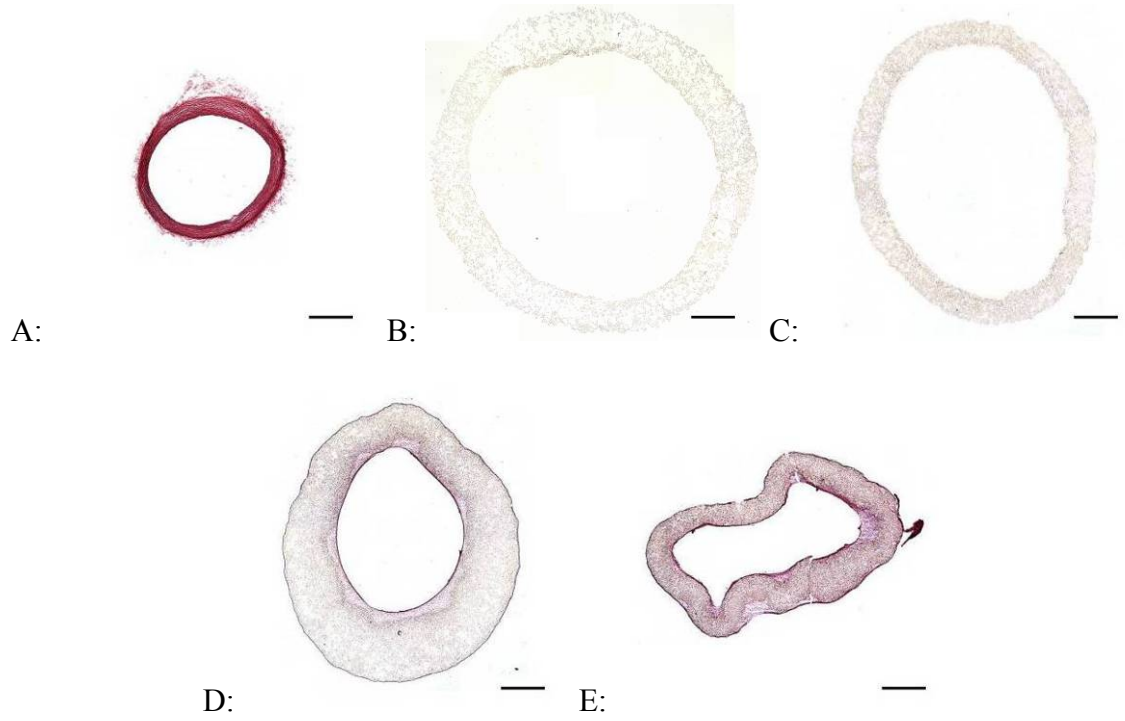

Figure 8.2: Effect of Scaffold Type on Histological Appearance of Engineered Constructs. Segments of baboon carotid arteries, type IV and V scaffolds cultured with adult baboon SMCs for 21 days, and uncultured type IV and V scaffolds were snap-frozen and cryosectioned. Cryosections were stained with H&E to qualitatively assess cell and protein distribution (scale bars = 1 mm). The *tunica adventitia* of baboon carotid arteries was removed prior to snap-freezing, and the artery cross-section shown has only the *tunicae media* and *intima* intact. (A) Baboon carotid arteries were dense and highly organized. (B) Uncultured type IV scaffolds showed minor absorption of H&E, as did (C) uncultured type V scaffolds. (D) Type IV constructs had concentrations of cell nuclei and proteins at the luminal and abluminal surfaces and cell nuclei distributed throughout the scaffold walls. The scaffold appeared wrinkled, probably as a result of compaction by SMCs. (E) Distribution of cells and protein in type V constructs appeared similar to type IV constructs, though type V constructs showed greater wrinkling and compaction.

Mechanical Properties of Engineered Constructs

Pressure-diameter Testing of Whole Constructs

Almost the entire length of each type IV or V construct was used for pressure-diameter testing to burst. (A small section near either end of each construct was cut off and set aside for cryosectioning and histological analysis prior to pressure-diameter testing.) In some cases the constructs were damaged during attachment to cannulae or stretch prior to testing, in which case the longest intact section of the construct was tested. In one case a type V construct was damaged too extensively for burst pressure testing. The mode of failure in constructs was generally short longitudinal slits (~5 mm) that were approximately linear (see Figure 11.4). Other failure modes included circumferential slits and pinholes. Hysteresis in baboon carotid arteries (Figure 8.3A) and engineered type IV and V constructs (Figure 8.3B) was observed only during the first cycle to each target pressure, with subsequent cycles demonstrating complete elastic recovery.

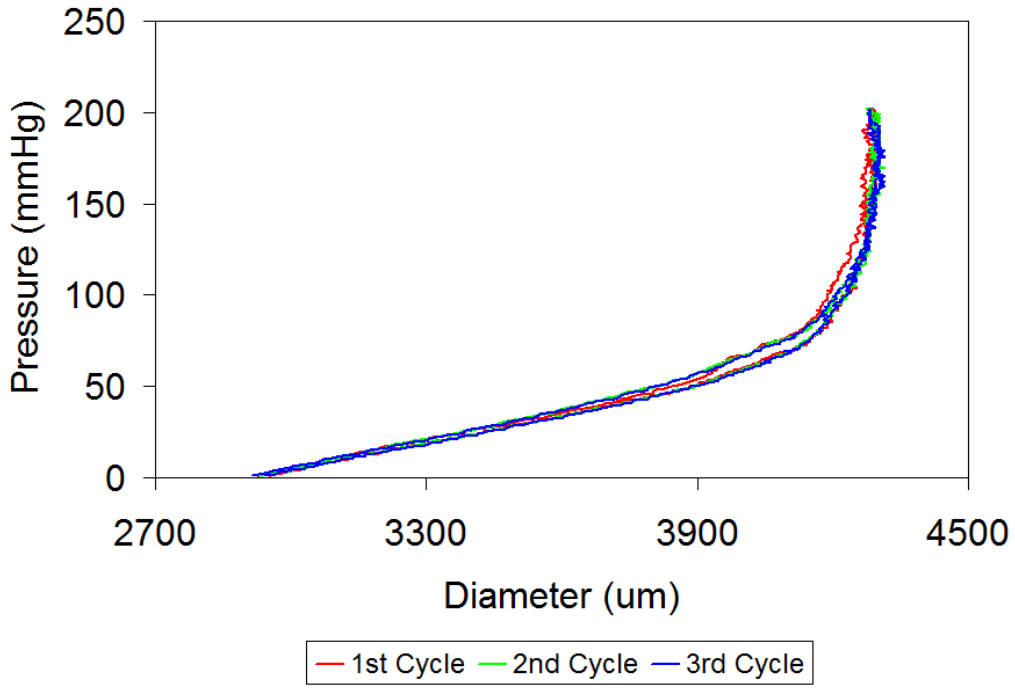

A:

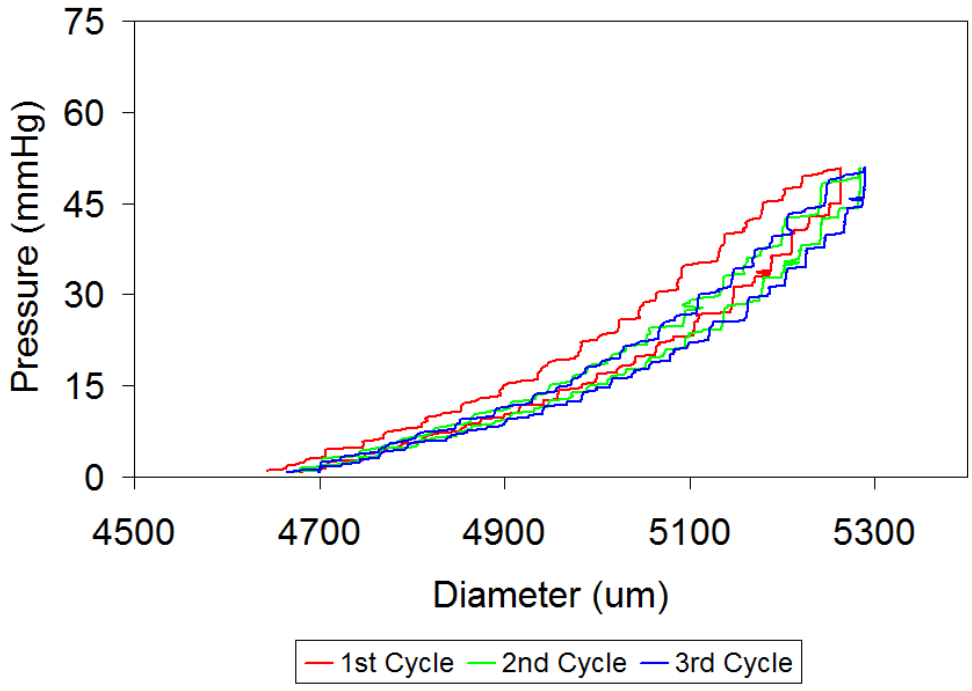

B:

Figure 8.3: Elastic Recovery of Whole Poly(glycerol sebacate)-based Type V Constructs Cultured for Twenty-one Days. Pressure-diameter testing of whole constructs was performed after type IV and V scaffolds were cultured for 21 days with adult baboon SMCs. Similar lengths of baboon carotid arteries were tested for comparison. The *tunica adventitia* of baboon carotid arteries was removed prior to

testing, and results therefore represent properties of the *tunicae media* and *intima* only. Complete elastic recovery was observed after the initial cycle to each target pressure in (A) baboon carotid arteries up to and including the highest pressure tested (200 mmHg) and in (B) type V constructs up to pressures near their burst pressure (cycles to a target pressure of 50 mmHg are shown for a construct with a burst pressure of 57 mmHg).

There was no significant difference between the compliance of baboon carotid arteries and type V constructs for any given target pressure (Figure 8.4). Type IV constructs were significantly less compliant than baboon carotid arteries for target pressures of 55 mmHg and less and significantly less compliant than type V constructs for a target pressure of 10 mmHg. Carotid arteries excised at different distances from the aorta showed the range of compliance in the baboon common carotid, with artery segments isolated at locations closer to the aorta showing higher compliance at a given pressure. Sharp increases in compliance immediately prior to vessel failure were most likely a result of tearing in luminal SMC sheets that had circumferentially wrinkled the scaffolds (see Visual Observations and Figures 8.2C-D).

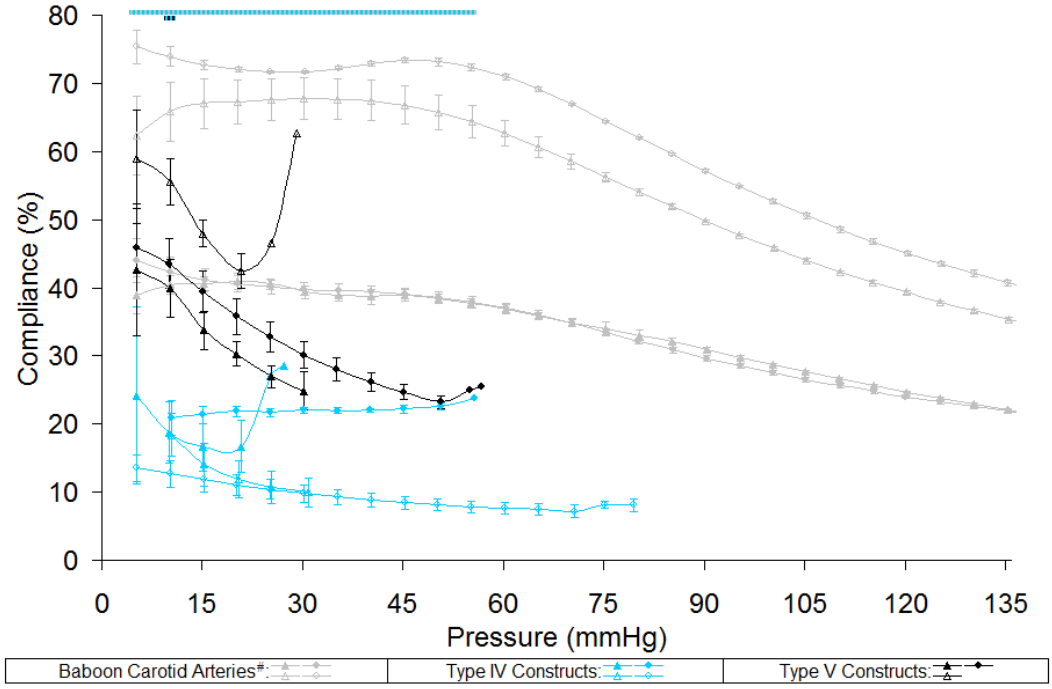

Figure 8.4: Effect of Scaffold Type on Compliance of Whole Engineered Constructs. Pressure-diameter testing of whole constructs was performed after type IV and V scaffolds were cultured for 21 days with adult baboon SMCs. Compliance was calculated for changes in diameter for each given zero-to-target pressure interval. Sharp increases in compliance immediately prior to vessel failure were most likely caused by tearing in luminal SMC sheets that circumferentially wrinkled the scaffolds (see Figure 8.2D-E). Similar lengths of baboon carotid arteries were tested for comparison. #The *tunica adventitia* of baboon carotid arteries was removed prior to testing, and results therefore represent properties of the *tunicae media* and *intima* only. There was no significant difference at any target pressure between the compliance of baboon carotid arteries (gray, n = 4) and type V constructs (black, n = 3). The gray-and-light blue striped line indicates that type IV constructs (light blue, n = 4) were significantly less compliant than baboon carotid arteries (gray, n = 4) for target pressures of 55 mmHg and less. The black-and-light blue striped line indicates that type IV constructs (light blue, n = 4) were significantly less compliant than type V constructs (black, n = 3) for a target pressure of 10 mmHg.

The mean burst pressures of type IV and V constructs were not significantly different (Figure 8.5).

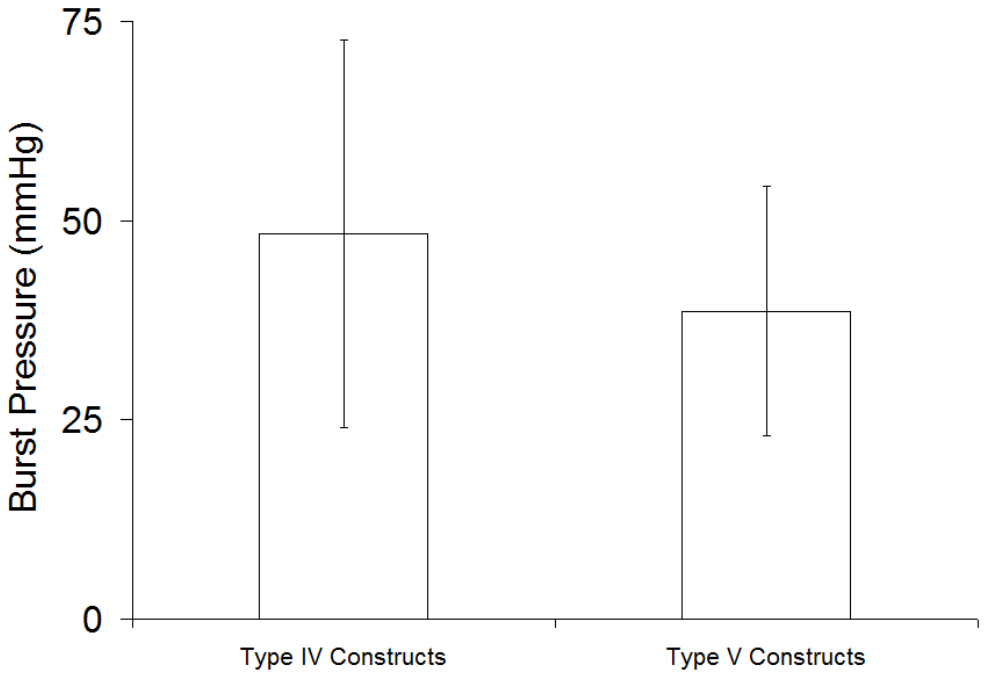

Figure 8.5: Effect of Scaffold Type on Burst Pressure of Whole Engineered Constructs. Pressure-diameter testing of whole constructs was performed after type IV and V scaffolds were cultured for 21 days with adult baboon SMCs. Burst pressure was taken as the highest pressure withstood by a construct at a rate of pressure increase of ~60 mmHg/min. Mean burst pressures of type IV and V constructs were not significantly different (n = 4 and 3 from left to right).

Extracellular Matrix Synthesis in Engineered Constructs

Collagen Content

Immunofluorescence

Baboon carotid arteries showed circumferentially-organized collagen I (FITC), collagen III (Rhodamine), and cell nuclei throughout the artery wall (Figure 8.6A). Uncultured type IV scaffolds (Figure 8.6B) and uncultured type V scaffolds (Figure 8.6C) absorbed DAPI and faintly autofluoresced but did not show antibody attachment. Type IV constructs showed collagen I and cell nuclei concentrated at the luminal and abluminal surfaces with collagens I and III and cell nuclei distributed throughout the construct wall (Figure 8.6D), as did type V constructs (Figure 8.6E).

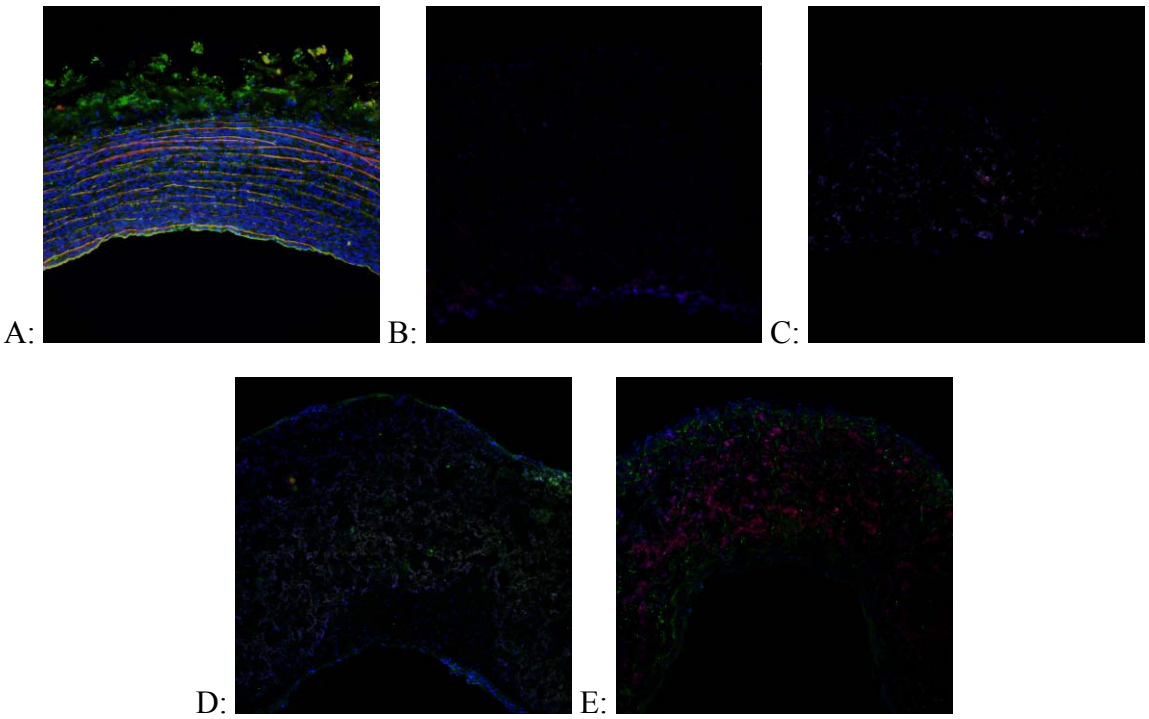

Figure 8.6: Effect of Scaffold Type on Distributions of Collagens I and III in Engineered Constructs. Segments of baboon carotid arteries, type IV and V scaffolds cultured with adult baboon SMCs for 21 days, and uncultured type IV and V scaffolds were snap-frozen and cryosectioned. Cryosections were immunofluorescently stained against collagen I (FITC) and collagen III (Rhodamine) to assess collagen distribution (magnification 10X). Staining with DAPI was used to assess distribution of SMCs. Collagens I and III and cell nuclei were stained and imaged in single locations, with images subsequently merged. All images are oriented with the luminal surface facing down. The *tunica adventitia* of baboon carotid arteries was removed prior to snap-freezing, and the artery cross-section shown has only the *tunicae media* and *intima* intact. (A) Baboon carotid arteries showed circumferentially-organized collagens I and III with cell nuclei throughout the artery wall. (B) Uncultured type IV scaffolds absorbed DAPI and faintly autofluoresced but did not show antibody attachment. (C) Uncultured type V scaffolds appeared similar to uncultured type IV scaffolds. (D) Type IV constructs showed collagen I and cell nuclei concentrated at the luminal and abluminal surfaces with collagens I and III and cell nuclei distributed throughout the construct wall. (E) Type V constructs showed cell nuclei concentrated at the luminal and abluminal surfaces with collagens I and III and cell nuclei distributed throughout the construct wall.

Colorimetric Analysis of Collagen Content

Baboon carotid arteries contained more collagen than type IV and V constructs by more than an order of magnitude (Figure 8.7A). A statistical analysis performed by excluding the positive control (to create a valid basis of statistical comparison between experimental groups and controls by equalizing magnitudes in the standard deviations of the data) showed that all constructs had significantly higher collagen content than uncultured type V scaffolds (Figure 8.7B). Type V constructs did not contain significantly more collagen than type IV constructs, suggesting that increased protein synthesis and ECM deposition could not be achieved by significantly reducing scaffold wall thickness (as in the case of type V scaffolds) to facilitate nutrient passage.

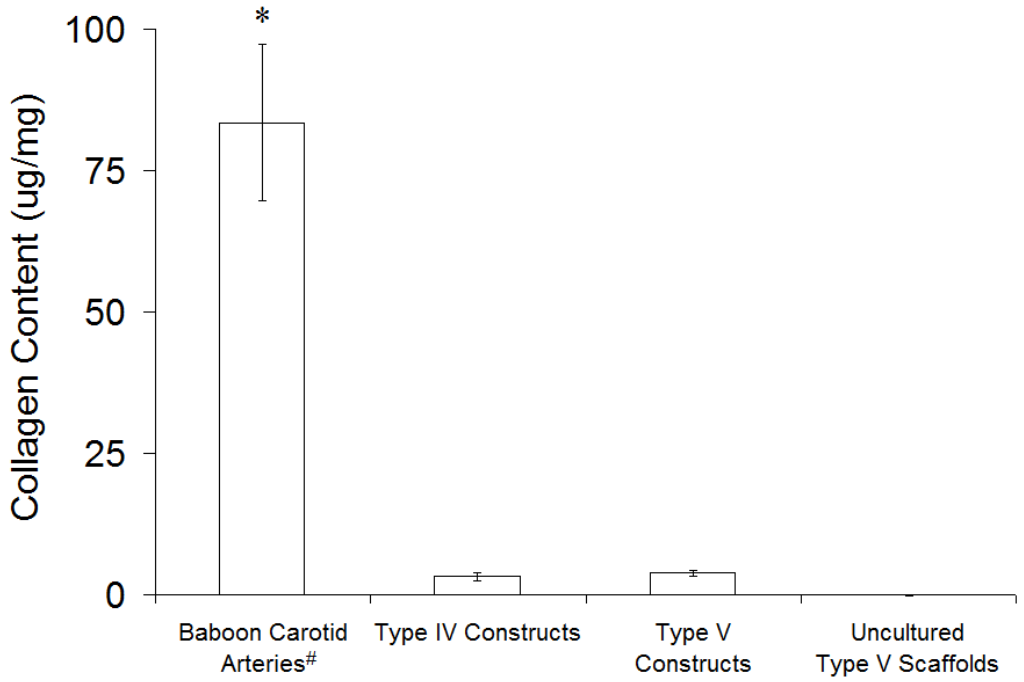

A:

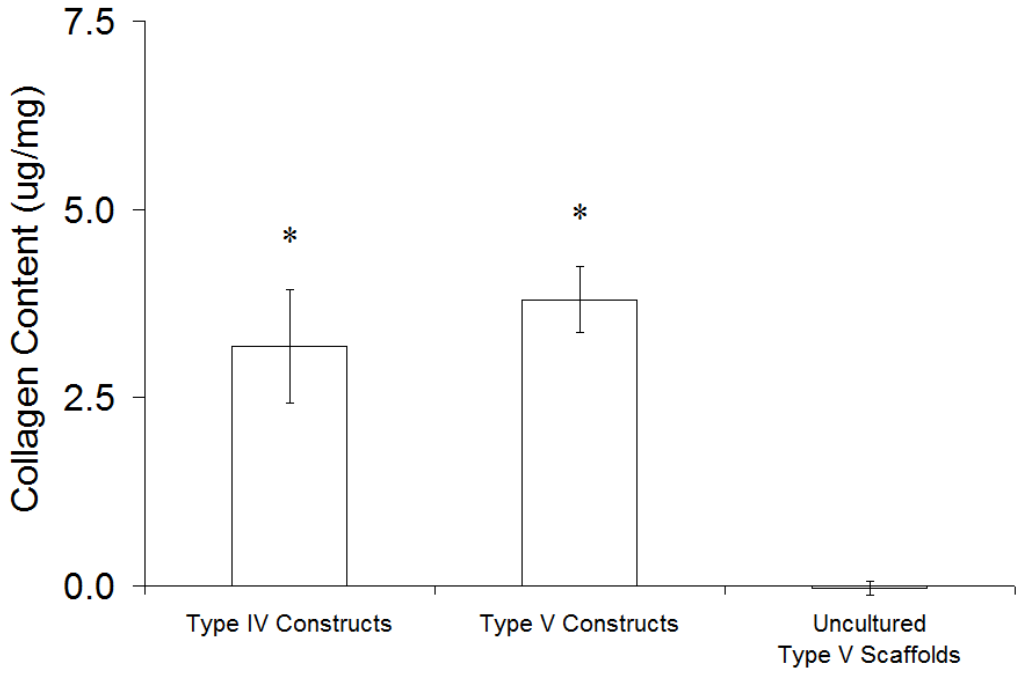

B:

Figure 8.7: Effect of Scaffold Type on Total Collagen Content in Engineered Constructs. Total collagen contents of baboon carotid arteries, type IV and V scaffolds cultured with adult baboon SMCs for 21 days, and uncultured type V scaffolds were measured indirectly by colorimetric quantification of hydroxyproline content. #The *tunica adventitia* of baboon carotid arteries was removed prior to testing, and results therefore

represent properties of the *tunicae media* and *intima* only. (A) All experimental groups and controls were initially included in the analysis (n = 4, 4, 4, and 8 from left to right). *Baboon carotid arteries had significantly higher collagen content than all other groups. (B) Dissimilar magnitudes of standard deviation between the positive control and all other groups prompted subsequent comparison of the experimental groups and the negative control only. *Type IV and V constructs contained significantly more collagen than uncultured type V scaffolds.

Elastin Content

Elastin Autofluorescence

Baboon carotid arteries showed circumferentially-organized elastin throughout the artery wall (Figure 8.8A). Uncultured type IV scaffolds (Figure 8.8B) and uncultured type V scaffolds (Figure 8.8C) were used for image thresholding and showed spots of faint autofluorescence under imaging conditions. Type IV constructs showed a concentration of elastin at the luminal surface (Figure 8.8D), while type V constructs showed concentrations of elastin at the luminal and abluminal surfaces (Figure 8.8E).

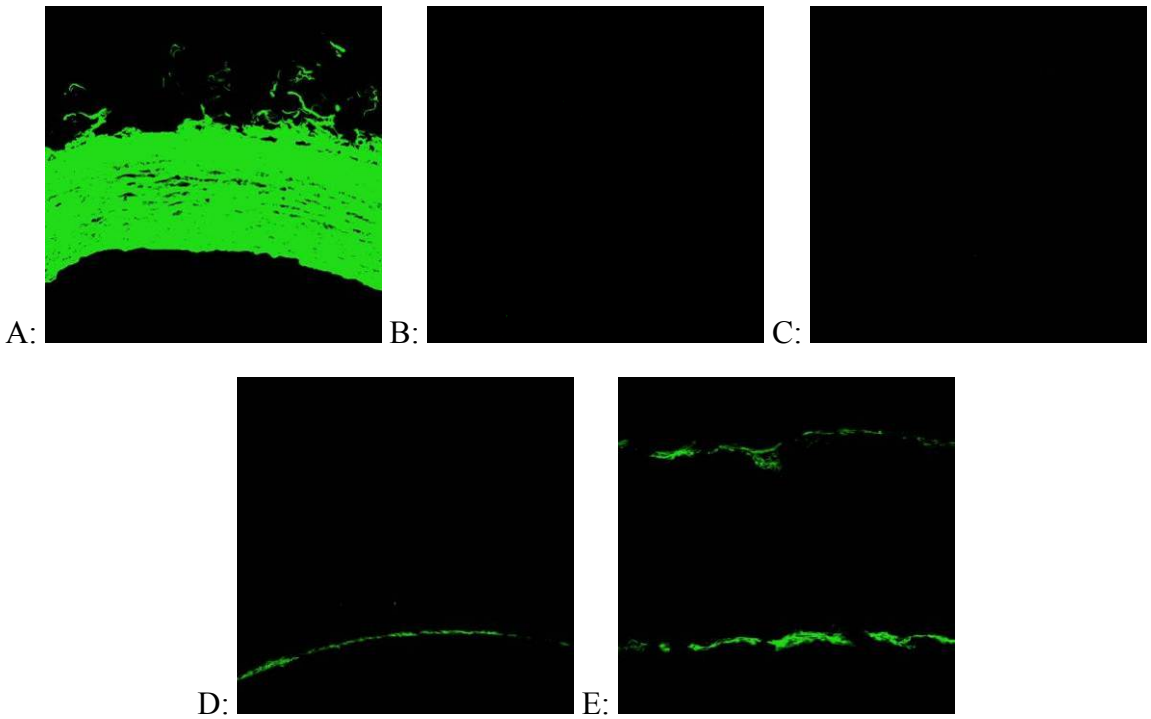

Figure 8.8: Effect of Scaffold Type on Elastin Distribution in Engineered Constructs. Segments of baboon carotid arteries, type IV and V scaffolds cultured with adult baboon SMCs for 21 days, and uncultured type IV and V scaffolds were snap-frozen and cryosectioned. Cryosections were excited at 488 nm and imaged to qualitatively assess elastin via autofluorescence (magnification 10X). All images are oriented with the luminal surface facing down. The *tunica adventitia* of baboon carotid arteries was removed prior to snap-freezing, and the artery cross-section shown has only the *tunicae media* and *intima* intact. (A) Baboon carotid arteries showed circumferentially-organized elastin throughout the artery wall. (B) The weak autofluorescence of uncultured type IV scaffolds and (C) uncultured type V scaffolds was used for image intensity thresholding. (D) Type IV constructs showed a concentration of elastin at the luminal surface. (E) Type V constructs showed concentrations of elastin at the luminal and abluminal surface.

Colorimetric Analysis of Soluble and Insoluble Elastin Content

The soluble elastin concentration in culture medium collected from type IV and V construct chambers was higher than unused culture medium incubated with uncultured type V scaffolds (Figure 8.9). This reinforced the suggestion by total collagen results that

increased protein synthesis and ECM deposition could not be achieved by significantly reducing scaffold wall thickness (as in the case of type V scaffolds) to facilitate nutrient passage.

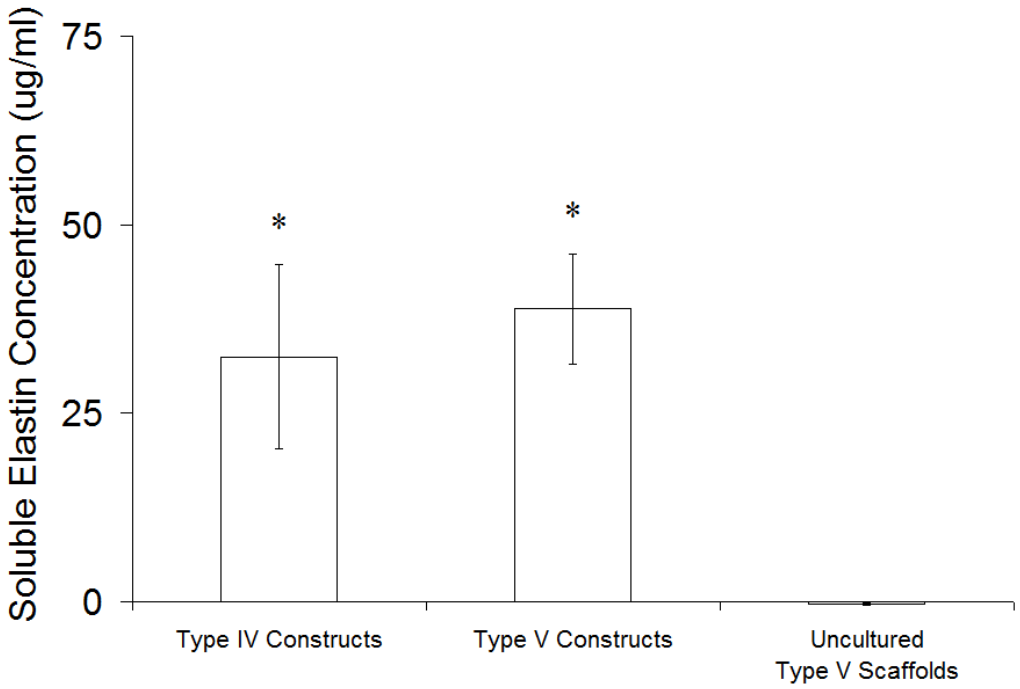

Figure 8.9: Effect of Scaffold Type on Soluble Elastin Concentration in Culture Medium of Engineered Constructs. Soluble elastin concentrations in culture medium collected at the termination of culture of type IV and V scaffolds for 21 days with adult baboon SMCs and in unused medium incubated with uncultured type V scaffolds were measured indirectly by a dye-binding assay and colorimetric quantification after centrifugation of medium to remove any insoluble elastin (n = 4, 4, and 10 from left to right). *Type IV and V constructs released similar concentrations of soluble elastin into the culture medium which were significantly higher than concentrations measured in unused medium incubated with uncultured type V scaffolds.

Baboon carotid arteries contained significantly more insoluble elastin than all other groups (Figure 8.10). Type V constructs contained significantly more insoluble elastin than type IV constructs and uncultured type V scaffolds. Type IV constructs contained significantly more insoluble elastin content than uncultured type V scaffolds. Significant differences in insoluble elastin content may have been caused by higher stresses and strains in type V scaffolds compared to type IV scaffolds during early stages of culture and higher compliance in type V constructs compared to type IV constructs during later stages of culture.

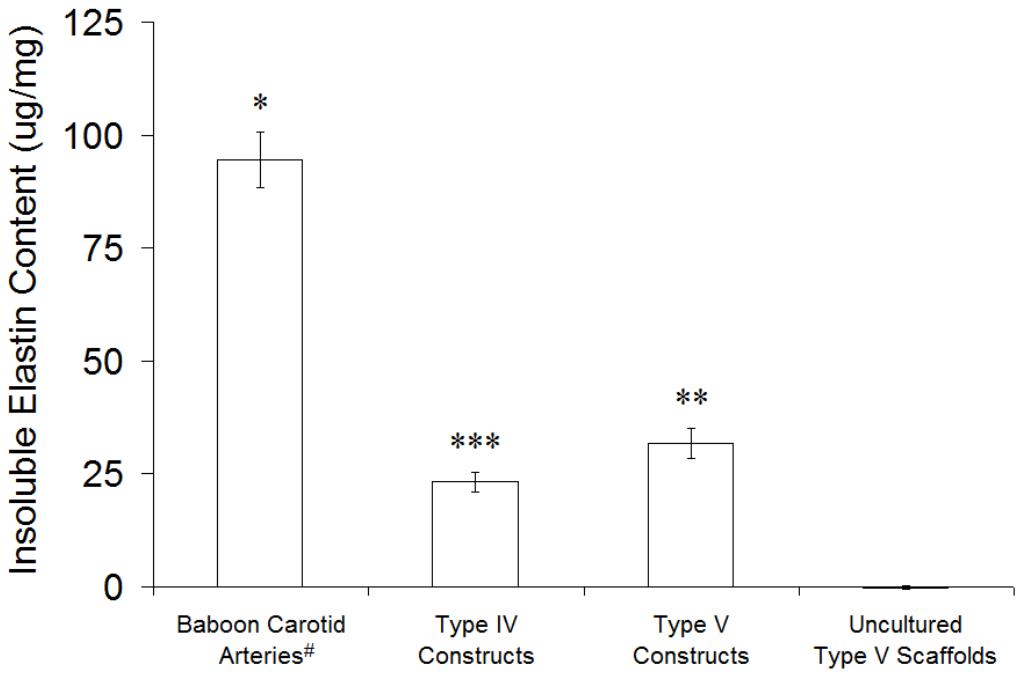

Figure 8.10: Effect of Scaffold Type on Insoluble Elastin Content in Engineered Constructs. Insoluble elastin contents of baboon carotid arteries, type IV and V scaffolds cultured with adult baboon SMCs for 21 days, and uncultured type V scaffolds were measured indirectly by a dye-binding assay and colorimetric quantification after acid hydrolysis of each construct, which destroyed all proteins except elastin, and centrifugation, which eliminated soluble elastin (n = 4, 4, 4, and 9 from left to right). #The *tunica adventitia* of baboon carotid arteries was removed prior to testing, and results therefore represent properties of the *tunicae media* and *intima* only. *Baboon carotid arteries contained significantly more insoluble elastin than all other groups. **Type V constructs contained significantly more insoluble elastin compared to type IV constructs and uncultured type V scaffolds. ***Type IV constructs contained significantly more insoluble elastin compared to uncultured type V scaffolds.

Limitations of the Experimental Approach and Recommendations

Causes of high variance in compliance and burst pressure of engineered constructs are probably attributable to inconsistent SMC seeding efficiency and initial SMC distribution on scaffold luminal surfaces, though scaffold properties may still play an obfuscatory role in variance. Additional evaluation of cell distribution within 24 hours

of seeding and improvements to seeding methods may enable further improvements in compliance and burst pressure of engineered constructs.

The burst pressures of engineered constructs were insufficient for grafting at high- or intermediate-pressure locations in an animal model without external reinforcement, which would reduce compliance. Construct burst pressures were especially inadequate for low-pressure clinical applications owing to high variance and the absence of any margin of safety.

Conclusions

Compliance was significantly higher in type V constructs compared to type IV constructs despite high variances. Culturing in type V rather than type IV scaffolds appeared to shift elastin from the luminal surface to both the luminal and abluminal surfaces and significantly increased insoluble elastin content. A combined discussion of results from this and all other chapters and their implications is presented in Chapter 12.

CHAPTER 9

ENGINEERED VASCULAR CONSTRUCTS – INVESTIGATION OF THE EFFECT OF IN VITRO CULTURE TIME

Introduction

The clinical application of tissue-engineered small-diameter arteries in urgent care will require shorter *in vitro* culture periods than those required by current benchmark blood vessel tissue engineering strategies. Shorter culture periods can also reduce costs and resources required for clinical care and decrease the possibility of undesirable tissue culture outcomes such as contamination. The purpose of this study was to compare engineered vascular constructs based on porous tubular PGS scaffolds cultured with adult vascular SMCs for 21 or 10 days, thereby providing insights into the effect of *in vitro* culture time on the properties of engineered vascular constructs. Materials and methods used in this chapter are described in Chapter 4.

Experimental Design

Baboon SMCs (passage 4-5) were seeded at normal density in two sets of four PGS type V scaffolds with through-wall flow for 15 min followed by luminal flow. All scaffolds were cultured on the first-generation bioreactor. The flow rate was increased steadily from 1.0 ml/min (1.1 dynes/cm^2) on day one to 10 ml/min (11 dynes/cm^2) on day 10, at which point one set of constructs was removed from the bioreactor for evaluation. For the remaining set of constructs, the flow rate was increased steadily from 10 ml/min (11 dynes/cm^2) on day 10 to 14 ml/min (15 dynes/cm^2) on day 14. Flow was maintained at 14 ml/min until the end of the culture period for the second set of construct (day 21). Medium was changed weekly with additional ascorbic acid being injected into the

medium reservoirs three and five days after medium exchange. Cultured type V scaffolds are denoted as type V constructs.

Qualitative comparisons of uncultured scaffolds, engineered constructs, and baboon carotid arteries (positive control) included gross construct morphology, SEM, staining with H&E, and visualization of immunofluorescently-labeled collagens I and III. Quantitative comparisons included mechanical properties, total collagen content and insoluble elastin content of wet tissue, and soluble elastin concentration in culture medium at the termination of culture.

Results and Discussion

Cell-Scaffold Interactions

Cell Seeding Efficiency

Cell seeding efficiency was evaluated qualitatively by macroscopically inspecting reservoir bottoms for cell aggregates and thick, confluent cell layers. Large cell aggregates and thick layers of cells had been visible within 24 hours of low-efficiency luminal (not through-wall) flow seeding (44 ± 8% versus 74 ± 4% seeding efficiency, respectively; see Chapter 5). No large aggregates or thick cell sheets were visible in any of the reservoirs at any time point.

Cellular Confluence

The luminal surface of baboon carotid arteries showed cellular confluence without cells adhering to the lumen (Figures 9.1A). Luminal surfaces of type V constructs cultured for 21 or 10 days had confluent cellular layers with SMCs aligned perpendicular to the direction of flow and individual SMCs visible on construct lumens (Figures 9.1B-C).

A:

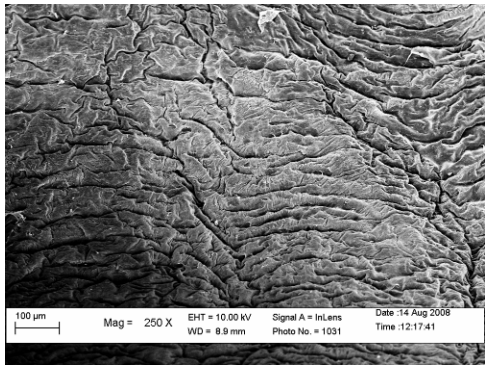

B:

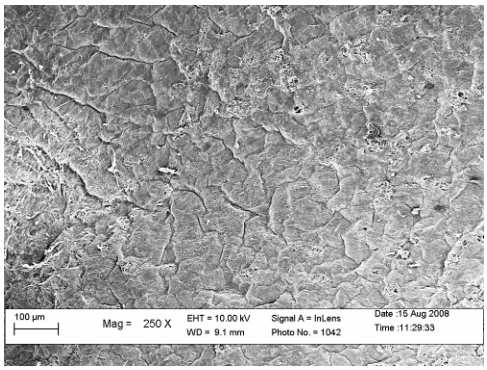

C:

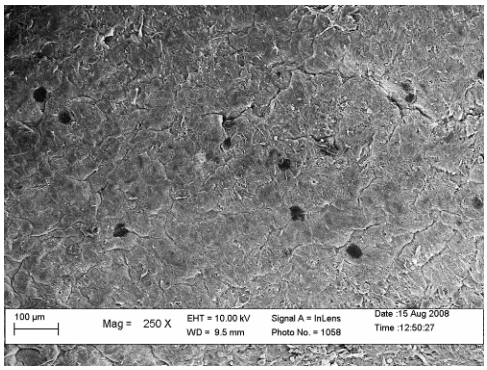

Figure 9.1: Effect of *in Vitro* Culture Time on Luminal Confluence of Adult Baboon Smooth Muscle Cells Cultured in Poly(glycerol sebacate) Type V Scaffolds for Twenty-one or Ten Days. Luminal surfaces of (A) baboon carotid arteries were confluent and devoid of cells, while luminal surfaces of (B) type V scaffolds cultured with adult baboon SMCs for 21 days and (C) type V constructs cultured for 10 days were confluent but had individual SMCs visible on their surfaces (scale bars = 100 µm).

Gross Construct Morphology

Visual Observations

Engineered constructs visibly distended in a cyclic manner while subjected to pulsatile perfusion during *in vitro* culture. Type V constructs retained a cylindrical shape upon removal from the bioreactor on day 21 or 10 and had a wrinkled appearance that varied from the smoother surface of baboon carotid arteries. Type V constructs cultured

for 10 days appeared less wrinkled compared to type V constructs cultured for 21 days. Greater scaffold compaction resulting from longer cultures times was the likely cause of the wrinkling. No differences in handling were noted for type V constructs cultured for 21 or 10 days, though both were less robust than baboon carotid arteries.

Histology

Baboon carotid arteries were compact and cells and protein were organized into circumferential bands within the artery wall, with some remaining *tunica adventitia* visible (Figure 9.2A). PGS type V scaffolds showed minor absorption of H&E (Figure 9.2B). Type V constructs cultured for 21 days had concentrations of cell nuclei and proteins at the luminal and abluminal surfaces, cell nuclei scattered throughout the scaffold walls, and circumferential wrinkles caused by compaction and filled by SMCs (Figure 9.2C), as did type V constructs cultured for 10 days (Figure 9.2D). Many of the engineered constructs showed the ability of the cells to fill macroscopic gaps after only days of *in vitro* culture, which indicated that culture periods employed by current benchmark blood vessel tissue engineering strategies may be excessive.

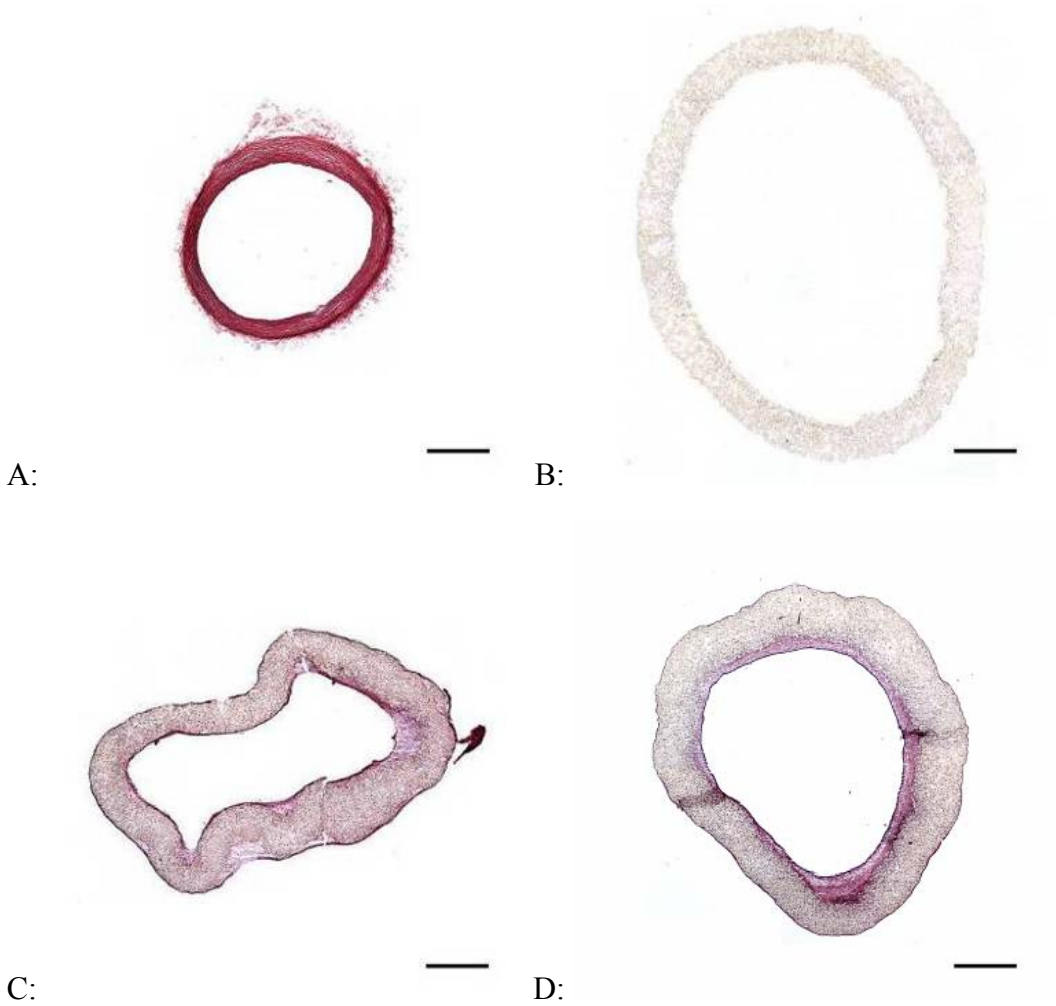

Figure 9.2: Effect of *in Vitro* Culture Time on Histological Appearance of Type V Constructs. Segments of baboon carotid arteries, type V scaffolds cultured with adult baboon SMCs for 21 or 10 days, and uncultured type V scaffolds were snap-frozen and cryosectioned. Cryosections were stained with H&E to qualitatively assess cell and protein distribution (scale bars = 1 mm). The *tunica adventitia* of baboon carotid arteries was removed prior to snap-freezing, and the artery cross-section shown has only the *tunicae media* and *intima* intact. (A) Baboon carotid arteries were dense and highly organized. (B) Uncultured type V scaffolds showed minor absorption of H&E. (C) Type V constructs cultured for 21 days had concentrations of cell nuclei and proteins at the luminal and abluminal surfaces and cell nuclei distributed throughout the scaffold walls. The scaffold appeared wrinkled, probably as a result of compaction by SMCs. (D) Type V constructs cultured for 10 days appeared similar to type V constructs cultured for 21 days, though type V constructs cultured for 21 days showed greater wrinkling and compaction.

Mechanical Properties of Engineered Constructs

Pressure-diameter Testing of Whole Constructs

Almost the entire length of each type V construct was used for pressure-diameter testing to burst. (A small section near either end of each construct was cut off and set aside for cryosectioning and histological analysis prior to pressure-diameter testing.) In some cases the constructs were damaged during attachment to cannulae or stretch prior to testing, in which case the longest intact section of the construct was tested. In one case a type V construct cultured for 21 days was damaged too extensively for burst pressure testing. The mode of failure in constructs was generally short longitudinal slits (~5 mm) that were approximately linear (see Figure 11.4). Other failure modes included circumferential slits and pinholes. Hysteresis in baboon carotid arteries and engineered constructs was observed only during the first cycle to each target pressure, with subsequent cycles demonstrating complete elastic recovery (see Figure 10.7).

There was no significant difference between the compliance of baboon carotid arteries and type V constructs cultured for 21 days for any given target pressure (Figure 9.3). Type V constructs cultured for 10 days were significantly more compliant than baboon carotid arteries for target pressures of 10 mmHg and less. Type V constructs cultured for 10 days were significantly more compliant than type V constructs cultured for 21 days for target pressures of 15 mmHg and less. Carotid arteries excised at different distances from the aorta showed the range of compliance in the baboon common carotid, with artery segments isolated at locations closer to the aorta showing higher compliance at a given pressure. Sharp increases in compliance immediately prior to vessel failure were most likely a result of tearing in luminal SMC sheets that had circumferentially wrinkled the scaffolds (see Visual Observations and Figure 9.2C), an idea which was reinforced by the absence of sharp increases in compliance prior to failure of type V constructs cultured for 10 days which showed less wrinkling (see Figure 9.2D).

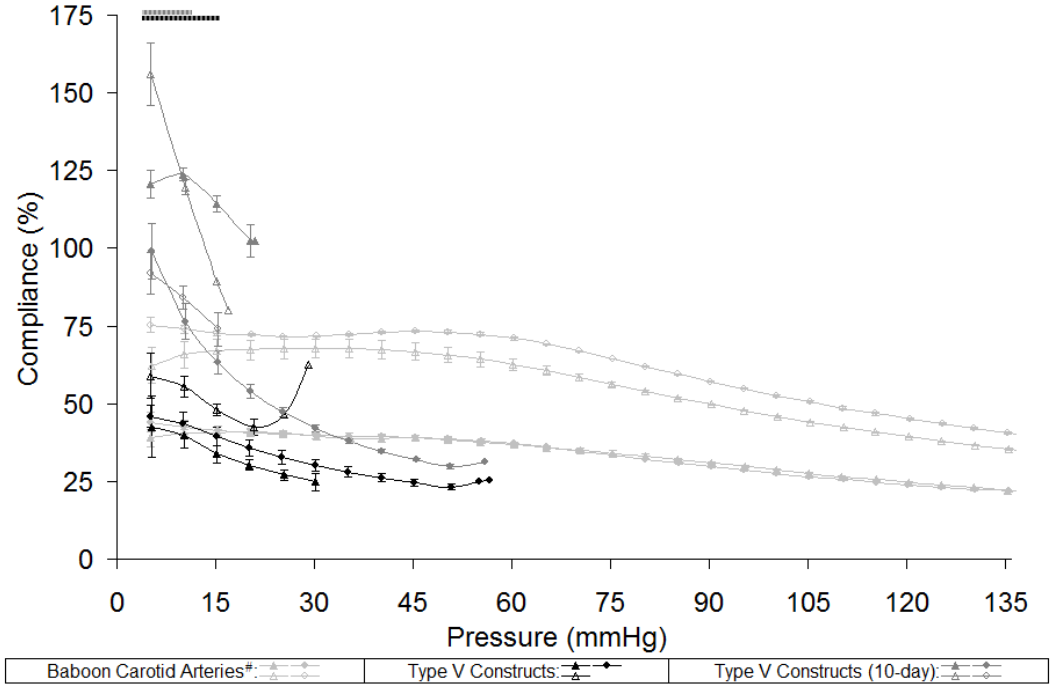

Figure 9.3: Effect of *in Vitro* Culture Time on Compliance of Whole Type V Constructs. Pressure-diameter testing of whole constructs was performed after type V scaffolds were cultured for 21 or 10 days with adult baboon SMCs. Compliance was calculated for changes in diameter for each given zero-to-target pressure value. Sharp increases in compliance immediately prior to vessel failure were most likely caused by tearing in luminal SMC sheets that circumferentially wrinkled the scaffolds (see Figure 9.2C). Similar lengths of baboon carotid arteries were tested for comparison. #The *tunica adventitia* of baboon carotid arteries was removed prior to testing, and results therefore represent properties of the *tunicae media* and *intima* only. There was no significant difference between the compliance of baboon carotid arteries (gray, n = 4) and type V constructs cultured for 21 days (black, n = 3) for any target pressure. The gray-and-dark gray striped line indicates that type V constructs cultured for 10 days (dark gray, n = 4) were significantly more compliant than baboon carotid arteries (gray, n = 4) for target pressures of 10 mmHg and less. The black-and-dark gray striped line indicates that type V constructs cultured for 10 days (dark gray, n = 4) were significantly more compliant than type V constructs cultured for 21 days (black, n = 3) for target pressures of 15 mmHg and less.

The mean burst pressures of type V constructs cultured for 21 or 10 days were not significantly different (Figure 9.4).

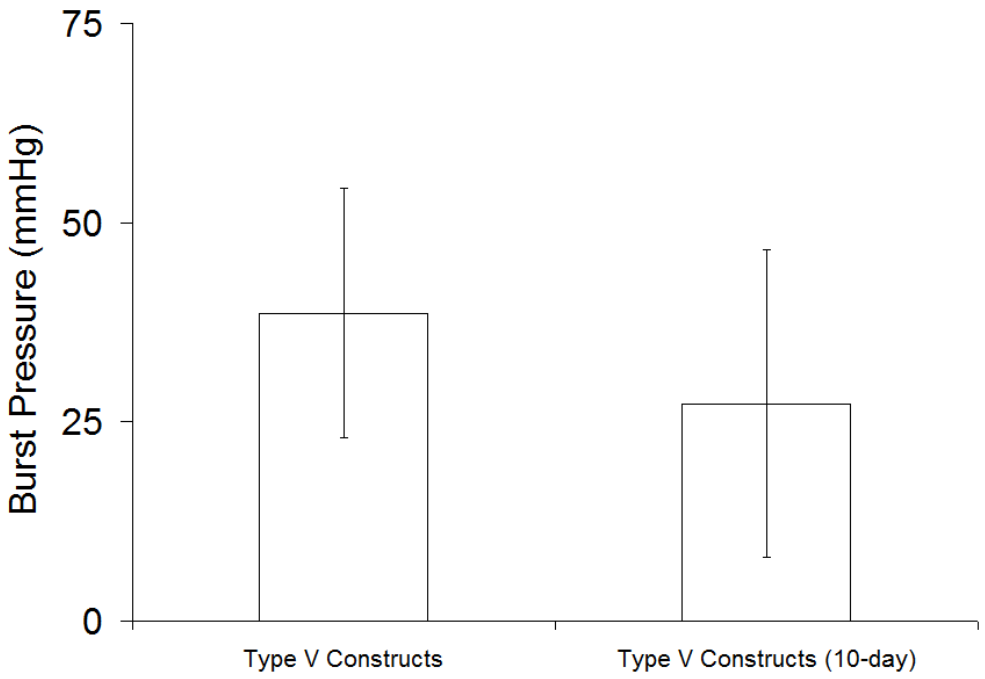

Figure 9.4: Effect of *in Vitro* Culture Time on Burst Pressure of Whole Type V Constructs. Pressure-diameter testing of whole constructs was performed after type V scaffolds were cultured for 21 or 10 days with adult baboon SMCs. Burst pressure was taken as the highest pressure withstood by a construct at a rate of pressure increase of ~60 mmHg/min. Mean burst pressures of type V constructs cultured for 21 or 10 days were not significantly different (n = 3 and 4 from left to right).

Extracellular Matrix Synthesis in Engineered Constructs

Collagen Content

Immunofluorescence

Baboon carotid arteries showed circumferentially-organized collagen I (FITC), collagen III (Rhodamine), and cell nuclei throughout the artery wall (Figure 9.5A). Uncultured type V scaffolds absorbed DAPI and faintly autofluoresced but did not show antibody attachment (Figure 9.5B). Type V constructs cultured for 21 days showed collagen I and cell nuclei concentrated at the luminal and abluminal surfaces with collagens I and III and cell nuclei distributed throughout the construct wall (Figure 9.5C), as did type V constructs cultured for 10 days (Figure 9.5D).

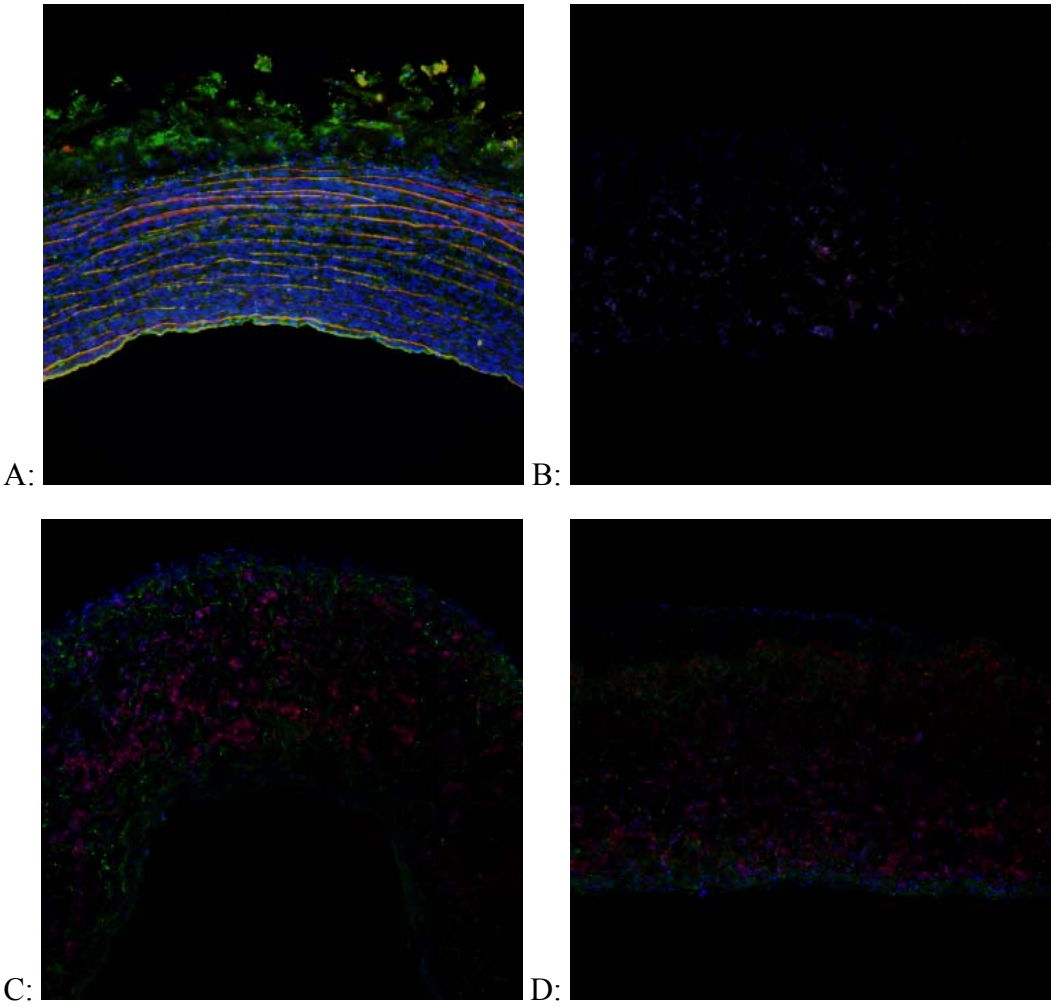

Figure 9.5: Effect of *in Vitro* Culture Time on Distributions of Collagens I and III in Type V Constructs. Segments of baboon carotid arteries, type V scaffolds cultured with adult baboon SMCs for 21 or 10 days, and uncultured type V scaffolds were snap-frozen and cryosectioned. Cryosections were immunofluorescently stained against collagen I (FITC) and collagen III (Rhodamine) to assess collagen distribution (magnification 10X). Staining with DAPI was used to assess distribution of SMCs. Collagens I and III and cell nuclei were stained and imaged in single locations, with images subsequently merged. All images are oriented with the luminal surface facing down. The *tunica adventitia* of baboon carotid arteries was removed prior to snap-freezing, and the artery cross-section shown has only the *tunicae media* and *intima* intact. (A) Baboon carotid arteries showed circumferentially-organized collagens I and III with cell nuclei throughout the artery wall. (B) Uncultured type V scaffolds absorbed DAPI and faintly autofluoresced but did not show antibody attachment. (C) Type V constructs cultured for 21 days showed collagen I and cell nuclei concentrated at the luminal and abluminal surfaces with collagens I and III and cell nuclei distributed throughout the construct wall, as did (D) type V constructs cultured for 10 days.

Colorimetric Analysis of Collagen Content

Baboon carotid arteries contained more collagen than all construct groups by more than an order of magnitude (Figure 9.6A). A statistical analysis performed by excluding the positive control (to create a valid basis of statistical comparison between experimental groups and controls by equalizing magnitudes in the standard deviations of the data) showed that all constructs had significantly higher collagen content than uncultured type V scaffolds and that type V constructs cultured for 21 days contained significantly more collagen than type V constructs cultured for 10 days (Figure 9.6B). The difference between type V constructs cultured for 21 or 10 days was likely due to the difference in culture length. Significantly higher collagen in type V constructs cultured for 21 days may have contributed to significantly lower compliance compared to type V constructs cultured for 10 days (see Figure 9.3).

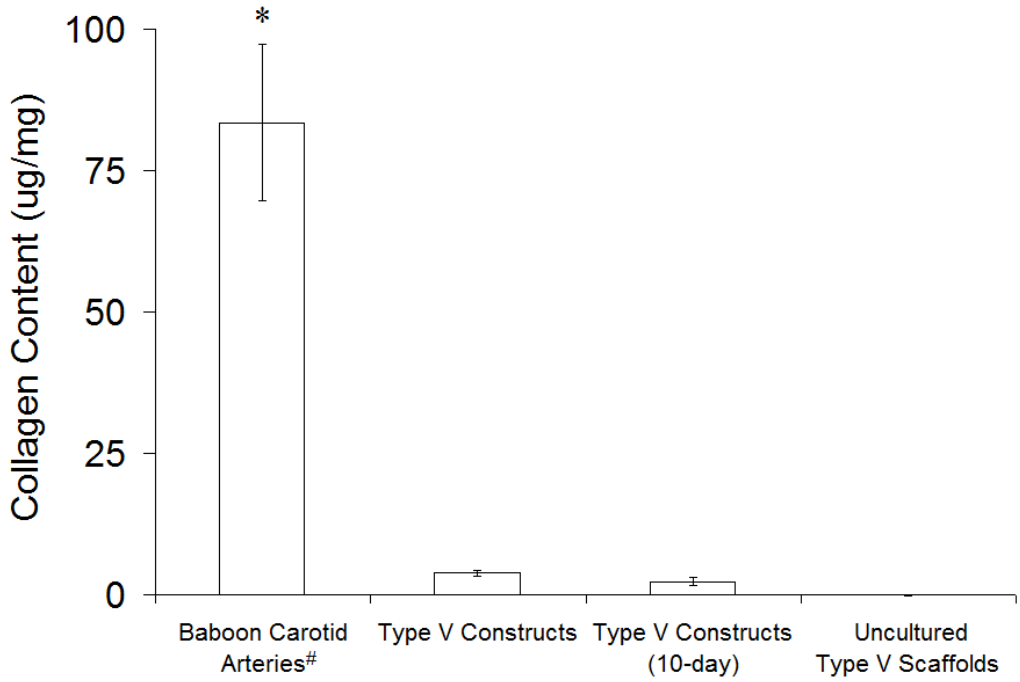

A:

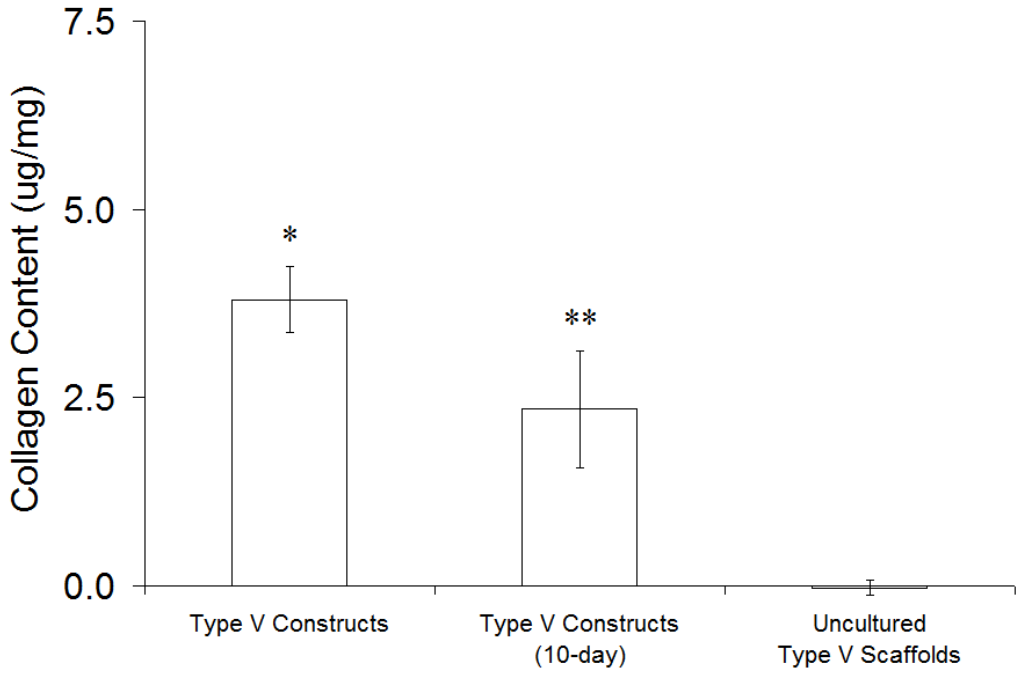

B:

Figure 9.6: Effect of *in Vitro* Culture Time on Total Collagen Content in Type V Constructs. Total collagen contents of baboon carotid arteries, type V scaffolds cultured with adult baboon SMCs for 21 or 10 days, and uncultured type V scaffolds were measured indirectly by colorimetric quantification of hydroxyproline content. #The *tunica adventitia* of baboon carotid arteries was removed prior to testing, and results therefore

represent properties of the *tunicae media* and *intima* only. (A) All experimental groups and controls were initially included in the analysis (n = 4, 4, 4, and 8 from left to right). *Baboon carotid arteries had significantly higher collagen content than all other groups. (B) Dissimilar magnitudes of standard deviation between the positive control and all other groups prompted subsequent comparison of the experimental groups and the negative controls only. *Type V constructs cultured for 21 days contained significantly more collagen than all other groups. **Type V constructs cultured for 10 days contained significantly more collagen than uncultured type V scaffolds.

Elastin Content

Elastin Autofluorescence

Baboon carotid arteries showed circumferentially-organized elastin throughout the artery wall (Figure 9.7A). Uncultured type V scaffolds were used for image thresholding and showed spots of faint autofluorescence under imaging conditions (Figure 9.7B). Type V constructs cultured for 21 days showed concentrations of elastin at the luminal and abluminal surfaces (Figure 9.7C), as did type V constructs cultured for 10 days (Figure 9.7D).

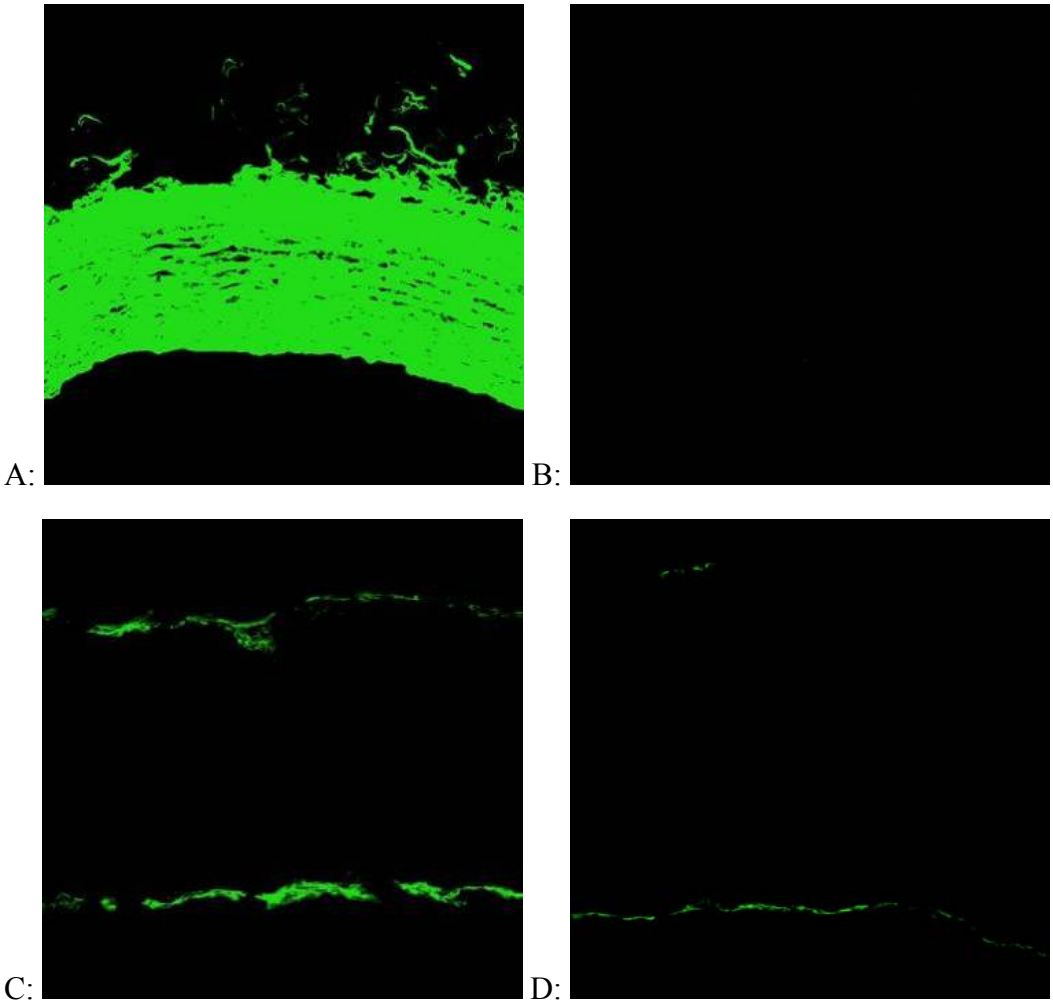

Figure 9.7: Effect of *in Vitro* Culture Time on Elastin Distribution in Type V Constructs. Segments of baboon carotid arteries, type V scaffolds cultured with adult baboon SMCs for 21 or 10 days, and uncultured type V scaffolds were snap-frozen and cryosectioned. Cryosections were excited at 488 nm and imaged to qualitatively assess elastin via autofluorescence (magnification 10X). All images are oriented with the luminal surface facing down. The *tunica adventitia* of baboon carotid arteries was removed prior to snap-freezing, and the artery cross-section shown has only the *tunicae media* and *intima* intact. (A) Baboon carotid arteries showed circumferentially-organized elastin throughout the artery wall. (B) The weak autofluorescence of uncultured type V scaffolds was used for image intensity thresholding. (C) Type V constructs cultured for 21 days showed concentrations of elastin at the luminal and abluminal surfaces, as did (D) type V constructs cultured for 10 days.

Colorimetric Analysis of Soluble and Insoluble Elastin Content

The soluble elastin concentration in culture medium collected from all construct chambers was higher than unused culture medium incubated with uncultured type V scaffolds (Figure 9.8). Soluble elastin concentration in medium collected from chambers of type V constructs cultured for 21 days was significantly higher than soluble elastin concentration in medium collected from chambers of type V constructs cultured for 10 days. As with total collagen content, the difference between elastin concentration in medium collected from type V constructs cultured for 21 or 10 days was likely due to the difference in culture length.

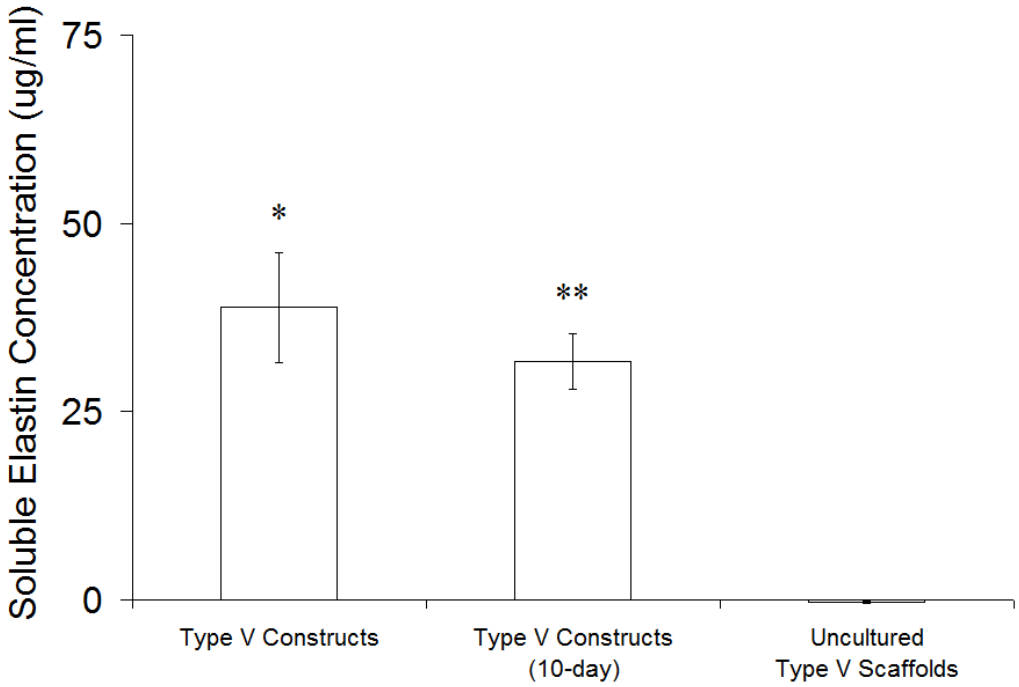

Figure 9.8: Effect of *in Vitro* Culture Time on Soluble Elastin Concentration in Culture Medium of Type V Constructs. Soluble elastin concentrations in culture medium collected at the termination of culture of type V scaffolds for 21 or 10 days with adult baboon SMCs and in unused medium incubated with uncultured type V scaffolds were measured indirectly by a dye-binding assay and colorimetric quantification after centrifugation of medium to remove any insoluble elastin (n = 4, 4, and 10 from left to right). *Constructs cultured for 21 days released significantly higher concentrations of soluble elastin into the culture medium compared to constructs cultured for 10 days and concentrations measured in unused medium incubated with uncultured type V scaffolds. **Constructs cultured for 10 days released significantly higher concentrations of soluble elastin into the culture medium compared to concentrations measured in unused medium incubated with uncultured type V scaffolds.

Baboon carotid arteries contained significantly more insoluble elastin than all other groups (Figure 9.9). All type V constructs had significantly more insoluble elastin content than uncultured type V scaffolds. Type V constructs cultured for 21 days contained significantly more insoluble elastin than type V constructs cultured for 10 days. As with total collagen content and soluble elastin concentration, the difference between

insoluble elastin content in type V constructs cultured for 21 or 10 days was likely due to the difference in culture length.

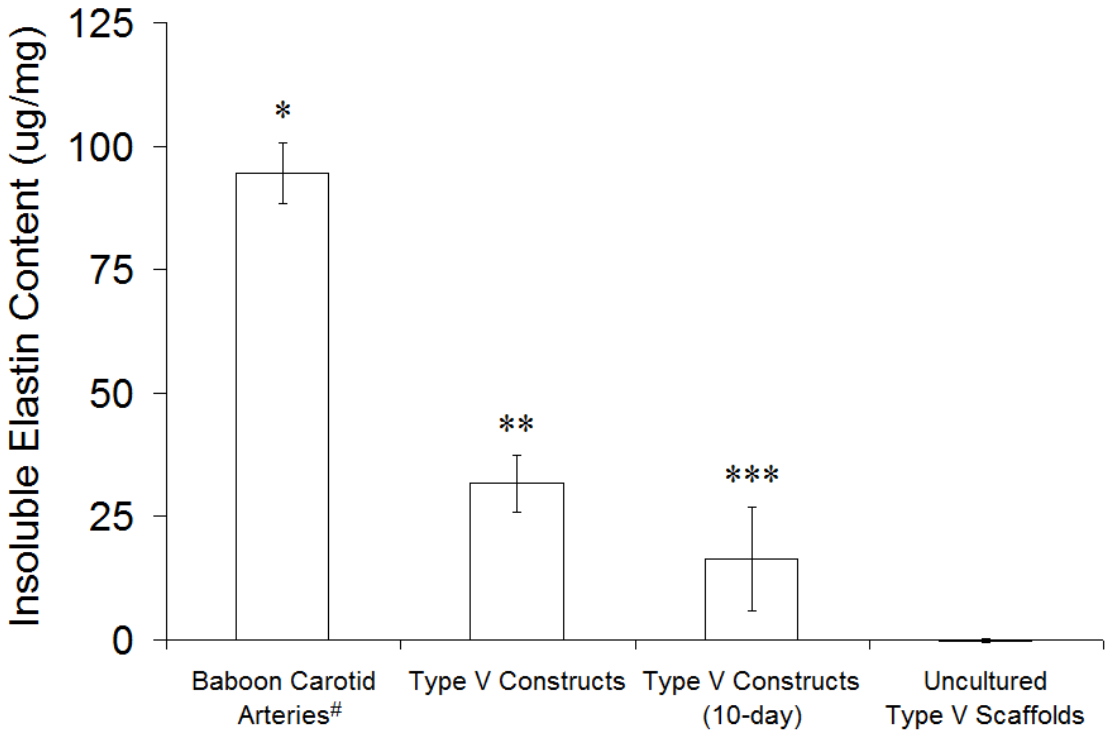

Figure 9.9: Effect of *in Vitro* Culture Time on Insoluble Elastin Content in Type V Constructs. Insoluble elastin contents of baboon carotid arteries, type V scaffolds cultured for 21 or 10 days with adult baboon SMCs, and uncultured type V scaffolds were measured indirectly by a dye-binding assay and colorimetric quantification after acid hydrolysis of each construct, which destroyed all proteins except elastin, and centrifugation, which eliminated soluble elastin (n = 4, 4, 4, and 9 from left to right). #The *tunica adventitia* of baboon carotid arteries was removed prior to testing, and results therefore represent properties of the *tunicae media* and *intima* only. *Baboon carotid arteries contained significantly more insoluble elastin than all other groups. **Type V constructs cultured for 21 days contained significantly more insoluble elastin compared to type V constructs cultured for 10 days and uncultured type V scaffolds. ***Type V constructs cultured for 10 days contained significantly more insoluble elastin compared to uncultured type V scaffolds.

Limitations of the Experimental Approach and Recommendations

While engineered construct culture time was relatively brief, it was still prohibitive in the development of this strategy for urgent care treatments. Increasing culture time may actually be desirable during continued development of a tissue engineering strategy to create highly compliant blood vessels based on PGS scaffolds. Longer culture times may provide insights for improvement of the constructs, ultimately enabling constructs to achieve clinically-relevant burst pressures with briefer culture times than those used in this study (21 or 10 days).

Burst pressures at the 10-day time point might be increased by early seeding with EPCs. A confluent layer of EPCs would protect SMCs from shear stress and prevent shear-induced inhibition of SMC proliferation,[57] providing a more physiologic culture conditions which could improve protein synthesis, ECM development and remodeling, and the mechanical properties of constructs. Once higher burst pressures are achieved, *in vitro* fatigue testing to look at long-term construct performance would be necessary before moving to animal studies and clinical applications.

Conclusions

Culturing type V constructs for 21 rather than 10 days appeared to increase wrinkling of the scaffold during compaction in culture without affecting the distribution of SMCs, collagens I and III, and elastin. Compliance significantly increased in type V constructs with longer culture time while elastic recovery and burst pressure were not significantly affected. Increasing culture time significantly increased total collagen and insoluble elastin content as well as the concentration of soluble elastin in culture medium. A combined discussion of results from this and all other chapters and their implications is presented in Chapter 12.

CHAPTER 10

ENGINEERED VASCULAR CONSTRUCTS – INVESTIGATION OF THE EFFECT OF SCAFFOLD MATERIAL

Introduction

Materials such as PLGA and its companions, PLA and PGA, evoke a more severe inflammatory response *in vivo* than PGS and therefore may be less suitable as synthetic scaffold materials for vascular tissue engineering.[90] Differences in surface chemistry and degradation by-products, including chemical groups presented to cells and pH, are likely to influence the development of engineered vascular constructs. In contrast to PLGA, PLA, and PGA, which are all rigid materials, PGS is a compliant elastomer with mechanical properties that more closely match the properties of cardiovascular tissues.[91] Scaffold stiffness and elastic deformability are expected to influence vascular cell behavior in vascular tissue engineering, including cell proliferation, protein synthesis, and incorporation of proteins into the ECM, particularly collagens and elastin. Collagens and elastin are the primary constituents of vascular ECM and key determinants of the mechanical properties of vascular tissue. Specifically, cyclic stretch of compliant PGS scaffolds is expected to increase SMC proliferation[63] and synthesis of collagen and glycosaminoglycans,[61] while PLGA scaffolds are expected to promote SMC elastin synthesis in comparison to PGS scaffolds.[64] The purpose of this study was to compare engineered vascular constructs based on porous tubular PGS or PLGA type V scaffolds cultured with adult vascular SMCs under identical conditions, thereby providing insights into the effect of scaffold material on the properties of engineered vascular constructs. Materials and methods used in this chapter are described in Chapter 4.

Experimental Design

Baboon SMCs (passage 5) were seeded in type V scaffolds composed of PGS or PLGA and cultured on the first-generation bioreactor for 10 days. The flow rate was increased steadily from 1.0 ml/min (1.1 dynes/cm^2) on day one to 10 ml/min (11 dynes/cm^2) on day 10, the termination point of the study. Medium was changed on day seven with additional ascorbic acid being injected into the medium reservoirs on days three and five. Cultured PGS or PLGA type V scaffolds are respectively denoted as PGS-based or PLGA-based constructs.

Qualitative comparisons of uncultured scaffolds, engineered constructs, and porcine carotid arteries (positive control) included gross construct morphology, SEM, staining with H&E, and visualization of immunofluorescently-labeled collagen I. Quantitative comparisons included mechanical properties, total collagen and insoluble elastin content of wet tissue, and soluble elastin concentration in culture medium at the termination of culture.

The mechanical properties of the constructs were assessed by pressure-diameter testing and by compression testing. Porcine carotid arteries and whole PGS-based constructs were pressure-diameter tested. After pressure-diameter testing, porcine carotid arteries and all constructs were sectioned and segments were tested in compression along a single axis perpendicular to each construct/segment axis (denoted as transverse compression testing). One segment from each vessel did not undergo transverse compression testing and was used instead for histological assessment of the tissue. Segments were assessed for ECM content subsequent to testing. Uncultured type V scaffolds fabricated from PGS or PLGA were similarly sectioned for transverse compression testing. Scaffold segments were tested in transverse compression after submersion in PBS for 24 hours or after sterile degradation in culture medium for 10 days to verify that degradation rates of the PGS and PLGA (mass loss and decrease in E_c) were comparable.

Note: PLGA-based constructs were originally intended for pressure-diameter testing, but this was not possible due to the degree of scaffold compaction and the rigid nature of PLGA-based constructs, which caused the constructs to break apart rather than conform to the cannulae of the testing apparatus and prevented sealing at the junction of the cannulae and the construct. Additionally, the culture time originally intended for this study was 21 days. However, PLGA scaffolds compacted so rapidly and significantly that culture was terminated on day 10 and transverse compression testing of construct segments rather than pressure-diameter testing of whole constructs was used for comparison. This seemed to be the best way to balance culture time (longer times increasing total ECM synthesis) against the preservation of initial scaffold geometry (more similar tissue geometries between the two groups providing a more valid comparison of mechanical properties in transverse compression).

Results and Discussion

Overall Process Yields and Scaffold Physical Properties

Overall Yields

A maximum of two type V scaffolds could be produced with each mold use. Yields were 1.93 ± 0.26 for PGS scaffolds or 1.87 ± 0.35 for PLGA scaffolds and were not significantly different.

Scaffold Geometry, Microstructure, and Porosity

Porosity of type V scaffolds composed of PGS was 84.6 ± 0.6% compared to 84.2 ± 0.9% for type V scaffolds composed of PLGA. Porosities were not significantly different. Luminal surfaces of PGS and PLGA scaffolds appeared similar (Figure 10.1A-B), including microstructural features that would be encountered by cells during initial adhesion and subsequent migration and proliferation (Figure 10.1C-D).

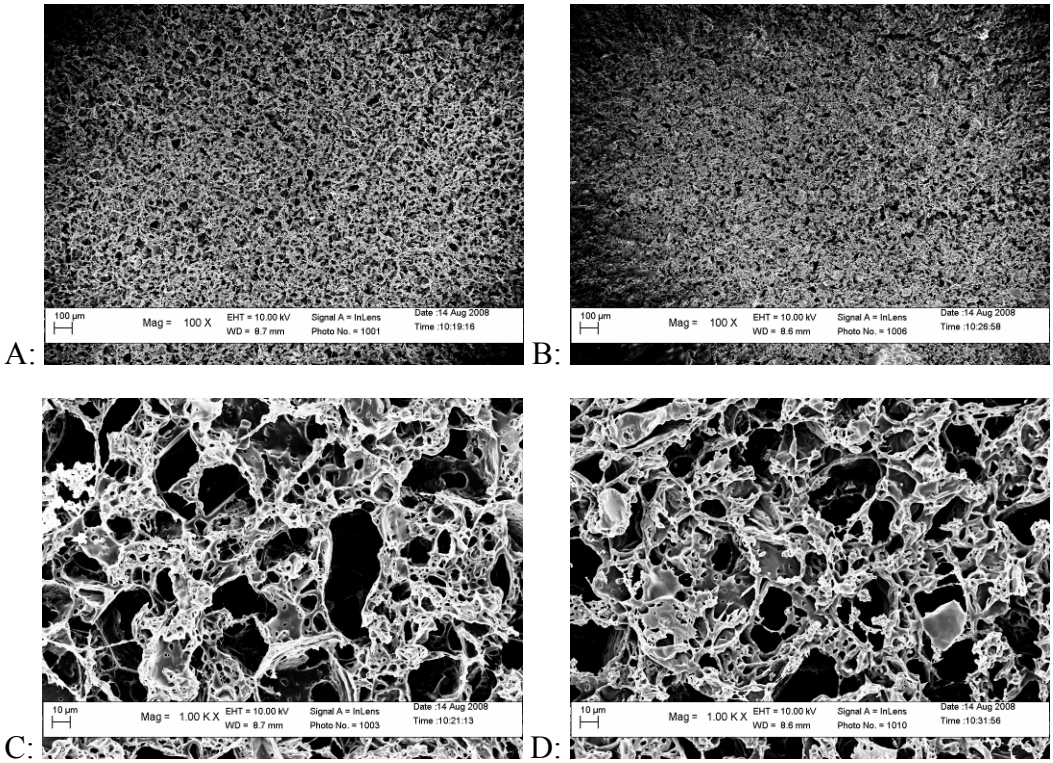

Figure 10.1: Effect of Material on Type V Scaffold Luminal Microstructure. Luminal surfaces appeared similar in micrographs of (A) PGS and (B) PLGA scaffolds (scale bars = 100 μm). Luminal microstructure also appeared similar in high-magnification micrographs of (C) PGS and (D) PLGA scaffolds (scale bars = 10 μm).

Cell-Scaffold Interactions

Cell Seeding Efficiency

Cell seeding efficiency was evaluated qualitatively by macroscopically inspecting reservoir bottoms for cell aggregates and thick, confluent cell layers. Large cell aggregates and thick layers of cells had been visible within 24 hours of low-efficiency luminal (not through-wall) flow seeding (44 ± 8% versus 74 ± 4% seeding efficiency,

respectively; see Chapter 5). No large aggregates or thick cell sheets were visible in the reservoirs at any time point.

Cellular Confluence

After 10 days of culture SMCs were confluent on the luminal surfaces of PGS- and PLGA-based constructs (Figures 10.2A-B), indicating that cell adhesion and proliferation were comparable for scaffolds made from the two materials. The microscopic appearance of cellular confluence was similar but not identical on the luminal surfaces of PGS- and PLGA-based constructs (Figures 10.2C-D), which could be attributed to differences in flow patterns at macroscopically smooth (PGS) versus rough (PLGA, post-compaction) luminal surfaces as evident from micrographs (Figures 10.2A-B) and differences in shear stress caused by difficulty maintaining luminal flow in post-compaction PLGA constructs during culture (see Visual Observations).

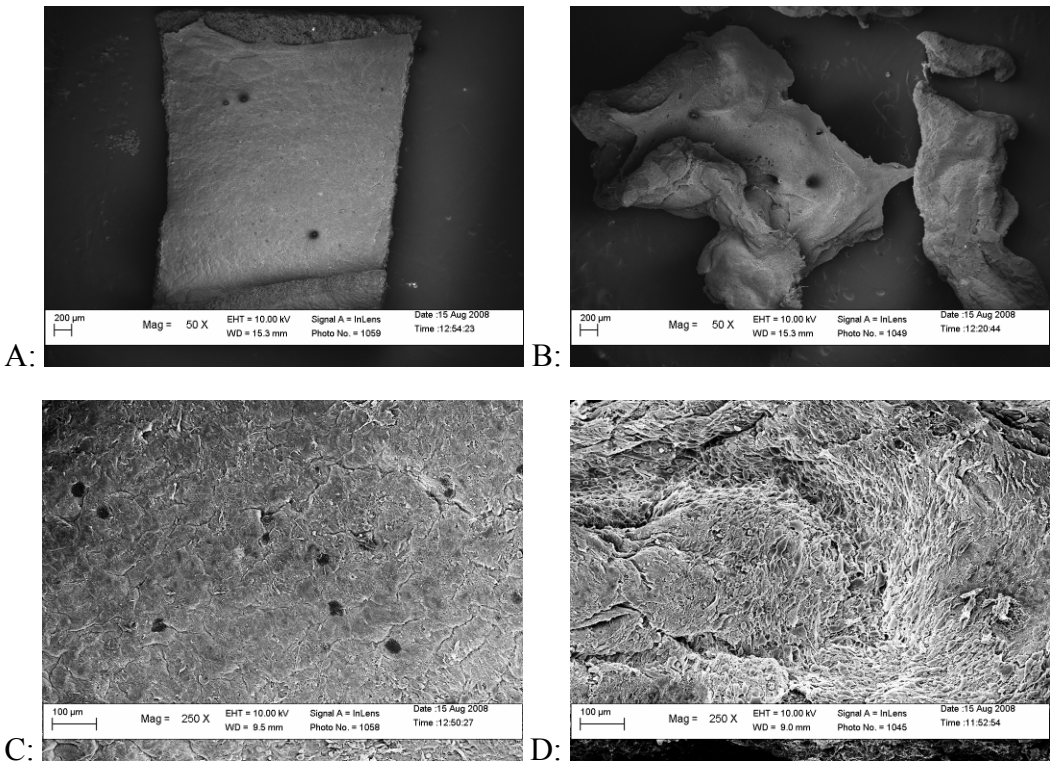

Figure 10.2: Effect of Material on Luminal Confluence of Adult Baboon Smooth Muscle Cells Cultured in Type V Scaffolds for Ten Days. Cellular confluence appeared equivalent on the luminal surfaces of (A) PGS and (B) PLGA type V scaffolds cultured with adult baboon SMCs for 10 days despite differences in gross morphology (scale bars = 200 µm). Luminal confluence appeared similar but not identical in high-magnification micrographs of (C) PGS and (D) PLGA type V construct lumens (scale bars = 100 µm). PLGA-based constructs had individual SMCs visible on their luminal surfaces in some locations.

Gross Construct Morphology

Visual Observations

Type V scaffolds composed of PGS or PLGA were geometrically indistinguishable prior to culture. PLGA scaffolds compacted so significantly in the longitudinal direction during the first five days of culture that their luminal tubing could

not be re-positioned to hold them in place for maintenance of luminal flow by day five. Radial compaction was also significant, and by day five the outer diameter of PLGA-based constructs matched the outer diameter of their luminal tubing (~4.0 mm). The rate of dimensional change appeared to decrease between day five and the termination of culture on day 10. Upon removal from culture, all engineered constructs appeared pinkish white and were similar in color to porcine carotid arteries (Figure 10.3). PLGA-based constructs maintained their geometry during handling with forceps, whereas PGS-based constructs held their shape but could be easily deformed during handling. Porcine carotid arteries maintained shape with greater definition and provided more resistance to deformation and damage than PGS-based constructs.

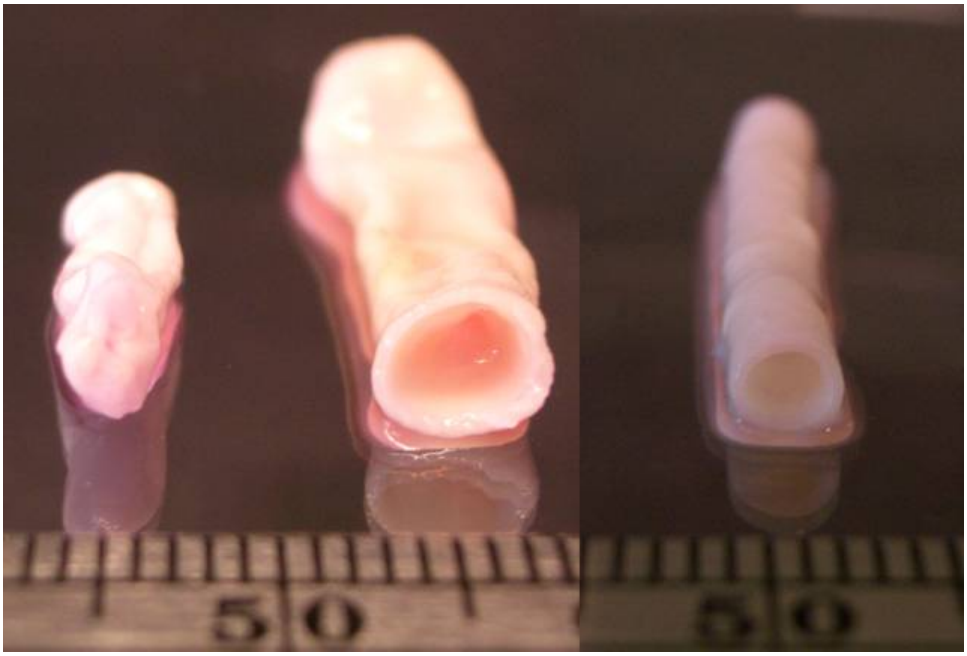

Figure 10.3: Effect of Material on Macroscopic Appearance of Whole Type V Constructs Cultured for Ten Days with Adult Baboon Smooth Muscle Cells. Differences in the macroscopic appearance of porcine carotid arteries (right), PGS type V scaffolds cultured for 10 days with adult baboon SMCs (center), and PLGA type V scaffolds cultured for 10 days with adult baboon SMCs (left) were readily apparent (ruler divisions = 1.0 mm). The *tunica adventitia* of porcine carotid arteries was removed prior to photographing, and the artery shown has only the *tunicae media* and *intima* intact.

Histology

Baboon carotid arteries were compact and cells and protein were organized into circumferential bands within the artery wall, with some remaining *tunica adventitia* visible (Figure 10.4A). PGS-based constructs had concentrations of cell nuclei and proteins at the luminal and abluminal surfaces and cell nuclei scattered throughout the scaffold walls (Figure 10.4B, with uncultured PGS scaffold shown in inset). PLGA-based constructs also had concentrations of cell nuclei and proteins at the luminal and abluminal surfaces and cell nuclei scattered throughout the scaffold walls, with scaffold

compaction evident (Figure 10.4C, with uncultured PLGA scaffold shown in inset). Equal concentrations of SMCs at the lumen and ablumen of PLGA-based constructs (rather than higher concentrations at the lumen as in PGS-based constructs) were most likely due to PLGA scaffold breaches caused by significant and rapid compaction soon after seeding and subsequent through-wall SMC migration and proliferation.

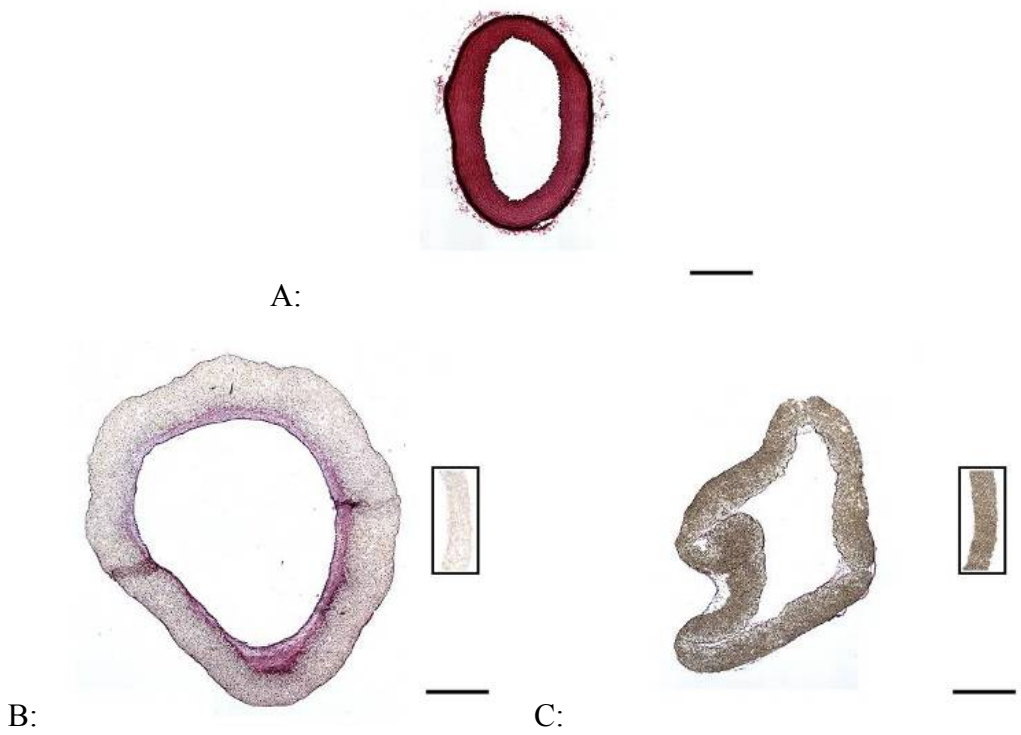

Figure 10.4: Effect of Material on Histological Appearance of Type V Constructs. Segments of porcine carotid arteries, PGS or PLGA type V scaffolds cultured with adult baboon SMCs for 10 days, and uncultured PGS or PLGA type V scaffolds were snap-frozen and cryosectioned. Cryosections were stained with H&E to qualitatively assess cell and protein distribution (scale bars = 1.0 mm). The *tunica adventitia* of porcine carotid arteries was removed prior to snap-freezing, and the artery cross-section shown has only the *tunicae media* and *intima* intact. (A) Porcine carotid arteries were dense and highly organized. (B) PGS-based constructs had concentrations of cell nuclei and proteins at the luminal and abluminal surfaces and cell nuclei distributed throughout the scaffold walls. (B, inset) Uncultured PGS type V scaffolds showed minor absorption of H&E. (C) PLGA-based constructs had concentrations of cell nuclei and protein at the luminal and abluminal surfaces and cell nuclei distributed throughout the scaffold walls. (C, inset) Uncultured PLGA type V scaffolds showed minor absorption of H&E coupled with discoloration from white to gray.

Mechanical Properties of Engineered Constructs

Transverse Compression Testing of Construct Segments

Segments of porcine carotid arteries and PGS-based constructs showed almost no measurable decrease in F_{max} at ε_{Cmax} through five compression cycles to 50% strain (Figure 10.5A-B). Each segment had nearly-identical force-extension values for all five cycles, indicating elastic and reversible deformation. PLGA-based construct segments required much greater force for equivalent deformation and strain, and F_{max} decreased for each subsequent cycle (Figure 10.5C). The initial compression cycle of PLGA-based segments showed a steady increase in force during platen extension, but subsequent cycles showed abrupt increases in force during late stages of platen extension, a behavior indicative of plastic deformation. Force-extension data of PGS and PLGA scaffolds likewise showed elastic and plastic deformation, respectively (Figure 10.5D-E).

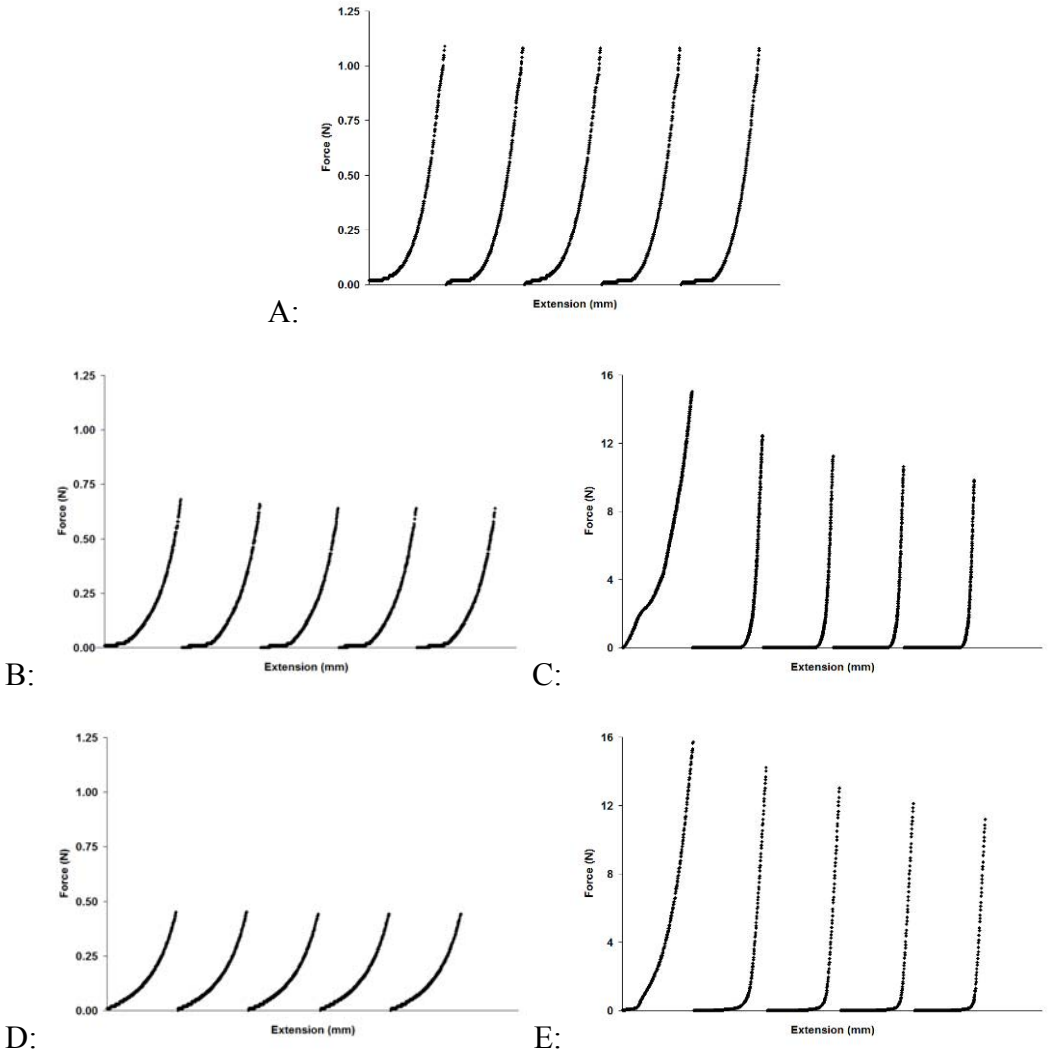

Figure 10.5: Effect of Material on Elastic Recovery of Type V Construct Segments in Transverse Compression. Segments of porcine carotid arteries, PGS or PLGA type V scaffolds cultured with adult baboon SMCs for 10 days, uncultured PGS or PLGA scaffolds, and uncultured PGS or PLGA scaffolds degraded in culture medium for 10 days were compressed perpendicular to their axis. Five force-extension cycles are shown in chronological sequence for each tested segment. The *tunica adventitia* of porcine carotid arteries was removed prior to testing, and results therefore represent properties of the *tunicae media* and *intima* only. Elastic recovery was observed in (A) porcine carotid artery segments and (B) PGS-based construct segments, while plastic deformation was observed in (C) PLGA-based construct segments. Scaffold segments composed of (D) PGS and (E) PLGA showed similar behavior to their construct counterparts.

E_c of PLGA-based constructs was significantly higher compared to E_c of all other groups, including PLGA scaffolds (Figure 10.6A). E_c of PLGA scaffolds was significantly higher compared to E_c of porcine carotid arteries, PGS-based constructs, and PGS scaffolds. Variances of E_c for PLGA groups were greater than variances of E_c for other groups. When data for porcine carotid arteries and PGS groups were compared independent of PLGA groups, E_c of porcine carotid arteries was significantly higher than E_c of all PGS groups and E_c of PGS-based constructs was significantly higher than E_c of PGS scaffolds (Figure 10.6B). Significant increases in E_c after culture with SMCs for 10 days indicated that SMCs were remodeling the scaffolds at measurable levels after only days of culture. There was no significant difference in E_c, F_{max}, or mass loss for degraded or undegraded scaffold samples of either PGS or PLGA, indicating comparable degradation rates for the polymers over the time course of this study. Since platen separation varied for artery and construct segments (to enable consistency in pre-loading and accommodate force limitations of the 50 N load cell) values of E_c were comparable between all groups but values of F_{max} were comparable only between scaffold groups.

A:

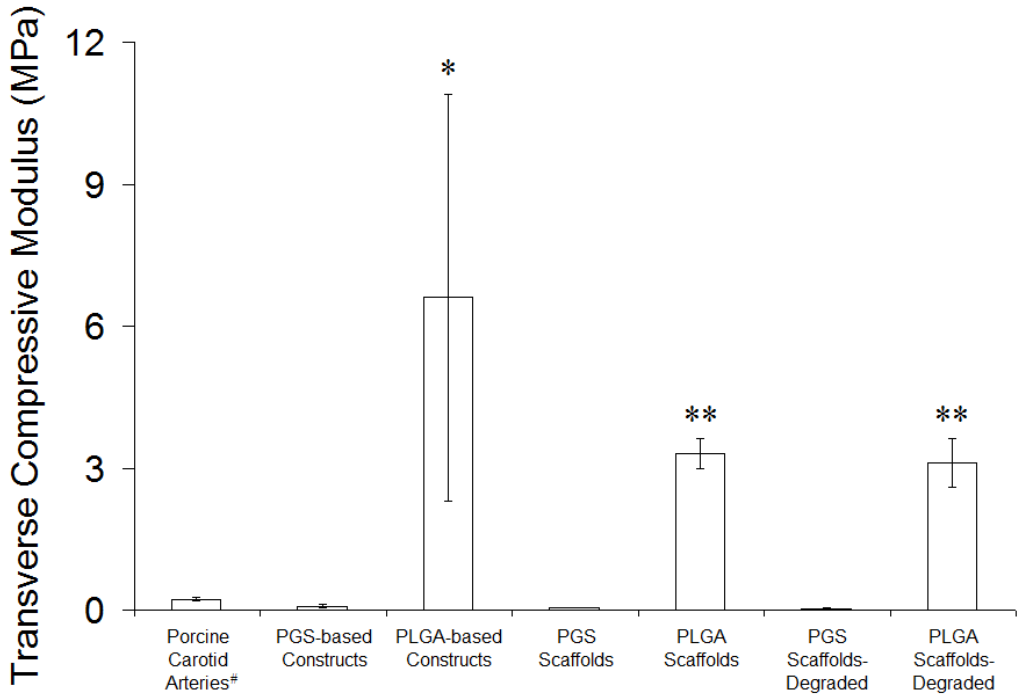

B:

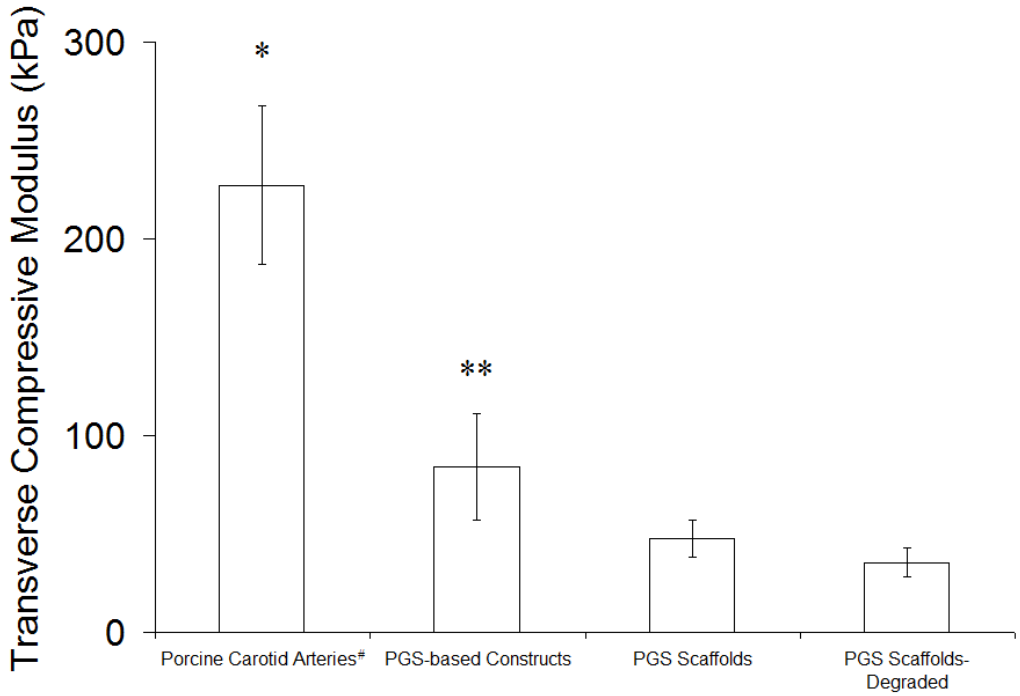

Figure 10.6: Effect of Material on Transverse Compressive Elastic Modulus of Type V Constructs and Scaffolds. Segments of porcine carotid arteries, PGS or PLGA type V scaffolds cultured with adult baboon SMCs for 10 days, uncultured PGS or PLGA scaffolds, and uncultured PGS or PLGA scaffolds degraded in culture medium for 10 days were compressed perpendicular to their axis. Five force-extension cycles were

recorded, and mean E_c was determined from the second, third, and fourth cycles. #The *tunica adventitia* of porcine carotid arteries was removed prior to testing, and results therefore represent properties of the *tunicae media* and *intima* only. (A) All experimental groups and controls were included in the initial analysis (n = 8, 10, 12, 12, 12, 12, and 12 from left to right). *E_c of PLGA-based constructs was significantly higher than all other groups. **E_c of undegraded and degraded PLGA scaffolds were significantly higher than E_c of porcine carotid arteries and all PGS groups. (B) Dissimilar magnitudes of standard deviation between the PLGA groups and all other groups prompted subsequent comparison of the positive control and PGS groups only (n = 8, 10, 12, and 12 from left to right). *E_c of porcine carotid arteries was significantly higher than all PGS groups. **E_c of PGS-based constructs was significantly higher than E_c of undegraded and degraded PGS scaffolds.

Force-extension data profiles (see Figure 10.5) and values of E_c (see Figure 10.6) provide the most likely explanation for the difference in PGS and PLGA scaffold compaction during culture. As SMCs exerted tensile forces on PLGA scaffold microstructure the structure plastically deformed, and the collective microscopic deformations caused by large numbers of SMCs over time resulted in macroscopic collapses and loss of scaffold integrity during culture. In contrast, as SMCs exerted tensile forces on PGS scaffold microstructure the scaffold elastically deformed and then returned to its original microscopic conformation as these forces changed over time, allowing the scaffold to retain a macroscopic geometry similar to its original shape during culture. In an environment of dynamic micro-forces collectively capable of compacting a scaffold with E_c on the order of MPa (PLGA), the ability to elastically deform at the microscopic level proved key to retaining macroscopic geometry.

Pressure-diameter Testing of Constructs

The stiff and brittle nature of PLGA-based constructs prevented attachment to and pressure-tight seals around even the smallest cannulae that could be practically used for pressure-diameter testing. Almost the entire length of each PGS-based construct was used

for pressure-diameter testing to burst. (A small section near either end of each construct was cut off and set aside for cryosectioning and histological analysis prior to pressure-diameter testing.) Hysteresis in porcine carotid arteries (Figure 10.7A) and PGS-based constructs (Figure 10.7B) was observed only during the first cycle to each target pressure, with subsequent cycles demonstrating complete elastic recovery.

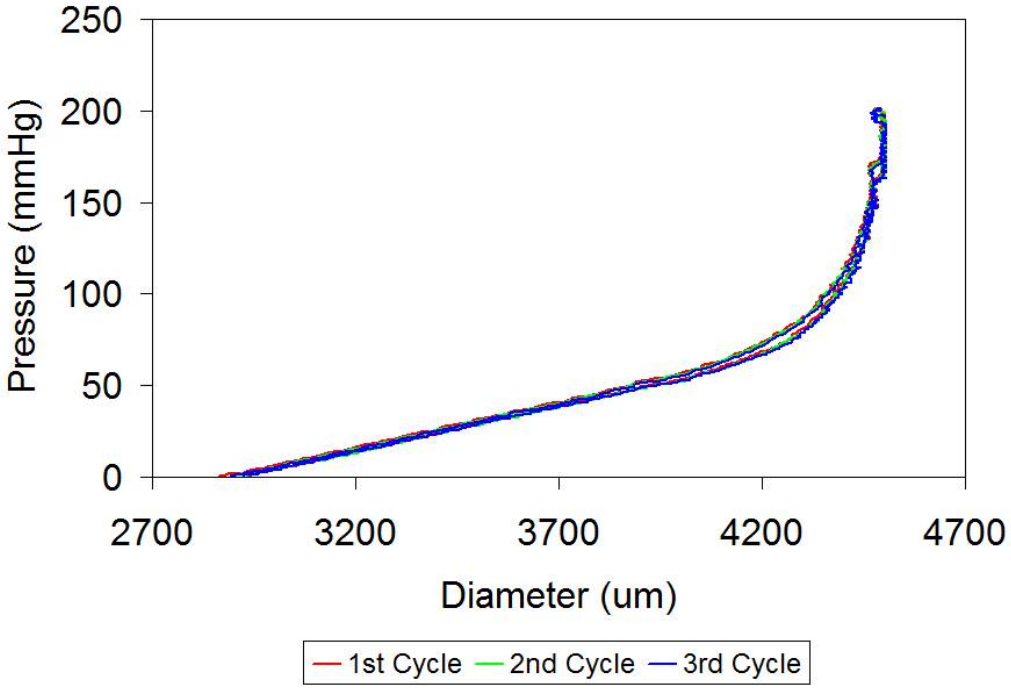

A:

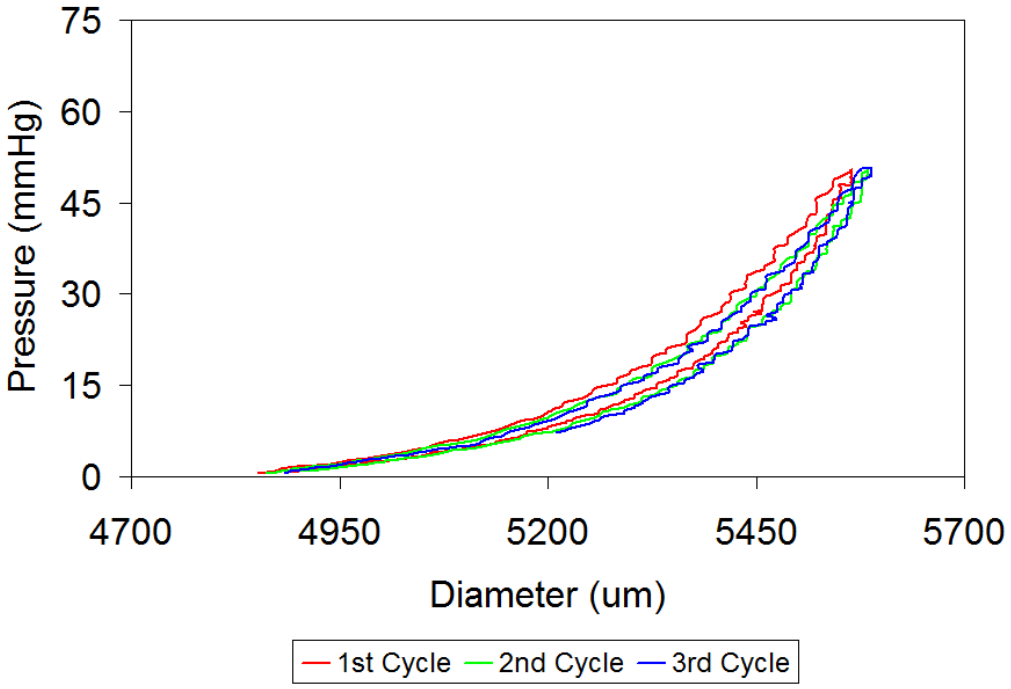

B:

Figure 10.7: Elastic Recovery of Whole Poly(glycerol sebacate)-based Type V Constructs Cultured for Ten Days. Pressure-diameter testing of whole constructs was performed after PGS type V scaffolds were cultured for 10 days with adult baboon SMCs. Similar lengths of porcine carotid arteries were tested for comparison. The *tunica adventitia* of porcine carotid arteries was removed prior to testing, and results therefore

represent properties of the *tunicae media* and *intima* only. Complete elastic recovery was observed after the initial cycle to each target pressure in (A) porcine carotid arteries up to and including the highest pressure tested (200 mmHg) and in (B) PGS-based constructs up to pressures near their burst pressure (cycles to a target pressure of 50 mmHg are shown for a construct with a burst pressure of 56 mmHg).

The compliance of porcine carotid arteries and PGS-based constructs was remarkably similar at pressures up to 56 mmHg, the highest burst pressure achieved for the PGS-based constructs (Figure 10.8). Carotid arteries excised at different distances from the aorta showed the range of compliance in the porcine common carotid, with artery segments isolated at locations closer to the aorta showing higher compliance at a given pressure. Mean burst pressure for PGS-based constructs was 27 ± 19 mmHg. Since the weakest section of the construct wall determined burst pressure, the large variance in burst pressure of 10-day PGS-based constructs was probably a reflection of how evenly-distributed cells and protein were longitudinally and circumferentially within construct lumens. Small differences in cell seeding efficiency may also have contributed to the large variance in burst pressure. In scaffolds with lower seeding efficiency a larger percentage of SMCs would be at the fluid-cell interface in the lumen, exposing these SMCs to non-physiologic shear stress and causing them to proliferate at a lower rate during early stages of culture,[57] thereby amplifying differences between constructs.

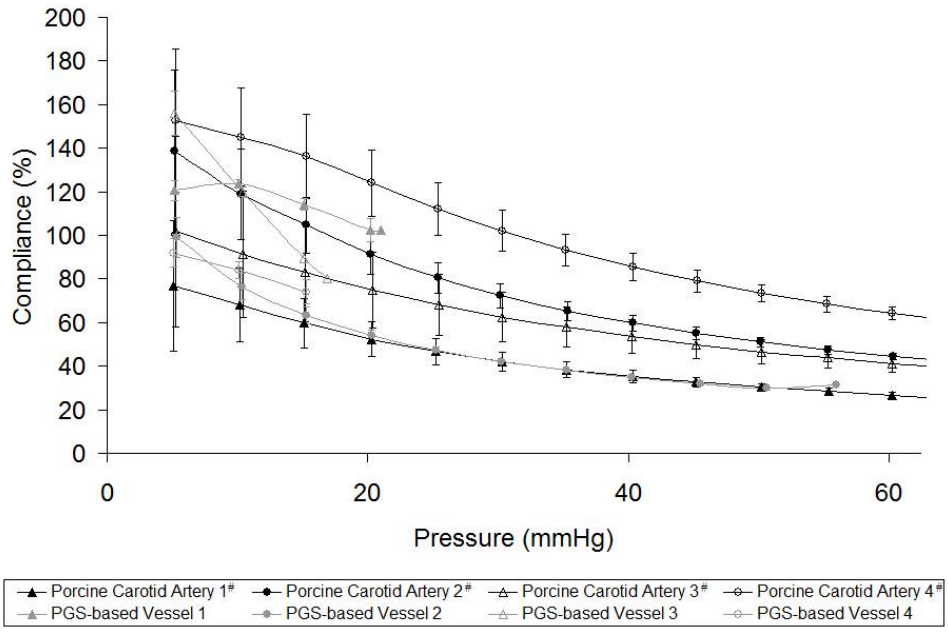

Figure 10.8: Low-pressure Physiologic Compliance of Whole Poly(glycerol sebacate)-based Type V Constructs Cultured for Ten Days. No statistical difference was found between the compliance of porcine carotid arteries (gray, n = 4) and PGS-based constructs cultured for 10 days with adult baboon SMCs (black, n = 4) at low pressures (<60 mmHg). Comparison at higher pressures was not possible because the maximum burst pressure achieved in the PGS-based constructs was 56 mmHg (group mean 27 ± 19 mmHg). #The *tunica adventitia* of porcine carotid arteries was removed prior to testing, and results therefore represent properties of the *tunicae media* and *intima* only.

Extracellular Matrix Synthesis in Engineered Constructs

Collagen Content

Colorimetric Analysis of Collagen Content

Porcine carotid arteries contained more collagen than PGS- and PLGA-based constructs by more than an order of magnitude (Figure 10.9A). A statistical analysis performed by excluding the positive control (to create a valid basis of statistical

comparison between experimental groups and controls by equalizing magnitudes in the standard deviations of the data) showed that all constructs had significantly higher collagen content than uncultured type V scaffolds of either material and that PLGA-based constructs contained significantly more collagen than PGS-based constructs (Figure 10.9B). The difference between PGS- and PLGA-based constructs was probably a result of material properties, including surface chemistry encountered at the cell-material interface, chemical composition of degradation by-products released into the medium during culture, and mechanical properties of the scaffolds such as stiffness and elastic deformability. Any of these factors, alone or in combination, could influence protein synthesis and incorporation into the ECM as well as subsequent ECM remodeling by SMCs. Scaffold stiffness may have increased collagen content in PLGA-based constructs by causing SMCs to attempt homeostatic maintenance of stiffness, which would result in increased synthesis and ECM incorporation of less compliant proteins such as collagens.

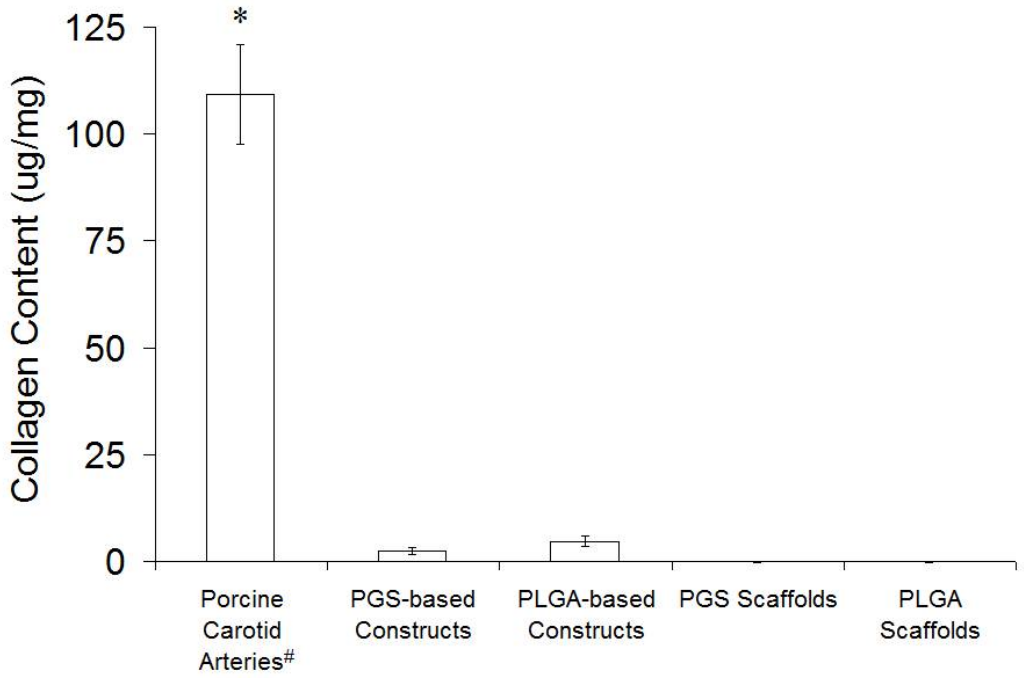

A:

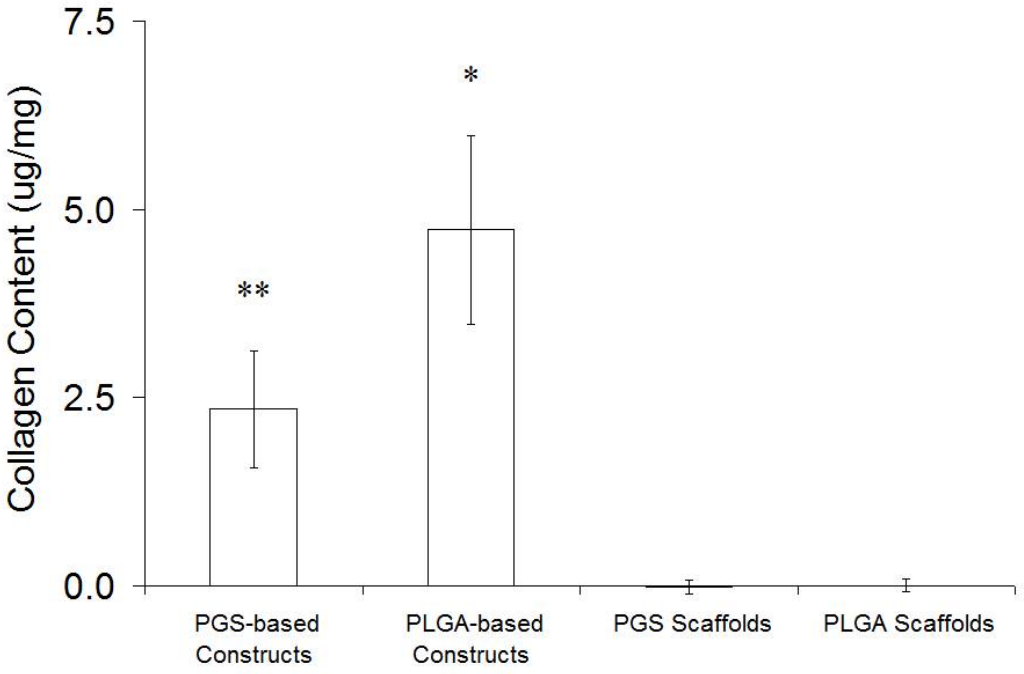

B:

Figure 10.9: Effect of Material on Total Collagen Content in Type V Constructs. Total collagen contents of porcine carotid arteries, PGS or PLGA type V scaffolds cultured for 10 days with adult baboon SMCs, and uncultured PGS or PLGA scaffolds were measured indirectly by colorimetric quantification of hydroxyproline content. #The *tunica adventitia* of porcine carotid arteries was removed prior to testing, and results

therefore represent properties of the *tunicae media* and *intima* only. (A) All experimental groups and controls were initially included in the analysis (n = 4, 4, 4, 8, and 8 from left to right). *Porcine carotid arteries had significantly higher collagen content than all other groups. (B) Dissimilar magnitudes of standard deviation between the positive control and all other groups prompted subsequent comparison of the experimental groups and the negative controls only. *PLGA-based constructs contained significantly more collagen than PGS-based constructs and uncultured scaffolds of either material. **PGS-based constructs contained significantly more collagen than uncultured scaffolds of either material.

Elastin Content

Colorimetric Analysis of Soluble and Insoluble Elastin Content

The soluble elastin concentration in culture medium collected from all construct chambers was higher than unused culture medium incubated with uncultured type V scaffolds (Figure 10.10). Soluble elastin concentrations in medium collected from chambers of PGS- or PLGA-based constructs cultured for 10 days were not significantly different. Therefore, scaffold material properties may not influence elastin synthesis. However, PGS-based constructs did contain significantly more insoluble elastin than PLGA-based constructs and uncultured scaffolds of either material, while PLGA-based constructs and uncultured scaffolds of either material did not significantly vary in their insoluble elastin content (Figure 10.11). These results strengthened the hypothesis that material properties such as surface chemistry, degradation by-products, stiffness, and elastic deformability play a role in protein incorporation into the ECM and subsequent ECM remodeling by SMCs. The elastin results also suggest that SMCs synthesize elastin on a continual basis but selectively control its crosslinking and incorporation into the ECM based on cues from the environment.

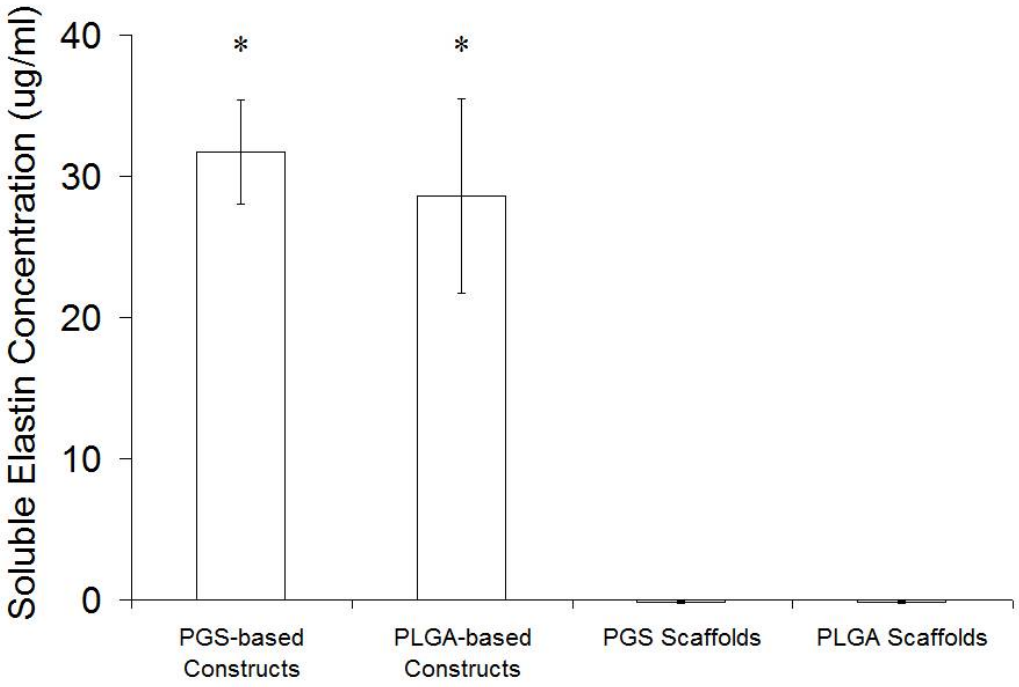

Figure 10.10: Effect of Material on Soluble Elastin Concentration in Culture Medium of Type V Constructs on Day Ten. Soluble elastin concentrations in culture medium collected at the termination of culture of PGS or PLGA type V scaffolds for 10 days with adult baboon SMCs were measured indirectly by a dye-binding assay and colorimetric quantification after centrifugation of medium to remove any insoluble elastin (n = 4, 4, 10, and 10 from left to right). *PGS- and PLGA-based constructs released similar amounts of soluble elastin into the culture medium that were significantly higher than concentrations measured in unused medium incubated with uncultured type V scaffolds of either material.

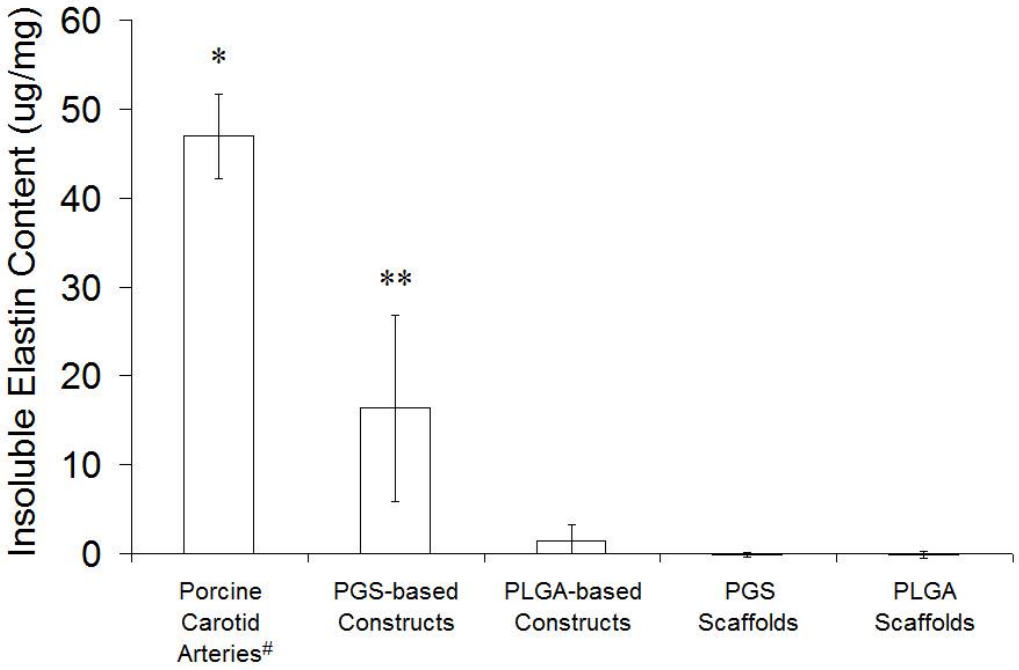

Figure 10.11: Effect of Material on Insoluble Elastin Content in Type V Constructs. Insoluble elastin contents of porcine carotid arteries, PGS or PLGA type V scaffolds cultured for 10 days with adult baboon SMCs, and uncultured PGS or PLGA type V scaffolds were measured indirectly by a dye-binding assay and colorimetric quantification after acid hydrolysis of each construct, which destroyed all proteins except elastin, and centrifugation, which eliminated soluble elastin (n = 4, 4, 4, 9, and 9 from left to right). #The *tunica adventitia* of porcine carotid arteries was removed prior to testing, and results therefore represent properties of the *tunicae media* and *intima* only. *Porcine carotid arteries contained significantly more insoluble elastin than all other groups. **PGS-based constructs contained significantly more insoluble elastin than PLGA-based constructs and uncultured scaffolds of either material, while PLGA-based constructs did not contain significantly more insoluble elastin in comparison to uncultured scaffolds of either material.

Limitations of the Experimental Approach and Recommendations

PLGA scaffold compaction by SMCs limited culture length and comparability of PGS- and PLGA-based constructs. In vascular constructs created by Niklason et al. from tubular non-woven PGA meshes, compaction by SMCs during culture was limited by

inserting a silicone rubber tube into the scaffold lumen during culture.[6,48] A similar approach could be used for comparing SMC culture in PGS and PLGA scaffolds, with cell seeding of the abluminal surfaces and primary perfusion rerouted through the scaffold chamber's abluminal inlet and outlet.

Surface chemistry and degradation by-products of PGS and PLGA varied and prevented conclusions about the effect of scaffold stiffness and elastic deformability on elastin synthesis, the incorporation of key proteins into the ECM by vascular SMCs *in vitro*, and the mechanical properties of engineered vascular constructs. PGS scaffold stiffness is proportional to crosslink density, which is indirectly controlled by three fabrication parameters: curing temperature, curing time, and the mass of PGS added to salt templates. This study investigated PGS scaffolds with identical fabrication parameters. One of these parameters could easily be varied during fabrication to create scaffolds with unique mechanical properties but with identical geometry, surface chemistry, and degradation by-products. Such scaffolds would enable direct comparison of more relevant criteria that could not be compared in this study, including compliance and burst pressure. When cultured under identical conditions these scaffolds might more clearly characterize the relationship between scaffold compliance, protein synthesis and incorporation into ECM by vascular cells, and mechanical properties of engineered vascular constructs.

Conclusions

Type V scaffolds composed of PLGA can be fabricated with high yield using methods previously developed for PGS type V scaffold fabrication. Scaffold porosity is not significantly affected by fabricating type V scaffolds from PLGA rather than PGS. SMC adhesion and luminal confluence are comparable in type V scaffolds composed of either PGS or PLGA after 10 days. Culture with SMCs for 10 days in scaffolds composed of either material significantly increased the scaffold E_c, a measure of stiffness, and

moved E_c of PGS scaffolds closer to that of porcine carotid arteries. Segments of porcine carotid arteries, PGS-based constructs, and PGS scaffolds underwent elastic deformation and recovery in transverse compression up to 50% strain, while segments of PLGA-based constructs and PLGA scaffolds underwent plastic deformation under identical testing conditions. PGS-based constructs and porcine carotid arteries demonstrated elastic recovery and had similar compliance with no significant difference at low pressures. Total collagen content was significantly higher in PLGA-based constructs. The concentration of soluble elastin in culture medium did not vary between PGS- and PLGA-based constructs, but insoluble elastin content was significantly higher PGS-based constructs. Protein synthesis and incorporation into the ECM may be regulated by SMCs in a homeostatic manner, with SMCs attempting to preserve the mechanical properties of their microenvironment through ECM regulation.[36] A combined discussion of results from this and all other chapters and their implications is presented in Chapter 12.

CHAPTER 11

ENGINEERED VASCULAR CONSTRUCTS – INVESTIGATION OF THE EFFECT OF HYDROSTATIC PRESSURE

Introduction

Native arteries experience much higher hydrostatic pressures than those used in earlier experiments. Increased hydrostatic pressure is known to increase SMC proliferation rates[66,67,119] at physiologic frequencies. Increased hydrostatic pressure may also promote a synthetic SMC phenotype, leading to increased synthesis of proteins and their incorporation into the ECM, thereby altering properties of engineered vascular constructs by accelerating development. Under pulsatile flow and increased hydrostatic pressure the developing construct may be remodeled in a more physiologic manner. The purpose of this study was to compare engineered constructs based on porous tubular PGS scaffolds cultured with adult vascular SMCs under identical conditions with the exception of hydrostatic pressure, thereby providing insights into the effect of hydrostatic pressure on the properties of engineered vascular constructs. Materials and methods used in this chapter are described in Chapter 4.

Experimental Design

Baboon SMCs (passage 4-5) were seeded at normal density in two sets of four PGS type V scaffolds with through-wall flow for 15 min followed by luminal flow. The flow rate was increased steadily from 1.0 ml/min (1.1 dynes/cm^2) on day one to 14 ml/min (15 dynes/cm^2) on day 14. Flow was maintained at 14 ml/min until the end of the culture period (day 21). One set of scaffolds was cultured on the first-generation bioreactor at baseline hydrostatic pressure of 10 ± 5 mmHg for the entire culture period.

The other set of scaffolds was cultured in the second-generation bioreactor at higher hydrostatic pressure, which was initially 60 ± 10 mmHg and was steadily raised to 120 ± 20 mmHg by day seven. Medium was changed weekly with additional ascorbic acid being injected into the medium reservoirs three and five days after medium exchange. Cultured type V scaffolds are denoted as type V constructs.

Qualitative comparisons of uncultured scaffolds, engineered constructs, and baboon carotid arteries (positive control) included gross construct morphology, SEM, staining with H&E, and visualization of immunofluorescently-labeled collagens I and III. Quantitative comparison included mechanical properties, total collagen and insoluble elastin content of wet tissue, and soluble elastin concentration in culture medium at the termination of culture.

Results and Discussion

Cell-Scaffold Interactions

Cell Seeding Efficiency

Cell seeding efficiency was evaluated qualitatively by macroscopically inspecting reservoir bottoms for cell aggregates and thick, confluent cell layers. Large cell aggregates and thick layers of cells had been visible within 24 hours of low-efficiency luminal (not through-wall) flow seeding (44 ± 8% versus 74 ± 4% seeding efficiency, respectively; see Chapter 5). No large aggregates or thick cell sheets were visible in any of the other reservoirs at any time point.

Cellular Confluence

The luminal surface of baboon carotid arteries showed cellular confluence without cells adhering to the lumen (Figures 11.1A). Luminal surfaces of type V constructs cultured at baseline or higher hydrostatic pressure had confluent cellular layers with

SMCs aligned perpendicular to the direction of flow and individual SMCs visible on construct lumens (Figures 11.1B-C).

A: 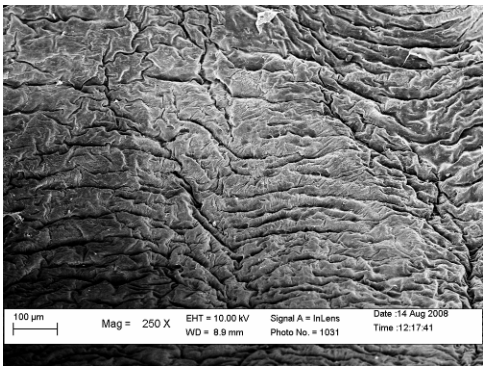

B: 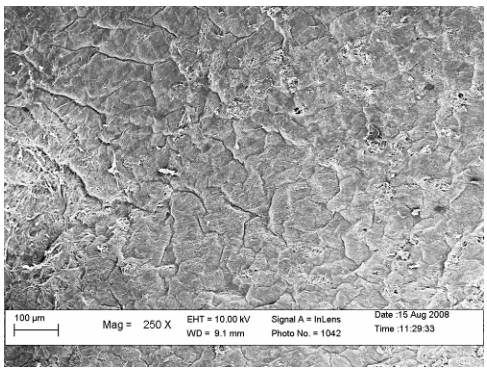

C: 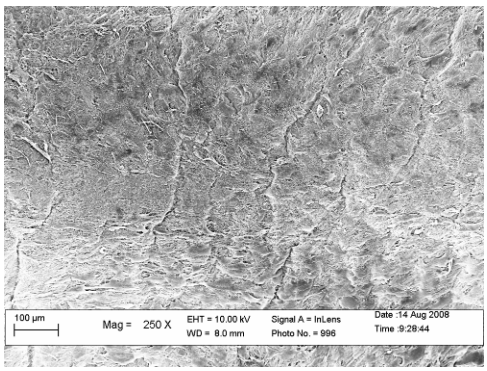

Figure 11.1: Effect of Hydrostatic Pressure on Luminal Confluence of Adult Baboon Smooth Muscle Cells Cultured in Poly(glycerol sebacate) Type V Scaffolds for Twenty-one Days. Luminal surfaces of (A) baboon carotid arteries were confluent and devoid of cells, while luminal surfaces of (B) type V scaffolds cultured with adult baboon SMCs at baseline hydrostatic pressure and (C) type V constructs cultured at higher hydrostatic pressure were confluent but had individual SMCs visible on their surfaces (scale bars = 100 µm).

Gross Construct Morphology

Visual Observations

Engineered type V constructs cultured in the first-generation bioreactor visibly distended in a cyclic manner while subjected to pulsatile perfusion during *in vitro* culture. Similar visible distension was observed in constructs cultured in the second-generation bioreactor, supporting the assumption that the addition of a needle valve to the flow circuit did not significantly diminish pulsatile flow. Near the end of culture distension ceased to be visible in constructs cultured at higher hydrostatic pressure. Type V constructs retained a cylindrical shape upon removal from the bioreactor and had a wrinkled appearance that varied from the appearance of baboon carotid arteries and uncultured type V scaffolds (Figure 11.2). No differences in handling were noted for type V constructs cultured at baseline or higher hydrostatic pressure, though both were less robust than baboon carotid arteries and more robust than uncultured scaffolds.

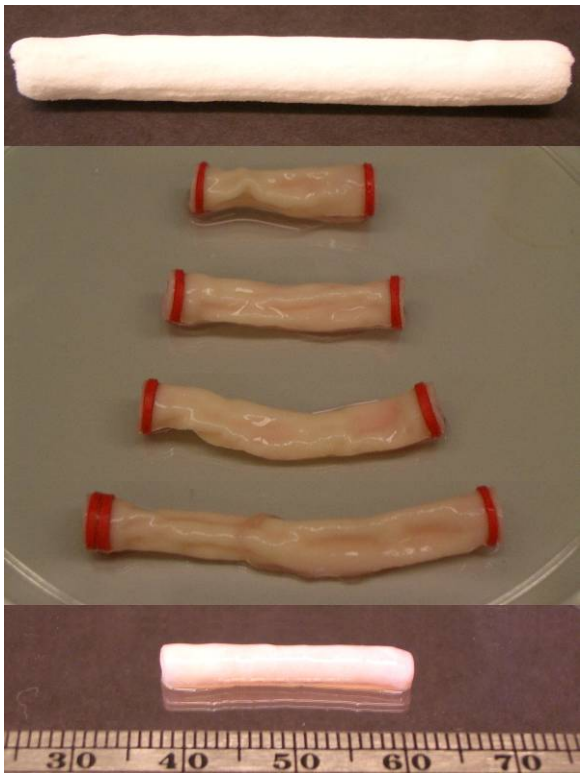

Figure 11.2: Macroscopic Appearance of Whole Type V Constructs Cultured for Twenty-one Days with Adult Baboon Smooth Muscle Cells at Higher Hydrostatic Pressure. Four type V scaffolds cultured for 21 days with adult baboon SMCs (middle) had a cylindrical shape with a wrinkled outer surface that appeared macroscopically different from baboon carotid arteries (bottom) and uncultured type V scaffolds (top), which had smoother abluminal surfaces and were more symmetrical about their axes (ruler divisions = 1 mm). The *tunica adventitia* of baboon carotid arteries was removed prior to photographing, and the artery shown has only the *tunicae media* and *intima* intact.

Histology

Baboon carotid arteries were compact and cells and protein were organized into circumferential bands within the artery wall, with some remaining *tunica adventitia* visible (Figures 11.3A). PGS type V scaffolds showed minor absorption of H&E (Figure 11.3B). Type V constructs cultured at baseline hydrostatic pressure had concentrations of

cell nuclei and proteins at the luminal and abluminal surfaces, cell nuclei scattered throughout the scaffold walls, and circumferential wrinkles caused by compaction and filled by SMCs (Figure 11.3C). Type V constructs cultured at higher hydrostatic pressure showed greater point-symmetry in cross-section with less wrinkling and compaction but resembled their baseline hydrostatic-pressure counterparts in other aspects (Figure 11.3D). Many of the engineered constructs showed the ability of the cells to fill macroscopic gaps after only days of *in vitro* culture, which indicated that culture periods employed by current benchmark blood vessel tissue engineering strategies may be excessive.

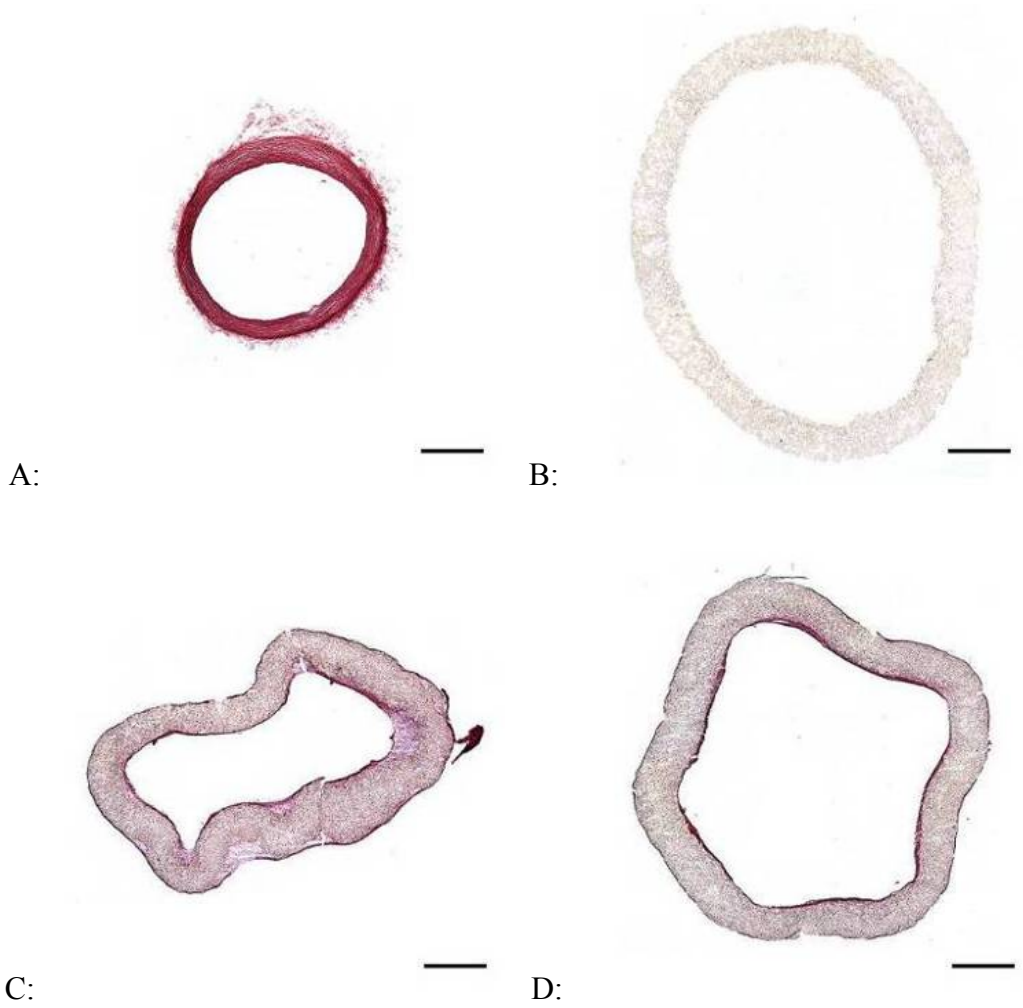

Figure 11.3: Effect of Hydrostatic Pressure on Histological Appearance of Type V Constructs. Segments of baboon carotid arteries, type V scaffolds cultured with adult baboon SMCs for 21 days at baseline or higher hydrostatic pressure, and uncultured type V scaffolds were snap-frozen and cryosectioned. Cryosections were stained with H&E to qualitatively assess cell and protein distribution (scale bars = 1 mm). The *tunica adventitia* of baboon carotid arteries was removed prior to snap-freezing, and the artery cross-section shown has only the *tunicae media* and *intima* intact. (A) Baboon carotid arteries were dense and highly organized. (B) Uncultured type V scaffolds showed minor absorption of H&E. (C) Type V constructs cultured at baseline hydrostatic pressure had concentrations of cell nuclei and proteins at the luminal and abluminal surfaces and cell nuclei distributed throughout the scaffold walls. The scaffold appeared wrinkled, probably as a result of compaction by SMCs. (D) Type V constructs cultured at higher hydrostatic pressure showed greater point symmetry and less wrinkling and compaction but otherwise appeared similar to type V constructs cultured at higher hydrostatic pressure.

Mechanical Properties of Engineered Constructs

Pressure-diameter Testing of Whole Constructs

Almost the entire length of each type V construct was used for pressure-diameter testing to burst. (A small section near either end of each construct was cut off and set aside for cryosectioning and histological analysis prior to pressure-diameter testing.) In some cases the constructs were damaged during attachment to cannulae or stretch prior to testing, in which case the longest intact section of the construct was tested. In one case a type V construct cultured at baseline hydrostatic pressure was damaged too extensively for burst pressure testing. The mode of failure in engineered constructs was generally short longitudinal slits (~5 mm) that were approximately linear (Figure 11.4). Other failure modes included circumferential slits and pinholes. Hysteresis in baboon carotid arteries (Figure 11.5A) and engineered constructs (Figure 11.5B) was observed only during the first cycle to each target pressure, with subsequent cycles demonstrating complete elastic recovery.

Figure 11.4: Common Failure Mode of Type V Constructs Cultured for Twenty-one Days with Adult Baboon Smooth Muscle Cells. The most common mode of failure in type V scaffolds cultured with adult baboon SMCs for 21 days was short longitudinal slits (~5 mm) that were approximately linear (ruler divisions = 1 mm). Culture at higher hydrostatic pressure did not appear to alter failure mode. Other failure modes included circumferential slits and pinholes.

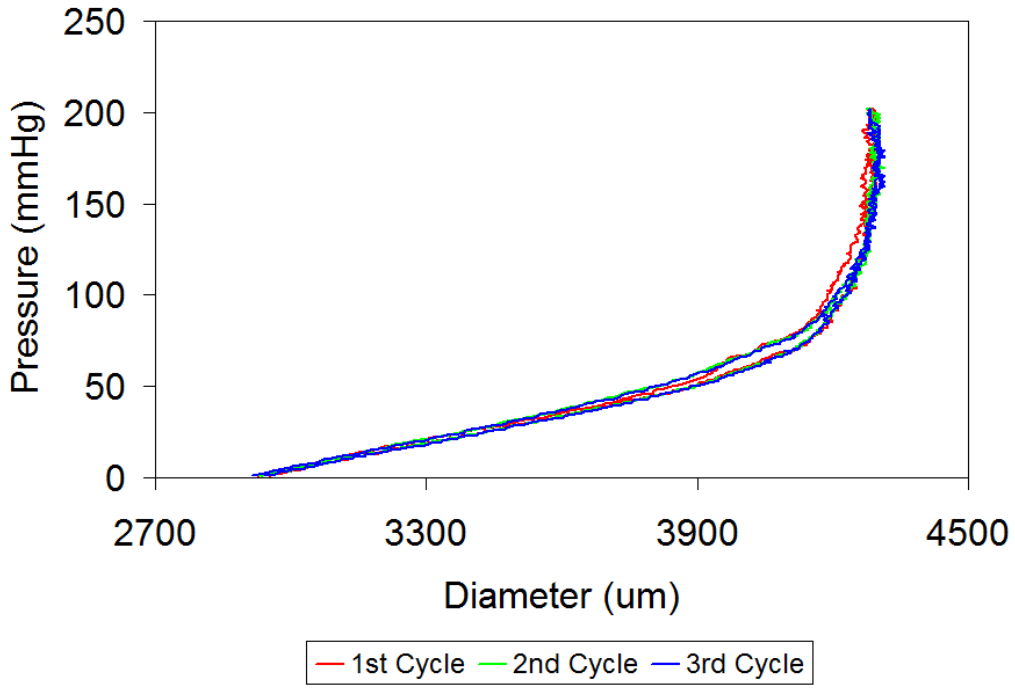

A:

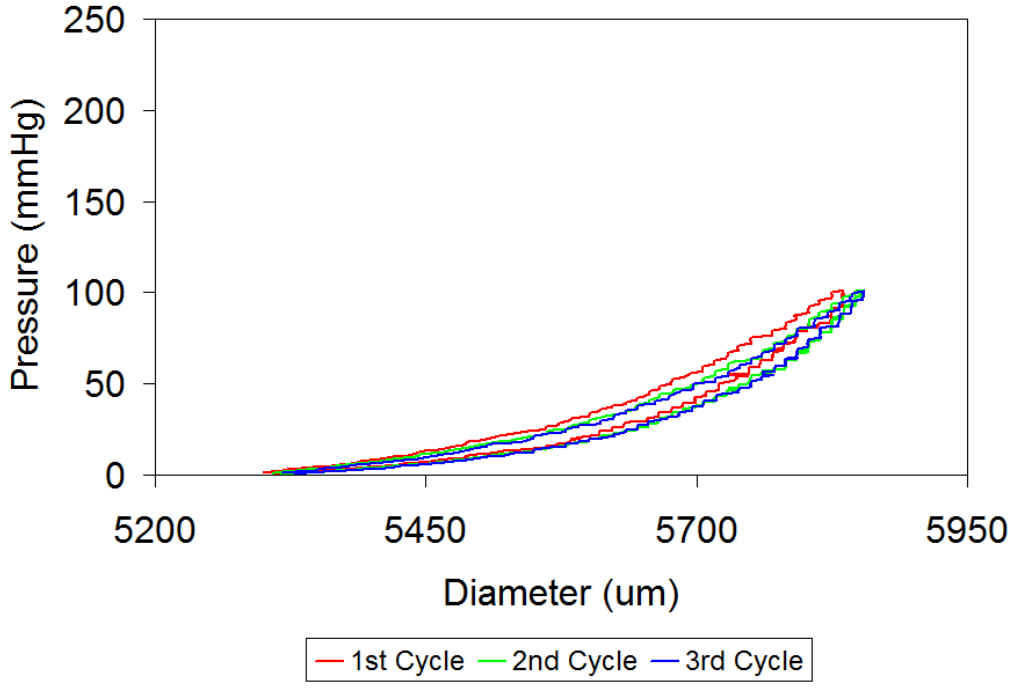

B:

Figure 11.5: Elastic Recovery of Whole Poly(glycerol sebacate)-based Type V Constructs Cultured for Twenty-one Days at Higher Hydrostatic Pressure. Pressure-diameter testing of whole constructs was performed after type V scaffolds were cultured for 21 days with adult baboon SMCs. Similar lengths of baboon carotid arteries were tested for comparison. The *tunica adventitia* of baboon carotid arteries was removed prior

to testing, and results therefore represent properties of the *tunicae media* and *intima* only. Complete elastic recovery was observed after the initial cycle to each target pressure in (A) baboon carotid arteries up to and including the highest pressure tested (200 mmHg) and in (B) type V constructs cultured at higher hydrostatic pressure up to pressures near their burst pressure (burst pressure of 110 mmHg for construct shown).

There was no significant difference between the compliance of baboon carotid arteries and type V constructs cultured at baseline hydrostatic pressure for any given target pressure (Figure 11.6). There was also no significant difference between the compliance of type V constructs cultured at baseline hydrostatic pressure and type V constructs cultured at higher hydrostatic pressure for any given target pressure. Type V constructs cultured at higher hydrostatic pressure were significantly less compliant than baboon carotid arteries for target pressures of 110 mmHg and less. Carotid arteries excised at different distances from the aorta showed the range of compliance in the baboon common carotid, with artery segments isolated at locations closer to the aorta showing higher compliance at a given pressure. Sharp increases in compliance immediately prior to vessel failure were most likely a result of tearing in luminal SMC sheets that had circumferentially wrinkled the scaffolds (see Visual Observations and Figure 11.3C) an idea which was reinforced by the absence of sharp increases in compliance prior to failure of type V constructs cultured at higher hydrostatic pressure which showed less wrinkling (see Figure 11.3D).

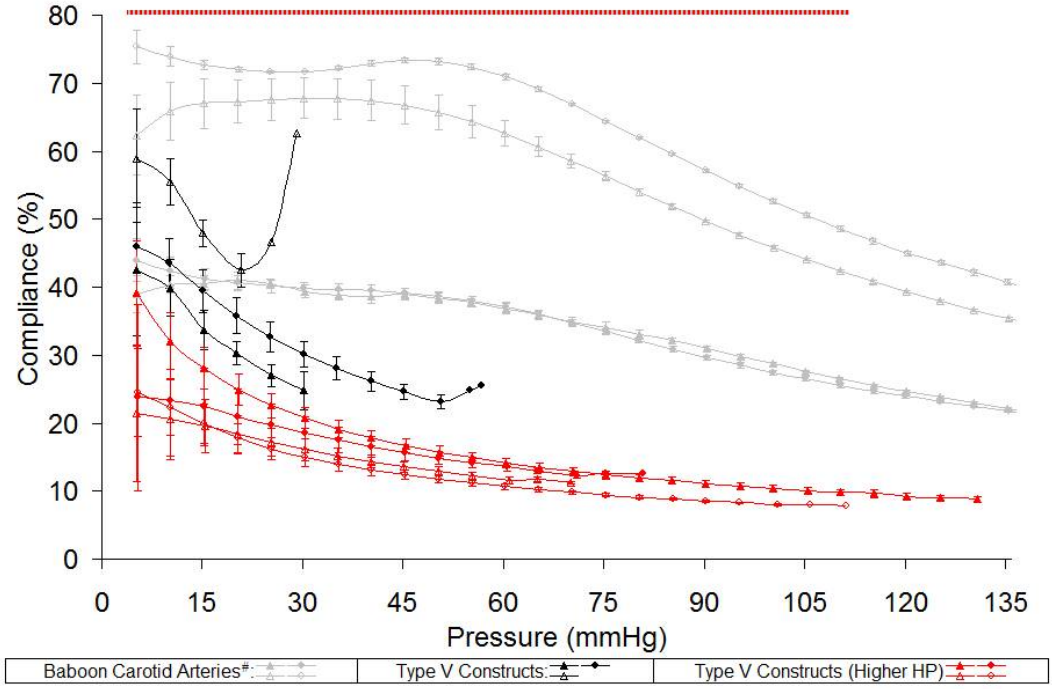

Figure 11.6: Effect of Hydrostatic Pressure on Compliance of Whole Type V Constructs. Pressure-diameter testing of whole constructs was performed after type V scaffolds were cultured for 21 days with adult baboon SMCs at baseline or higher hydrostatic pressure. Compliance was calculated for changes in diameter for each given zero-to-target pressure value. Sharp increases in compliance immediately prior to vessel failure were most likely caused by tearing in luminal SMC sheets that circumferentially wrinkled the scaffolds (see Figure 11.3C). Similar lengths of baboon carotid arteries were tested for comparison. #The *tunica adventitia* of baboon carotid arteries was removed prior to testing, and results therefore represent properties of the *tunicae media* and *intima* only. There was no significant difference at any target pressure between the compliance of baboon carotid arteries (gray, n = 4) and type V constructs cultured at baseline hydrostatic pressure (black, n = 3). Likewise, there was no significant difference at any target pressure between the compliance of type V constructs cultured at baseline hydrostatic pressure (black, n = 3) or at higher hydrostatic pressure (red, n = 4). The gray-and-red striped line indicates that type V constructs cultured at higher hydrostatic pressure (red, n = 4) were significantly less compliant than baboon carotid arteries (gray, n = 4) for target pressures of 110 mmHg and less.

The mean burst pressure of type V constructs cultured at higher hydrostatic pressure was significantly higher than the mean burst pressure of type V constructs cultured at higher hydrostatic pressure (Figure 11.7). Significantly higher burst pressure of constructs cultured at higher hydrostatic pressure could have resulted from (1) increased ECM deposition or (2) increased ECM organization and remodeling rates, either of which could have been caused by (1) increased SMC proliferation[66,67,119] or (2) higher hydrostatic pressure directly altering SMC behavior.[70,71]

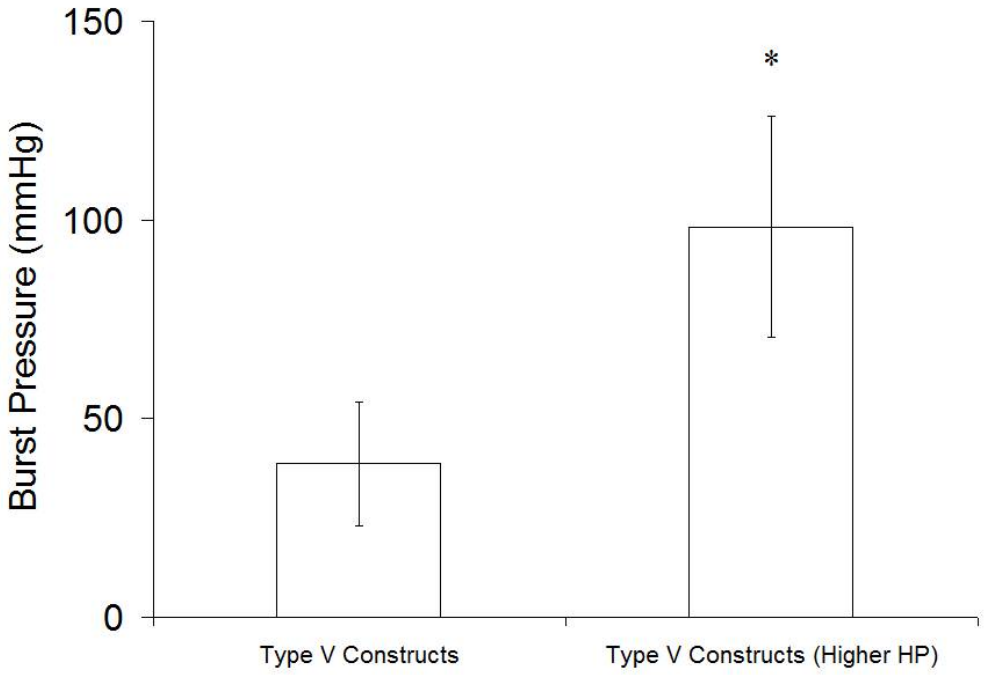

Figure 11.7: Effect of Hydrostatic Pressure on Burst Pressure of Whole Type V Constructs. Pressure-diameter testing of whole constructs was performed after type V scaffolds were cultured for 21 days with adult baboon SMCs at baseline or higher hydrostatic pressure. Burst pressure was taken as the highest pressure withstood by a vessel at a rate of pressure increase of ~60 mmHg/min. *Mean burst pressure of type V constructs cultured at higher hydrostatic pressure was significantly higher than mean burst pressure of type V constructs cultured at baseline hydrostatic pressure (n = 3 and 4 from left to right).

Extracellular Matrix Synthesis in Engineered Constructs

Collagen Content

Immunofluorescence

Baboon carotid arteries showed circumferentially-organized collagen I (FITC), collagen III (Rhodamine), and cell nuclei throughout the artery wall (Figure 11.8A). Uncultured type V scaffolds absorbed DAPI and faintly autofluoresced but did not show antibody attachment (Figure 11.8B). Type V constructs cultured at baseline hydrostatic pressure showed collagen I and cell nuclei concentrated at the luminal and abluminal surfaces with collagens I and III and cell nuclei distributed throughout the construct wall (Figure 11.8C), as did type V constructs cultured at higher hydrostatic pressure (Figure 11.8D).

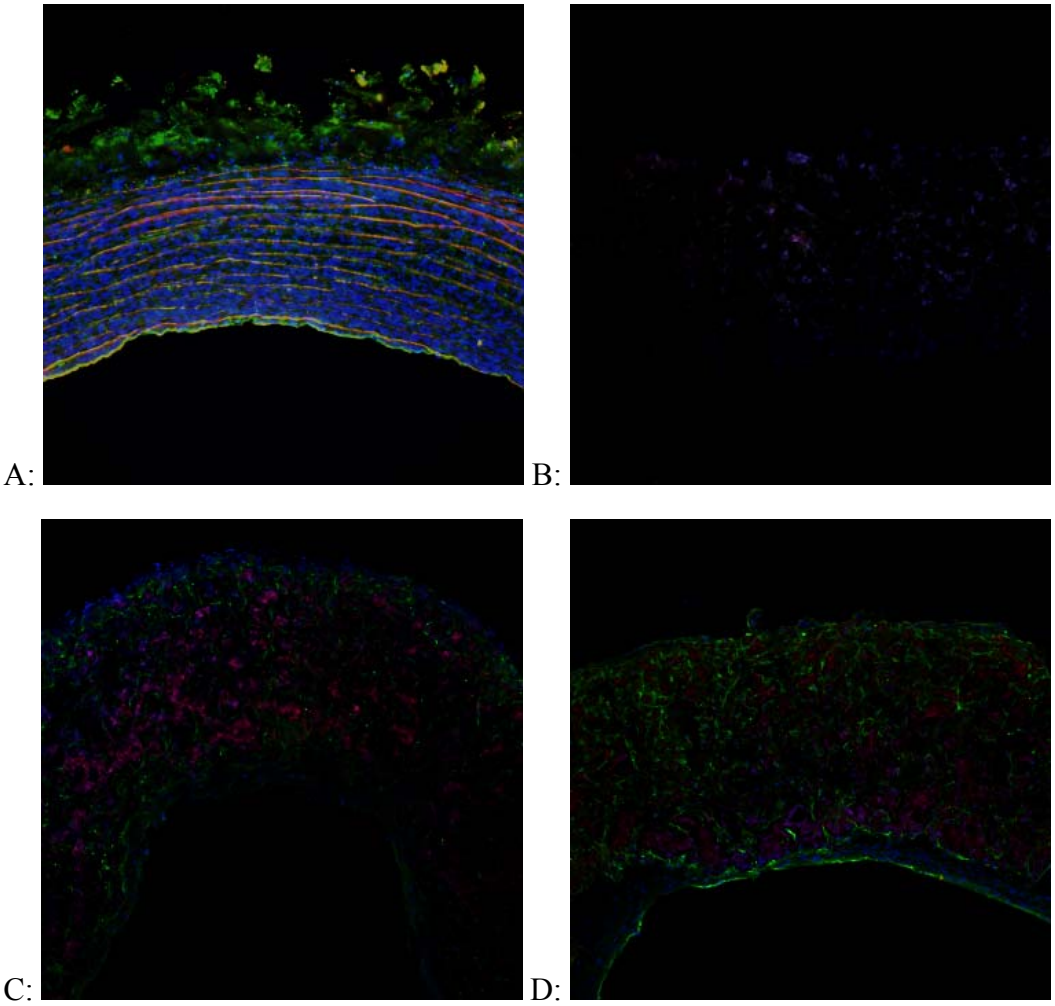

Figure 11.8: Effect of Hydrostatic Pressure on Distributions of Collagens I and III in Type V Constructs. Segments of baboon carotid arteries, type V scaffolds cultured with adult baboon SMCs for 21 days at baseline or higher hydrostatic pressure, and uncultured type V scaffolds were snap-frozen and cryosectioned. Cryosections were immunofluorescently stained against collagen I (FITC) and collagen III (Rhodamine) to assess collagen distribution (magnification 10X). Staining with DAPI was used to assess distribution of SMCs. Collagens I and III and cell nuclei were stained and imaged in single locations, with images subsequently merged. All images are oriented with the luminal surface facing down. The *tunica adventitia* of baboon carotid arteries was removed prior to snap-freezing, and the artery cross-section shown has only the *tunicae media* and *intima* intact. (A) Baboon carotid arteries showed circumferentially-organized collagens I and III with cell nuclei throughout the artery wall. (B) Uncultured type V scaffolds absorbed DAPI and faintly autofluoresced but did not show antibody attachment. (C) Type V constructs cultured at baseline hydrostatic pressure showed collagen I and cell nuclei concentrated at the luminal and abluminal surfaces with collagens I and III and cell nuclei distributed throughout the construct wall, as did (D) type V constructs cultured at higher hydrostatic pressure.

Colorimetric Analysis of Collagen Content

Baboon carotid arteries contained more collagen than all construct groups by more than an order of magnitude (Figure 11.9A). A statistical analysis performed by excluding the positive control (to create a valid basis of statistical comparison between experimental groups and controls by equalizing magnitudes in the standard deviations of the data) showed that all constructs had significantly higher collagen content than uncultured type V scaffolds and that type V constructs cultured at higher hydrostatic pressure contained significantly more collagen than type V constructs cultured at baseline hydrostatic pressure (Figure 11.9B). The difference between type V constructs cultured at baseline or higher hydrostatic pressure supported the theory that burst pressures were significantly higher because of significant increases in ECM deposition and remodeling.

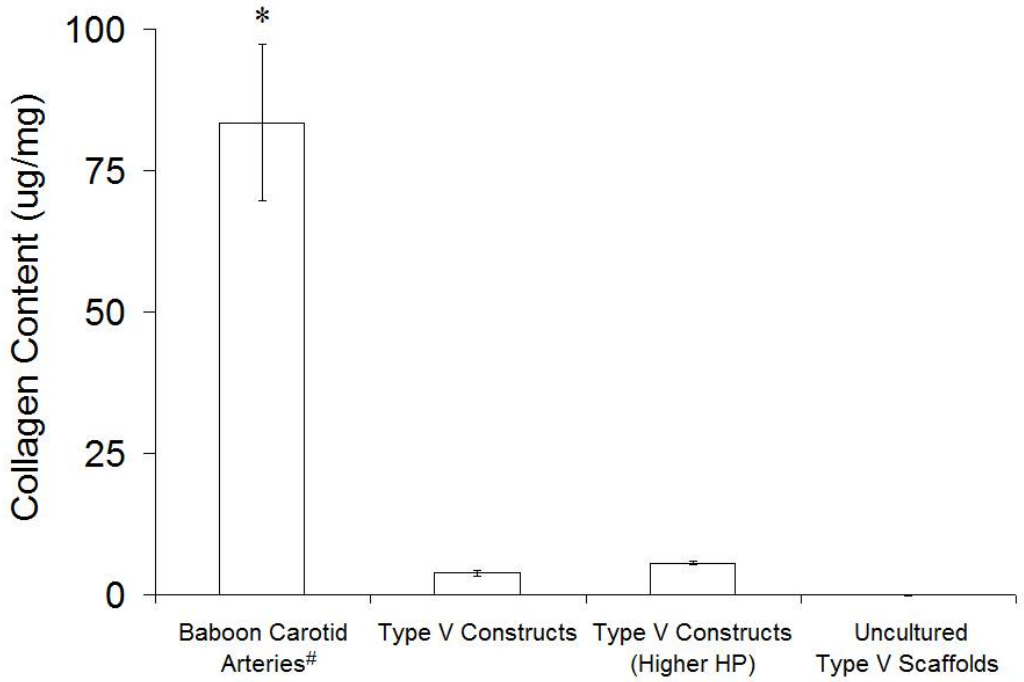

A:

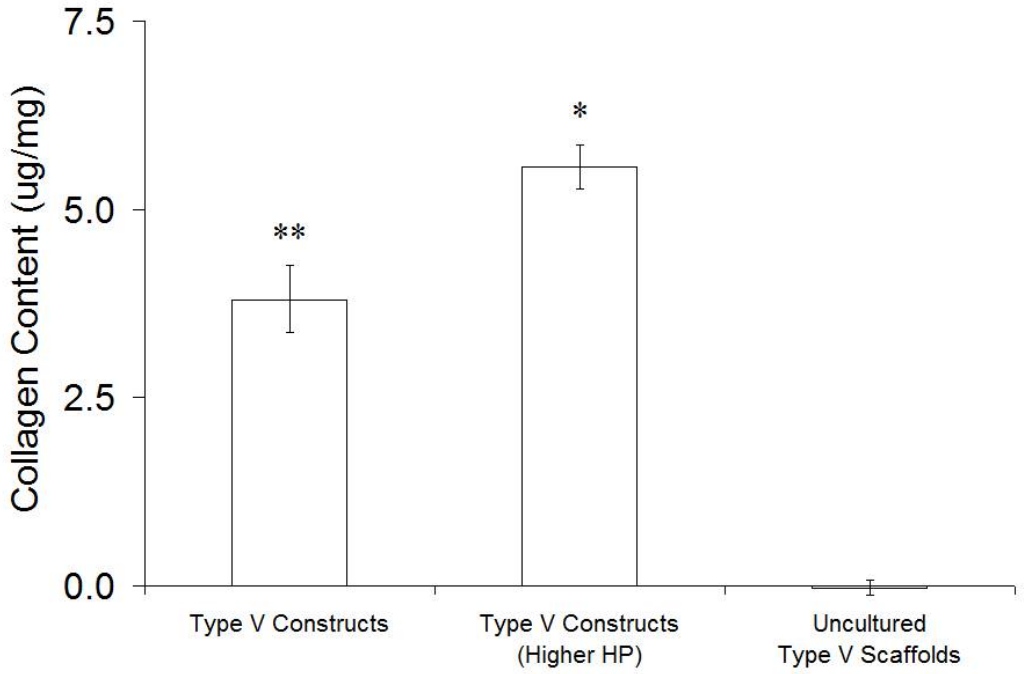

B:

Figure 11.9: Effect of Hydrostatic Pressure on Total Collagen Content in Type V Constructs. Total collagen contents of baboon carotid arteries, type V scaffolds cultured with adult baboon SMCs for 21 or 10 days, and uncultured type V scaffolds were measured indirectly by colorimetric quantification of hydroxyproline content. #The *tunica adventitia* of baboon carotid arteries was removed prior to testing, and results therefore

represent properties of the *tunicae media* and *intima* only. (A) All experimental groups and controls were initially included in the analysis (n = 4, 4, 4, and 8 from left to right). *Baboon carotid arteries had significantly higher collagen content than all other groups. (B) Dissimilar magnitudes of standard deviation between the positive control and all other groups prompted subsequent comparison of the experimental groups and the negative controls only. *Type V constructs cultured at higher hydrostatic pressure contained significantly more collagen than all other groups. ** Type V constructs cultured at baseline hydrostatic pressure contained significantly more collagen than uncultured type V scaffolds.

Elastin Content

Elastin Autofluorescence

Baboon carotid arteries showed circumferentially-organized elastin throughout the artery wall (Figure 11.10A). Uncultured type V scaffolds were used for image thresholding and showed spots of faint autofluorescence under imaging conditions (Figure 11.10B). Type V constructs cultured at baseline hydrostatic pressure showed concentrations of elastin at the luminal and abluminal surfaces (Figure 11.10C), as did type V constructs cultured at higher hydrostatic pressure (Figure 11.10D).

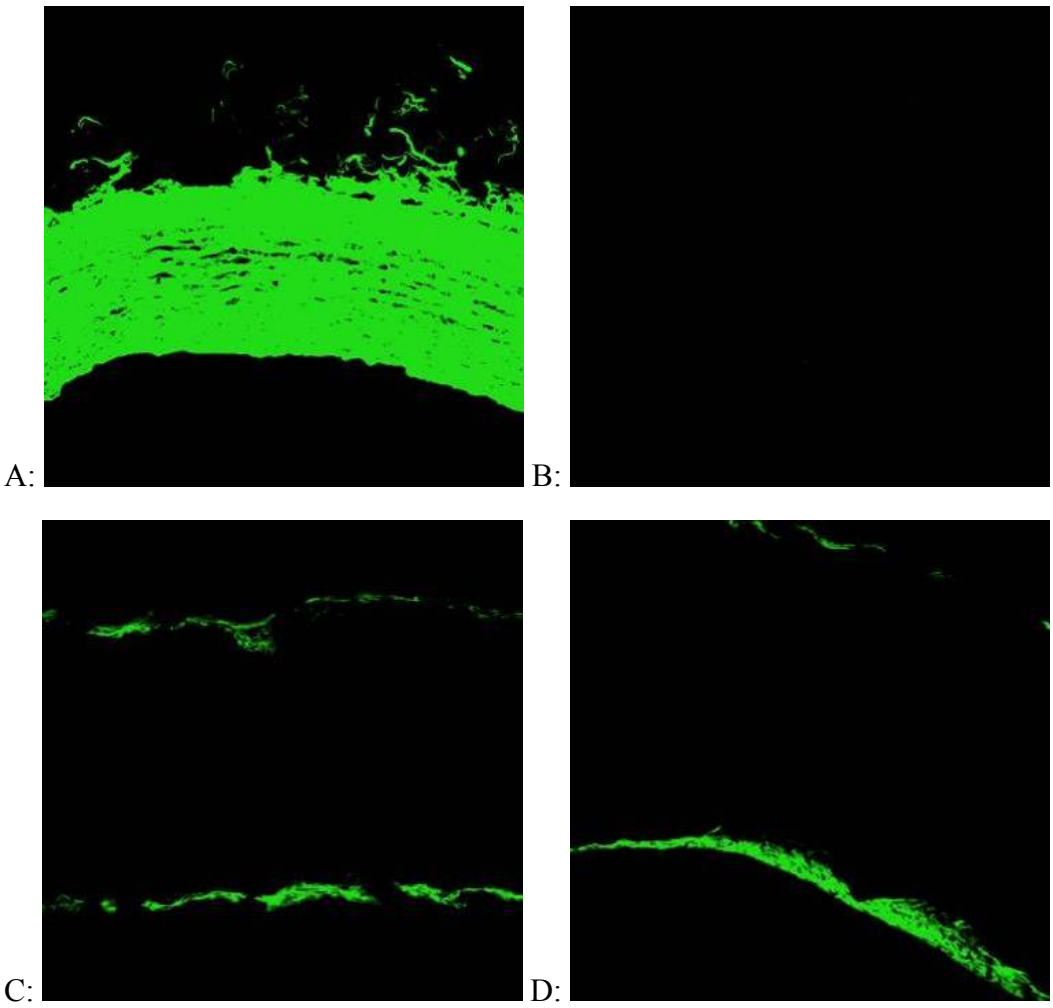

Figure 11.10: Effect of Hydrostatic Pressure on Elastin Distribution in Type V Constructs. Segments of baboon carotid arteries, type V scaffolds cultured with adult baboon SMCs for 21 or 10 days, and uncultured type V scaffolds were snap-frozen and cryosectioned. Cryosections were excited at 488 nm and imaged to qualitatively assess elastin via autofluorescence (magnification 10X). All images are oriented with the luminal surface facing down. The *tunica adventitia* of baboon carotid arteries was removed prior to snap-freezing, and the artery cross-section shown has only the *tunicae media* and *intima* intact. (A) Baboon carotid arteries showed circumferentially-organized elastin throughout the artery wall. (B) The weak autofluorescence of uncultured type V scaffolds was used for image intensity thresholding. (C) Type V constructs cultured at baseline hydrostatic pressure showed concentrations of elastin at the luminal and abluminal surface, as did (D) type V constructs cultured at higher hydrostatic pressure.

Colorimetric Analysis of Soluble and Insoluble Elastin Content

The soluble elastin concentration in culture medium collected from all construct chambers was higher than unused culture medium incubated with an uncultured scaffold (Figure 11.11). Soluble elastin concentration in medium collected from chambers of type V constructs cultured at higher hydrostatic pressure was significantly higher than soluble elastin concentration in culture medium collected from chambers of type V constructs cultured at baseline hydrostatic pressure.

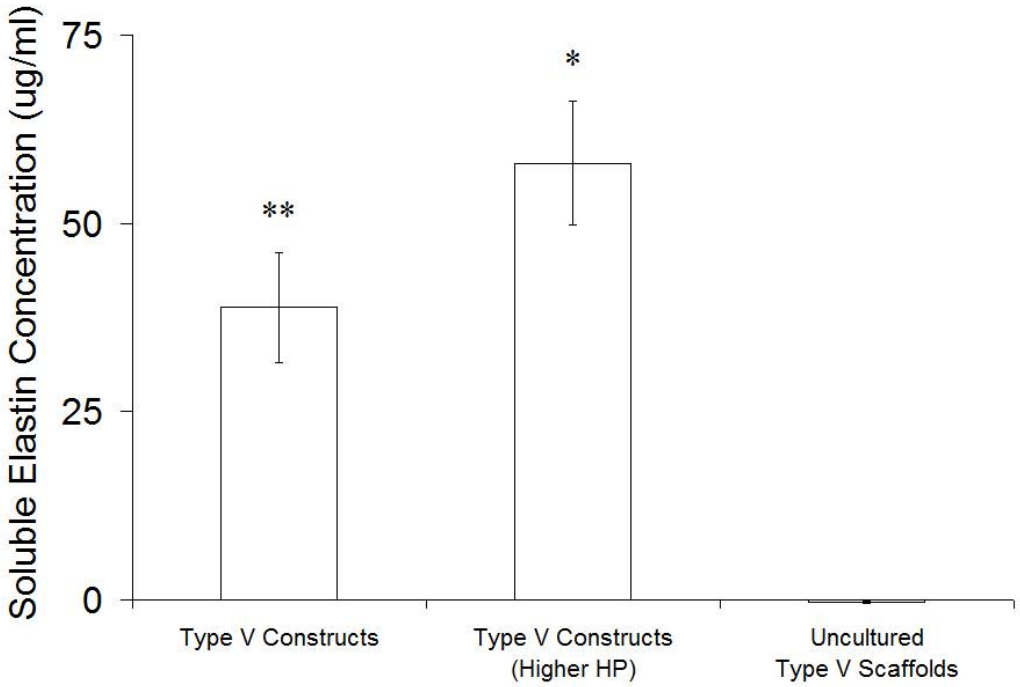

Figure 11.11: Effect of Hydrostatic Pressure on Soluble Elastin Concentration in Culture Medium of Type V Constructs. Soluble elastin concentrations in culture medium collected at the termination of culture of type V scaffolds for 21 days with adult baboon SMCs at baseline or higher hydrostatic pressure and in unused medium incubated with uncultured type V scaffolds were measured indirectly by a dye-binding assay and colorimetric quantification after centrifugation of medium to remove any insoluble elastin (n = 4, 4, and 10 from left to right). *Type V constructs cultured at higher hydrostatic pressure released significantly higher concentrations of soluble elastin into the culture medium compared to type V constructs cultured at baseline hydrostatic pressure. **Type V constructs cultured at baseline hydrostatic pressure released significantly higher concentrations of soluble elastin into the culture medium compared to concentrations measured in unused medium incubated with uncultured type V scaffolds.

Baboon carotid arteries contained significantly more insoluble elastin than all other groups (Figure 11.12). All type V constructs had significantly more insoluble elastin content than uncultured type V scaffolds. Type V constructs cultured at higher hydrostatic pressure contained significantly more insoluble elastin than type V constructs cultured at baseline hydrostatic pressure. The difference between type V constructs

cultured at baseline or higher hydrostatic pressure supported the theory that burst pressures were significantly higher because of significant increases in ECM deposition and remodeling.

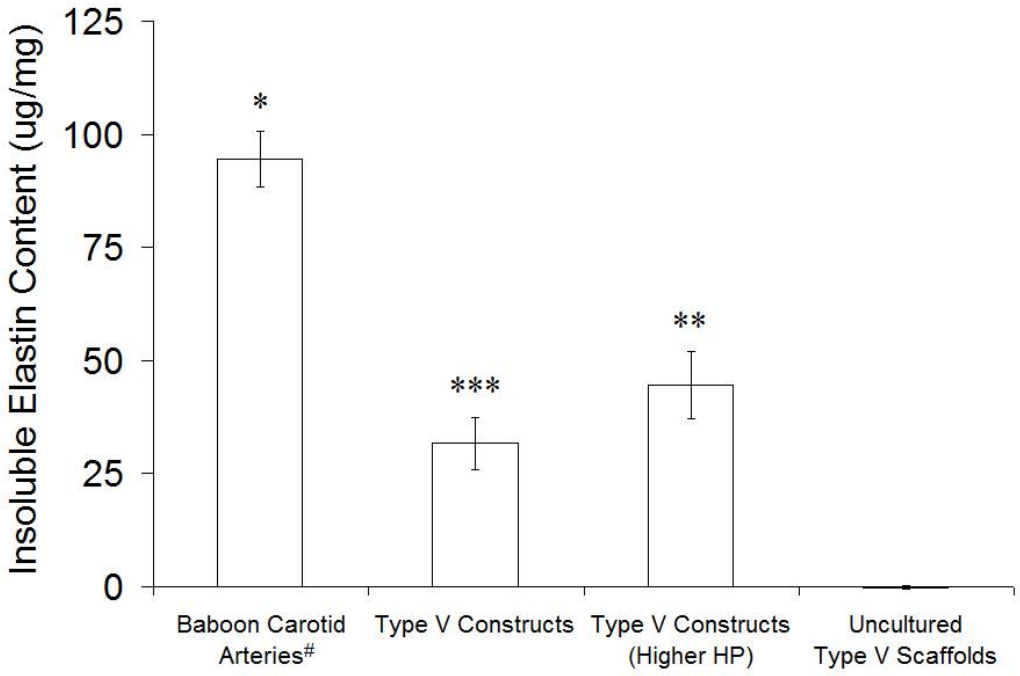

Figure 11.12: Effect of Hydrostatic Pressure on Insoluble Elastin Content in Type V Constructs. Insoluble elastin contents of baboon carotid arteries, type V scaffolds cultured for 21 days with adult baboon SMCs at baseline or higher hydrostatic pressure, and uncultured type V scaffolds were measured indirectly by a dye-binding assay and colorimetric quantification after acid hydrolysis of each construct, which destroyed all proteins except elastin, and centrifugation, which eliminated soluble elastin (n = 4, 4, 4, and 9 from left to right). #The *tunica adventitia* of baboon carotid arteries was removed prior to testing, and results therefore represent properties of the *tunicae media* and *intima* only. *Baboon carotid arteries contained significantly more insoluble elastin than all other groups. **Type V constructs cultured at higher hydrostatic pressure contained significantly more insoluble elastin compared to type V constructs cultured at baseline hydrostatic pressure and uncultured type V scaffolds. ***Type V constructs cultured at baseline hydrostatic pressure contained significantly more insoluble elastin compared to uncultured type IV scaffolds.

Limitations of the Experimental Approach and Recommendations

Hydrostatic pressure in the second-generation bioreactor was conducted at arterial pressures but was probably below that of arterial *tunicae in vivo* due to its unconstrained state (the lack of surrounding tissue). ECM deposition and remodeling, and therefore burst pressures, would increase with physiologic and perhaps even super-physiologic hydrostatic pressure. Increased hydrostatic pressure could be easily implemented in the second-generation bioreactor, though pressure monitors with higher range would need to be used. Concurrent monitoring of construct diameter may also be incorporated into the second-generation bioreactor using a laser micrometer.

Organization of ECM was assessed only qualitatively in this study. Immunofluorescence and autofluorescence at high magnification may show collagen and elastin fibril orientation and could be quantitatively assessed by image analysis. Quantitative indirect measurements of ECM elements such as glycosaminoglycans, procollagen relative to total collagen, and desmosine, which crosslinks elastin molecules, and could be completed using commercially-available kits or protocols established in the literature. Gene regulation in scaffolds with different compliance was also not evaluated but could be used in future studies to investigate how vascular cells regulate the synthesis of key proteins and other biomolecules.

Note: An effort to reproduce data generated by culturing adult baboon SMCs on type V scaffolds in the second-generation bioreactor at higher hydrostatic pressure failed because of contamination. The source of contamination was identified (non-sterile manifolds due to inadequate bleaching, with residual water mitigating autoclave sterilization) and corrected. A second effort to reproduce the data by other laboratory members was underway at the time of thesis submission.

Conclusions

Culturing type V constructs at higher hydrostatic pressure appeared to increase point symmetry in transverse construct cross-sections and decrease wrinkling of the scaffold during compaction in culture without affecting elastic recovery or the distribution of SMCs, collagens I and III, and elastin. Compliance of type V constructs cultured at higher hydrostatic pressure but not at baseline hydrostatic pressure was significantly lower than compliance of baboon carotid arteries. Culturing type V constructs at higher hydrostatic pressure also significantly increased burst pressure, total collagen and insoluble elastin content, and the concentration of soluble elastin in culture medium. A combined discussion of results from this and all other chapters and their implications is presented in Chapter 12.

CHAPTER 12

CONTRIBUTIONS, IMPLICATIONS, LIMITATIONS, AND FUTURE DIRECTIONS OF THE PRESENTED RESEARCH

Contributions of the Research

These studies pursued two avenues of contribution to the field of biomedical engineering generally and tissue engineering specifically: (1) the generation of new methods for engineering tubular tissues; and (2) the formation of insights into PGS-based engineered vasculature. This section outlines contributions of this research to the fields of biomedical and tissue engineering.

New Scaffold Fabrication Techniques for Tissue Engineering

A high-yield process to create porous tubular PGS scaffolds was developed. The process was adaptable and offered control of scaffold pore size, pore interconnectivity, porosity, wall thickness, inner diameter, and length (see Figures 5.1 and 5.2). Creation of PLGA scaffolds using the same process further demonstrated its adaptability. The use of a heat-shrinkable mandrel within the tubular scaffolds significantly increased yield, and coating glass tubes with hyaluronic acid at the outer scaffold surface enabled scaffold wall thickness to be significantly decreased (see Figure 4.5).

New Cell Seeding Techniques for Tissue Engineering

A method for culturing SMCs within the scaffolds was developed and demonstrated how to create continuous tubular constructs (a combination of smooth muscle tissue and remodeled scaffold) in a time period of less than one week (see Figure 6.5). The SMC culture method included a new approach for significantly increasing cell retention in engineered tissue under pulsatile perfusion by passing the cell suspension

through the scaffold walls during seeding (see Figure 4.9), as well as a new approach for evenly distributing cells on the luminal surface of a tubular scaffold by slowly rotating the scaffold horizontal to its axis after seeding but prior to perfusion (see Figure 4.11).

Investigations of Bioreactor Conditions and Their Effect on Construct Properties

This research provided new insights into the effect of bioreactor conditions on biological and mechanical properties of smooth muscle constructs based on PGS scaffolds: (1) higher initial SMC density significantly increases collagen content, significantly decreases elastin crosslinking, and affects collagen distribution and construct compliance (see Chapter 7); (2) scaffold properties affect elastin crosslinking, but not elastin synthesis, and also affect construct compliance (see Chapter 8); (3) briefer culture periods significantly decrease collagen content, crosslinked elastin content, and elastin synthesis and significantly increase construct compliance (see Chapter 9); (4) culture on PGS promotes constructs that resemble arteries in their elastic deformability and stiffness, significantly increases elastin crosslinking without affecting elastin synthesis, and significantly decreases collagen content in contrast to culture on PLGA (see Chapter 10); and (5) increased hydrostatic pressure significantly increases construct burst pressure (up to 130 mmHg after 21 days of culture), decreases construct compliance, and significantly increases collagen content, elastin synthesis, and elastin crosslinking (crosslinked elastin content up to 47% of baboon carotid arteries after 21 days of culture; see Chapter 11). These insights may have implications in and applications to other biomedical and tissue engineering research. However, it is important to point out that the experiments on which these insights are based have not yet been repeated and reproducing the results is necessary to confirm these insights.

Demonstration of Physiologic Compliance in Tissue-engineered Vascular Constructs

The most important contribution of this work may be the demonstration that elastomer-based tissue-engineered constructs cultured *in vitro* can match the compliance of native arteries (see Figure 10.8). The second most important contribution, which is probably related to compliance, is the demonstration that SMCs co-express collagen and elastin, a rarity in vascular tissue engineering,[33,53] when cultured in PGS scaffolds but not in PLGA scaffolds with equivalent physical properties (see Figures 10.9, 10.10, and 10.11). The contributions of this work are considered alongside the contributions of other investigators in the field of vascular tissue engineering in Table 12.1. The sub-physiologic burst pressure of PGS-based constructs is a key weakness of the approach as characterized by current results and contrasts with the strengths of the approach such as briefer *in vitro* preparation time. It should be noted that the response of PGS-based constructs to vasodilators and vasoconstrictors and the bioactivity and stability of their EPC-derived endothelium are not yet investigated. A non-thrombogenic endothelium that can withstand physiologic shear is of utmost importance in avoiding short-term graft failure. Due consideration of this biomimetic property and the associated duration of *in vivo* patency should take priority once physiologic burst pressures are achieved for PGS-based constructs.

Table 12.1: Successes in Blood Vessel Tissue Engineering Revisited. Contributions of this work considered alongside contributions of other investigators. See text accompanying Table 3.1 for citations.

Investigator	**Kaushal et al.**	**Campbell et al.**	**L'Heureux et al.**	**Niklason et al.**	**Tranquillo et al.**	**Crapo et al.**
Graft Material	Decellularized Porcine Iliac Vessels	Peritoneal ECM (Derived *In Vivo)*	ECM & Cell Sheets (Derived *In Vitro*)	PGA	Fibrin Gel	PGS
Cell Source	Ovine	Rat or Rabbit	Human	Bovine or Porcine	Rat	Baboon
Cell Type	EPC	Fibroblast, SMC, Mesothelial	Fibroblast, EC	SMC, EC	Neonatal SMC	SMC, EPC
↓ Biomimetic Property ↓						
Physiologic Burst Pressure	X	X	X	X	?	
Response to Vasodilators	X	X	X	?	?	?
Response to Vasoconstrictors	X	X	X	X	?	?
Stable Endothelium Under Physiologic Shear Stress (~15 dynes/cm^2)	X		X	?	X	?
Elastin & Collagen Co-expressed	?	X			X	X
Physiologic Compliance	?	?			?	X
Animal Model	Ovine	Rat or Rabbit	Rat	Porcine	N/A	
Position of *In Vivo* Testing	Carotid Artery	Descending Aorta or Carotid Artery	Aorta	Saphenous Artery	N/A	N/A
Duration of *In Vitro* Preparation (Days)	2	14	~200	56	42	>21
Duration of *In Vivo* Patency (Days)	130+	120+	225	28+	?	?

Comprehensive Analyses and Context

Correlations between Construct Protein Contents and Mechanical Properties

A comprehensive comparison of all data indicated possible relationships between the protein contents and mechanical properties of individual constructs. Total collagen content appeared to be proportional to burst pressure (Figure 12.1). Insoluble elastin content appeared to also be proportional to burst pressure (Figure 12.2). These trends were expected since greater ECM deposition should tend to strengthen engineered constructs. Discrepancies between individual data points and these trends were most likely a result of differences in ECM crosslinking and how evenly SMCs were distributed in the scaffolds during seeding, which would cause uneven distributions of ECM and weak points in the construct wall.

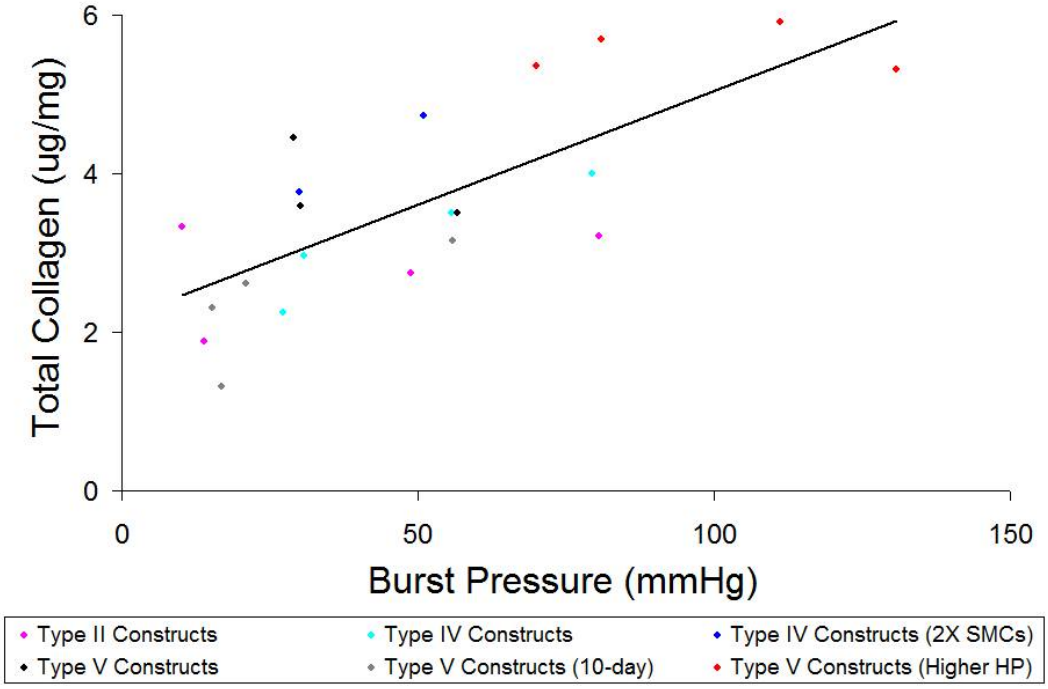

Figure 12.1: Effect of Total Collagen Content on Burst Pressure of Engineered Constructs. Total collagen content and burst pressure of individual constructs (all scaffold types, all culture lengths and conditions) were plotted to discover any trends in the data. There appeared to be a proportional relationship (black linear trend-line) between total collagen content and burst pressure.

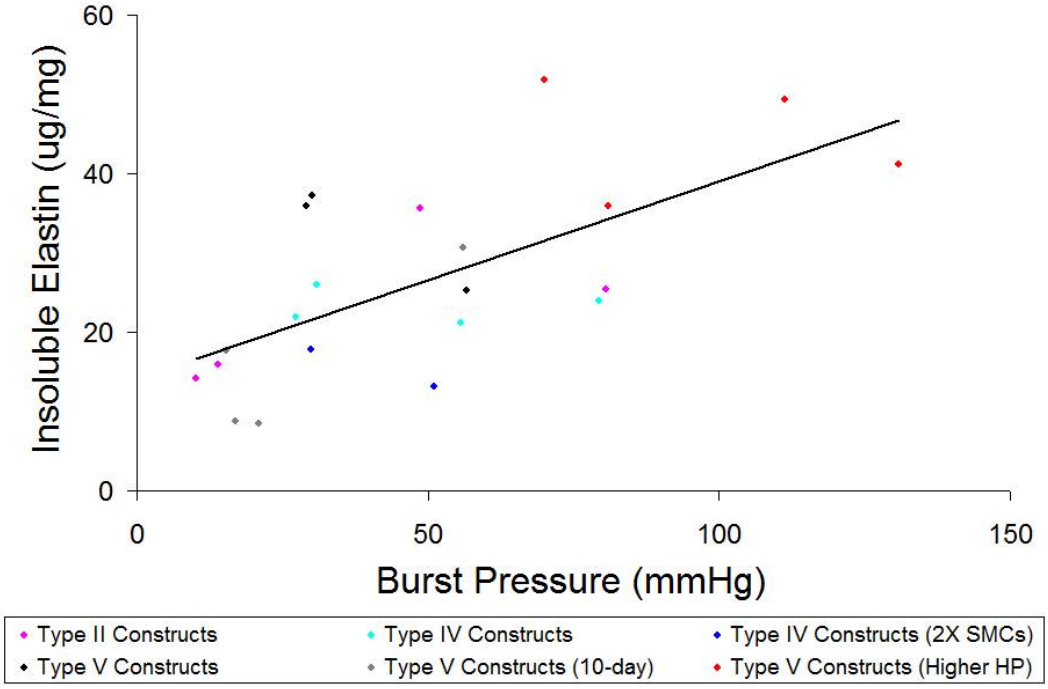

Figure 12.2: Effect of Insoluble Elastin Content on Burst Pressure of Engineered Constructs. Insoluble elastin content and burst pressure of individual constructs (all scaffold types, all culture lengths and conditions) were plotted to discover any trends in the data. There appeared to be a proportional relationship (black linear trend-line) between insoluble elastin content and burst pressure.

Total collagen content was compared to compliance at 15 mmHg, a pressure which maximized the number of constructs included in the analysis. No relationship between total collagen content and compliance was initially apparent until different scaffold types were considered separately, which was reasonable considering that scaffold type was known to significantly affect compliance (see Figure 8.4). Total collagen content appeared to be inversely proportional to compliance, an expected trend based on collagen being a stiffer ECM component (Figure 12.3).[32] The presence of separate trends in different scaffold types suggested differences in collagen organization and crosslinking in constructs based on different scaffold types. However, this

explanation seemed unlikely since type II and IV constructs grouped closely together but type II and IV scaffold properties differed significantly in their mean wall thickness and all mechanical properties.

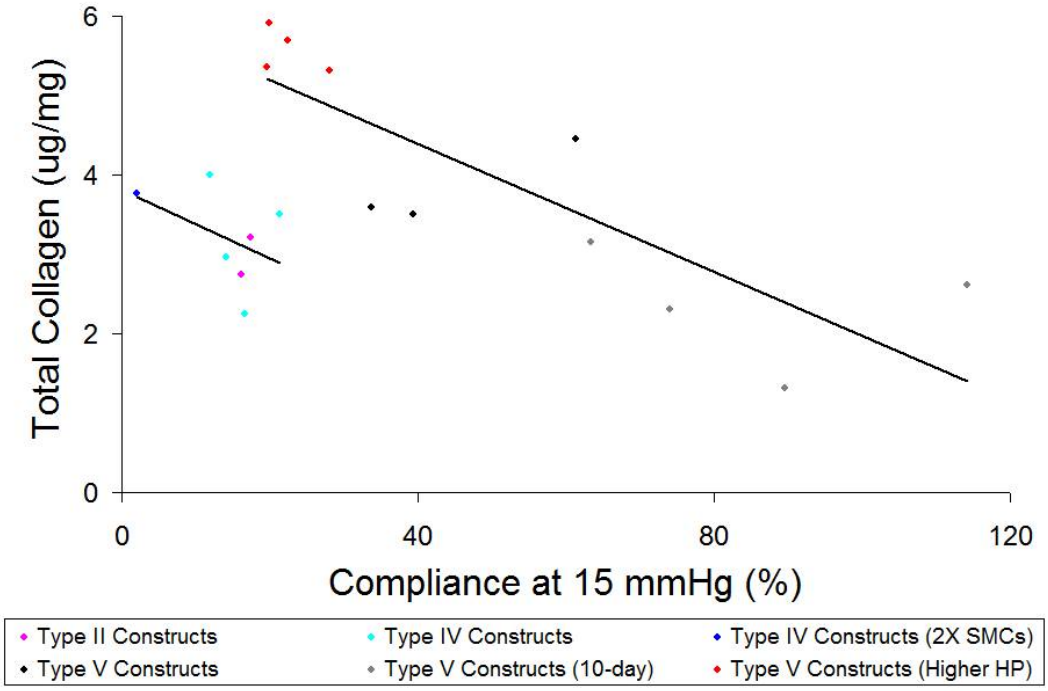

Figure 12.3: Effect of Total Collagen Content on Compliance of Engineered Constructs. Total collagen content and compliance of individual constructs (all scaffold types, all culture lengths and conditions) were plotted to discover any trends in the data. Compliance at 15 mmHg was used to maximize the quantity of constructs included in the analysis. There appeared to be an inverse relationship (black linear trend-lines) between total collagen content and compliance that was scaffold-dependent (longer line represents the trend in type V constructs and shorter line represents the trend in all other construct types combined).

Another possible reason for scaffold-dependent trends in the relationship between total collagen content and compliance was construct compressibility associated with

scaffold type. True compliance reflects changes in internal volume which accommodate pulsatile perfusion, but compliance in these studies (which might be termed apparent compliance) was calculated from measurements of outer diameter rather than luminal diameter or volume (see Chapter 4). Type V scaffolds varied significantly from all other scaffold types in their wall thickness, porosity, strength (σ_{max}), and stiffness (E_{linear}). Lower porosity and thinner scaffold walls would each be expected to reduce construct compressibility and therefore increase apparent compliance. Significant differences in scaffold porosity were especially likely to influence compressibility since type II and IV constructs grouped closely together.

Considering type IV and V constructs only, the significantly difference in construct compliance may have been a result of significant differences in type IV and V scaffold mechanical properties and wall thicknesses. An examination of type IV and V scaffold behavior during uniaxial tensile testing revealed that while the respective mean values of ε_{Tmax} for type IV and V scaffolds were 39 ± 4% and 47 ± 5% (see Figure 6.4), the respective mean values of F_{max} for type IV and V scaffolds were 125 ± 66 mN and 75 ± 12 mN. In other words, less force was required to produce higher circumferential strain in type V scaffolds. Therefore, considering the significantly lower mean wall thickness of type V scaffolds and equal pulsatile flow rates exerting equivalent forces on type IV and V scaffolds, there would be higher strains in type V scaffold walls during construct development. Reducing the strain at failure of type IV scaffolds by a ratio of 75:125 would produce a respective 1:2 difference in the magnitude of strain in type IV and V scaffolds prior to remodeling in culture. Higher strain would induce circumferential orientation of SMC and collagen fibrils[60] and increase synthesis of collagen and some glycosaminoglycans.[61] Cyclic strain at pulsatile perfusion rates used in this study (~0.5-2.5 Hz) would also increase SMC proliferation if serum proteins such as fibronectin or vitronectin mediated SMC adhesion.[63] Therefore, significantly higher compliance in type

V constructs may have directly arisen from the influence of scaffold-dependent strain on collagen synthesis and organization in constructs during culture.

If total collagen content and compliance of constructs are related in a scaffold-dependent manner, construct compliance could be further increased by culturing SMCs in a type VI scaffold with significantly thinner walls than type V scaffolds. The effect of increased strain in type VI scaffold walls might be amplified throughout the culture period by causing SMCs to lay down more compliant collagen fibrils during early stages of culture, which would alter collagen synthesis and organization in subsequent stages. Compliance of type VI constructs would be higher than compliance of type V constructs cultured for the same time period. In this way, thinner scaffold walls and associated increases in strain could be used to combat decreases in construct compliance associated with increases in construct burst pressure, *in vitro* culture time, and hydrostatic pressure during culture.

Insoluble elastin content was compared to compliance at 15 mmHg, a pressure which maximized the number of constructs included in the analysis. Ignoring the established effect of scaffold type on construct compliance (see Figure 8.4) provided no correlation between insoluble elastin content and compliance (Figure 12.4). Separation of scaffold types showed an apparent trend toward a median compliance value of ~20% at 15 mmHg. Unexpectedly, type V constructs showed an inverse relationship between insoluble elastin content and compliance in contrast to all other construct types, which showed insoluble elastin content and compliance to be proportional as expected. The lack of any apparent relationship between insoluble elastin content and compliance suggested at least five possibilities: (1) insoluble elastin content was not a key determinant of compliance, and that factors such as total collagen content dominated individual construct compliance (see Figure 12.3); (2) calculations of compliance based on external diameter measurements were not accurate because of construct compressibility; (3) SMC phenotype was inconsistent in constructs and led to differences in ECM deposition and

remodeling; (4) constructs varied widely in their organization of insoluble elastin, specifically the degree of crosslinking and alignment of fibrils within construct walls; and (5) increasing deposition of insoluble elastin actually shifted construct compliance toward a limit of ~20% compliance at 15 mmHg (see convergence of linear trend-lines in Figure 12.4).

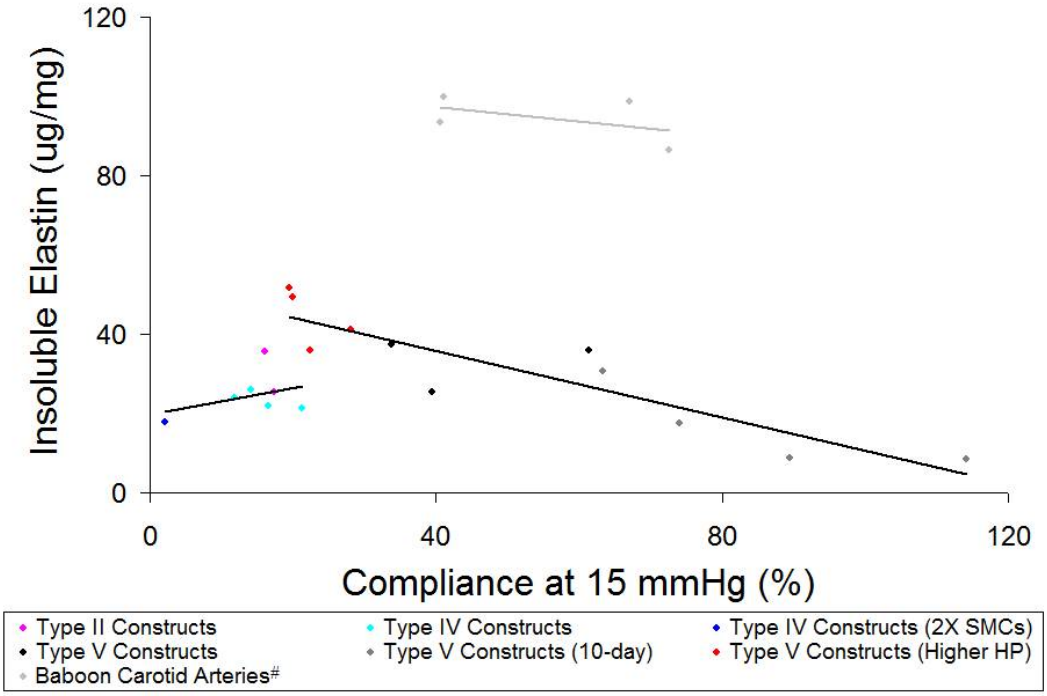

Figure 12.4: Effect of Insoluble Elastin Content on Compliance of Engineered Constructs. Insoluble elastin content and compliance of individual constructs (all scaffold types, all culture lengths and conditions) were plotted to discover any trends in the data. Compliance at 15 mmHg was used to maximize the quantity of constructs included in the analysis. Grouping all constructs together showed no correlation between insoluble elastin content and compliance. There appeared to be an inverse relationship between insoluble elastin content and compliance in type V constructs (longer black linear trend-line). Insoluble elastin content and compliance appeared to be directly proportional in all other construct types (shorter black linear trend-line). Construct compliance appeared to approach a limit of ~20% compliance at 15 mmHg (convergence of black trend-lines). The lack of correlation between insoluble elastin content and compliance in baboon carotid arteries (gray linear trend-line) suggested that differences in the organization of insoluble elastin in baboon carotid arteries and engineered constructs were responsible for different compliances at 15 mmHg. #The *tunica adventitia* of baboon carotid arteries was removed prior to testing, and results therefore represent properties of the *tunicae media* and *intima* only.

If total collagen content dominated compliance then the addition of key regulators of collagen deposition and crosslinking such as TGF-β1,[52] insulin,[52] and lysyl oxidase[117] or their antagonists could be added to the culture medium, which would alter collagen

and elastin crosslinking and therefore the compliance of collagen and elastin fibrils as they are incorporated into the ECM. If compliance measurements were inaccurate then a method for measuring either luminal volume or internal diameter should be implemented for future data collection during pressure-diameter testing. Inconsistencies in SMC phenotype could be addressed by decreasing cell passaging and altering serum concentration during passaging and construct culture. If elastin organization varied widely in constructs then culture conditions could be altered to shift elastin deposition, or at least elastin crosslinking, to earlier stages of the culture period, using medium additives such as cupric sulfate[117] and lysyl oxidase[117] that accelerate elastin crosslinking in culture. However, if increases in insoluble elastin content did shift compliance toward a limit of 20% at only 15 mmHg then basic components of the system, including scaffold properties prior to culture and cell seeding density, would need to be modified to alter the compliance limit itself and shift it toward physiologic values (40-70% for baboon carotid arteries at 15 mmHg). The lack of correlation between insoluble elastin content and compliance in baboon carotid arteries at 15 mmHg (see Figure 12.4, gray linear trend-line) encouraged the idea that insoluble elastin organization influenced compliance.

Placing Poly(glycerol sebacate)-based Construct Compliance in Context

Resting systolic and diastolic pressures in the human circulatory system are 120 and 80 mmHg, and compliance of human arteries in this range is commonly used as an *in vitro* benchmark for vascular graft compliance. Baboon carotid arteries tested in this research had a systolic/diastolic benchmark compliance of 7.1 ± 1.0%, and the single PGS-based construct with a burst pressure above 120 mmHg had a systolic/diastolic benchmark compliance of 3.8 ± 0.6% during its second and third (non-hysteretic) cycles (see Figures 11.5 and 11.6). In contrast, systolic/diastolic benchmark compliances of other tissue-engineered grafts reported in the literature are ~1.0% for a graft based on PGA cultured with bovine SMCs and ECs[48] and 1.5 ± 0.3% for a graft based on rolled

sheets of human fibroblast-derived ECM and human fibroblasts cultured with ECs,[5] the latter currently in human clinical trials as an arteriovenous shunt. The systolic/diastolic benchmark compliance of human internal thoracic and radial arteries measured by the same group had a range of 4.5-6.2%, and human saphenous vein systolic/diastolic benchmark compliance had a range of 0.7-1.5%. It is noteworthy that pressure was cycled at a rate of 480 mmHg/min during pressure-diameter testing of engineered grafts and human arteries and veins by this group, and elastic deformation rates in vessels and grafts may cause underestimation of compliance at this rate. Pressure was cycled at a rate of 40-60 mmHg/min during pressure-diameter testing of baboon carotid arteries and PGS-based constructs to minimize inaccuracies in burst pressure and compliance measurements.

Placing Material Effects in Context

This research has shown that elastin and collagen deposition by SMCs are material-dependent: culture on PGS scaffolds increases elastin deposition and culture on 50:50 PLGA scaffolds increases collagen deposition (see Chapter 10). Previous studies have also demonstrated a relationship between scaffold material and elastin and collagen synthesis and deposition by SMCs. A study by Kim et al. showed that the rate of elastin synthesis by SMCs cultured on PGA, 85:15 PLGA, or collagen I without mechanical stimulation for 11 days was highest within PGA and lowest within collagen I, and that the trend was exactly reversed for collagen synthesis by SMCs on the same materials.[64] ECM deposition followed the same trend for PGA and collagen I, with elastin deposition higher in PGA scaffolds and collagen deposition higher in collagen I scaffolds. A second study by Kim et al. subjecting SMCs on PGA or collagen I to cyclic strain at 1.0 Hz for 14 days showed that mechanical stimulation increases elastin and collagen synthesis regardless of scaffold material and that the material-dependent differences in elastin and collagen synthesis on PGA but not collagen I held true for SMCs subjected to cyclic strain.[63] The combined results of all three studies suggest that PLGA may promote higher SMC elastin

synthesis than PGS without mechanical stimulation but that cyclic strain at 1.2 Hz (range: 0.5-1.7 Hz) in PGS scaffolds compensates for any difference in elastin synthesis. Combined results also suggest that collagen content in PGS-based constructs could be increased by coating scaffolds with collagen gel prior to cell seeding, though such a modification might compromise PGS promotion of elastin deposition and crosslinking.

Placing Hydrostatic Pressure Effects in Context

The concluding study presented in this research demonstrated that increased hydrostatic pressure promoted elastin synthesis and collagen and elastin deposition by SMCs in PGS scaffolds subjected to pulsatile flow and associated cyclic strain (see Chapter 11). Increases in SMC proliferation within PGS-based constructs as a result of higher pulsatile hydrostatic pressure probably contributed to increases in ECM synthesis and deposition.[66,67] Previous studies indicate that baseline hydrostatic pressure used in our research should not increase SMC protein synthesis compared to two-dimensional SMC culture.[69] However, increased pulsatile hydrostatic pressure has been shown to directly increase SMC collagen synthesis under conditions similar to those used in our study (100 ± 20 mmHg at 1.167 Hz compared to 120 ± 20 mmHg at 1.8 Hz (range: 0.5-2.5 Hz) for the majority of the PGS-based construct culture period).[70] In fact, increasing pulsatile hydrostatic pressure to super-physiologic levels (140 ± 20 mmHg at 1.167 Hz) further increased collagen synthesis, and increasing the pulsatile frequency to 2.0 Hz produced a two-fold increase in sulfated glycosaminoglycans synthesis with a coordinate but non-significant increase in collagen synthesis.

Increased hydrostatic pressure also decreased PGS scaffold compaction and PGS-based construct compliance. SMC migration increases with hydrostatic pressure, especially when pulsatile,[65] and may have contributed to apparently tighter grouping of PGS-based construct compliance compared to culture under all other conditions (see Figures 7.4, 9.3, and 11.6) by causing redistribution of SMCs during culture and thereby

reinforcing weaker sections of construct walls. Shorter residence time of SMCs on scaffold surfaces would allow the elastomeric PGS microstructure to rebound more regularly and more readily and could therefore contribute to decreases in scaffold wrinkling and compaction.

Limitations of the Research and Recommended Future Studies

Limitations and recommendations have been offered with the individual studies from this research (see Limitations of the Experimental Approach and Recommendations in Chapters 5-11). Finite resources require selective implementation of the recommendations included with this work, and the most promising ideas, as gauged by their potential to increase knowledge in the fields of biomedical and tissue engineering and to develop a potential treatment for urgent clinical care, are presented in greater depth in this section. Prospective studies are sequential and intended to progress from fundamental to applied research and include all graft properties that might be perceived as critical. Some of the steps for graft development presented in this section could be omitted based on their perceived value.

Characterize Hyaluronic Acid Residues in Poly(glycerol sebacate) Scaffolds

The molecular weight of hyaluronic acid residues in PGS type V scaffolds should be characterized.[120] Hyaluronic acid oligomers have recently been demonstrated to increase elastin synthesis and crosslinking,[120] especially in conjunction with TGF-β1,[121] although this may decrease SMC proliferation.[121] The effect of hyaluronic acid oligomers is increased when they are presented on a surface rather than as a medium supplement.[122] Hyaluronic acid residues on type V scaffolds may have contributed to a non-significant increase in elastin synthesis (see Figure 8.9) and a significant increase in insoluble elastin content (see Figure 8.10) in type V constructs compared to type IV constructs. The use of hyaluronic acid in future scaffold fabrication methods should therefore be retained.

Directly Measure Cell Proliferation and Apoptosis in Scaffolds

Changes in SMC quantity over time did not directly measure proliferation or eliminate the possibility of cytotoxicity. However, the effects of PGS scaffolds on cell proliferation and apoptosis are likely to influence *in vitro* burst pressures of PGS-based constructs as well as *in vivo* outcomes. Incorporation of BrdU should be used to directly measure the rate of SMC proliferation in PGS scaffolds. A live/dead assay such as TUNEL should be used to compare SMC apoptosis in PGS type V scaffolds, and results should be compared to two-dimensional culture on TCPS. Time points of 24 hours and seven days could be used. EPC apoptosis should also be investigated. If any significant differences in SMC or EPC apoptosis exist then a secondary comparison between TCPS and two-dimensional PGS films could be used to determine whether PGS itself elicits DNA fragmentation. Cytotoxicity in SMCs and EPCs on PGS films has been assessed previously using a MTT assay, which showed that mitochondria activity in cells was not altered by PGS but did not conclusively disprove cytotoxicity.[99] (Increased mitochondrial activity or proliferation rates could obscure cytotoxicity as assessed by MTT assay.) It is therefore recommended that cytotoxicity be directly assessed by examining cell apoptosis in tubular PGS scaffolds.

Investigate the Effect of Scaffold Pore Size on Cell Seeding and Cellular Confluence

Cell seeding efficiency in tubular PGS scaffolds was ~80% using through-wall flow, and approximately seven days were required to reach luminal cellular confluence. The effect of pore size on cell seeding efficiency and cellular confluence should be investigated. Scaffolds with a pore size closer to the diameter of individual SMCs could be fabricated using smaller salt porogen size. Similar diameters of pores relative to individual cell size may help SMCs to adhere more readily to scaffolds by increasing the contact surface area between the SMCs and the pores. Smaller pores could decrease cell washout, thereby increasing cell seeding efficiency and decreasing culture time required

for confluence. Smaller pores may also more evenly distribute SMCs in scaffold lumens, causing a reduction in the variance of PGS-based construct compliance and possibly altering burst pressure and compliance.

Scaffolds with smaller pores are more likely to retain unreacted monomers and residual salt unless scaffold pretreatment times are extended to allow equivalent ethanol penetration and subsequent removal by PBS. Smaller pores are likely to decrease cell penetration into scaffold walls during seeding and through-wall flow. Nutrient and metabolite diffusion within and through scaffold walls is also likely to be decreased by smaller pores. A decrease in pore size may also decrease the adhesion of confluent SMC layers to scaffold lumens, adversely affecting the biological and mechanical properties of PGS-based construct.

Investigate the Effect of Scaffold Stiffness on Construct Properties

The effect of scaffold stiffness and elasticity should be investigated by comparing culture in PGS type V scaffolds fabricated with all parameters except curing time being identical. Extended curing time will increase polymer crosslinking and therefore increase scaffold stiffness. Scaffold degradation should be investigated before culture to determine whether mass loss and decreases in mechanical properties vary significantly with different durations of scaffold curing. SMC proliferation on the scaffolds should also be investigated prior to construct analysis to determine whether differences in PGS crosslinking and increased oxidation during scaffold curing change scaffold surface chemistry and by-products and therefore affect SMC behavior. Scaffolds curing times of 24 hours (used in this work) or 96 hours could be compared, since we have qualitatively noted different stiffness in handling of scaffolds cured at these times. Once two curing times have been identified that produce scaffolds with significantly different mechanical properties but without significantly different degradation characteristics and SMC proliferation rates, PGS-based constructs can be compared and conclusions can be drawn

about the effect of scaffold stiffness on the biological and mechanical properties of engineered constructs.

It should be noted that mechanical and degradation properties of PGS scaffolds may be coupled too tightly to produce a significant difference in stiffness but not in degradation. Even if mechanical and degradation properties of PGS scaffolds can be decoupled they may have a confounding effect on the biological and mechanical properties of PGS-based constructs, causing statistical significance that is not solely attributable to a change in scaffold mechanical properties. An alternative approach to investigate the effect of scaffold stiffness on constructs properties would be to cure a solid sheet of PGS around the scaffold ablumen and varying the sheet thickness. A second alternative approach would be to fabricate scaffolds using PGS pre-polymers with different molecular weights (pre-polymer chain lengths). It should be noted that these alternatives would alter culture conditions such as the magnitude of luminal shear stress in the former case or polymer degradation in the latter case.

Transition to Primary Adult Human Cells

Properties of engineered grafts are known to be species-dependent.[5] Primary adult human SMCs and EPCs might be obtained from unusable blood donations and biopsy tissue samples collected in the clinic. Using human cells to create PGS-based constructs would widen the implications of this research and decrease the timeline to potential FDA approval for clinical testing of the technology. If human cells (SMCs and/or EPCs) cultured in PGS-based constructs co-expressed elastin and collagen this finding would be unprecedented and potentially revolutionize the field of tissue engineering. The remaining sections in this chapter assume continued use of baboon cells but are generally applicable to PGS-based constructs derived from cells of any mammalian species.

Increase Collagen Content in Poly(glycerol sebacate)-based Constructs

Collagen content in PGS-based constructs was less than 10% of collagen content in baboon and porcine carotid arteries. Long et al. showed that adding TGF-β1 at 2.0 ng/ml and insulin at 2.0 μg/ml resulted in a 20-fold increase in collagen synthesis by neonatal rat SMCs in fibrin gels *in vitro*.[52] Niklason et al. demonstrated significant increases in SMC proliferation and burst pressure by supplementing culture medium with PDGF and amino acids, respectively.[6] It is therefore recommended that these medium additives be used to increase collagen content in PGS-based constructs. It is likely that culture medium could be saturated with amino acids without any adverse effects on construct properties. PDGF, TGF-β1, and insulin could initially be investigated at the same concentrations reported previously to improve PGS-based construct mechanical properties. If increased collagen content reduces compliance then it is recommended that either: (1) concentrations of PDGF, TGF-β1, and insulin be reduced or one or more be eliminated completely; (2) lysyl oxidase also be added to the culture medium to increase crosslinking of both elastin and collagen and thereby alter construct compliance;[117,118] or (3) protein crosslinking in PGS-based constructs be reduced, or at least delayed until later stages of culture, by supplementing medium with hydroxylysyl pyridinoline[117] to decrease lysyl oxidase crosslinking of collagen within constructs or by supplementing medium with antibodies against lysyl oxidase to directly decrease its activity in culture.

Further Characterize the Extracellular Matrix of Poly(glycerol sebacate)-based Constructs

A wide variety of ECM molecules other than elastin and collagen contribute to the mechanical properties of arteries, and their presence and distribution should be assessed within the ECM of PGS-based constructs. A colorimetric assay to quantify sulfated glycosaminoglycans is commercially available (Blyscan™ Glycosaminoglycan Assay kit; Biocolor Ltd.) and could be used to quantitatively compare PGS-based

constructs in the future. Single cryosections immunofluorescently stained against elastin and associated proteins such as fibrillin-1[52] and desmosine[118,120] may provide insights into elastin organization in PGS-based constructs. Layers of elastic fibers and SMCs alternate in the *tunica media* of arteries,[32-34] and similarities between the structure of arteries and PGS-based constructs might be assessed by coordinate immunofluorescent staining against α-smooth muscle actin and elastin or collagens I and III. Once collagen and elastin content in PGS-based constructs is increased, the alignment of elastic fibers should be assessed. Fiber angles could be analyzed in high-magnification images using Masson's trichrome stain (collagen), Verhoeff's stain (elastin), immunofluorescence (collagen or elastin), or autofluorescence at 488 nm (elastin). An internal elastic lamina composed of collagen IV, laminin, elastin, and fibronectin resides between the *tunicae media* and *intima* of arteries,[30,31] and the presence of an elastic lamina in PGS-based constructs cocultured with SMCs and EPCs could be probed using immunofluorescent antibodies against one or more of these proteins.

Incorporate a Functional Endothelium into Poly(glycerol sebacate)-based Constructs

A functional endothelium must be incorporated into PGS-based constructs for non-thrombogenic functionality *in vivo*. EPCs can be cocultured with SMCs in PGS-based constructs (see Chapter 5), and EPCs in cocultured tubular PGS scaffolds remain at the luminal surface and express vWF.[95] L'Heureux et al. showed that ECs remain adherent to *in vitro*-derived ECM under physiologic shear stress after only three days of *in vitro* conditioning,[5] and Isenberg et al. showed EC adherence to SMC-only fibrin-based constructs under physiologic shear after only two days.[7] Perhaps most applicable to our studies is the demonstration by Kaushal et al. of EPC adherence under physiologic shear after only two days of *in vitro* conditioning on uncultured ePTFE.[3] Based on these results from the literature, the introduction of EPCs on day 7 of a 21-day culture in an

effort to ensure endothelium integrity may be premature,[95] though possible benefits of early EPC seeding to the biological and mechanical properties of whole PGS-based constructs are unknown. It is recommended that EPCs be introduced into SMC-only PGS-based constructs on day 18 of a 21-day culture, and that EPC adherence under physiologic shear stress be tested at the termination of culture by vWF immunofluorescence in cryosections cut from shear-stress-tested constructs at regular intervals. A side study could investigate the relationship between earlier EPC introduction (perhaps on day 9) and the biological and mechanical properties of PGS-based constructs, especially since a shear-protective layer of confluent EPCs in coculture is likely to increase SMC proliferation and protein content in PGS-based constructs.[57] Construct reaction to vasodilators and vasoconstrictors should be evaluated only after a method to create stable endothelium is established. Exposure to acetylcholine should be included in this analysis since functional endothelium produces vasodilation but dysfunctional endothelium produces vasoconstriction.[123]

Evaluate Short-term Patency of Poly(glycerol sebacate)-based Constructs

Once the endothelium appears to function normally *in vitro*, cocultured PGS-based constructs should be tested in an *ex vivo* baboon arteriovenous shunt model to assess whether EPCs remain adherent to construct lumens and prevent thrombosis and occlusion in a time-frame of hours.[124] Platelet deposition and thrombus formation could be assessed directly at the termination of the shunt study,[3,5] and immunofluorescence of sections cut at regular intervals from each tested PGS-based construct could be used to determine *ex vivo* endothelium integrity. Short-term patency should also be assessed by monitoring shunt recipients for signs of thromboembolism such as stroke or myocardial infarct.

Evaluate Fatigue in Poly(glycerol sebacate)-based Constructs

After physiologic burst pressure and compliance in endothelialized PGS-based constructs are achieved, *in vitro* fatigue testing over thousands of cycles should be performed prior to *in vivo* animal studies. These tests should neglect the effect of surrounding tissue and should be completed in a shallow bath of medium at 37°C to minimize external hydrostatic pressure around the construct and kinetic effects caused by non-physiologic temperatures. Fatigue testing of PGS-based constructs should be done at physiologic frequencies to ensure complete construct distension during each cycle and at super-physiologic transmural pressures to provide a margin of safety.

Evaluate Long-term Patency of Poly(glycerol sebacate)-based Constructs

The development of PGS-based constructs with physiologic burst pressure and compliance, *ex vivo* endothelium function and short-term patency, and lack of creep during *in vitro* fatigue testing leaves only long-term *in vivo* patency uninvestigated. Long-term patency would preferably be assessed in a baboon model such as a carotid interposition graft[3] but could be tested for periods of months in the same *ex vivo* baboon arteriovenous shunt model used to assess short-term patency.[124] I*n vivo* imaging techniques such as ultrasound[3,5,6] or computed tomographic angiography[5] could be used to assess long-term patency.

Overall Conclusions

Scaffold fabrication using heat-shrinkable mandrels and glass tubes coated with hyaluronic acid significantly decreased tolerances of wall thickness and mechanical properties, improved handling, and decreased culture time required to reach luminal cellular confluence compared to scaffolds made with other fabrication techniques. The initial density of SMCs in PGS-based constructs altered ECM deposition and organization. PGS scaffold properties determined biological and mechanical properties of

their derivative constructs. ECM deposition increased with SMC-only culture time, and ECM deposition and remodeling during culture influenced construct compliance. PGS compared favorably to PLGA, a benchmark biomaterial, as a scaffold material for vascular tissue engineering. Compared to PLGA scaffolds, PGS scaffolds promoted elastin crosslinking by SMCs and elastic tissue properties but attenuated collagen deposition. Hydrostatic pressure promoted ECM synthesis and deposition by SMCs and altered construct compliance. Collagen and crosslinked elastin content in constructs correlated positively with construct burst pressure, and a negative correlation dependent on scaffold type was found between collagen content and construct compliance at low pressures.

Biological and mechanical properties of constructs created by culturing adult baboon vascular cells on porous tubular PGS scaffolds demonstrated potential for PGS-based vascular tissue engineering. The central hypothesis of this work, that grafts engineered from PGS scaffolds and adult vascular cells under biomimetic *in vitro* culture conditions can possess compliance comparable to autologous vessels, was proven true at low pressures. However, results regarding compliance at pressures in excess of 60 mmHg were inconclusive, and the central hypothesis of this work therefore was only partially validated. Future studies are required to conclusively prove whether culturing adult vascular cells on PGS scaffolds under biomimetic *in vitro* culture conditions can produce engineered grafts with compliance comparable to autologous vessels at peak systolic and diastolic pressures. Overall, this work provides a foundation for PGS-based vascular tissue engineering.

REFERENCES

1. Braunwald H. A Textbook of Cardiovascular Medicine. Philadelphia: Saunders; 1997.

2. Shin'oka T, Matsumura G, Hibino N, Naito Y, Watanabe M, Konuma T, Sakamoto T, Nagatsu M, Kurosawa H. Midterm clinical result of tissue-engineered vascular autografts seeded with autologous bone marrow cells. J Thorac Cardiovasc Surg 2005;129(6):1330-8.

3. Kaushal S, Amiel GE, Guleserian KJ, Shapira OM, Perry T, Sutherland FW, Rabkin E, Moran AM, Schoen FJ, Atala A, Soker S, Bischoff J, Mayer JE Jr. Functional small-diameter neovessels created using endothelial progenitor cells expanded ex vivo. Nat Med 2001;7(9):1035-40.

4. Campbell JH, Efendy JL, Campbell GR. Novel vascular graft grown within recipient's own peritoneal cavity. Circ Res 1999;85(12):1173-8.

5. L'Heureux N, Dusserre N, Konig G, Victor B, Keire P, Wight TN, Chronos NA, Kyles AE, Gregory CR, Hoyt G, Robbins RC, McAllister TN. Human tissue-engineered blood vessels for adult arterial revascularization. Nat Med 2006;12(3):361-5.

6. Niklason LE, Gao J, Abbott WM, Hirschi KK, Houser S, Marini R, Langer R. Functional arteries grown in vitro. Science 1999;284(5413):489-93.

7. Isenberg BC, Williams C, Tranquillo RT. Endothelialization and flow conditioning of fibrin-based media-equivalents. Ann Biomed Eng 2006;34(6):971-85.

8. Stankus JJ, Guan J, Fujimoto K, Wagner WR. Microintegrating smooth muscle cells into a biodegradable, elastomeric fiber matrix. Biomaterials 2006;27(5):735-44.

9. Matsumura G, Miyagawa-Tomita S, Shin'oka T, Ikada Y, Kurosawa H. First evidence that bone marrow cells contribute to the construction of tissue-engineered vascular autografts in vivo. Circulation 2003;108(14):1729-34.

10. Fujiyama S, Amano K, Uehira K, Yoshida M, Nishiwaki Y, Nozawa Y, Jin D, Takai S, Miyazaki M, Egashira K, Imada T, Iwasaka T, Matsubara H. Bone marrow

monocyte lineage cells adhere on injured endothelium in a monocyte chemoattractant protein-1-dependent manner and accelerate reendothelialization as endothelial progenitor cells. Circ Res 2003;93(10):980-9.

11. Ma PX, Choi JW. Biodegradable polymer scaffolds with well-defined interconnected spherical pore network. Tissue Eng 2001;7(1):23-33.

12. Yang C, Sodian R, Fu P, Luders C, Lemke T, Du J, Hubler M, Weng Y, Meyer R, Hetzer R. In vitro fabrication of a tissue engineered human cardiovascular patch for future use in cardiovascular surgery. Ann Thorac Surg 2006;81(1):57-63.

13. Guan J, Fujimoto KL, Sacks MS, Wagner WR. Preparation and characterization of highly porous, biodegradable polyurethane scaffolds for soft tissue applications. Biomaterials 2005;26(18):3961-71.

14. Yang J, Motlagh D, Webb AR, Ameer GA. Novel biphasic elastomeric scaffold for small-diameter blood vessel tissue engineering. Tissue Eng 2005;11(11-12):1876-86.

15. Fromstein JD, Woodhouse KA. Elastomeric biodegradable polyurethane blends for soft tissue applications. J Biomater Sci Polym Ed 2002;13(4):391-406.

16. Nagapudi K, Brinkman WT, Thomas BS, Park JO, Srinivasarao M, Wright E, Conticello VP, Chaikof EL. Viscoelastic and mechanical behavior of recombinant protein elastomers. Biomaterials 2005;26(23):4695-706.

17. Lu Q, Ganesan K, Simionescu DT, Vyavahare NR. Novel porous aortic elastin and collagen scaffolds for tissue engineering. Biomaterials 2004;25(22):5227-37.

18. Berglund JD, Nerem RM, Sambanis A. Incorporation of intact elastin scaffolds in tissue-engineered collagen-based vascular grafts. Tissue Eng 2004;10(9-10):1526-35.

19. Roeder R, Wolfe J, Lianakis N, Hinson T, Geddes LA, Obermiller J. Compliance, elastic modulus, and burst pressure of small-intestine submucosa (SIS), small-diameter vascular grafts. J Biomed Mater Res 1999;47(1):65-70.

20. L'Heureux N, McAllister TN, de la Fuente LM. Tissue-engineered blood vessel for adult arterial revascularization. N Engl J Med 2007;357(14):1451-3.

21. Abbott WM, Megerman J, Hasson JE, L'Italien G, Warnock DF. Effect of compliance mismatch on vascular graft patency. J Vasc Surg 1987;5(2):376-82.

22. Trubel W, Moritz A, Schima H, Raderer F, Scherer R, Ullrich R, Losert U, Polterauer P. Compliance and formation of distal anastomotic intimal hyperplasia in Dacron mesh tube constricted veins used as arterial bypass grafts. ASAIO J 1994;40(3):M273-8.

23. Hofstra L, Bergmans DC, Hoeks AP, Kitslaar PJ, Leunissen KM, Tordoir JH. Mismatch in elastic properties around anastomoses of interposition grafts for hemodialysis access. J Am Soc Nephrol 1994;5(5):1243-50.

24. Trubel W, Schima H, Moritz A, Raderer F, Windisch A, Ullrich R, Windberger U, Losert U, Polterauer P. Compliance mismatch and formation of distal anastomotic intimal hyperplasia in externally stiffened and lumen-adapted venous grafts. Eur J Vasc Endovasc Surg 1995;10(4):415-23.

25. Sarkar S, Salacinski HJ, Hamilton G, Seifalian AM. The mechanical properties of infrainguinal vascular bypass grafts: their role in influencing patency. Eur J Vasc Endovasc Surg 2006;31(6):627-36.

26. Rosamond W, Flegal K, Furie K, Go A, Greenlund K, Haase N, Hailpern SM, Ho M, Howard V, Kissela B, Kittner S, Lloyd-Jones D, McDermott M, Meigs J, Moy C, Nichol G, O'Donnell C, Roger V, Sorlie P, Steinberger J, Thom T, Wilson M, Hong Y; American Heart Association Statistics Committee and Stroke Statistics Subcommittee. Heart disease and stroke statistics--2008 update: a report from the American Heart Association Statistics Committee and Stroke Statistics Subcommittee. Circulation 2008;117(4):e25-146.

27. Daemen J, Serruys PW. Optimal revascularization strategies for multivessel coronary artery disease. Curr Opin Cardiol 2006;21(6):595-601.

28. Desai ND, Fremes SE. Radial artery conduit for coronary revascularization: as good as an internal thoracic artery. Curr Opin Cardiol 2007;22(6):534-40.

29. Suma H. Arterial grafts in coronary bypass surgery. Ann Thorac Cardiovasc Surg 1999;5:141-5.

30. Carey DJ. Control of growth and differentiation of vascular cells by extracellular matrix proteins. Annu Rev Physiol 1991;53:161-77.

31. Jaffe JA. Inflammation: basic principles and clinical correlates. New York: Raven Press, Ltd; 1988.

32. Silver FH, Horvath I, Foran DJ. Viscoelasticity of the vessel wall: the role of collagen and elastic fibers. Crit Rev Biomed Eng 2001;29(3):279-301.

33. Patel A, Fine B, Sandig M, Mequanint K. Elastin biosynthesis: The missing link in tissue-engineered blood vessels. Cardiovasc Res 2006;71(1):40-9.

34. Gleason RL, Hu JJ, Humphrey JD. Building a functional artery: issues from the perspective of mechanics. Front Biosci 2004;9:2045-55.

35. www.sci.sdsu.edu/histology/ci07.htm.

36. Kassab GS, Navia JA. Biomechanical considerations in the design of graft: the homeostasis hypothesis. Annu Rev Biomed Eng 2006;8:499-535.

37. Sonoda H, Takamizawa K, Nakayama Y, Yasui H, Matsuda T. Coaxial double-tubular compliant arterial graft prosthesis: time-dependent morphogenesis and compliance changes after implantation. J Biomed Mater Res A 2003;65(2):170-81.

38. Okuhn SP, Connelly DP, Calakos N, Ferrell L, Pan MX, Goldstone J. Does compliance mismatch alone cause neointimal hyperplasia. J Vasc Surg 1989;9(1):35-45.

39. Fei DY, Thomas JD, Rittgers SE. The effect of angle and flow rate upon hemodynamics in distal vascular graft anastomoses: a numerical model study. J Biomech Eng 1994;116(3):331-6.

40. Stewart SF, Lyman DJ. Effects of an artery/vascular graft compliance mismatch on protein transport: a numerical study. Ann Biomed Eng 2004;32(7):991-1006.

41. Melbin J, Ho PC. Stress reduction by geometric compliance matching at vascular graft anastomoses. Ann Biomed Eng 1997;25(5):874-81.

42. Sterpetti AV, Cucina A, Randone B, Palumbo R, Stipa F, Proietti P, Saragosa MT, Santoro-D'Angelo L, Cavallaro A. Growth factor production by arterial and vein grafts: relevance to coronary artery bypass grafting. Surgery 1996;120(3):460-7.

43. Dardik H, Ibrahim IM, Dardik I. Modified and unmodified umbilical vein allografts and xenografts as arterial substitutes: morphologic assessment. Surg Forum 1975;26:286-7.

44. Yeager A, Callow AD. New graft materials and current approaches to an acceptable small diameter vascular graft. ASAIO Trans 1988;34(2):88-94.

45. Seifalian A, Giudiceandrea A, Schmitz-Rixen T. Tissue Engineering of Vascular Prosthetic Grafts: R.G. Landes Bioscience; 1999.

46. Tissue engineering of blood vessel. New York: Marcel Dekker; 2004.

47. Weinberg CB, Bell E. A blood vessel model constructed from collagen and cultured vascular cells. Science 1986;231(4736):397-400.

48. Niklason LE, Abbott W, Gao J, Klagges B, Hirschi KK, Ulubayram K, Conroy N, Jones R, Vasanawala A, Sanzgiri S, Langer R. Morphologic and mechanical characteristics of engineered bovine arteries. J Vasc Surg 2001;33(3):628-38.

49. Ratcliffe A. Tissue engineering of vascular grafts. Matrix Biol 2000;19(4):353-7.

50. Grassl ED, Oegema TR, Tranquillo RT. A fibrin-based arterial media equivalent. J Biomed Mater Res A 2003;66(3):550-61.

51. Grassl ED, Oegema TR, Tranquillo RT. Fibrin as an alternative biopolymer to type-I collagen for the fabrication of a media equivalent. J Biomed Mater Res A 2002;60(4):607-12.

52. Long JL, Tranquillo RT. Elastic fiber production in cardiovascular tissue-equivalents. Matrix Biol 2003;22(4):339-50.

53. Isenberg BC, Williams C, Tranquillo RT. Small-diameter artificial arteries engineered in vitro. Circ Res 2006;98(1):25-35.

54. Laflamme K, Roberge CJ, Labonte J, Pouliot S, D'Orleans-Juste P, Auger FA, Germain L. Tissue-engineered human vascular media with a functional endothelin system. Circulation 2005;111(4):459-64.

55. L'Heureux N, Stoclet JC, Auger FA, Lagaud GJ, Germain L, Andriantsitohaina R. A human tissue-engineered vascular media: a new model for pharmacological studies of contractile responses. FASEB J 2001;15(2):515-24.

56. L'Heureux N, Paquet S, Labbe R, Germain L, Auger FA. A completely biological tissue-engineered human blood vessel. FASEB J 1998;12(1):47-56.

57. Ueba H, Kawakami M, Yaginuma T. Shear stress as an inhibitor of vascular smooth muscle cell proliferation. Role of transforming growth factor-beta 1 and tissue-type plasminogen activator. Arterioscler Thromb Vasc Biol 1997;17(8):1512-6.

58. Sterpetti AV, Cucina A, D'Angelo LS, Cardillo B, Cavallaro A. Shear stress modulates the proliferation rate, protein synthesis, and mitogenic activity of arterial smooth muscle cells. Surgery 1993;113(6):691-9.

59. Kohler TR, Kirkman TR, Kraiss LW, Zierler BK, Clowes AW. Increased blood flow inhibits neointimal hyperplasia in endothelialized vascular grafts. Circ Res 1991;69(6):1557-65.

60. Kanda K, Matsuda T. Mechanical stress-induced orientation and ultrastructural change of smooth muscle cells cultured in three-dimensional collagen lattices. Cell Transplant 1994;3(6):481-92.

61. Leung DY, Glagov S, Mathews MB. Cyclic stretching stimulates synthesis of matrix components by arterial smooth muscle cells in vitro. Science 1976;191(4226):475-7.

62. Dethlefsen SM, Shepro D, DAmore PA. Comparison of the effects of mechanical stimulation on venous and arterial smooth muscle cells in vitro. J Vasc Res 1996;33(5):405-13.

63. Kim BS, Nikolovski J, Bonadio J, Mooney DJ. Cyclic mechanical strain regulates the development of engineered smooth muscle tissue. Nat Biotechnol 1999;17(10):979-83.

64. Kim BS, Nikolovski J, Bonadio J, Smiley E, Mooney DJ. Engineered smooth muscle tissues: regulating cell phenotype with the scaffold. Exp Cell Res 1999;251(2):318-28.

65. Tada T, Nawata J, Wang H, Onoue N, Zhulanqiqige D, Ito K, Sugimura K, Fukumoto Y, Shimokawa H. Enhanced pulsatile pressure accelerates vascular smooth muscle migration: implications for atherogenesis of hypertension. Cardiovasc Res 2008;Epub:2008 Aug 25.

66. Watase M, Awolesi MA, Ricotta J, Sumpio BE. Effect of pressure on cultured smooth muscle cells. Life Sci 1997;61(10):987-96.

67. Stover J, Nagatomi J. Cyclic pressure stimulates DNA synthesis through the PI3K/Akt signaling pathway in rat bladder smooth muscle cells. Ann Biomed Eng 2007;35(9):1585-94.

68. Vouyouka AG, Jiang Y, Basson MD. Pressure alters endothelial effects upon vascular smooth muscle cells by decreasing smooth muscle cell proliferation and increasing smooth muscle cell apoptosis. Surgery 2004;136(2):282-90.

69. Kolpakov V, Rekhter MD, Gordon D, Wang WH, Kulik TJ. Effect of mechanical forces on growth and matrix protein synthesis in the in vitro pulmonary artery. Analysis of the role of individual cell types. Circ Res 1995;77(4):823-31.

70. Xing Y, Warnock JN, He Z, Hilbert SL, Yoganathan AP. Cyclic pressure affects the biological properties of porcine aortic valve leaflets in a magnitude and frequency dependent manner. Ann Biomed Eng 2004;32(11):1461-70.

71. Xing Y, He Z, Warnock JN, Hilbert SL, Yoganathan AP. Effects of constant static pressure on the biological properties of porcine aortic valve leaflets. Ann Biomed Eng 2004;32(4):555-62.

72. Benitz WE, Kelley RT, Anderson CM, Lorant DE, Bernfield M. Endothelial heparan sulfate proteoglycan. I. Inhibitory effects on smooth muscle cell proliferation. Am J Respir Cell Mol Biol 1990;2(1):13-24.

73. Herman IM, Castellot JJ Jr. Regulation of vascular smooth muscle cell growth by endothelial-synthesized extracellular matrices. Arteriosclerosis 1987;7(5):463-9.

74. Castellot JJ Jr, Addonizio ML, Rosenberg R, Karnovsky MJ. Cultured endothelial cells produce a heparinlike inhibitor of smooth muscle cell growth. J Cell Biol 1981;90(2):372-9.

75. Zempo N, Koyama N, Kenagy RD, Lea HJ, Clowes AW. Regulation of vascular smooth muscle cell migration and proliferation in vitro and in injured rat arteries by a synthetic matrix metalloproteinase inhibitor. Arterioscler Thromb Vasc Biol 1996;16(1):28-33.

76. Levesque MJ, Nerem RM, Sprague EA. Vascular endothelial cell proliferation in culture and the influence of flow. Biomaterials 1990;11(9):702-7.

77. Sumpio BE, Banes AJ, Levin LG, Johnson G Jr. Mechanical stress stimulates aortic endothelial cells to proliferate. J Vasc Surg 1987;6(3):252-6.

78. Shin HY, Gerritsen ME, Bizios R. Regulation of endothelial cell proliferation and apoptosis by cyclic pressure. Ann Biomed Eng 2002;30(3):297-304.

79. Vouyouka AG, Powell RJ, Ricotta J, Chen H, Dudrick DJ, Sawmiller CJ, Dudrick SJ, Sumpio BE. Ambient pulsatile pressure modulates endothelial cell proliferation. J Mol Cell Cardiol 1998;30(3):609-15.

80. Dardik A, Yamashita A, Aziz F, Asada H, Sumpio BE. Shear stress-stimulated endothelial cells induce smooth muscle cell chemotaxis via platelet-derived growth factor-BB and interleukin-1alpha. J Vasc Surg 2005;41(2):321-31.

81. Orlidge A, D'Amore PA. Inhibition of capillary endothelial cell growth by pericytes and smooth muscle cells. J Cell Biol 1987;105(3):1455-62.

82. Waybill PN, Hopkins LJ. Arterial and venous smooth muscle cell proliferation in response to co-culture with arterial and venous endothelial cells. J Vasc Interv Radiol 1999;10(8):1051-7.

83. Werner N, Nickenig G. Clinical and therapeutical implications of EPC biology in atherosclerosis. J Cell Mol Med 2006;10(2):318-32.

84. Jin H, Aiyer A, Su J, Borgstrom P, Stupack D, Friedlander M, Varner J. A homing mechanism for bone marrow-derived progenitor cell recruitment to the neovasculature. J Clin Invest 2006;116(3):652-62.

85. Luttun A, Carmeliet G, Carmeliet P. Vascular progenitors: from biology to treatment. Trends Cardiovasc Med 2002;12(2):88-96.

86. Hirschi KK, Rohovsky SA, Beck LH, Smith SR, D'Amore PA. Endothelial cells modulate the proliferation of mural cell precursors via platelet-derived growth factor-BB and heterotypic cell contact. Circ Res 1999;84(3):298-305.

87. Dodge AB, Lu X, D'Amore PA. Density-dependent endothelial cell production of an inhibitor of smooth muscle cell growth. J Cell Biochem 1993;53(1):21-31.

88. Lindner V, Reidy MA. Proliferation of smooth muscle cells after vascular injury is inhibited by an antibody against basic fibroblast growth factor. Proc Natl Acad Sci USA 1991;88(9):3739-43.

89. MacLeod DC, Strauss BH, de Jong M, Escaned J, Umans VA, van Suylen RJ, Verkerk A, de Feyter PJ, Serruys PW. Proliferation and extracellular matrix synthesis of smooth muscle cells cultured from human coronary atherosclerotic and restenotic lesions. J Am Coll Cardiol 1994;23(1):59-65.

90. Wang Y, Ameer GA, Sheppard BJ, Langer R. A tough biodegradable elastomer. Nat Biotechnol 2002;20(6):602-6.

91. Chen QZ, Bismarck A, Hansen U, Junaid S, Tran MQ, Harding SE, Ali NN, Boccaccini AR. Characterisation of a soft elastomer poly(glycerol sebacate) designed to match the mechanical properties of myocardial tissue. Biomaterials 2008;29(1):47-57.

92. Lee MC, Haut RC. Strain rate effects on tensile failure properties of the common carotid artery and jugular veins of ferrets. J Biomech 1992;25(8):925-7.

93. Wang Y, Kim YM, Langer R. In vivo degradation characteristics of poly(glycerol sebacate). J Biomed Mater Res A 2003;66(1):192-7.

94. Sundback CA, Shyu JY, Wang Y, Faquin WC, Langer RS, Vacanti JP, Hadlock TA. Biocompatibility analysis of poly(glycerol sebacate) as a nerve guide material. Biomaterials 2005;26(27):5454-64.

95. Gao J, Crapo P, Nerem R, Wang Y. Co-expression of elastin and collagen leads to highly compliant engineered blood vessels. J Biomed Mater Res A 2008;85(4):1120-8.

96. Bettinger CJ, Weinberg E, Wang Y, Borenstein J, Langer R. Endothelialized elastomeric biodegradable microfluidic scaffolds. Adv Mater 2006;18:165-9.

97. Gao J, Crapo PM, Wang Y. Macroporous elastomeric scaffolds with extensive micropores for soft tissue engineering. Tissue Eng 2006;12(4):917-25.

98. Fidkowski C, Kaazempur-Mofrad MR, Borenstein J, Vacanti JP, Langer R, Wang Y. Endothelialized microvasculature based on a biodegradable elastomer. Tissue Eng 2005;11(1-2):302-9.

99. Gao J, Ensley AE, Nerem RM, Wang Y. Poly(glycerol sebacate) supports the proliferation and phenotypic protein expression of primary baboon vascular cells. J Biomed Mater Res A 2007;83(4):1070-5.

100. Murphy WL, Dennis RG, Kileny JL, Mooney DJ. Salt fusion: an approach to improve pore interconnectivity within tissue engineering scaffolds. Tissue Eng 2002;8(1):43-52.

101. Hsu YY, Gresser JD, Trantolo DJ, Lyons CM, Gangadharam PR, Wise DL. Effect of polymer foam morphology and density on kinetics of in vitro controlled release of isoniazid from compressed foam matrices. J Biomed Mater Res 1997;35(1):107-16.

102. Ho ST, Hutmacher DW. A comparison of micro CT with other techniques used in the characterization of scaffolds. Biomaterials 2006;27(8):1362-76.

103. Zhang R, Ma PX. Poly(alpha-hydroxyl acids)/hydroxyapatite porous composites for bone-tissue engineering. I. Preparation and morphology. J Biomed Mater Res 1999;44(4):446-55.

104. Ramanujan S. Modular Equations and Approximations to Pi. Quart J Pure Appl Math 1914;45:350-72.

105. Ensley AE, Nerem RM. Endothelial progenitor cell coagulation potential is altered in response to fluid shear stress and substrate.:Manuscript in preparation.

106. Van Wezel AL. Growth of cell-strains and primary cells on micro-carriers in homogeneous culture. Nature 1967;216(5110):64-5.

107. Peterson LH, Jensen RE, Parnell J. Mechanical properties of arteries in vivo. Circ Res 1960;8:622-39.

108. Strauss BH, Chisholm RJ, Keeley FW, Gotlieb AI, Logan RA, Armstrong PW. Extracellular matrix remodeling after balloon angioplasty injury in a rabbit model of restenosis. Circ Res 1994;75(4):650-8.

109. Woessner JF Jr. The determination of hydroxyproline in tissue and protein samples containing small proportions of this imino acid. Arch Biochem Biophys 1961;93:440-7.

110. Wong LC, Langille BL. Developmental remodeling of the internal elastic lamina of rabbit arteries: effect of blood flow. Circ Res 1996;78(5):799-805.

111. Lee WK, Bell J, Kilpatrick E, Hayes M, Lindop GB, Dominiczak MH. Collagen-linked fluorescence in human atherosclerotic plaques. Atherosclerosis 1993;98(2):219-27.

112. Briones AM, González JM, Somoza B, Giraldo J, Daly CJ, Vila E, González MC, McGrath JC, Arribas SM. Role of elastin in spontaneously hypertensive rat small mesenteric artery remodelling. J Physiol 2003;552(1):185-95.

113. Crapo PM, Gao J, Wang Y. Seamless tubular poly(glycerol sebacate) scaffolds: high-yield fabrication and potential applications. J Biomed Mater Res A 2008;86(2):354-63.

114. Nasseri BA, Pomerantseva I, Kaazempur-Mofrad MR, Sutherland FW, Perry T, Ochoa E, Thompson CA, Mayer JE Jr, Oesterle SN, Vacanti JP. Dynamic rotational seeding and cell culture system for vascular tube formation. Tissue Eng 2003;9(2):291-9.

115. Cummings CL, Gawlitta D, Nerem RM, Stegemann JP. Properties of engineered vascular constructs made from collagen, fibrin, and collagen-fibrin mixtures. Biomaterials 2004;25(17):3699-706.

116. Hirose M, Kosugi H, Nakazato K, Hayashi T. Restoration to a quiescent and contractile phenotype from a proliferative phenotype of myofibroblast-like human aortic smooth muscle cells by culture on type IV collagen gels. J Biochem 1999;125(6):991-1000.

117. Dahl SL, Rucker RB, Niklason LE. Effects of copper and cross-linking on the extracellular matrix of tissue-engineered arteries. Cell Transplant 2005;14(6):367-74.

118. Elbjeirami WM, Yonter EO, Starcher BC, West JL. Enhancing mechanical properties of tissue-engineered constructs via lysyl oxidase crosslinking activity. J Biomed Mater Res A 2003;66(3):513-21.

119. Haberstroh KM, Kaefer M, Retik AB, Freeman MR, Bizios R. The effects of sustained hydrostatic pressure on select bladder smooth muscle cell functions. J Urol 1999;162(6):2114-8.

120. Joddar B, Ramamurthi A. Elastogenic effects of exogenous hyaluronan oligosaccharides on vascular smooth muscle cells. Biomaterials 2006;27(33):5698-707.

121. Kothapalli CR, Taylor PM, Smolenski RT, Yacoub MH, Ramamurthi A. TGF-beta1 and Hyaluronan Oligomers Synergistically Enhance Elastin Matrix Regeneration by Vascular Smooth Muscle Cells. Tissue Eng Part A 2008;Epub:2008 Oct 10.

122. Joddar B, Ibrahim S, Ramamurthi A. Impact of delivery mode of hyaluronan oligomers on elastogenic responses of adult vascular smooth muscle cells. Biomaterials 2007;28(27):3918-27.

123. Furchgott RF, Zawadzki JV. The obligatory role of endothelial cells in the relaxation of arterial smooth muscle by acetylcholine. Nature 1980;288(5789):373-6.

124. Bass A, Krupski WC, Hanson SR, Dodson T, Lumsden A, White D, Harker LA, Kelly AB. Exteriorized chronic aorto-caval arteriovenous access shunts in the baboon (Papio cynocephalus). J Med Primatol 1993;22(6):331-9.